

BORATE MODIFIED BIOGLASS CONTAINING SCAFFOLDS FOR DENTAL  
TISSUE ENGINEERING APPLICATIONS

A THESIS SUBMITTED TO  
THE GRADUATE SCHOOL OF NATURAL AND APPLIED SCIENCES  
OF  
MIDDLE EAST TECHNICAL UNIVERSITY

BY

REZA MOONESI RAD

IN PARTIAL FULLFILLMENT OF THE REQUIREMENTS  
FOR  
THE DEGREE OF DOCTOR OF PHILOSOPHY  
IN  
BIOTECHNOLOGY

JANUARY 2018



Approval of the thesis:

**BORATE MODIFIED BIOGLASS CONTAINING SCAFFOLDS FOR  
DENTAL TISSUE ENGINEERING APPLICATIONS**

Submitted by **REZA MOONESI RAD** in partial fulfillment of the requirements for the degree of **Doctor of Philosophy in Biotechnology Department, Middle East Technical University** by,

Prof. Dr. Gülbin Dural Ünver  
Dean of Graduate School of Natural and Applied Sciences \_\_\_\_\_

Assoc. Prof. Dr. Can Özen  
Head of Department, Biotechnology \_\_\_\_\_

Prof. Dr. Ayşen Tezcaner  
Supervisor, Engineering Sciences Dept., METU \_\_\_\_\_

Prof. Dr. Zafer Evis  
Co-Supervisor, Engineering Sciences Dept., METU \_\_\_\_\_

**Examining Committee Members:**

Prof. Dr. Dilek Keskin  
Engineering Sciences Dept., METU \_\_\_\_\_

Prof. Dr. Ayşen Tezcaner  
Engineering Sciences Dept., METU \_\_\_\_\_

Assoc. Prof. Dr. Senih Gürses  
Engineering Sciences Dept., METU \_\_\_\_\_

Prof. Dr. Volkan Şahin  
Prosthodontics Dept., Kırıkkale University \_\_\_\_\_

Assist. Prof. Dr. Özge Erdemli  
Molecular Biology and Genetics Dept., Başkent University \_\_\_\_\_

**Date:** 31/01/2018

**I hereby declare that all information in this document has been obtained and presented in accordance with academic rules and ethical conduct. I also declare that, as required by these rules and conduct, I have fully cited and referenced all material and results that are not original to this document.**

Name, Last name: Reza Moonesi Rad

Signature:

## **ABSTRACT**

### **BORATE MODIFIED BIOGLASS CONTAINING SCAFFOLDS FOR DENTAL TISSUE ENGINEERING APPLICATIONS**

Moonesi Rad, Reza

Ph.D., Department of Biotechnology

Supervisor: Prof. Dr. Ayşen Tezcaner

Co-Supervisor: Prof. Dr. Zafer Evis

January 2018, 220 pages

Dental tissue engineering has gained increasing attention in recent years. Dentures or implants are used as replacements of the lost teeth. High cost of these restorations and rejection possibility of the implants are their main drawbacks. For this reason, a regenerative approach for repairing of the damaged dentin-pulp complex or generating a new tissue is needed. The properties associated with bioglass like biocompatibility and bioactivity are very attractive for dental applications. In this thesis, bioactive glass nanoparticles (BG-NPs) modified with borate at different ratios (7%, 14%, and 21%) were synthesized using combination of sol-gel/co-precipitation and quick alkali-mediated sol-gel methods. Their effect on the odontogenic differentiation of human dental pulp stem cells (hDPSCs) was investigated. Additionally, 3D cellulose acetate/pullulan/gelatin (CA/PULL/GEL) based dentin-like constructs containing 10 or 20% BG-NPs was studied to explore their potential for dentin regeneration. SEM and XRD analyses showed that synthesized BGs were nano-sized and amorphous in nature, respectively. Characteristic functional groups of BGs were observed in FTIR and FT-Raman spectral analysis. ICP analysis revealed that BGs synthesized possessed the expected and compositions close to the theoretical ones. The purpose of modification of

bioglass with borate was to achieve increased biodegradability. Increase of  $B_2O_3$  in BG content positively affected the bioactivity of BG. Higher ion release in SBF resulted in higher amounts of calcium phosphate deposited on BG discs. Three-dimensional porous scaffolds with tubular pore structures were successfully produced using two methods: thermally induced phase separation/porogen leaching (TIPS/PL) and freeze-drying/metal mold pressing (FD/MMP) and crosslinked with glutaraldehyde. KCl was added as porogen for increasing porosity of the scaffolds in TIPS/PL method. Bioactivity tests showed apatite like depositions on scaffolds. BG addition enhanced bioactivity of the scaffolds. Furthermore, borate modification resulted in higher deposition than observed in scaffolds with BG. Scaffolds without BG possessed the highest porosity percentage. Addition of 10% BG improved the mechanical properties of scaffolds. For cell culture studies hDPSCs were isolated from patient's extracted tooth and flow cytometry analysis showed that isolated hDPSCs were mesenchymal origin. 6.25 mg/ml was chosen as the optimum BG concentration from dose dependent cytotoxicity study and used for differentiation tests. All of BG groups enhanced odontogenic differentiation of hDPSCs and presence of borate increased cell viability. hDPSCs proliferated on scaffolds prepared by both methods and presence of borate modified BGs increased cell viability observed on scaffolds. Immunohistochemical and histochemical stainings showed that scaffolds positively affected the odontoblastic differentiation of the hDPSCs.

In this thesis, results showed that borate modified BG-NPs and dentin-like constructs hold promise for use in dental tissue engineering applications.

Keywords: Regenerative Dentistry, Borate Modified Bioglass Nanoparticles, Cellulose Acetate, Pullulan, Gelatin, Tissue Engineering

## ÖZ

### **DIŞ DOKU MÜHENDİSLİĞİ UYGULAMALARI İÇİN BORAT İLE MODİFİYE EDİLMİŞ BİOCAM İÇEREN TAŞIYICILAR**

Moonesi Rad, Reza

Doktora, Biyoteknoloji

Tez Yöneticisi: Prof. Dr. Ayşen Tezcaner

Ortak Tez Yöneticisi: Prof. Dr. Zafer Evis

Ocak 2018, 220 sayfa

Diş dokusu mühendisliği son yıllarda giderek artan bir ilgi görmektedir. Kaybedilen dişler yerine maliyeti yüksek protezler veya rejeksiyon olasılığı olan implantlar kullanılmaktadır. Bu nedenle hasarlı dentin-pulpa kompleksinin rejeneratif bir yaklaşımla onarımına veya yerine yeni doku oluşturulmasına ihtiyaç vardır. Biyocamın, biyouyumluluk ve biyoaktivite gibi özellikleri, diş uygulamaları için oldukça ilgi çekicidir. Bu tezde borat ile farklı oranlarda (%7, 14 ve 21) modifiye edilerek hazırlanan biyocam nanopartikülleri (BG-NPs) iki farklı metod ile (sol-jel ve çöktürme metodu ve hızlı alkali-aracılı sol-jel metodu) hazırlanıp, karakterize edilmiş ve elde edilen biyocamların diş pulpası kökenli kök hücreler üzerindeki etkileri incelenmiştir. Ayrıca borat ile modifiye edilmiş BG-NPs'ler %10 ve %20 ağırlık oranlarında sellüloz asetat/pullulan/jelatin (SA/PULL/JEL) eklenerek üç boyutlu dentin benzeri yapılarına eklenerek, dentin rejenerasyonuna yönelik kullanım potansiyeli araştırılmıştır. Üretilen biocamların SEM ve XRD analizleri, sırasıyla sentezlenen BG'lerin nano boyutlu ve yapısal olarak amorf olduğunu göstermiştir. BG'lerin karakteristik fonksiyonel grupları FTIR ve FT-Raman sanalizlerinde gözlenmiştir. ICP analizi sentezlenen BG'lerin, beklenen kompozisyonlara sahip olduklarını göstermiştir. Borat ile modifikasyonun amacı, biyocamın

biyobozunurluğunu arttırmaktır.  $B_2O_3$  içeriğinin artması, SBF'de serbest bırakılan iyonların daha yüksek konsantrasyonda ve BG disklerinde üzerinde biriken kalsiyum fosfatın daha yüksek miktarda olmasına neden olup, BG biyoaktivitesini olumlu yönde etkilemiştir. Taşıyıcılar iki metod (termal indükleme/porojen uzaklaştırma ve liyofilizasyon /metal kalıplama) kullanılarak hazırlanmış ve glutaraldehit ile çapraz bağlanmıştır. Gözenekliliğin artırılması için taşıyıcılara KCl porojen olarak eklenmiştir. Her iki yöntemle yönlü ve tübüler yapıya sahip taşıyıcılar başarıyla üretilmiş ve in vitro bioaktivite testlerinde kalsiyum fosfat içerikli çökteller oluştuğu gözlenmiştir. BG ilavesi taşıyıcıların biyoaktivitesini arttırmıştır. Ayrıca, borat ile modifikasyon, taşıyıcıların üstünde daha çok depozisyona neden olmuştur. En yüksek gözeneklik yüzdesine BG içermeyen grubun sahip olduğu bulunmuştur. Hazırlanan taşıyıcılara, %10 biyocam ilavesinin, mekanik özellikleri arttırdığı gözlenmiştir. Hücre kültür çalışmaları için hastaların dental pulpa hücreleri (hDPSC) izole edilmiş ve akış sitometri analizi ile mezenkimal kök hücre kökenli olduğu gösterilmiştir. Yapılan doza bağlı sitotoksikite testlerinden optimum konsantrasyon olarak 6.25 mg/ml belirlenmiş ve bu konsantrasyonun tüm BG grupları için hDPSC'lerin odontojenik farklılaşmasını sağladığı gözlenmiştir. Her iki yöntem ile hazırlanan taşıyıcılar üzerinde hDPSC'ler çoğalmıştır ve borat ilaveli biyocamın varlığı, hücre canlılığını arttırmıştır. İmmunohistokimyasal ve histokimyasal boyamalar sonucunda, taşıyıcıların (hDPSCs) hücrelerin odontontoblast yönünde farklılaşmasını olumlu şekilde etkilediği görülmüştür.

Bu tezde elde edilen sonuçlar üretilen borat ile modifiye edilmiş (BG-NPs) ve geliştirilen dentin benzeri yapıların diş doku mühendisliği uygulamaları için yeni bir yaklaşım getirdiğini göstermektedir.

Anahtar kelimeler: Rejeneratif Diş Hekimliği, Borat ile Modifiye Biyocam Nanopartikülleri, Seluloz Asetat, Pullulan, Jelatin, Doku Mühendisliği



*To my beloved family*

*and*

*To all human beings who know values of nature and cultural heritage*

## ACKNOWLEDGEMENTS

I would like to express my foremost gratitude to my supervisor Prof. Dr. Ayşen Tezcaner for her continuous guidance, unsurpassed knowledge and generous support that she has provided me throughout my thesis study. I would like to express my special appreciation to my co-supervisor Prof. Dr. Zafer Evis for his contribution and encouragement during my thesis study.

I also would like to express my special thanks to Prof. Dr. Dilek Keskin for her valuable suggestions and encouragement throughout my thesis study. I would also like to thank Assoc. Prof. Dr. Senih Gürses, as member of my thesis monitoring committee for his support and suggestions throughout my Ph.D. study.

I would also like to express my thanks of gratitude to Prof. Dr. Korhan Altunbaş, for allowing me to study in his laboratory at Afyon Kocatepe University, Veterinary Faculty, Histology and Embryology Department. I would also like to thank Elif Ece Akgün and Tayfun Dikmen for their assistance in the experiments. I also thank Dr. Sıla Şahin for her valuable cooperation for providing teeth for stem cell isolation.

I would like to thank all my lab friends, Dr. Özge Erdemli, Dr. Ayşegül Kavas, Dr. Ömer Aktürk, Dr. Aydın Tahmasebifar, Dr. Bengi Yılmaz, Dr. Ammar Z. Alshemary, Dr. Tuğçe Aktar, Zeynep Gürtürk, Sibel Turkan, Merve Güldiken, Nil Göl, Hazal Aydoğdu, Alişan Kayabölen, Sina Khoshsima, Said Murat Kayhan, Yağmur Çalışkan, Milad Fathi, Elmira Pourreza, Gülçin Çiçek, Sepren Öncü, Buşra Yedekçi, Bahadır Güner, Duygu Deniz Akolpoğlu, Gerçem Altunordu, Gülhan Işık, Hani Alem, Mustafa Nakipoğlu, Hosein Jodati, Saba Najari Hagh for their valuable helps during the experiments and also providing a friendly environment in the lab, which is full of good memories.

I am thankful for Deniz Atila for helping me all the time in my lab experiments and also preparing scientific reports. I also give my thanks to Engin Pazarçeviren, and Ali Deniz Dalgıç, for their valuable supports for my lab works.

I thank my friends Dr. Aslan Massahi, Dr. Kaveh Dehganian, Dr. Ali Etemadi, Yashar Oskouei, and Hamed Asadi for their moral support during my thesis work.

I would like to thank to The Scientific and Technological Research Council of Turkey for the support they provided (Project no: 114R042).

I would like to give my special thanks to my parents, Mohammad Ali Mounesi Rad, and Shahin Eslamnour for their endless supports and precious contributions to every stage of my life and this study. Many Thanks to my sisters Dr. Shokoufeh Mounesi Rad, Banafsheh Mounesi Rad, and my brother, Pouria Mounesi Rad, for their valuable encouragement during my thesis study.

## TABLE OF CONTENTS

ABSTRACT.....	v
ÖZ.....	vii
ACKNOWLEDGMENTS.....	x
TABLE OF CONTENTS.....	xii
LIST OF TABLES.....	xviii
LIST OF FIGURES.....	xx
LIST OF ABBREVIATIONS.....	xxvii
CHAPTERS	
1. INTRODUCTION.....	1
1.1. Strategies for Tooth Regeneration.....	2
1.1.1. Selection of Biomaterials for Dental Tissue Engineering.....	2
1.1.1.1. Bioactive Glasses.....	3
1.1.1.1.1. Methods for Bioactive Glass Synthesis.....	6
1.1.1.1.2. Application of Bioactive Glass in Tissue Engineering..	7
1.2. Tissue Engineering Approaches for the Regeneration of Dentin- Pulp Complex.....	11
1.2.1. Biomaterials Used for Preparation of the Scaffolds in This Study.....	16
1.2.1.1. Cellulose.....	16
1.2.1.2. Pullulan.....	17
1.2.1.3. Gelatin.....	22
1.2.2. Stem Cells.....	26
1.2.2.1. Embryonic Stem Cells.....	26
1.2.2.2. Mesenchymal Stem Cells.....	27
1.2.2.2.1. Adult Stem Cells of Non-Dental Origin.....	27
1.2.2.2.2. Adult Stem Cells of Dental Origin.....	28

1.2.2.2.2.1. Stem Cells from Human Exfoliated Deciduous Teeth (SHED) .....	28
1.2.2.2.2.2. Dental Follicle Stem Cells (DFPCs) .....	29
1.2.2.2.2.3. Stem Cells from the Apical Papilla (SCAPs) .....	30
1.2.2.2.2.4. Periodontal Ligament Stem Cells (PDLSCs) .....	31
1.2.2.2.2.5. Dental Pulp Stem Cells (DPSCs) .....	32
1.2.2.3. Induced Pluripotent Stem Cells.....	33
1.3. Aim of the Study.....	34
2. MATERIALS & METHODS.....	37
2.1. Materials.....	37
2.2. Methods.....	41
2.2.1. Synthesis of Pure and Borate Modified BG-NPs.....	41
2.2.1.1. Preparations of Pure and Borate Modified BG-NPs by Combination of Sol-Gel and Coprecipitation Methods.....	42
2.2.1.2. Preparations of Pure and Borate Modified BG-NPs by a Quick Alkali-Mediated Sol-Gel Method.....	43
2.3. Characterization of Pure and Borate Modified BG-NPs.....	44
2.3.1. X-Ray Diffraction (XRD) Analysis.....	44
2.3.2. Fourier Transform Infrared Spectroscopy (FTIR) Analysis.....	44
2.3.3. Scanning Electron Microscopy (SEM) Analysis.....	45
2.3.4. Inductively Coupled Plasma Mass Spectrometry (ICP-MS) Analysis.....	45
2.3.5. Porosimetry Analysis.....	46
2.3.6. In Vitro Bioactivity Tests.....	46
2.4. Preparation of Three Dimensional CA/PULL/GEL Scaffolds.....	47
2.4.1. Periodate Oxidation of PULL.....	47
2.4.1.1. Determination of Oxidation Degree of Oxidized PULL.....	47
2.4.2. Carboxylation of PULL.....	48
2.4.2.1. Determination of Degree of Substitution of Carboxylated PULL.....	48

2.4.3. Preparation of Polymer Solutions.....	49
2.4.4. Preparation of Three Dimensional Scaffolds.....	50
2.4.4.1. Preparation of Three Dimensional Scaffolds by (TIPS/PL) Method.....	50
2.4.4.2. Preparation of Three Dimensional Scaffolds by (FD/MMP) Method.....	53
2.4.5. Cross-linking of Three-Dimensional Scaffolds.....	56
2.4.6. In Vitro Degradation Analysis.....	57
2.4.7. Water Absorption Capacity Measurement of the Scaffolds.....	57
2.4.8. Scanning Electron Microscopy (SEM) Analysis.....	58
2.4.9. In Vitro Biomineralization Analysis.....	58
2.4.10. Porosity Measurements.....	59
2.4.11. Mechanical Tests.....	60
2.5. Cell Culture Studies.....	61
2.5.1. Isolation of hDPSCs.....	61
2.5.2. Characterization of Human DPSCs.....	61
2.5.3. In Vitro Cytotoxicity Assessment of Pure and Borate Modified BG-NPs.....	62
2.5.4. Evaluation of Effect of Pure and Borate Modified BG-NPs on Differentiation of Dental Pulp Stem Cells.....	63
2.5.4.1. Measurement of Alkaline Phosphatase (ALP) Enzyme Activity and Intracellular Calcium Amounts of DPSCs.....	63
2.5.5. Immunohistochemical Staining.....	64
2.5.6. Cell Viability Assays.....	65
2.5.7. Measurement of ALP Activity and Intracellular Calcium Amounts of hDPSCs Seeded on Scaffolds.....	66
2.5.8. Immunohistochemical and Histological Analysis of hDPSCs Seeded Scaffolds.....	66
2.6. Statistical Analysis.....	67
3. RESULTS AND DISCUSSION.....	69

3.1. Characterization of the Synthesized BG-NPs.....	69
3.1.1. Scanning Electron Microscopy (SEM) Analysis.....	69
3.1.1.1. Combination of Sol-Gel and Co-Precipitation Methods.....	69
3.1.1.2. Quick Alkali-Mediated Sol-Gel Method.....	70
3.1.2. X-Ray Diffraction (XRD) Analysis.....	72
3.1.2.1. Combination of Sol-Gel and Co-Precipitation Methods.....	72
3.1.2.2. Quick Alkali-Mediated Sol-Gel Method.....	72
3.1.3. Inductively Coupled Plasma Mass Spectrometry (ICP-MS) Analysis.....	75
3.1.3.1. Combination of Sol-Gel and Co-Precipitation Methods.....	75
3.1.3.2. Quick Alkali-Mediated Sol-Gel Method.....	76
3.1.4. Fourier Transform Infrared Spectroscopy (FTIR) Analysis.....	77
3.1.5. Fourier Transform Raman (FT-Raman) Spectroscopy.....	79
3.1.6. Porosimetry Analysis.....	79
3.1.7. In Vitro Bioactivity Tests.....	80
3.2. Preparation of Three Dimensional CA/PULL/GEL.....	85
3.2.1. Determination of Oxidation Degree of Oxidized PULL and Degree of Substitution of Carboxyl Groups of Carboxylated PULL.....	85
3.2.2. In Vitro Degradation Analysis.....	87
3.2.2.1. Scaffolds Prepared by (TIPS/PL) Method.....	89
3.2.2.2. Scaffolds Prepared by (FD/MMP) Method.....	92
3.2.3. Water Absorption Capacity of the Scaffolds.....	98
3.2.3.1. Scaffolds Prepared by (TIPS/PL) Method.....	98
3.2.3.2. Scaffolds Prepared by (FD/MMP) Method.....	99
3.2.4. Scanning Electron Microscopy (SEM) Results.....	102
3.2.4.1. Scaffolds Prepared by (TIPS/PL) Method.....	102
3.2.4.2. Scaffolds Prepared by (FD/MMP) Method.....	106
3.2.5. In Vitro Bioactivity Tests.....	109
3.2.5.1. Scaffolds Prepared by TIPS/PL Method.....	109

3.2.5.2. Scaffolds Prepared by FD/MMP Method.....	114
3.2.6. Porosity Measurements.....	118
3.2.6.1. Porosity Results of Scaffolds Prepared by TIPS/PL Method.....	118
3.2.6.2. Porosity Results of Scaffolds Prepared by FD/MMP Method.....	122
3.2.7. Mechanical Tests.....	124
3.3. Cell Culture Studies.....	127
3.3.1. Isolation of hDPSCs.....	127
3.3.2. Characterization of hDPSCs.....	128
3.3.3. In Vitro Cytotoxicity Assessment of BG and Borate Modified BG.....	131
3.3.4. Evaluation of Effect of BG Nanoparticles on Differentiation of Dental Pulp Stem Cells.....	132
3.3.4.1. Measurement of Alkaline Phosphatase (ALP) Enzyme Activity and Intracellular Calcium amounts of DPSCs.....	132
3.3.4.2. Immunohistochemical Staining.....	137
3.3.5. Cell Viability Assays for the 3-Dimensional Scaffolds.....	138
3.3.5.1. Scaffolds Prepared by TIPS/PL Method.....	138
3.3.5.2. Scaffolds Prepared by FD/MMP Method.....	146
3.3.6. Evaluation of Differentiation of hDPSCs Seeded on Three Dimensional Scaffolds.....	151
3.3.6.1. Measurement of ALP Activity and Intracellular Calcium Amounts of hDPSCs Seeded on Three Dimensional Scaffolds.....	151
3.3.6.1.1. Scaffolds Prepared by TIPS/PL Method.....	151
3.3.6.1.2. Scaffolds Prepared by FD/MMP Method.....	153
3.3.6.2. Immunohistochemical and Histological Analysis of hDPSCs Seeded Scaffolds.....	156
3.3.6.2.1. Scaffold Prepared by TIPS/PL Method.....	156



3.3.6.2.2. Scaffolds Prepared by FD/MMP Method.....	166
4. CONCLUSION.....	181
REFERENCES.....	183
APPENDICES	
A. ETHICS COMMITTEE REPORT.....	211
B. CALIBRATION CURVE FOR ALP ASSAY.....	213
C. CALIBRATION CURVE FOR DETERMINATION OF INTRACELLULAR CALCIUM.....	215
D. CALIBRATION CURVE FOR DETERMINATION OF DNA	217
CURRICULUM VITAE.....	219

## LIST OF TABLES

<b>Table 1.</b> Different compositions of bioactive glasses (Abbasi et al., 2015).....	4
<b>Table 2.</b> Different commercial brands of bioactive glass (Montazerian & Dutra Zanotto, 2016, Kumar et al., 2015).....	5
<b>Table 3.</b> Tissue engineering applications of different forms of PULL.....	23
<b>Table 4.</b> List of materials used for bioactive glass nanoparticles synthesis.....	37
<b>Table 5.</b> List of chemicals used in the preparation of three-dimensional scaffolds...	38
<b>Table 6.</b> List of materials used in cell culture experiments.....	40
<b>Table 7.</b> Nominal compositions of Bx-BG samples.....	43
<b>Table 8.</b> Nominal compositions of Bx-BG samples.....	44
<b>Table 9.</b> Solubility of polymers in different solvents.....	50
<b>Table 10.</b> Different solvent systems used for preparation of the scaffolds.....	51
<b>Table 11.</b> Experimental groups used for preparing the three dimensional scaffolds by using the (TIPS/PL) method.....	54
<b>Table 12.</b> Ion concentrations in SBF solution.....	59
<b>Table 13.</b> Chemical composition of BG and borate modified BG materials obtained with ICP-MS.....	76
<b>Table 14.</b> Chemical composition of BG and borate modified BG materials obtained with ICP-MS.....	77
<b>Table 15.</b> BET and BJH analyses results of BG and B <sub>2</sub> O <sub>3</sub> modified BGs.....	81
<b>Table 16.</b> Ca/P ratio of apatite layer formed after immersion of samples in SBF solution.....	87
<b>Table 17.</b> pH of PBS (0.1 M, pH 7.4) in which 6 hours GTA cross-linked CA/Ox-PULL/GEL scaffolds incubated at 37°C for different periods (n=3). Scaffolds were prepared by (TIPS/PL) method.....	93
<b>Table 18.</b> pH of PBS (0.1 M, pH 7.4) in which CA/Ox-PULL/GEL scaffolds cross-linked with 5% GTA solution for 30 minutes before mold pressing and for 12 hours after mold pressing, were incubated at 37°C for different periods (n=3). Scaffolds were prepared by (FD/MMP) method.....	97

<b>Table 19.</b> Water absorption results of GTA cross-linked (6 hours) CA/Ox-PULL/GEL scaffolds in PBS (0.1 M, pH 7.4) at 37°C that were prepared by the method of (TIPS/PL) (n=3).....	99
<b>Table 20.</b> Water absorption measurement results of GTA cross-linked (30 minutes before mold pressing and for 12 hours after mold pressing) CA/Ox-PULL/GEL scaffolds in PBS (0.1 M, pH 7.4) at 37°C that were prepared by the method of (FD/MMP) (n=3).....	101
<b>Table 21.</b> Porosity percentages of the scaffolds prepared by the TIPS/PL method (n=3).....	122
<b>Table 22.</b> Results of porosity measurements of the scaffolds prepared by the FD/MMP method (n=3).....	125
<b>Table 23.</b> Compression test results of the scaffolds prepared by the (TIPS/PL) method (n=3).....	129
<b>Table 24.</b> Immunophenotypic properties of hDPSCs cells (n=2). Numbers in the table indicate the percentages of CD positive and CD negative cells.....	130

## LIST OF FIGURES

<b>Figure 1.</b> (a) Anatomy of tooth (Boling, 2017); (b) SEM image of natural dentinal tubules with odontoblasts processes (Torabinejad, 2015).....	2
<b>Figure 2.</b> Chemical structure of PULL (Pereira, 2013).....	18
<b>Figure 3.</b> Mechanism of cross-linking of PULL with sodium trimetaphosphate (STMP) (Dulong et al., 2011).....	19
<b>Figure 4.</b> Schematic representation of cross-linking of oxidized PULL and proteins (Asma et al., 2014).....	20
<b>Figure 5.</b> Chemical structure of gelatin (Ge et al., 2012).....	24
<b>Figure 6.</b> Crosslinking mechanism of gelatin with GTA (Migneault et al., 2004)....	24
<b>Figure 7.</b> Schematic representation of amide bond formation as a result of cross-linking of gelatin with EDC/NHS (Rose et al., 2014).....	25
<b>Figure 8.</b> A system prepared from aluminum plate and foam in order to freeze the polymers solution in one direction (a) view from the foam side with the glass containers – (b) view from the aluminum plate side.....	52
<b>Figure 9.</b> Schematic image of the metal mold consisting of pins with 400 $\mu\text{m}$ diameter and distance of 400 $\mu\text{m}$ between (a); Image of the designed and produced metal mold consisting of pins with 400 $\mu\text{m}$ diameter and distance of 400 $\mu\text{m}$ between them, side view (b); view from above (c); Image of the designed and produced metal mold consisting of pins with 500 $\mu\text{m}$ diameter and distance of 600 $\mu\text{m}$ between them, side view (d); view from above (e).....	55
<b>Figure 10.</b> SEM image and particle size distribution curve of B0-BG synthesized by combination of sol-gel and co-precipitation methods.....	69
<b>Figure 11.</b> SEM images and particle size distribution curves of a) B0-BG, b) B7-BG, synthesized by the quick alkali-mediated sol-gel method.....	70
<b>Figure 12.</b> XRD spectra of synthesized a) B0-BG, b) B7-BG, c) B14-BG synthesized by combination of sol-gel and co-precipitation methods.....	73
<b>Figure 13.</b> XRD spectra of synthesized B0-BG, B7-BG, B14-BG, B21-BG synthesized by the quick alkali-mediated sol-gel method.....	74

<b>Figure 14.</b> FTIR spectra of different compositions of BG-NPs, A) B0-BG, B) B7-BG, C) B14-BG, D) B21-BG , respectively. All samples were calcined at 600°C for 2 h.....	78
<b>Figure 15.</b> FT-Raman spectra of different compositions of BG-NPs, A) B0-BG, B) B7-BG, C) B14-BG, D) B21-BG, respectively. All samples were calcined at 600 °C for 2 h.....	80
<b>Figure 16.</b> N <sub>2</sub> adsorption-desorption isotherm of synthesized a) B0-BG, b) B7-BG, c) B14-BG, d) B21-BG synthesized by the quick alkali-mediated sol–gel method.....	82
<b>Figure 17.</b> SBF incubation studies for B0-BG and borate modified BG; Release of a) Si ion, b) Ca <sup>+2</sup> ion, c) B ion, and d) changes in pH of SBF with time groups.....	83
<b>Figure 18.</b> SEM images of B0-BG and borate modified BG samples after soaking in SBF for various periods of time.....	86
<b>Figure 19.</b> Weight loss of GTA cross-linked CA/PULL/GEL scaffold samples (%50 CA, %15 PULL, %35 GEL, with total polymer concentration of %2.5), in PBS (0.1 M, pH 7.4) at 37°C (n=3).....	88
<b>Figure 20.</b> Weight loss of GTA cross-linked CA/Ox-PULL/GEL scaffold samples (%50 CA, %15 Ox-PULL, %35 GEL, with total polymer concentration of %2.5) in PBS (0.1 M, pH 7.4) at 37°C (n=3).....	89
<b>Figure 21.</b> Weight loss of EDC/NHS cross-linked CA/Carboxyl-PULL/GEL scaffold samples (50% CA, 15% Carboxyl-PULL, 35% GEL, with total polymer concentration of %2.5) in PBS (0.1 M, pH 7.4) at 37°C (n=3).....	89
<b>Figure 22.</b> Weight loss of GTA cross-linked (6 hours) CA/Ox-PULL/GEL scaffolds in PBS (0.1 M, pH 7.4) at 37°C (n=3). Scaffolds were prepared by (TIPS/PL) method (50% CA, 15% PULL, 35% GEL, with total polymer concentration of 2.5%).....	92
<b>Figure 23.</b> Weight loss of GTA cross-linked (30 minutes before mold pressing and for 12 hours after mold pressing) CA/Ox-PULL/GEL scaffolds in PBS (0.1 M, pH 7.4) at 37°C (n=3). Scaffolds were prepared by the (FD/MMP) method (50% CA, 15% PULL, 35% GEL, with total polymer concentration of 5%).....	95
<b>Figure 24.</b> Cross-sectional SEM images of the scaffolds composed of CA/Ox-PULL/GEL prepared by the (TIPS/PL) method (Freezing temperatures: -196°C)..	104

<b>Figure 25.</b> Cross-sectional SEM images of the CA/Ox-PULL/GEL scaffolds prepared by the TIPS/PL method and using KCl as porogen at different amounts (a) 100% (b) 50% (C) 25% of the total polymer concentration. (Freezing temperatures: -80°C).....	105
<b>Figure 26.</b> Cross-sectional SEM images of the CA/Ox-PULL/GEL scaffolds prepared by the TIPS/PL method using KCl as %100 of the total polymer weight, (a) B0-10 group (b) B14-20 group. (Freezing temperatures: -80°C).....	106
<b>Figure 27.</b> SEM images of the scaffolds prepared by the FD/MMP method, a) without BG, b) B0 – 10, c) B0 – 20, d) B7 – 10, e) B7 – 20, f) B14 – 10, g) B14 – 20, h) B21 – 10, and i) B21 – 20.....	108
<b>Figure 28.</b> SEM images of macropores walls of the scaffolds prepared by the FD/MMP method, a) without BG, and b) 14B – 10, (arrow shows wall of the macropore).....	109
<b>Figure 29.</b> SEM images of the scaffolds prepared by the TIPS/PL method, and kept in SBF for 7 and 14 days: a) without BG, day 7; b) without BG, day 14; c) B0-10, day 7; d) B0-10, day 14; e) B0-20, day 7; f) B0-20, day 14.....	111
<b>Figure 30.</b> SEM images of the scaffolds prepared by the FD/MMP method, and kept in SBF for 7 and 14 days: a) withoutBG, day 7; b) without BG, day 14; c) B0-10, day 7; d) B0-10, day 14; e) B0-20, day 7; f) B0-20, day 14.....	115
<b>Figure 31.</b> Pore size distribution of CA/Ox-PULL/GEL scaffold prepared by the TIPS/PL) method, measured by the mercury porosimetry device.....	119
<b>Figure 32.</b> Phase contrast microscopy images of the isolated hDPSCs (a) 3 days and (b) 5 days after isolation.....	128
<b>Figure 33.</b> Flow cytometry analysis results for expression of surface markers by hDPSCs for mesenchymal stem cells markers (CD44, CD 73, CD90, CD105), endothelial stem cells marker (CD31) and hematopoietic stem cells marker (CD45).....	130
<b>Figure 34.</b> Effect of extracts of BG-NPs prepared with different concentrations on the viability of DPSCs (n=4) 1, 3, and 7 days after incubation. Cell viability is given as relative cell viability where viability of untreated DPSCs was taken as 100%. ( $\alpha$ ,	

$\beta$ , and  $\gamma$ : denote the statistically highest groups among all BG compositions at day 1.  
 $\alpha$ : denotes the statistically highest group among all BG compositions at day 3.  $\alpha$ , and  
 $\beta$ : denote the statistically highest groups among all BG compositions at day 7,  
 $p < 0.05$ ).....134

**Figure 35.** (a) ALP activity and (b) intracellular calcium amounts of DPSCs cells treated with extracts obtained with 6.25 mg/ml in odontogenic differentiation medium (DMEM containing 10% FBS, 1% penicillin-streptomycin, 50  $\mu$ g/ml ascorbic acid, 10 mM  $\beta$ -glycerophosphate, and 10 nM dexamethasone) at different incubation periods (n=4). For ALP activity, # denotes the statistical difference between groups at week 2 and for intracellular calcium amounts, # denotes the statistical difference between group B21-BG and groups (without BG, and B0-BG) at week 1 ( $p < 0.05$ ).....136

**Figure 36.** Results of immunocytochemical staining of DPSCs incubated in medium containing 6.25 mg/ml BG extracts after 7 days, (a,b,c,d) [DSPP (green) and DAPI (blue) staining for group B0-BG, group B7-BG, group B14-BG, group B21-BG; (e, f, g, h) [Osteopontin (green) and DAPI (blue) staining for group B0-BG, group B7-BG, group B14-BG, group B21-BG; (i, j, k, l) [Collagen type I (green) and DAPI (blue) staining for group B0-BG, group B7-BG, group B14-BG, group B21-BG; (scale bar: 100  $\mu$ m).....139

**Figure 37.** Results of immunocytochemical staining of DPSCs incubated in medium containing 6.25 mg/ml BG extracts after 14 days, (a, b, c, d) [DSPP (green) and DAPI (blue) staining for group B0-BG, group B7-BG, group B14-BG, group B21-BG; (e, f, g, h) [Osteopontin (green) and DAPI (blue) staining for group B0-BG, group B7-BG, group B14-BG, group B21-BG; (i, j, k, l) [Collagen type I (green) and DAPI (blue) staining for group B0-BG, group B7-BG, group B14-BG, group B21-BG; (scale bar: 100  $\mu$ m).....140

**Figure 38.** Result of proliferation assay of hDPSCs cultured on scaffolds prepared by the TIPS/PL method with Alamar blue assay for 7 days (n=3).....142

**Figure 39.** SEM images of hDPSCs seeded on the scaffolds prepared by the TIPS/PL method: a) without BG, day 1; b) without BG, day 7; c) B0-10, day 1; d) B0-10, day 7; e) B0-20, day 1; f) B0-20, day 7 (scale bar: 50  $\mu\text{m}$ ).....143

**Figure 40.** Result of proliferation assay of hDPSCs cultured on scaffolds prepared by the FD/MMP method with Alamar blue assay for 7 days (n=3).....147

**Figure 41.** SEM images of hDPSCs seeded on the scaffolds prepared by the FD/MMP method a) without BG, day 1; b) without BG, day 7; c) B0-10, day 1; d) B0-10, day 7; e) B0-20, day 1; f) B0-20, day 7 (scale bar: 200  $\mu\text{m}$ , inserts: 20  $\mu\text{m}$ ), white arrows show cells.....148

**Figure 42.** ALP enzyme activity of hDPSCs seeded on scaffolds prepared by the (TIPS/PL) method (n=4). # designates the groups that are significantly different than groups (without BG, B0-10, and B21-10) at week 2 (p<0.05).....152

**Figure 43.** Intracellular calcium amounts of hDPSCs seeded on scaffolds prepared by the (TIPS/PL) method (n=4). # designates the groups that were significantly different than all groups at week 2 (p<0.05).....153

**Figure 44.** ALP enzyme activity of hDPSCs seeded on scaffolds prepared by the FD/MMP method (n=4). # designates the group significantly different than all groups (except B0-20, and B7-10) at week 2 (p<0.05).....155

**Figure 45.** Intracellular calcium amounts of hDPSCs that were seeded on scaffolds prepared by the FD/MMP method (n=4). # designates the group significantly different than all groups (except: B14-20) at week 2 (p<0.05).....156

**Figure 46.** Results of immunohistochemical staining of DPSCs seeded on the scaffolds prepared by the TIPS/PL method, [DSPP (green) and DAPI (blue)], a) without BG, day 14; b) without BG, day 21; c) B0-10, day 14; d) B0-10, day 21; e) B7-10, day 14; f) B7-10, day 21, (distance of stained sections from the scaffold surface was 150  $\mu\text{m}$ ) (scale bar: 20  $\mu\text{m}$ ).....159

**Figure 47.** Results of immunohistochemical staining of DPSCs seeded on the scaffolds prepared by the TIPS/PL method, [OPN (green) and DAPI (blue)], a) without BG, day 14; b) without BG, day 21; c) B0-10, day 14; d) B0-10, day 21; e)



B7-10, day 14; f) B7-10, day 21, distance of stained sections from the scaffold surface was 150 $\mu\text{m}$ ) (scale bar: 20 $\mu\text{m}$ ).....	161
<b>Figure 48.</b> Results of immunohistochemical staining of DPSCs seeded on the scaffolds prepared by the TIPS/PL method, [COLI (green) and DAPI (blue)], a) without BG, day 14; b) without BG, day 21; c) B0-10, day 14; d) B0-10, day 21; e) B7-10, day 14; f) B7-10, day 21 distance of stained sections from the scaffold surface was 150 $\mu\text{m}$ ) (scale bar: 20 $\mu\text{m}$ ).....	163
<b>Figure 49.</b> Results of Von Kossa staining of DPSCs seeded on the scaffolds prepared by the TIPS/PL method, a) without BG, day 14; b) without BG, day 21; c) B0-10, day 14; d) B0-10, day 21; e) B7-10, day 14; f) B7-10, day 21, distance of stained sections from the scaffold surface was 150 $\mu\text{m}$ ) (scale bar: 20 $\mu\text{m}$ ).....	165
<b>Figure 50.</b> Results of immunocytochemical staining of DPSCs seeded on the scaffolds prepared by the FD/MMP method [DSPP (green) and DAPI (blue)], a) without BG, day 14; b) without BG, day 21; c) B0-10, day 14; d) B0-10, day 21; e) B0-20, day 14; f) B0-20, day 21, distance of stained sections from the scaffold surface was 150 $\mu\text{m}$ ) (scale bar: 20 $\mu\text{m}$ ).....	169
<b>Figure 51.</b> Results of immunocytochemical staining of DPSCs seeded on the scaffolds prepared by the FD/MMP method [OPN (green) and DAPI (blue)], a) without BG, day 14; b) without BG, day 21; c) B0-10, day 14; d) B0-10, day 21; e) B0-20, day 14; f) B0-20, day 21, distance of stained sections from the scaffold surface was 150 $\mu\text{m}$ ) (scale bar: 20 $\mu\text{m}$ ).....	172
<b>Figure 52.</b> Results of immunocytochemical staining of DPSCs seeded on the scaffolds prepared by the FD/MMP method [COLI (green) and DAPI (blue)], a) without BG, day 14; b) without BG, day 21; c) B0-10, day 14; d) B0-10, day 21; e) B0-20, day 14; f) B0-20, day 21, distance of stained sections from the scaffold surface was 150 $\mu\text{m}$ ) (scale bar: 20 $\mu\text{m}$ ).....	175
<b>Figure 53.</b> Results of Von Kossa staining of DPSCs seeded on the scaffolds prepared by the FD/MMP method, a) without BG, day 7; b) without BG, day 14; c) B0-10,	

day 7; d) B0-10, day 14; e) B0-20, day 7; f) B0-20, day 14, (distance of stained sections from the scaffold surface was 150 $\mu\text{m}$ ) (scale bar: 20 $\mu\text{m}$ ).....	178
<b>Figure 54.</b> Calibration curve for ALP assay constructed with para-nitrophenol as standard.....	213
<b>Figure 55</b> Calibration curve of calcium using various $\text{CaCl}_2$ concentrations as standard (n=5).....	215
<b>Figure 56.</b> Calibration curve of DNA constructed with different concentrations of calf thymus DNA as standard for the determination of total DNA content in cell lysates in ALP assay (n=3).....	217

## LIST OF ABBREVIATIONS

Al: Aluminum

ALP: Alkaline Phosphatase

ANOVA: Analysis of Variance

BET: Brunauer–Emmett–Teller

BCA: Bicinchoninic Acid

BG: Bioglass

BG-NPs: Bioactive Glass Nanoparticles

BJH: Barret–Joyner–Halenda

BMP2: Bone Morphogenetic Protein 2

BMSCs: Bone Marrow-derived Mesenchymal Stem Cells

BP: Biopolymer

BSA: Bovine Serum Albumin

$\beta$  TCP: Beta Tricalcium Phosphate

CA: Cellulose Acetate

CMP: Carboxymethylpullulan

CS: Calcium Sulphate

DBM: Demineralized Bone Matrix

DEX: Dexamethasone

DFPCs: Dental Follicle Stem Cells

DMA: Dimetilasetamid

DMEM: Dulbecco's modified Eagle's medium

DMF: Dimethylformamid

DMSO: Dimethyl Sulphoxide

DMP1: Dentin Matrix Protein 1

DNA: Deoxyribonucleic Acid

DPP: Dentin Phosphoprotein

DPSCs: Dental Pulp Stem Cells

DSP: Dentin Sialoprotein

DSPP: Dentin Sialophosphoprotein

EB: Embryoid Body

ECM: Extracellular Matrix

EDC: 1-ethyl-3-(3-dimethylaminopropyl) carbodiimide

ESCs: Embryonic Stem Cells

FBS: Fetal Bovine Serum

FD/MMP: Freeze-Drying/Metal Mold Pressing

FTIR: Fourier Transform Infrared Spectroscopy

GEL: Gelatin

HA: Hydroxyapatite

HCA: Hydroxycarbonate Apatite

hDPSCs: Human Dental Pulp Stem Cells

HUVEC: Human Umbilical Vein Endothelial Cells

ICP-MS: Inductively Coupled Plasma Mass Spectrometry

ifhU-iPSCs: Integration-free Human Urine Induced Pluripotent Stem Cells

iPSCs: Induced Pluripotent Stem Cells

JBMSCs: Jaw Bone Mesenchymal Stem Cells

Li: Lithium

MBNs-NH<sub>2</sub>: Aminated Mesoporous Bioactive Nanoparticles

MDF: Mouse Dental Follicle

MEPE: Matrix Extracellular Phosphoglycoprotein

Mg: Magnesium

MSCs: Mesenchymal Stem Cells

MTT: 3-(4,5-dimethylthiazol-2-yl)-2,5-diphenyltetrazolium bromide

MW: Molecular Weight

NBG: Nano Bioactive Glass

NBG-NPs: Nano Bioactive Glass Nanoparticles

NBO: Non-bridging Oxygen

NF: Nanofibrous

NHS: N-hydroxysuccinimide

NMMO: N-methylmorpholine-N-oxide

PBS: Phosphate Buffered Saline

PCL: Polycaprolactone

PD: Population Doublings

PDL: Periodontal Ligament

PDLSCs: Periodontal Ligament Stem Cells

PEG: Poly Ethylene Glycol

PHB: Poly (Hydroxybutyrate)

PGA: Poly Glycolic Acid

PLGA: Poly Glycolic Poly Lactic Acid

PLLA: Poly-L-lactic Acid

PNIPAAm: Peptide- poly(N-isopropylacrylamide)

pNPP: p-nitrophenyl phosphate

PRF: Platelet-rich Fibrin

PULL: Pullulan

rhVEGF<sub>165</sub>: Recombinant Vascular Endothelial Growth Factor

RT: Room temperature

SEM: Scanning Electron Microscopy

SBF: Simulated Body Fluid

SCAPs: Stem Cells from the Apical Papilla

SHED: Stem Cells from Human Exfoliated Deciduous Teeth

STAT3: Signal Transducer and Activator of Transcription 3

STMP: Sodium Trimetaphosphate

TBDC: Teicoplanin-loaded Borate Bioactive Glass

TDM: Treated Dentin Matrix

TEOS: Tetra Ethyl Ortho Silicate

TEP: Triethyl Phosphate

TIPS/PL: Thermally Induced Phase Separation/Porogen Leaching

VEGF: Vascular Endothelial Growth Factor

VEGFR1: Vascular Endothelial Growth Factor Receptor 1

WA: Water Absorption

XRD: X-ray Diffraction





## **CHAPTER 1**

### **INTRODUCTION**

Dental caries is the most common health disorder after common cold disease. Dental caries is a transmissible bacterial disease process. The bacteria causing caries, use fermentable carbohydrates in the mouth and form organic acids. As a result of diffusion of acids into pores of tooth mineral parts and dissolving them, demineralization occurs. Demineralization starts in the enamel layer and goes to the dentin layer when not treated. Enamel and dentin are mineralized tissues of the tooth being affected (Featherstone, 2008). Caries progress more quickly in the dentin layer, which is less resistant to caries than enamel (Wolff & Larson, 2009).

Dentin is similar to bone tissue in terms of composition and structure. Dentin is formed by odontoblasts which are arranged as a layer of cells lining the pulpal surface of dentin through a life-long process (Arana-Chavez & Massa, 2004). In the structure of the dentin, the odontoblastic extensions are found in a highly mineralized fluid. The dentinal tubules are well aligned and parallel to each other and divide into branches that are narrower. The anatomy of the tooth, and SEM image of natural dentinal tubules are shown in Figure 1.

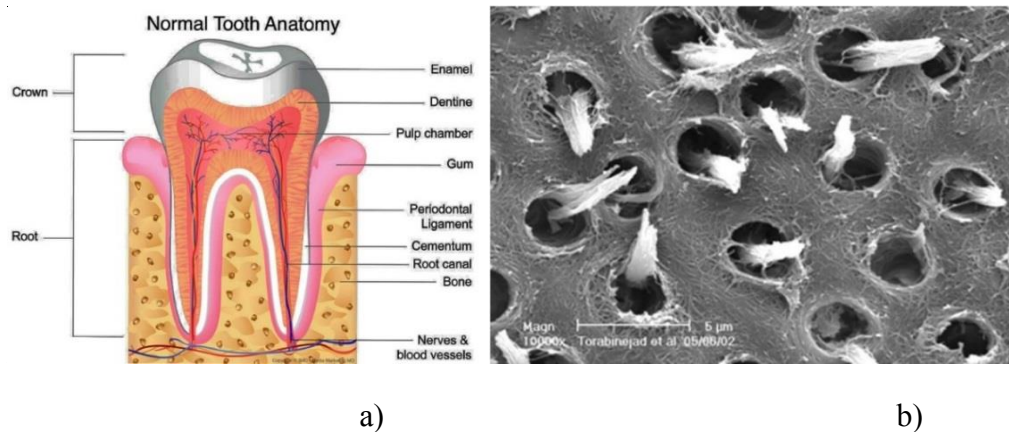


**Figure 1.** (a) Anatomy of tooth (Boling, 2017); (b) SEM image of natural dentinal tubules with odontoblasts processes (Torabinejad, 2015).

## 1.1. Strategies for Tooth Regeneration

There are two strategies in tooth tissue engineering: 1- entire tooth regeneration, 2- regeneration of different parts of tooth (enamel, dentin, pulp, cementum, periodontal ligament and alveolar bone) (Sharma et al., 2014).

### 1.1.1. Selection of Biomaterials for Dental Tissue Engineering

Biomaterials for preparation of scaffolds could be natural/synthetic. Examples of natural biomaterials used in dental tissue engineering are: 1- proteins like collagen (Prescott et al., 2008), and silk (Zhang et al., 2011), 2- polysaccharides like chitosan (Boynueğri et al., 2009), hyaluronic acid (Inuyama et al., 2010), alginate (Srinivasan et al., 2012). Synthetic biomaterials used in dental tissue engineering include organic polymers like poly glycolic acid (PGA) (Tonomura et al., 2010), and polycaprolactone (PCL) (Park et al., 2010) or inorganic calcium phosphate materials

like hydroxyapatite (HA) (Teti et al., 2015) or beta tricalcium phosphate ( $\beta$  TCP) (Gala-Garcia et al., 2010) and glass ceramics like niobium doped fluorapatite glass ceramic (Kushwaha et al., 2012).

#### **1.1.1.1. Bioactive Glasses**

Glasses are silica based materials (Laczka et al., 2000). Glass ceramics are glasses containing Lithium/Aluminum (Li/Al) or Magnesium/Aluminum (Mg/Al) crystals. In bioglasses, some of the silica groups have been replaced by calcium, phosphorus, or sodium ( $\text{SiO}_2$ ,  $\text{Na}_2\text{O}$ ,  $\text{CaO}$ ,  $\text{P}_2\text{O}_5$ ). Calcium and phosphate ions released from the glass, together with those present in the solution, form a calcium phosphate rich layer on the surface of the biomaterial in contact with body fluids.  $\text{Na}^+$  leaches quickly and  $\text{Ca}^{2+}$ ,  $\text{PO}_4^{3-}$ , and  $\text{Si}^{4+}$  dissolve congruently at the glass surface. A polycondensated silica-rich layer then forms on the glass bulk resulting in calcium phosphate (Ca/P) layer deposits on outer surface (Hench & Wilson, 1993). This phosphate is initially amorphous and then crystallizes into hydroxycarbonate apatite (HCA) layer by addition of carbonate ions from the solution. These bioglasses are highly bioactive and chemical bonding occurs between the tissue and the implant (Nandi et al., 2011). However, when compared to high-density (cortical) bone, medical applications of bioactive glass are limited to low load-bearing areas due to their low fracture toughness (Kükürtcü, 2015). Most important features of bioactive glasses are; to support the formation of three-dimensional vascular structures, to help differentiate mesenchymal cells in bone tissue and to bind to bone tissue with organic bonds (Abbasi et al., 2015). In other words, bioactive glasses promote both osteoconductivity and osteointegration (Kumar, 2009). When bone is able to grow on the surface of a biomaterial, that material is so called osteoconductive material and bone growth occurs on its surface or down into its pores, channels or pipes (Albrektsson & Johansson, 2001). Osseointegration means a direct structural and functional contact between ordered, living bone and surface of the implant (Anil et

al., 2011). Bioglass<sup>®</sup> particulates, of equivalent size in two compositions (with and without fluoride) have been tested for restoration of osseous tissues in treatment of periodontal disease in a monkey model. Both alveolar bone and periodontal ligament were restored as a result of osteoconductivity of this material (Wilson & Low, 1992). In one study, gradient coatings composed of bioactive glass and nanohydroxyapatite (BG-nHA) on titanium-alloy orthopaedic implants were tested in vivo. Histological and histomorphometric studies revealed enhancement of implant osteointegration. They observed that bone formation was facilitated and bone absorption around the materials was delayed (Xie et al., 2010).

**Table 1.** Different compositions of bioactive glasses (Abbasi et al., 2015).

Bioactive glasse	Composition (%mol)
45S5 (Bioglass <sup>®</sup> )	46.1% SiO <sub>2</sub> , 24.4% Na <sub>2</sub> O, 26.9% CaO ve 2.6% P <sub>2</sub> O <sub>5</sub>
58S (Synthesized by the sol-gel method)	60% SiO <sub>2</sub> , 36% CaO ve 4% P <sub>2</sub> O <sub>5</sub>
70S30C	70% SiO <sub>2</sub> , 30% CaO.
S53P4	53% SiO <sub>2</sub> , 23% Na <sub>2</sub> O, 20% CaO ve 4% P <sub>2</sub> O <sub>5</sub>

**Table 2.** Different commercial brands of bioactive glass (Montazerian & Dutra Zanotto, 2016, Kumar et al., 2015).

Brand name	Application
PerioGlas®	Dental bone grafting
Bio-Oss®	Dental bone grafting
Cerabone®	Dental bone grafting
UltraDEX®	Treatment of dentin hypersensitivity & repair of dental caries
Biosilicate®	Regeneration bone tissue & treatment of dental hypersensitivity
NovaMin®	Dentistry (remineralization)
NovaBone®	Bone graft substitute (orthopedic & facial reconstruction)
NovaBone-C/M®	Bone graft substitute (orthopedic & facial reconstruction)
Bioverit® I & II	Bone substitution (head & neck surgery)
Activioss™	Bone substitution (oral surgery)
Bioglass® 45S5	Bone substitution

#### **1.1.1.1.1. Methods for Bioactive Glass Synthesis**

Bioactive glasses are synthesized by the conventional melting method (Lombardi et al., 2013) and sol-gel method (Fadzli et al., 2016). When using the melting method, the source of  $\text{SiO}_2$  is sand,  $\text{Na}_2\text{O}$  and  $\text{CaO}$  are obtained from carbonate compounds.  $\text{P}_2\text{O}_5$  is added as an oxide before melting the glass. The bioactive glass batch is melted in a Pt-Rh pot at 1350-1400°C and after homogenization, the melt is poured into the mold. Bioactive glass prepared by the melting method is dense and does not contain any organic compounds or water. Therefore, when used as an implant, contact surface area with tissue fluids is limited. Bioactive glasses synthesized by this method are in the micro-size range (Ducheyne et al., 2011).

The standard bioactive glass formula is commonly known as 45S5 and is synthesized by conventional melting method at high temperatures (1300 - 1500°C). Composition of this glass is: 45%  $\text{SiO}_2$ , 24.5%  $\text{Na}_2\text{O}$  and  $\text{CaO}$  and 6%  $\text{P}_2\text{O}_5$  (wt. %). When the material is modified, the  $\text{SiO}_2$  component is varied while the  $\text{P}_2\text{O}_5$  component is kept constant. Keeping the silica ratio below 60% by weight and keeping the  $\text{CaO}/\text{P}_2\text{O}_5$  ratio high during the production of the material ensures that the material has a highly reactive surface (Gerhardt & Boccaccini, 2010).

Sol-gel technique is another method for synthesis of bioactive glasses. This method differs from the conventional melting method in a way that bioactive glass is obtained from solution at room temperature, instead of melting at high temperature. For this reason, it is also defined as the cold method. The sol-gel method generally consists of the following steps: 1- Hydrolysis of the precursor, 2- Alcohol or water condensation 3- Gelation, 4- Aging, 5- Drying, 6- High temperature treatment. The starting materials are generally alkoxides and metal salts. As a result of hydrolysis and condensation reactions in the solutions prepared by mixing with water, acid or alcohol, formation of gel occurs. Then, the gels are converted to bioactive glass by heat treatment (600 - 700°C) (Vichery & Nedelec, 2016). This takes place in the

calcination step during which unwanted components left from the hydrolysis and condensation reactions are removed and gel stabilizes chemically. Environmental stability and bioactivity are also obtained as a result of this step. Usually 600°C is used as the calcination temperature for bioactive glasses and it is known that minimum stabilization temperature is needed in order to have maximum bioactivity (Jones et al., 2006, M. Mukundan et al., 2013).

Bioactive glasses were first synthesized in micron and then in nano size range. Micron sized bioactive glasses were first obtained when using the conventional melting method. Prof. L. L. Hench synthesized the first bioactive glass (Bioglass®) at the University of Florida in 1969 (Hench, 2006). Both micron and nano-sized bioactive glass particles are considered for clinical applications. By reducing the size of the bioactive glass particles to nanoscale during the synthesis process, it is aimed to increase the reactivity of the particles. By reducing the particle size of bioactive glasses to nano levels, the performance of the material is improved and the material gains new application areas like hard tissue (bones, teeth) regeneration and repair, soft tissue regeneration, wound healing and drug delivery. Both faster ion release and higher protein adsorption from the surface of the glass particles are achieved, thereby increasing the bioactivity (Kumar, 2009, Vichery & Nedelec, 2016).

#### **1.1.1.1.2. Application of Bioactive Glass in Tissue Engineering**

In recent years, there is an increase in the number of publications on bioactive glass nanoparticle based nanobiocomposites, for engineering of different hard and soft tissues (Srinivasan et al., 2012, Hafezi et al., 2012, Zhang et al., 2016, Murphy et al., 2017). Sowmya et al. (2011) prepared a nanobiocomposite scaffold composed of  $\beta$ -chitin hydrogel and nanobioglass for periodontal bone regeneration. Biocompatibility of nanocomposite scaffolds was assessed by in vitro cytotoxicity assays with human osteosarcoma (MG63) and human primary osteoblast (POB) cells. Better results were

obtained for porosity, swelling, bioactivity and degradation tests comparing to the control group. The composite scaffolds showed no toxicity on (MG63) and (POB) cells and also attachment, spreading and proliferation of the cells were enhanced. The group reported that the nanocomposite scaffolds showed favorable porosity and biocompatibility for regeneration of periodontal bone defects and also could be used as a coating layer in dental implants (Sowmya et al., 2011).

In previous studies on bioglass conducted in Turkey, micro- and nano-sized bioglasses have been used in the treatment of bone tissue disorders. Sakallioğlu et al. (2006) evaluated the effectiveness of bioactive-glass alloplastic bone grafts for reconstruction of interproximal component bone defects and demonstrated that using bioglass could yield successful results in terms of new periodontal tissue formation (Sakallioğlu et al., 2006). Ceyhan et al. (2007) prepared a bioglass-ceramic by the sol-gel method, with the composition of  $30\text{SiO}_2\text{-}17\text{MgO-}53\text{Ca}_3(\text{PO}_4)_2$ . For in vitro tests, phase analysis of samples was done by XRD after their immersion in simulated body fluid (SBF) for 10, 30, and 40 days. After 30, and 40 days, peaks related to hydroxyapatite crystals at the 2<sup>nd</sup> and 3<sup>rd</sup> degree phases were observed. This is because of exchange of Ca, P elements on the particule surfaces which is indicative of surface reactivity of the prepared glass-ceramic. For in vivo tests, samples were histologically assessed after 4, 6, and 8 weeks of placement in tibial metaphyses of Sprague-Dawley rats. After 8 weeks, glass-ceramic material had been converted completely to lamellar bone tissue. Full osteointegration was observed because of continuous increase in size of osteoid tissue without presence of any fibrous tissue in between. The results indicated that the prepared material was suitable for bone substitute applications (Ceyhan et al., 2007).

Erdemli et al. (2010) investigated the effect of demineralized bone matrix (DBM) or calcium sulphate (CS) addition to polycaprolactone/bioglass (PCL/BG) bone implants in vitro and in vivo. In this study PerioGlas<sup>®</sup> with composition of 45%  $\text{SiO}_2$ , 24.5%  $\text{CaO}$ , 24.5%  $\text{NaO}_2$ , and 6%  $\text{P}_2\text{O}_5$  was used. According to in vitro bioactivity test results, crystal structures were observed on discs of three groups



(PCL/BG, PCL/BG/CS and PCL/ BG/DBM) and Ca/P ratio was 1.42 in PCL/BG/CS and 1.53 in PCL/ BG/DBM group which was closer to that of hydroxy- carbonate apatite crystals. Water uptake increased in groups containing fillers. PCL/BG/DBM group showed significantly higher water uptake and the highest weight loss. All experimental groups were found cytocompatible. Addition of fillers (BG, DBM, CS) caused an increase in the initial mechanical properties of the implants. In vivo tests were performed on defects created in the rabbit humeri. Histological analysis revealed osteoblastic activity in PCL/BG implants at the bone-implant interface owing to osteoconductive property of BG. DBM addition facilitated bone formation around and into implant and CS enhanced formation of cartilage tissue around the implant. In general, enhanced bone ingrowth and new bone formation at the interface were observed in all groups (Erdemli et al., 2010).

The effect of incorporation of different ions to composition of BGs has been evaluated (Nandi et al., 2016b). In researches aiming to regenerate dental tissues, boron containing bioactive glass has not been used till today. The reason for use of boron modified bioactive glass in tissue engineering relies on its distinguished biological properties like stimulating release of growth factors and cytokines, and increase of the extracellular matrix turnover. Dzondo-Gadet and co-workers tested the effect of boric acid on release of growth factors at the molecular level. VEGF and TGF $\beta$  (factors effective in angiogenesis - wound healing) were detected, but FGF1 and TNF $\alpha$  were not observed. Therefore, local treatment with boron, in vivo, on cicatrization (scar formation at the site of a healing wound) was suggested. (Dzondo-Gadet et al., 2002). Role of boron in bone physiology has been shown. Boron influences composition and physical characteristics of bone by altering hormones effective in bone growth. Nielsen (2004) evaluated the effect of dietary boron, oil and gender on bone shape and strength, and plasma lipid and glutathione concentrations in rats. Female and male rats received diets with supplemental boron and canola oil (low in  $\alpha$ -linolenic acid) or palm oil (high in  $\alpha$ -linolenic acid). Femur strength, tibial boron, calcium, phosphorus, zinc and potassium concentrations; and plasma alkaline phosphatase increased as a result of presence of boron in diet.

Replacing canola oil with palm oil caused decrease of plasma cholesterol in male rats receiving boron. The same trend was seen about plasma triglycerides. In total, synergic effect of boron and a diet high in  $\alpha$ -linolenic acid on bone formation was shown which also was influenced by gender (Nielsen, 2004).

Boron can prevent some chronic bone illnesses by increasing the secretion of some steroid hormones, (Hunt, 1998). According to the researches, the increase of boron in the diet leads to increase of estrogen, testosterone and plasma ionized calcium concentrations, and decrease of calcium urinary excretion (Nielsen, 1994). It also alleviates problems caused by deficiency of vitamin D and magnesium (Pizzorno, 2015). All of these factors are responsible for the increase of bone mineral density in humans in an effective manner, especially in postmenopausal women (Devirian & Volpe, 2003).

Over the past years, borate and borosilicate bioglasses with different compositions have been developed and evaluated for biomedical applications. In one study, it was shown that substitution of  $B_2O_3$  with  $SiO_2$  in the 45S5 glass enhanced the degradation of the 45S5 bioglass and its conversion to hydroxyapatite in the phosphate solution. Full conversion of borate glass took less than 4 days, but silicate (45S5) and borosilicate compositions did not convert completely even after 70 days (Huang et al., 2006). In the same year, in the study conducted by Gorustovich et al., melt-derived glasses with two compositions as: a base 45S5 bioactive glass and 2% wt boron oxide modified 45S5 (45S5.2B) were prepared and implanted into the intramedullary canal of rat tibiae. According to histological and histomorphometric analyses, significantly larger area of neoformed bone tissue around the 45S5.2B particles was observed 15 days after surgery, while there was no significant difference for two compositions (45S5, 45S5.2B) after 30 days of implantation. At all time-points, osseointegrated tissue on 45S5.2B BG particles had significantly higher thickness. It was concluded that the boron-modified 45S5 bioglass promoted the formation of new bone tissue more than the standard 45S5 bioactive glass (Gorustovich et al., 2006).

Zhang et al. (2010) tested efficiency of pellets composed of a chitosan-bonded mixture of borate bioactive glass (mol%: 6 Na<sub>2</sub>O, 8 K<sub>2</sub>O, 8 MgO, 22 CaO, 54 B<sub>2</sub>O<sub>3</sub>, 2 P<sub>2</sub>O<sub>5</sub>) and teicoplanin powder for treatment of chronic osteomyelitis in vitro and in vivo results. The group reported a sustained release of teicoplanin for about 30 days and formation of hydroxyapatite after 7 days in PBS at 37 °C. When the pellets were implanted in a rabbit tibia osteomyelitis model, teicoplanin was detected in the blood for about 9 days. 12 weeks post-implantation, new bone was formed as a result of complete conversion of implants to HA graft. According to microbiological, histological and SEM results, osteomyelitis was cured completely. As a result of microbiological tests, teicoplanin-loaded borate bioactive glass (TBDC) treated animals showed 86% negativity for MRSA infection in comparison to 43% negativity in animals receiving intravenous injection of teicoplanin. Transmitted light images of H&E stained sections of group with TBDC pellets implantation, showed no infection or fibrosis. SEM images of the surfaces of the implanted TBDC pellets revealed good connection of converted implant to the old bone. Consistent with other studies, it has been shown that boron enhances biodegradation and conversion of bioactive glass to hydroxyapatite and does not cause toxic effects (Zhang et al., 2010).

## **1.2. Tissue Engineering Approaches for the Regeneration of Dentin-Pulp Complex**

There are several studies in the literature about the repair and/or reconstruction of dentin-pulp complex with tissue engineering approach. Several methods have been implemented for induction of odontogenic differentiation or regeneration of dentin, dental pulp or dentin-pulp complex. Examples for polymeric scaffolds are: thermally induced phase separation/porogen leaching (TIPS/PL) (Qu et al., 2015), solvent casting/particulate leaching technique (El-Backly et al., 2008), gas foaming/particulate leaching process (Huang et al., 2009), for bioceramic scaffolds:

wet precipitation method (AbdulQader et al., 2013), for nanocomposite scaffolds: dual-phase mixing method (Gala-Garcia et al., 2010), fiber- templating method (Vallés Lluch et al., 2009), electrospinning method (Bae et al., 2012) and for hydrogels: demineralization and decellularization (Paduano et al., 2016). In one study, magnetic nanocomposite scaffolds composed of magnetic nanoparticles (MNPS) and polycaprolactone (PCL) were prepared and tested for adhesion, growth, migration and odontogenic differentiation of human dental pulp cells (hDPCs). The magnetic nanocomposite scaffolds were proposed as candidates for dentin-pulp tissue engineering because of supporting migration, adhesion, and odontogenic differentiation of hDPCs (Yun et al., 2015). In another research, odontogenic differentiation of DPSCs on collagen I (Col-I) scaffolds and hydrogel scaffolds made of bone extracellular matrix (bECM) was compared. Bovine bone was demineralized and decellularized for preparation of bECM hydrogels. It was reported that bECM hydrogel scaffolds provided better conditions for odontogenic differentiation of DPSCs than Col-I hydrogel scaffolds and found suitable for dentin-pulp regeneration (Paduano et al., 2016).

In one study, hDPSCs and human periodontal ligament stem cells were seeded on a decellularized 3D extracellular matrix (ECM) and, odontogenic differentiation of the stem cells was achieved without using growth factors. In vivo studies were performed by subcutaneous implantation of scaffolds in male nude mice. Fluorescent images of H&E stained sections revealed neovascularization in the scaffolds. Alizarin Red staining showed enhancement of extracellular calcium deposition in the scaffolds. Immunohistochemical analysis revealed a slight increase in the expression of dentin matrix protein 1 (DMP1) and distinct increase in the expression of dentin sialoprotein (DSP) and dentin phosphoprotein (DPP) were observed in the ECM scaffolds as a result of (Ravindran et al., 2013). Qu et al. (2015) prepared 3D nanofibrous (NF)-gelatin scaffolds by (TIPS/PL) method and investigated the effect of the stiffness of the scaffold on the regeneration of the dental pulp-dentin complex. Crosslinking duration affected mechanical strength of the scaffolds and according to that, they were classified into low, medium and high stiffness groups. In vitro cell

culture studies showed that attachment and spread of DPSCs on scaffolds were enhanced on high-stiffness (NF-gelatin) scaffolds. Von Kossa staining results showed that more and evenly distributed mineral deposition occurred in the high-stiffness scaffolds and stem cells seeded on these scaffolds expressed marker genes for odontogenic differentiation more compared to other scaffold groups. These results showed that DPSCs differentiated into odontoblasts on the 3D NF-gelatin scaffolds with high stiffness and formed mineralized tissue while pulp-like tissue regeneration was provided on scaffolds with low stiffness. This group also developed a single scaffold comprising both low and high-stiffness NF-gelatin for pulp-dentin complex regeneration. According to differentiation studies, mineralization was observed in the peripheral (high-stiffness) area, which caused formation of a ring-like structure. After subcutaneous implantation of the DPSC/S-scaffold in nude mice highly mineralized dentin was observed in the periphery the construct and also formation of blood vessels in the center of construct was observed. Immunohistochemical analysis revealed expression of DSPP as the dentin-specific marker of odontoblasts, in the peripheral area. As a result, it was concluded that complete regeneration of pulp-dentin complex was achieved in vitro and in vivo (Qu et al., 2015). Lu et al. (2015) investigated the use of injectable PEG-fibrinogen hydrogels as scaffolds for DPSCs for tooth pulp tissue engineering purposes. It has been reported that 3D microenvironment of PF-hydrogels triggered the differentiation of human DPSC cells and these cells mineralized the scaffolds according to results of alizarin red staining and calcium quantitative assay. The group concluded these scaffolds could be useful for regenerative endodontic applications (Lu et al., 2015).

For restoration and regeneration of dental mineralized tissues, composites and nanobiocomposites incorporating bioceramics and different polymers are used. In 2009, Gala-Garcia and colleagues prepared a composite material containing beta-tricalcium phosphate-hydroxyapatite or calcium hydroxide as bioceramics and PLGA (poly-glycolic-poly-lactic acid) as a polymer) by the dual-phase mixing method for dental pulp repair. This study was successful in reorganizing the dentin-pulp

complex (Gala-Garcia et al., 2010). Abdul Qader et al. (2013) developed a biphasic calcium phosphate scaffold by the wet precipitation method for dentin regeneration. In this study, hydroxyapatite/beta-tricalcium phosphate was used as the bioceramic. These scaffolds possessed 65% total porosity and spherical macro pores of 300  $\mu\text{m}$  size. Meanwhile, microporous structure of the scaffold was preserved. Micropores were useful for the flow of nutrients and presence of macropores enhanced the arrangement of dental pulp stem cells and their differentiation (AbdulQader et al., 2013). Teti et al. (2015) prepared a hybrid hydrogel of carboxymethyl cellulose-hydroxyapatite for investigating its potential for inducing osteogenic and odontogenic differentiation of dental pulp cells (DPSCs). In vitro osteogenic and odontogenic differentiation of DPSCs was in the presence of hybrid hydrogel reported by the group. DPSCs seeded hydrogels were shown to be suitable for dentin-pulp complex regeneration and periodontal tissue engineering (Teti et al., 2015).

In another study, researchers developed a nanocomposite scaffold by fiber-templating method using poly (ethyl methacrylate-co-hydroxyethyl acrylate) [P (EMAcO- HEA)] and  $\text{SiO}_2$  for the regeneration of dentin layer of the tooth. For organic phase formation,  $\text{SiO}_2$  was obtained by sol-gel method using tetra ethyl ortho silicate (TEOS). SEM images of the scaffolds revealed their resemblance to natural dentin. According to IR spectroscopy results, presence of silica at the surfaces of the hybrids was confirmed. Different silica contents didnot have distinct effect on porosity of the hybrids. Hybrid scaffolds with percentages of silica above 10 wt % enhanced the mechanical properties and positively affected precipitation of apatite on surfaces of the scaffolds. According to the results, prepared nanohybrids could be used for dentin regeneration (Vallés Lluch et al., 2009).

In literature nano-bioactive glasses used for regeneration of dentin and other mineral structures of the tooth, are now remarked as a new generation biomaterial with favorable properties like anti-inflammatory and pro-angiogenic (Gerhardt et al., 2011, Haro Durand et al., 2017, Chandrasekar et al., 2015). Vollenweider et al.

(2007) compared the effect of 45S5 bioactive glasses on micro- and nano-scale on remineralization of the dentin layer under in vitro conditions. This study showed that nanoscale bioactive glass provides faster remineralization (Vollenweider et al., 2007). Bae et al. (2012) prepared a nanocomposite scaffold containing collagen (Col) and (BG-NPs) by the electrospinning method for dentin-pulp regeneration and evaluated cellular responses of human dental pulp cells (hDPSCs) to the scaffold regarding their proliferation and odontogenic differentiation. It was observed that the nanocomposite Col/nBG matrix was more efficient for promoting growth and odontogenic differentiation of hDPCs than Col matrix and was considered suitable for dentin-pulp complex regeneration (Bae et al., 2012). In one study, zinc phosphate bioglass (ZnBG) was added to phosphate cements (CPC,  $\alpha$ -tricalcium phosphate-based) and cellular responses of dental pulp stem cells (DPSCs) to this biomaterial was assessed in terms of odontogenic differentiation and angiogenesis. Incorporation of Zn-BGN was shown to be considerably effective for the in vitro odontogenic differentiation and angiogenesis and therefore the composite cements are candidates to be used in regenerative endodontics (Zhang et al., 2015). Lim et al. (2016) studied the odontogenic differentiation of dental pulp stem cells (DPSCs) cultured on dexamethasone (DEX) loaded nanofiber matrices composed of BG-NPs, gelatin and polycaprolactone (PCL). DEX was added because of its stimulatory effect on odontogenic differentiation of (DPSCs). There were three experimental groups (only polymers, BG incorporated, BG-DEX incorporated). According to cell culture results, viability and proliferation of HDPCs on DEX-releasing BGN matrices increased. Results of tests for alkaline phosphatase activity, mRNA expression of genes, and mineralization, were also favorable for this group. Mechanistic study on signaling pathways revealed integrins, bone morphogenetic protein, and mTOR signaling pathways, as the possible molecular mechanisms were involved in odontoblastic differentiation of HDPCs. In total, the prepared nanofiber matrices were shown to induce differentiation of DPSCs and have been proposed for regeneration of dentin–pulp complex (Lim et al., 2016).

## **1.2.1. Biomaterials Used for Preparation of the Scaffolds in This Study**

### **1.2.1.1. Cellulose**

Cellulose is the most abundant polymer in nature. Cellulose and its derivatives are preferred for tissue engineering applications due to their high biocompatibility and tensile strength (Ko et al, 2010). Cellulose is degraded by microbial or fungal enzymes in nature by breakage of glycosidic bonds. The lack of these enzymes in animals and humans limits the biodegradability of cellulose and its derivatives (Helenius et al., 2006). Cellulose acetate (CA) is one of the most important derivatives of cellulose and has been used for engineering of soft tissues like nerve (Du et al., 2014), skin (Atila et al., 2015) and heart (Chainoglou et al., 2016) and also hard tissue like bone (Petrauskaite et al., 2016).

The reasons for widespread use of cellulose acetate in medical applications are its good mechanical properties, low toxicity, good hydrolytic stability, cost-efficient and eco-friendly properties (Li et al., 2012). Gouma et al. (2012) prepared a nano-hydroxyapatite and cellulose acetate nanocomposite as a cell scaffold by electrospinning technique for bone tissue engineering application. Cell culture studies showed that the developed scaffold had a positive effect on attachment and differentiation of SaOS-2 cells (Gouma et al., 2012). Lee et al. (2015) prepared cellulose acetate/nano-hydroxyapatite (nHAP) composite fibers by electrospinning with different amounts of nHAP and cross-linked them by using acetone and benzyl alcohol as the solvent. According to the results, solvent composition affected the structural properties of the fibers and cross-linked structures with nHAP content less than 40 vol. % were preserved. It was also shown that mechanical properties of the prepared fibrous scaffold could be controlled by altering its nHAP content. With increase of HAP, tensile strength and ultimate strain decreased, but elastic modulus increased (Lee et al., 2015). In another study, nanofibrous scaffolds of poly (hydroxybutyrate) (PHB)/cellulose acetate were prepared by the electrospinning



method. According to SEM results, scaffolds possessed well interconnected porous fibrous structure. Weight ratio of PHB/CA determined the mechanical properties and biodegradability of the blend nanofiber scaffolds which was much higher than PHB scaffolds. 3T3 fibroblast cells that were seeded on the blend scaffold, adhered and proliferated well after 48 hours of incubation. According to the mentioned results which confirms bioactivity and biocompatibility of PHB/CA blend scaffolds, they were suitable for wound dressing or tissue engineering applications (Zhijiang et al., 2016).

Atila et al. (2016) prepared a 3D fibrous network from pullulan and cellulose acetate by the wet electrospinning method and crosslinked it with trisodium trimetaphosphate (STMP) in order to improve mechanical properties and reduce weight loss. Because of presence of more uniform fibers in P50/CA50 group, its cross-linking was more successful and showed the least weight loss among groups. Its mechanical properties were improved as a result of cross-linking. This group also possessed more uniform pores, that's why it was used for further studies. After immersion in SBF, apatite-like structures were formed on the fibers and cytocompatibility results using SaOS-2 cells were acceptable in terms of adhesion, proliferation and differentiation. It was suggested that crosslinked P50/CA50 scaffolds could be used for bone tissue engineering applications (Atila et al., 2016).

#### **1.2.1.2. Pullulan**

Pullulan (PULL), is a neutral polysaccharide produced extracellularly by a yeast-like fungus *Aureobasidium pullulans* (Singh et al., 2008). This biopolymer is economically important with increasing applications in the food, pharmaceutical, agriculture and chemical sectors. As it is non-toxic, non-mutagenic and non-immunogenic and biocompatible, this polymer has different applications in the

biomedical field (tissue engineering, targeted drug and gene delivery, bio-imaging) (Mishra et al., 2011). Figure 2 shows the chemical structure of PULL.

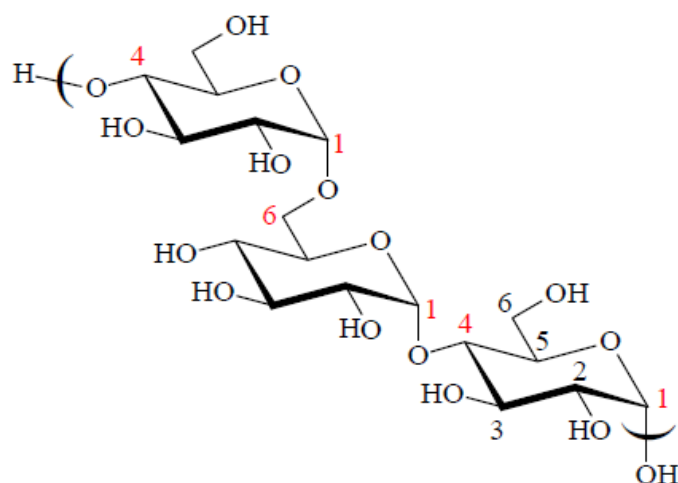


**Figure 2.** Chemical structure of PULL (Pereira, 2013).

The regular exchange of  $\alpha$  (1  $\rightarrow$  4) and  $\alpha$  (1  $\rightarrow$  6) bonds causes PULL to be easily soluble and structurally flexible (Shingel, 2004). Pullulan has high water solubility. Derivatives of PULL with low-solubility or no-solubility in water have been obtained and used for different purposes (Rekha & Sharma, 2007). As an example, carbonated PULL was proposed to be useful for drug delivery applications (Bruneel & Schacht, 1993), and carboxymethylpullulan (CMP) hydrogel was prepared as a wound dressing material (Li et al., 2011a). In the study by Li and colleagues, they prepared hydrogels by cross-linking CMP different diamines and dihydrazides. When cystamine was used as the cross-linker, mechanical properties of the hydrogels was improved. Gentamycin was loaded into hydrogels prepared with different cystamine–CMP ratios. Release of the drug was very fast during the first 2h, gradual till 40 h and release then slowed down. In this study they also showed that hydrogels with less cross-linking degree released the drug more. According to the results, good

swelling capacity, high water absorption and quick water absorption velocity, good mechanical strength were achieved.

There is a need for cross-linking of PULL in order to protect structural integrity of the three-dimensional scaffolds composed of this polymer. Mechanism of cross-linking of PULL with sodium trimetaphosphate (STMP) is shown in Figure 3. In the first step, alkoxides in strong alkaline media react with phosphate groups which causes cyclic structure of STMP to open and as a result of this reaction a tripolyphosphated polymer is obtained. In the second step, due to adding a new polymer chain, cross-linking of the polymer is achieved and as a result of the cross-linking reaction, formation of pyrophosphate links occurs. After reaction between STMP and PULL, different PULL-phosphates are obtained (Dulong et al., 2011).

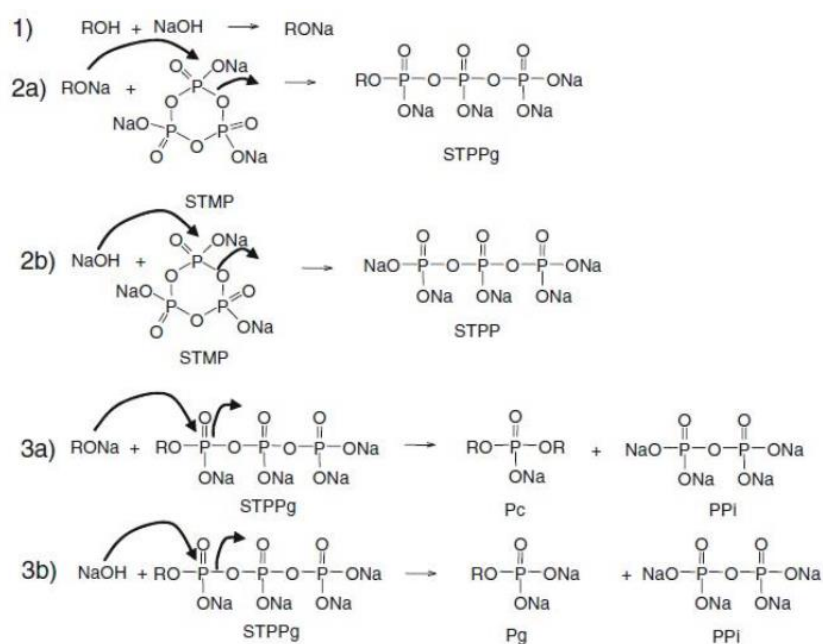


**Figure 3.** Mechanism of cross-linking of PULL with sodium trimetaphosphate (STMP) (Dulong et al., 2011).

Mechanism of cross-linking of ox-PULL/GEL by glutaraldehyde is shown in Figure 4. In ox-PULL, C=O groups are present. GTA is reactive to the NH<sub>2</sub> groups of the proteins ( $\epsilon$ -amino group of lysine) and can be dissolved in aqueous media to form stable covalent bonds (Migneault et al., 2004).

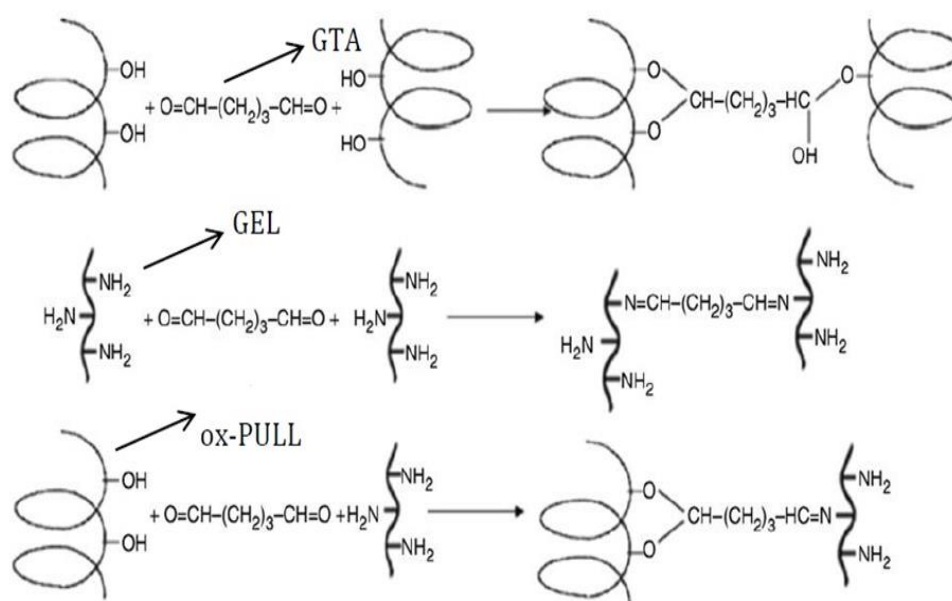


**Figure 4.** Schematic representation of cross-linking of oxidized PULL and proteins (Asma et al., 2014).

Na et al. (2003) conjugated carboxymethyl pullulan (CMP) with heparin and evaluated the effect of heparin immobilized PULL on growth of endothelial cells. The reason for use of carboxylated pullulan was its processability and biocompatibility. Human umbilical vein endothelial cells (HUVEC) attached and proliferated on heparin-conjugated carboxylated pullulan covered glasses, but proliferation of smooth muscle cells was inhibited. Heparin being a constituent of the extracellular matrix of blood vessels, is known to enhance endothelial cell growth in

vitro and inhibit proliferation and migration of vascular smooth muscle cells (Na et al., 2003). Fricain et al. (2013), developed PULL based scaffolds incorporating nanocrystalline hydroxyapatite particles (nHA). Human bone marrow stromal cells formed, multicellular aggregates on PULL based scaffolds and they also expressed bone specific markers. When composite scaffolds were implanted heterotopically under the skin of mice and into intramuscular sites of the goat, a dense mineralized tissue on the scaffolds was formed at both sites implanted in mice and goat. Concentration of local growth factors of vascular endothelial growth factor 165 (VEGF165) and bone morphogenetic protein 2 (BMP2) was retained in mice and biological apatite was grown on the scaffolds. Formation of osteoid tissue was observed in composites implanted intramuscularly in goat. In continuation of in vivo studies, implantation of scaffolds in orthotopic preclinical models in small and large animals (the femoral condyle of rat, a transversal mandibular defect and a tibial osteotomy in goat), revealed presence of a highly mineralized tissue, osteoid tissue and regenerated bone tissue. In conclusion, addition of mineral phase to natural polysaccharides has caused differentiation of host mesenchymal stem cells and formation of bone (Fricain et al., 2013). Arora et al. (2015) reinforced pullulan hydrogels with nano-crystalline hydroxyapatite (nHAP) and poly (3-hydroxybutyrate) (PHB) fibers. Addition of nHAP enhanced the mechanical properties, while combination of two fillers (composite PHB fibers and nHAP) increased the mechanical properties ten times. In order to deposit HA on pore walls, a novel double diffusion method was used. As a result, adhesion and proliferation of human osteosarcoma MG63 cells on scaffolds were improved. Maximum stress before failure increased higher than 3 times (0.058 MPa for double composites and greater than 0.186 MPa for triple composites) (Arora et al., 2015). Takahata et al. (2015) developed the phosphorylated PULL/ $\beta$ -TCP composite for bone tissue engineering. It was observed that the PULL/ $\beta$ -TCP composite was biocompatible and supported bone formation when applied in a load bearing bone model (Takahata et al., 2015). In another study, three-dimensional scaffolds were prepared from a mixture of PULL cross-linked with STMP and collagen for skin tissue engineering

purposes. As a result of in vitro and in vivo tests, it was shown that highly porous pullulan/collagen hydrogels could be applied for wound healing purposes (Iswariya et al., 2016). In another study, PULL microspheres were either coated with silk fibroin (SF) or incubated in SBF for biomineralization. Surface modified microspheres showed positive effects on bone cells adhesion and proliferation. It was concluded that surface modified microspheres were applicable for bone tissue engineering applications (Aydogdu et al., 2016). Table 3. gives some examples of PULL used in tissue engineering applications.

### **1.2.1.3. Gelatin**

Gelatin, produced through partial hydrolysis of collagen, is the most abundant protein of the body (skin, tendon, cartilage and bone) and it is present in the natural extracellular matrix (Qian et al., 2011). Because of its biodegradability, biocompatibility and low cost, this protein is widely used in tissue engineering. Because of their lower immunogenicity and better solubility in aqueous media, it is more advantageous compared to collagen. Figure 5 shows chemical structure of GEL.

**Table 3.** Tissue engineering applications of different forms of PULL.

Form	Purpose	Author
PULL, nanocrystalline hydroxyapatite and poly (3-hydroxybutyrate) microfibers	Bone tissue engineering	(Arora et al., 2015)
Pullulan / tannic acid / chitosan composite nanofibers	Wound dressing	(Xu et al., 2015)
Pullulan nanoparticles	Drug delivery	(Ravi et al., 2014)
Nano-hydroxyapatite - pullulan / dextran polysaccharide composite microporous material	Bone tissue engineering	(Fricain et al., 2013)
Multi-responsive pullulan hydrogels	Drug delivery	(Mocanu et al., 2012)
Pullulan-collagen hydrogel scaffold	Skin tissue engineering	(Wong et al., 2010)

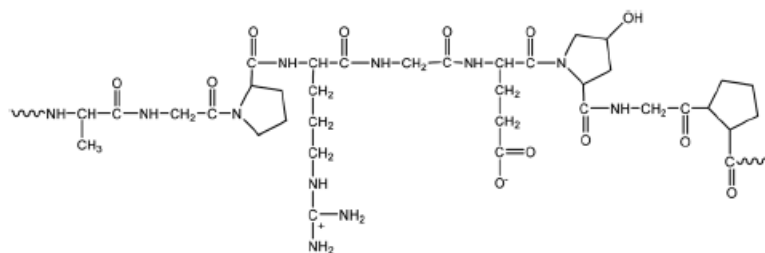


**Figure 5.** Chemical structure of gelatin (Ge et al., 2012).

Gelatin is cross-linked in order to change its mechanical and biochemical properties (Rose et al., 2014). Cross-linking of the gelatin with glutaraldehyde, occurs between the unprotonated amino groups of lysine and hydroxylysine and the amino groups of the N-terminal amino acid (Schrieber & Gareis, 2007). Mechanism of cross-linking of gelatin with GTA is shown in Fig. 6.



**Figure 6.** Crosslinking mechanism of gelatin with GTA (Migneault et al., 2004).

Crosslinking of the gelatin with 1-ethyl-3-(3-dimethylaminopropyl) carbodiimide (EDC) is carried out by forming the amide bond, which as a result of that, activation of the carboxylic acid residues of aspartic and glutamic acids and their conversion



into O-acylisourea groups occurs. Nucleophilic attack of free amine groups of lysine on the activated carboxylic acid, causes the amide bond formation (Kuijpers et al., 2000). In order to activate the carboxylic acid group, N-hydroxysuccinimide (NHS) is often used along EDC, which could increase yield of the crosslinking reaction (Fagerholm et al., 2010). These steps are schematically shown in Fig. 7.

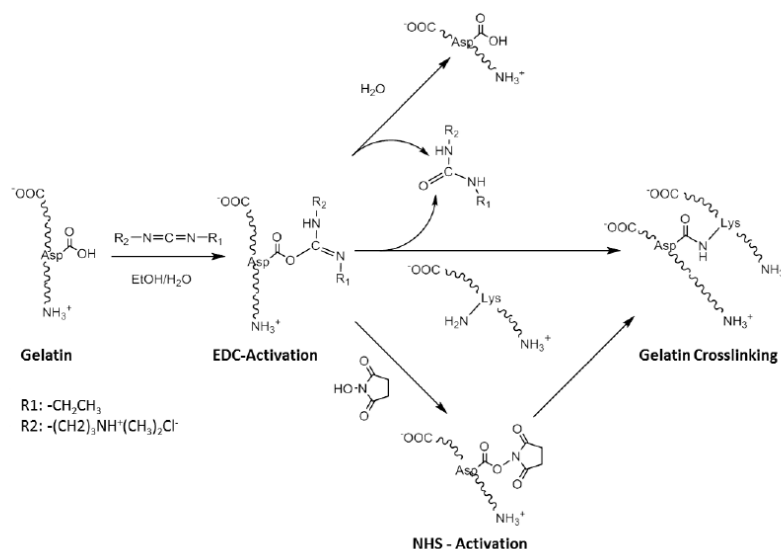


**Figure 7.** Schematic representation of amide bond formation as a result of cross-linking of gelatin with EDC/NHS (Rose et al., 2014).

Zhou et al. (2013) developed a scaffold for bone tissue engineering composed of gelatin/hyaluronic acid (Gel/HA) containing nano-bioactive glass (NBG). The tested materials were porous in structure and showed no cytotoxicity (Zhou et al., 2013). Li et al. (2011) tested the osteogenic differentiation potential of human dental pulp derived stem cells (hDPSCs) seeded on 3-dimensional scaffolds composed of gelatin for bone tissue engineering applications. In vitro studies showed that hDPSCs could differentiate osteogenically and in vivo studies revealed that hDPSCs grown on gelatin scaffolds could form bone structure (Li et al., 2011b). Kabashima et al. (2013) used an autologous blood clot in combination with gelatin for periodontal tissue regeneration in a clinical treatment trial. Regeneration was shown to be successful because of slow degradation of the gelatin hydrogel which made release

of growth factors from the clot possible (Kabashima et al., 2013). Maji et al. (2016) prepared scaffolds composed of bioactive glass (58S) and natural biopolymers (chitosan, gelatin) for bone regeneration. It was observed that the addition of 58S bioactive glass nanoparticles increased human umbilical cord mesenchymal stem cells (MSCs) adhesion, proliferation and osteogenic differentiation. The developed composite scaffolds were proposed for bone regeneration applications (Maji et al., 2016). In another study, electrospun PCL/gelatin composite fibrous scaffolds with different mixing ratios were prepared. PCL/gelatin (2:1) composite scaffold showed the highest tensile strength and elongation rate and at the same time provided best conditions for attachment, spreading, and cytoskeleton organization of mesenchymal stem cells (MSCs) (Yao et al., 2016).

### **1.2.2. Stem Cells**

Cells are one of the most basic components in order to form artificial tissues by tissue engineering. For engineering of dental tissues, embryonic stem cells, adult stem cells and induced pluripotent stem cells are used. The most common cell source, are stem cells isolated from the target tissue.

#### **1.2.2.1. Embryonic Stem Cells**

Embryonic stem cells (ESCs) could self-renewal and differentiate into different types of functional tissue cells. In the study by Ning et al. (2010), murine ESCs (mESCs) were derived from the inner cell mass of mouse blastocysts and cultured in ameloblasts serum-free conditioned medium (ASF-CM). In vitro tests showed higher expression of ameloblast-specific proteins in mESCs obtained with embryoid body (EB) formation rather than in mESCs obtained without EB formation. As a result of

in vivo studies after transplantation of murine EBs (mEBs) in immunocompromised mice, odontogenic epithelial-like structures were formed. In total, odontogenic differentiation of mESCs was confirmed and EB-derived mESCs could promote odontogenesis under in vitro and in vivo conditions (Ning et al., 2010).

#### **1.2.2.2. Mesenchymal Stem Cells**

For engineering of dental tissues, both non-dental and dental mesenchymal stem cells have been used. Non-dental stem cells have been shown to differentiate into dental-like cells, but in comparison to dental stem cells, their capabilities are low. This is because of a close relationship between dental stem cells and mature dental tissues (Huang & Thesleff, 2013). For this reason, use of dental stem cells for engineering of dental tissues, is more widespread.

##### **1.2.2.2.1. Adult Stem Cells of Non-Dental Origin**

They are pluripotent stem cells present in various tissues and organs which support tissue homeostasis and maintain their regenerative potential after lesion (Baudry et al., 2016). Hashmi et al. (2017), prepared thermoresponsive [H-Gly-Arg-Gly-Asp-Ser-OH (GRGDS) peptide- poly(N-isopropylacrylamide)] (GRGDS-PNIPAAm) compressive scaffolds coated with Collagen VI. As a result of in vitro culture studies with murine adult bone marrow stromal cells (BMSCs), increased expression of critical markers of tooth differentiation was observed. After implanting the cell-scaffold construct under the kidney capsule of mice, histological analyses revealed local mineralization, calcification and production of dentin-like tissue. In general, chemically modified compressive scaffolds were shown to induce adult bone

marrow-derived mesenchymal stem cells (BMSCs) to undergo a lineage switch and begin to form dentin-like tissue (Hashmi et al., 2017).

#### **1.2.2.2.2. Adult Stem Cells of Dental Origin**

Application of dental stem cells in engineering of dental tissues is intriguing. They possess properties of mesenchymal stem cells (MSCs) and are isolated from different parts of dental tissues. Until now, five different types of dental stem cells have been isolated from permanent and deciduous teeth.

##### **1.2.2.2.2.1. Stem Cells from Human Exfoliated Deciduous Teeth (SHED)**

Pulp tissue of the extracted deciduous teeth is considered as a suitable source for isolation of the stem cells. These cells are positive for embryonic stem cell and mesenchymal stem cell markers and negative for hematopoietic stem cell markers. Permanent and primary teeth differ from each other in terms of development, morphological characteristics and physiological processes. SHED are more proliferative than dental pulp stem cells (DPSCs), form sphere-like cell aggregation and their differentiation capabilities are greater (Rosa et al., 2016, Liu et al., 2015). Casagrande et al. (2010), prepared tooth slice/scaffolds by casting Poly-L-lactic acid (PLLA) in the pulp cavity of human tooth slices. After in vitro culture of SHED on the scaffolds for 28 days, cell-scaffold constructs were implanted subcutaneously into immunodeficient mice. At two different time points, mice were sacrificed, implants were removed and RNA extraction was done for gene expression analysis. According to the results, markers of odontoblastic differentiation dentin sialophosphoprotein (DSPP), DMP-1, matrix extracellular phosphoglycoprotein

(MEPE) were expressed in both in vitro and in vivo conditions when tooth slice/scaffolds were used, but were not expressed in deproteinized tooth slice/scaffolds, or scaffolds without a tooth slice. It was concluded that presence of dentin-derived BMP-2 is essential for odontoblastic differentiation of SHED (Casagrande et al., 2010). In the research conducted by Sakai et al. (2010), after culturing SHED in tooth slice/scaffolds (PLLA casted human tooth slices), they were grown in presence of recombinant human vascular endothelial growth factor (rhVEGF<sub>165</sub>) under in vitro conditions and also were transplanted into immunodeficient mice. Regulation of the signal transducer and activator of transcription 3 (STAT3) and AKT pathways by vascular endothelial growth factor (VEGF) signaling [through vascular endothelial growth factor receptor 1 (VEGFR1)] was investigated to understand the mechanism of differentiation of SHED into endothelial cells. As a result of in vivo tests, tetracycline staining and confocal microscopy revealed differentiation of SHED into functional odontoblasts which formed tubular dentin and their differentiation into vascular endothelial cells was confirmed by beta-galactosidase staining of LacZ-tagged SHED. As for a successful dental pulp tissue engineering, odontoblasts and endothelial cells are needed, SHED are proposed to fulfill this requirement (Sakai et al., 2010).

#### **1.2.2.2.2. Dental Follicle Stem Cells (DFPCs)**

The dental follicle is an ectomesenchyme-derived tissue surrounding the developing tooth germ before the eruption. DFPCs were isolated from the third molar teeth follicle. They have a remarkable differentiation capacity and they can differentiate into chondrocytes, adipocytes, neuronal cells, periodontal ligament (PDL), osteoblasts, cementoblasts and fibroblast cells [(Liu et al., 2015); (Khazaei et al., 2016)]. In the study by Yokoi et al. (2007), presence of PDL progenitors in mouse dental follicle (MDF) cells was reported. MDF cells were isolated from mouse

incisor tooth germs and then immortalized using a mutant human papilloma virus type 16 E6 gene. MDF cells expressing the mutant E6 gene (MDFE6-EGFP cells) possessed over 150 population doublings (PD), while that of normal MDF cells did not exceed 10. MDFE6-EGFP cells could express tendon/ligament phenotype-related genes. When they were transplanted into immunodeficient mice, after 4 weeks they formed a PDL-like tissue that could express periostin, Scx, and type XII collagen and the fibrillar assembly of type I collagen. These results indicated that immortalized dental follicle cells could recreate a new PDL after *in vivo* implantation (Yokoi et al., 2007).

#### **1.2.2.2.3. Stem Cells from the Apical Papilla (SCAPs)**

SCAPs are isolated from apical dental papilla, a tissue which later is converted into dental pulp. SCAPs have been shown to differentiate into osteoblasts, odontoblasts and adipocytes in *in vitro* conditions. In comparison to DPSCs, their differentiation capabilities and dental tissue regeneration capacities are greater (Bakopoulou et al., 2011). Since origin of SCAPs is an embryonic-like tissue, in comparison to DPSCs, they are less differentiated and this increases their potential for dentin regeneration. Number of adult stem cells present in dental papilla, are higher than those in the mature dental pulp (cheung, 2010). Bakopoulou et al. (2010), isolated DPSCs and SCAPs from human third molars and evaluated their *in vitro* osteo/odontogenic differentiation potential. Their growth characteristics, mineralization potential and differentiation markers were assessed under osteo/odontogenic differentiation condition. Both types of cells differentiated into odontoblast-like cells with proper migration, organization and mineralization properties which finally formed 3D mineralized structures. Differentiation markers specific for osteodentin were expressed positively. Population doubling capacity, proliferation rate and

mineralization rate of SCAPs was higher than that of DPSCs (Bakopoulou et al., 2011).

#### **1.2.2.2.2.4. Periodontal Ligament Stem Cells (PDLSCs)**

Periodontal ligament is a structure located between the teeth and the alveolar bone, which consists of the fibers that attach tooth to the jaw. Periodontal ligament could be obtained from root of the extracted tooth and is source of PDLSCs. These cells could differentiate into adipocytes, osteoblasts, chondrocytes in vitro (Zhu & Liang, 2015). Gao et al. (2015), investigated effect of nanotopography on PDLSC sheet based periodontal regeneration. Titania nanotubes layered on titanium (Ti) were prepared and a specific sandwich-like model was used for in vivo experiments. In vitro results showed favorable adhesion and spread of PDLSCs and also collagen secretion. As a result of ectopic implantation of a Ti/cell sheets/hydroxyapatite (HA) complex into immunocompromised mice, PDLSC sheets regenerated the PDL tissue, after being combined with bone marrow mesenchymal stem cell (BMSC) sheets and HA. It was concluded that the formation of functionally aligned collagen fiber bundles was because of presence of NTs (Gao et al., 2015). Wang et al. (2016), isolated human PDL stem cells (PDLSCs) and jaw bone mesenchymal stem cells (JBMSCs) and prepared cell sheets by the ascorbic acid-rich method. Bioabsorbable fibrin scaffolds were developed from Platelet-rich fibrin (PRF). PDLSC sheet/PRF/JBMSC sheet composites were put in a simulated periodontal space containing human treated dentin matrix (TDM) and hydroxyapatite (HA)/tricalcium phosphate (TCP) frameworks and the whole construct was implanted into nude mice. After eight weeks, periodontal tissue-like structures containing PDL- and bone-like tissues were formed. As a conclusion, this cell transplantation method was suggested for periodontal tissue regeneration (Wang et al., 2016).

#### **1.2.2.2.5. Dental Pulp Stem Cells (DPSCs)**

Dental pulp stem cells (DPSCs) are highly proliferative and immunosuppressive and are suitable for regeneration of dentin-pulp-like complex (Liu et al., 2015). Mesenchymal stem cell markers of DPSCs include CD29, CD44, CD73, CD105, CD106, CD146 and their osseous-specific markers are known to be alkaline phosphatase (ALP), osteopontin, and osteocalcin. In addition, they can differentiate into osteoblasts, odontoblasts, chondrocytes, myocytes, cardiomyocytes, active neurons, melanocytes and hepatocyte-like cells (Khazaei et al., 2016).

In a study of using stem cells for dentin regeneration, DPSCs were isolated and seeded on a PLGA based scaffold prepared by the solvent casting/particulate leaching technique, and then tested *in vivo*. As a result, osteodentin-like and tubular structures were obtained (El-Backly et al., 2008). Wang et al. (2011) investigated the effect of scaffold structure on odontogenic differentiation of hDPSCs by developing nanofibrous and solid-walled poly (L-lactic acid) (PLLA) scaffold. As a result of *in vitro* and *in vivo* experiments, nanofibrous PLLA scaffolds resulted in better adhesion and proliferation of hDPSCs and also their odontogenic differentiation and dentin-like tissue formation (Wang et al., 2011). In another study, stem cells from apical papilla and dental pulp stem cells were isolated, cultured on poly-D, L-lactic/glycolic acid scaffolds prepared by the gas foaming/particulate leaching process and then placed in tooth fragments. For *in vivo* experiments, cell-scaffold constructs were implanted into subcutaneous space of nude mice. As a result of the *in vivo* study, pulp-like tissue was formed in the root canal area with favorable degree of vascularity and also a continuous dentin-like layer on the canal wall. According to results of immunohistochemistry analyses (positive expression of dentin sialophosphoprotein, bone sialoprotein, alkaline phosphatase, and CD105), formation of the dentin-like structure was done by a layer of newly formed odontoblast-like cells. In total, results confirmed favorable effects of stem/progenitor cell-mediated tissue engineering for pulp/dentin regeneration (Huang et al., 2009). In one study,



odontogenic differentiation of hDPSCs on nanofibrous composites prepared from biopolymer (BP) blend polycaprolactone-gelatin (BP) and mesoporous bioactive glass nanoparticles (BG-NPs) was evaluated. (BG-NPs)-BP composite nanomatrices were prepared by the electrospinning method with 10 and 20 wt% of BGN incorporation. Odontogenic differentiation of the HDPCs was assessed by ALP activity assay, calcified nodule formation, and mRNA expression for markers. There was not much difference between results of cells attachment and proliferation on BP and BGN-BP groups, but results of ALP activity, mineralized nodule formation, and mRNA expressions were much better for (BG-NPs)-BP. Nanocomposite scaffold has been shown to be suitable for dentin tissue engineering, because of supporting the differentiation of hDPSCs through the integrin, BMP, and mitogen-activated protein kinases signaling pathway (Kim et al., 2015). Lee et al. (2016) examined the effect of the aminated mesoporous bioactive nanoparticles (MBNs-NH<sub>2</sub>) on the differentiation of rat dental pulp stem cells (rDPSCs). rDPSCs viability, their uptake of MBNs-NH<sub>2</sub> and odontogenic differentiation were tested in vitro. According to the results, MBNA-NH<sub>2</sub> were reported to promote odontogenic differentiation of rDPSCs and were proposed to be used for dentin regeneration applications (Lee et al., 2016). In our study, hDPSCs are isolated and used for the experiments.

### **1.2.2.3. Induced Pluripotent Stem Cells**

Because of safety concerns of ESCs, and problems regarding isolation and use of adult stem cells in dental clinics, induced pluripotent stem cells (iPSCs) are suggested as candidates for dental tissue regeneration (Baudry et al., 2016). Cai et al. (2013), prepared integration-free human urine induced pluripotent stem cells (ifhU-iPSCs). After differentiation of them into epithelial sheets, they were recombined with E14.5 mouse dental mesenchymes. After 1–2 days in vitro culture of the explants, they were implanted under subrenal capsule of mouse for 3 weeks. Tooth-like structures were formed that contained enamel with ameloblast-like cells

and had physical properties resembling natural human teeth. In conclusion, human iPSCs were proposed to be used in regenerative dentistry (Cai et al., 2013).

### **1.3. Aim of the Study**

Dental caries is a dental disease affecting public health, which results with many socio-economic consequences. This disease causes loss of tooth hard tissue and subsequent inflammation and loss of the dental pulp. Every year a large number of dental restorations is carried out in the world and most of them do not succeed. High cost of these restorations and rejection possibility of the implants are their drawbacks. For this reason, a regenerative approach for repairing of the damaged dentin-pulp complex or generating a new tissue is needed.

In this study, it was aimed to develop and characterize borate modified BG-NPs containing (CA/ox-PULL/GEL) three dimensional scaffolds with tubular morphology for dentin regeneration. The biocompatibility and bioactivity of bioactive glass are very attractive for dental applications. The purpose of modification with borate was to achieve increased biodegradability of the bioactive glass. In this thesis, the effect of borate modified bioactive glass on hDPSCs and its application in dentin tissue engineering was studied for the first time in the literature. CA is a derivative of cellulose and is used in tissue engineering of soft and hard tissues as a scaffold. The neutral extracellular polysaccharide PULL was used for the first time in a composition with cellulose acetate and BG-NPs. This polysaccharide has wide applications in a range of fields as well as tissue engineering in recent years. Gelatin is a partial derivative of collagen and as a composite with other materials, can simulate ECM structure of the human tissues and organs. Diacyl forms of pullulan with high water solubility were obtained by periodate oxidation to crosslink with gelatin in order to obtain a structurally stable carrier.

The three-dimensional nano biocomposite structure were prepared by mixing borate modified BG-NPs with (CA/ox-PULL/GEL) and processing by [(TIPS/PL) and (FD/MMP)] methods.

The purpose of this study can be summarized as:

- to investigate the use of borate modified BG-NPs in dentistry and orthopedic applications,
- to analyze the effect of borate modified BG-NPs on hDPSCs,
- to prepare porous nano biocomposite scaffolds using borate modified BG-NPs and three polymers (CA/ox-PULL/GEL) and explore its use in dentin regeneration,
- to develop dentin like constructs using hDPSCs and CA/ox-PULL/GEL scaffolds,



## CHAPTER 2

### 2. MATERIALS & METHODS

#### 2.1. Materials

Materials used for bioactive glass nanoparticles synthesis, formulas and companies that they were purchased from, are given in Table 4.

**Table 4.** List of materials used for bioactive glass nanoparticles synthesis.

Materials	Formulas	Company
Calcium nitrate	$\text{Ca}(\text{NO}_3)_2$	Sigma-Aldrich (USA)
Ethanol	$\text{C}_2\text{H}_6\text{O}$	Sigma-Aldrich (USA)
Citric acid	$\text{C}_6\text{H}_8\text{O}_7$	Sigma-Aldrich (USA)
Polyethylene glycol	$\text{C}_2\text{H}_6\text{O}_2$	Sigma-Aldrich (USA)
Ammonium dibasic phosphate	$(\text{NH}_4)_2\text{HPO}_4$	Sigma-Aldrich (USA)
Boric acid	$\text{H}_3\text{BO}_3$	Sigma-Aldrich (USA)

**Table 4 - Continued.** List of materials used for bioactive glass nanoparticles synthesis.

Tetraethyl orthosilicate (TEOS)	$(C_2H_5O)_4Si$	Merck (USA)
Triethyl phosphate (TEP)	$(C_2H_5O)_3PO$	Merck (USA)
Ammonium hydroxide	$NH_4OH$	Merck (USA)
Nitric acid	$HNO_3$	Merck (USA)

The chemicals used for the preparation of three-dimensional scaffolds and for the isolation and proliferation of hDPSCs are listed in Tables 5 and 6, respectively.

**Table 5.** List of chemicals used in the preparation of three-dimensional scaffolds.

<b>Materials</b>	<b>Formulas</b>	<b>Company</b>
Cellulose acetate	$C_{76}H_{114}O_{49}$	Sigma-Aldrich (USA)
Pullulan	$(C_6H_{12}O_5)_n$	Hayashibara Inc (Okayama, Japan)
Gelatin		Sigma-Aldrich (USA)
Glutaraldehyde	$C_5H_8O_2$	Sigma-Aldrich (USA)
Sodium periodate	$NaIO_4$	Sigma-Aldrich (USA)

**Table 5 - Continued.** List of chemicals used in the preparation of three-dimensional scaffolds.

Sodium hydroxide	NaOH	Sigma-Aldrich (USA)
Glycerine	C <sub>3</sub> H <sub>8</sub> O <sub>3</sub>	Sigma-Aldrich (USA)
Methyl orange dye	C <sub>14</sub> H <sub>14</sub> N <sub>3</sub> NaO <sub>3</sub> S	Sigma-Aldrich (USA)
Hydroxylamine hydrochloride	HONH <sub>2</sub> ·HCl	Sigma-Aldrich (USA)
Succinic anhydride	C <sub>4</sub> H <sub>4</sub> O <sub>3</sub>	Sigma-Aldrich (USA)
Acetic acid	C <sub>2</sub> H <sub>4</sub> O <sub>2</sub>	Sigma-Aldrich (USA)
1-ethyl-3-(3-dimethylaminopropyl) carbodiimide hydrochloride (EDC)	C <sub>8</sub> H <sub>17</sub> N <sub>3</sub> ·HCl	Sigma-Aldrich (USA)
N-hydroxysuccinimide (NHS)	C <sub>4</sub> H <sub>5</sub> NO <sub>3</sub>	Sigma-Aldrich (USA)
Glycine	C <sub>2</sub> H <sub>5</sub> NO <sub>2</sub>	Sigma-Aldrich (USA)
Ethanol	C <sub>2</sub> H <sub>6</sub> O	Sigma-Aldrich (USA)
Dimetilformamid (DMF)	C <sub>3</sub> H <sub>7</sub> NO	Sigma-Aldrich (USA)

**Table 6.** List of materials used in cell culture experiments.

<b>Materials</b>	<b>Company</b>
Collagenase Type I	Sigma-Aldrich (USA)
Dispase	Sigma-Aldrich (USA)
Fetal bovine serum (FBS)	Biochrom (Germany)
Penicillin / Streptomycin	Biochrom (Germany)
DMEM (Dulbecco's modified Eagle medium)	Biochrom (Germany)
Trypsin -EDTA	Biochrom (Germany)
Alamar blue dye	Sigma-Aldrich (USA)
CD31 Mouse monoclonal antibody	Cell Signalling (USA)
CD44 Mouse monoclonal antibody	Cell Signalling (USA)
CD45 Rabbit monoclonal antibody	Cell Signalling (USA)
CD73 Mouse monoclonal antibody	Abcam (Britain)
CD90 Mouse monoclonal antibody	Abcam (Britain)
CD105 Mouse monoclonal antibody	Abcam (Britain)
Mouse mAb IgG1 isotype control	Cell Signalling (USA)
Rabbit mAb IgG isotype control	Cell Signalling (USA)
Anti-mouse IgG secondary antibody	Cell Signalling (USA)



**Table 6 - Continued.** List of materials used in cell culture experiments.

Anti-rabbit IgG secondary antibody	Cell Signalling (USA)
Thiazolyl blue tetrazolium bromide	Sigma-Aldrich (USA)
Bicinchoninic acid solution	Sigma-Aldrich (USA)
Copper sulphate	Sigma-Aldrich (USA)
Anti-collagen I antibody	Abcam (Britain)
Anti-DSPP antibody	Abcam (Britain)
Anti-osteopontin antibody	Abcam (Britain)
Donkey anti-rabbit IgG secondary antibody	Abcam (Britain)
Triton X-100	Sigma-Aldrich (USA)
Bovine serum albumin	Sigma-Aldrich (USA)

## **2.2. Methods**

### **2.2.1. Synthesis of Pure and Borate Modified BG-NPs**

For preparation of BG-NPs, two different methods i) combination of sol-gel and co-precipitation methods and ii) quick alkali-mediated sol-gel method) were used.

### **2.2.1.1. Preparations of Pure and Borate Modified BG-NPs by Combination of Sol-Gel and Coprecipitation Methods**

The procedure followed for preparing the BG-NPs (58S)(SiO<sub>2</sub>:CaO:P<sub>2</sub>O<sub>5</sub>) (58:38:4 mol%) was as follows: 7.26 g calcium nitrate was dissolved in 120 ml of deionized water at room temperature to prepare the calcium precursor solution. The tetraethyl orthosilicate (TEOS)-ethanol solution was prepared by diluting 9.76 g of TEOS in 60 ml of ethanol and added to the calcium nitrate solution. Citric acid was then added to the solution for adjusting the pH value to 1–2. The reaction mixture was kept stirring until a homogeneous and transparent solution was obtained. Under vigorous stirring, the homogenous solution was added dropwise into ammoniated deionized water containing 15 g of PEG 20000, in which 0.855 g of ammonium dibasic phosphate was dissolved in advance. During this addition the pH value of solution was kept at around 11.5 using ammonia water. After stirring for 48 h and aging for 24 h, the precipitate was separated from the reaction solution by centrifugation at 7000 rpm and washed three times with deionized water. The precipitate was freeze dried (Labconco, USA) and calcined at 700°C in a muffle furnace (Protherm Furnace - PLF 140/5 – Turkey) for 3 h, after which the white BG nanoparticles were obtained (Hong et al., 2009).

The steps followed for preparing borate modified BG-NPs were the same as described above. For borate modification, SiO<sub>2</sub> was partly replaced by B<sub>2</sub>O<sub>3</sub> with 7% and 14% (Table 7). Boric acid was used as a precursor for obtaining B<sub>2</sub>O<sub>3</sub>. After diluting TEOS with ethanol, boric acid was added to the TEOS-ethanol solution which was then added to the calcium nitrate-water solution (Laczka et al., 2000).

### 2.2.1.2. Preparations of Pure and Borate Modified BG-NPs by a Quick Alkali-Mediated Sol-Gel Method

For preparation of BG-NPs ( $\text{SiO}_2:\text{CaO}:\text{P}_2\text{O}_5$ ) (58:38:4 mol%), quick alkali-mediated sol-gel method was used. After mixing TEOS (20 ml), distilled water (13.9 ml) and 2 M nitric acid (2.8 ml) in ethanol (50 ml) and stirring for 30 min, TEP (2.15 ml) was added and stirred for 20 min. Calcium nitrate (14 g) was added. Ammonia solution (1 molar) (10 ml) was added dropwise under vigorous stirring after obtaining a clear acid

**Table 7.** Nominal compositions of Bx-BG samples.

Sample ID	Reactants (Mole %)			
	$\text{SiO}_2$	CaO	$\text{P}_2\text{O}_5$	$\text{B}_2\text{O}_3$
B0-BG	58	38	4	0
B7-BG	51	38	4	7
B14-BG	44	38	4	14

sol. After swift gelation of sol, we used a muddler to mix the gel well and then dried the gel in the oven at 60°C for 1 day. Afterwards, calcination step was done at 600°C in a muffle furnace (Protherm Furnace - PLF 140/5 – Turkey) for 2 h (Xia & Chang, 2007). For borate modification, the mole ratio of  $\text{SiO}_2$  was partly replaced by 7%, 14% and 21%  $\text{B}_2\text{O}_3$  (Table 8). Boric acid was used as a precursor for obtaining  $\text{B}_2\text{O}_3$ . After diluting TEOS with ethanol, boric acid was added in the TEOS-ethanol solution and the other steps were the same as stated above (Laczka et al., 2000).

**Table 8.** Nominal compositions of Bx-BG samples.

Sample ID	Reactants (Mole %)			
	SiO <sub>2</sub>	CaO	P <sub>2</sub> O <sub>5</sub>	B <sub>2</sub> O <sub>3</sub>
B0-BG	58	38	4	0
B7-BG	51	38	4	7
B14-BG	44	38	4	14
B21-BG	37	38	4	21

### 2.3. Characterization of Pure and Borate Modified BG-NPs

#### 2.3.1. X-Ray Diffraction (XRD) Analysis

Phase purity analysis was investigated using X-ray diffraction analysis (XRD, Model D/ MAX2200 / PC - Japan) (Metallurgical and Materials Engineering Department, METU). A full scan (from 10-80 degrees) was run for all samples to find peak positions.

#### 2.3.2. Fourier Transform Infrared Spectroscopy (FTIR) Analysis

For examining the functional groups by Fourier Transform Infrared Spectroscopy (FTIR), (Bruker IFS 66/S, FRA 106/ S, HYPERION 1000, RAMANSCOPE II)

(Central Laboratory, METU), the nanoparticles were pressed with KBr into a small disc form. Before measurements, the powders were dried overnight at 100°C to remove the moisture. The FTIR spectra were recorded from 400 to 4000  $\text{cm}^{-1}$  with a resolution of 4  $\text{cm}^{-1}$ .

### **2.3.3. Scanning Electron Microscopy (SEM) Analysis**

Morphology and particle size of the synthesized pure and borate modified BG-NPs was studied with Scanning Electron Microscopy (SEM) analysis. Synthesized particles were coated with ultrafine (10 nm) gold layer by precision etching coating system (682 PECS, Gatan, Inc., USA) and then imaged via (FEI, Nova Nano SEM 430, USA) (Metallurgical and Materials Engineering Department, METU) before analysis.

### **2.3.4. Inductively Coupled Plasma Mass Spectrometry (ICP-MS) Analysis**

Elemental analysis of pure and borate modified BG-NPs was conducted by ICP-MS, (Elmer DRC II model ICP-MS, USA). The particles were dissolved in 2%  $\text{NO}_3$  solution for analysis. Molar percentages of  $\text{SiO}_2$ ,  $\text{CaO}$ , and  $\text{P}_2\text{O}_5$  were determined by the lithium metaborate fusion method (Valliant et al., 2013) and mole percentage of  $\text{B}_2\text{O}_3$  was determined by the sodium peroxide fusion method (Richaud et al., 2000).

### **2.3.5. Porosimetry Analysis**

The specific surface area, pore volume and pore size of pure and borate modified BG-NPs were determined by Brunauer–Emmett–Teller (BET) and Barret–Joyner–Halenda (BJH) analyses (Tristar3000, Micromeritics, USA). The samples were degassed in vacuum at 200°C for 3 h prior to the nitrogen adsorption analysis to remove moisture from the pores (Luz & Mano, 2011).

### **2.3.6. In Vitro Bioactivity Tests**

The prepared pure and borate modified BG-NPs were compressed in disc forms (Diameter: 12.6 mm, and height: 2.3 mm) with equal weights and discs were immersed in falcon tubes containing 50 ml of Simulated Body Fluid (SBF) (Kokubo & Takadama, 2006) and incubated at 37°C for 14 days. After different incubation periods, samples were removed from SBF solution and washed 3 times with deionized water. They were then freeze-dried for 20 hours. The samples were gold sputter coated and imaged by SEM in order to investigate the apatite formation on discs (Kokubo & Takadama, 2006). ICP-MS analysis was also used to determine the concentrations of ions in SBF at different time points. After 1, 3, 7, and 14 days of treatment, SBF solution was collected and sent to analysis on the same day. Release of different ions from BG during SBF treatment period, was studied by ICP-MS according to Section 2.3.4 in order to determine the degree of bioactivity of the material (Polini et al., 2013).

## **2.4. Preparation of Three Dimensional CA/PULL/GEL Scaffolds**

### **2.4.1. Periodate Oxidation of PULL**

Pullulan was modified by periodate oxidation for crosslinking with gelatin to obtain a structurally stable scaffold due to its high solubility in aqueous environment (Balmayor et al., 2012). Briefly, PULL (1 g) was dissolved in 8 ml distilled water in a light protected container and 0.125 ml of sodium iodate (100 mg/ml) was added per ml of PULL solution. The solution was stirred at low speed for 30 min at room temperature using a magnetic stirrer. Glycerin (0.1 ml/ml) was added to stop the reaction and stirring continued for 10 min. Then, solution was dialyzed against distilled water for 2 days and after dialysis, oxidized pullulan solution was freeze-dried for 24 hours and was stored at 4°C in a light protected container until use.

#### **2.4.1.1. Determination of Oxidation Degree of Oxidized PULL**

Aldehyde content was determined to assess the degree of oxidation of PULL. The procedure was as follows: For this, first 0.1 g of dialdehyde PULL (DPULL), was dissolved in 12.5 ml of distilled water and the pH was adjusted to 7 with 0.1 N sodium hydroxide (NaOH). Then 0.5 N N- hydroxylamine hydrochloride - methyl orange solution ( $\text{H}_2\text{NOHHCl}$ ) was added to 12.5 ml PULL solution, and the mixture was stirred for 2 hours. It was then titrated with a 0.1 N sodium hydroxide solution until the red-to-yellow endpoint and the color of the solution was matched at pH 7 with an oxidized PULL solution (blank) at the same concentration.

The number of aldehyde groups per 100 anhydroglucose units was measured using the following formula:

$$AC = N_{NaOH} \cdot V_{NaOH} \cdot \frac{MW}{m_{DPULL}} \cdot \frac{100}{S} \cdot 10^{-3} \quad (1)$$

where AC is aldehyde content;  $N_{NaOH}$  is the concentration of standardized sodium hydroxide solution [N];  $V_{NaOH}$  is the volume of NaOH [ml]; MW is the molecular weight of PULL [Da];  $m_{DPULL}$  is the weight of DPULL sample [g]; S is the number of anhydroglucose units in the chain of PULL with a MW (Kulikowska et al., 2013).

## **2.4.2. Carboxylation of PULL**

We aimed to obtain a structurally stable scaffold through amide bond formation between carboxyl groups of carboxylated PULL and amine groups in gelatin with EDC / NHS crosslinking. For this end, PULL was mixed with succinic anhydride (4% weight of PULL) in dH<sub>2</sub>O for 60 minutes. This mixture was then dialyzed against distilled water for 1 day, and the carboxylated PULL was stored at 4 ° C in a light protected container (Li et al., 2013).

### **2.4.2.1. Determination of Degree of Substitution of Carboxylated PULL**

Acid/base titration was used to measure the DS of CPULL. After dissolving CPULL (0.2 g) in 40 ml of distilled water, the pH of the solution was adjusted to 2 with hydrochloric acid and then CPULL was titrated with 0.1 N NaOH. The volume of NaOH and pH values were recorded.



This test was repeated three times for each sample. DS was determined as follows:

$$DS = \frac{M_{Pru} \times (n_{ep})}{0.2 - (M_C \times n_{ep})} \quad (2)$$

where  $M_{Pru}$  is the molecular weight of PULL repeating unity (164),  $n_{ep}$  the number of moles of carboxyl groups at the ending point of the titration, and  $M_C$  is the molecular weight of the carboxyl groups placed in the natural structure of PULL (Mendes et al., 2012).

### 2.4.3. Preparation of Polymer Solutions

The solubility of the polymers that will be used for preparation of the scaffolds was tested in different solvent systems (Table 9). N-methylmorpholine-N-oxide (NMMO) and Dimethyl sulfoxide (DMSO) were not used for preparation of different solvent systems because they could not be freeze-dried. Solvents were added at different volume percentages in order to find a solvent composition to obtain a clear and homogeneous solution (Table 10). Finally, acetic acid + dH<sub>2</sub>O, with a total content of 58% acetic acid, was chosen as the solvent system for preparation of the polymer solution. When other solvent systems were used (DMF, dH<sub>2</sub>O), (DMA, dH<sub>2</sub>O), (DMF, NMMO), freeze-drying step was problematic. This problem was related to different melting points of the solvents which would result in a melting point of the mixture at temperatures less than -80 °C and eventual melting of the frozen mixture during freeze-drying.

**Table 9.** Solubility of polymers in different solvents

Polymer	DMA	DMF	Acetic acid + dH <sub>2</sub> O	DMSO	dH <sub>2</sub> O	NMMO	THF	TFE	HFIP
CA	+	+	+	+			+	+	+
PULL		+	+	+	+	+	+		
GEL			+	+	+	+		+	+

(GEL solution was prepared by heating at 40°C)

Scaffolds were prepared by two different methods.

#### **2.4.4. Preparation of Three Dimensional Scaffolds**

##### **2.4.4.1. Preparation of Three Dimensional Scaffolds by (TIPS/PL) Method**

CA/Oxidized PULL/GEL scaffolds were prepared using (TIPS/PL) method. Polymers were dissolved in 58% acetic acid solution at 40°C and transferred to glass containers. At this stage, solutions were ready for phase separation. To induce phase

**Table 10.** Different solvent systems used for preparation of the scaffolds.

System	Solvents	Volume added (%)	Result
1	CA: DMF PULL: DMF GEL: dH <sub>2</sub> O	DMF: 83.4 dH <sub>2</sub> O: 16.6	clear and homogeneous solution
2	CA: DMA PULL: dH <sub>2</sub> O GEL: dH <sub>2</sub> O	DMA: 87.5 dH <sub>2</sub> O: 12.5	clear and homogeneous solution
3	CA: acetic acid + dH <sub>2</sub> O PULL: dH <sub>2</sub> O GEL: dH <sub>2</sub> O	acetic acid: 58 dH <sub>2</sub> O: 42	clear and homogeneous solution

separation, the temperature was reduced by cooling the mixture in one direction using a system that involves foam fixed onto the aluminum plate where glass bottles can be placed in holes formed on foam (Figure 8). Aluminum is a good thermal conductor and the foam is chosen for insulation. Two different temperatures (-196°C and -80°C) were used for phase separation. The glass containers were placed in this system and the solutions were poured into them and frozen at either -196°C or -80°C. The frozen mixture was then lyophilized using a freeze-dryer (Labconco, USA) for 72 hours (Chen et al, 2008).

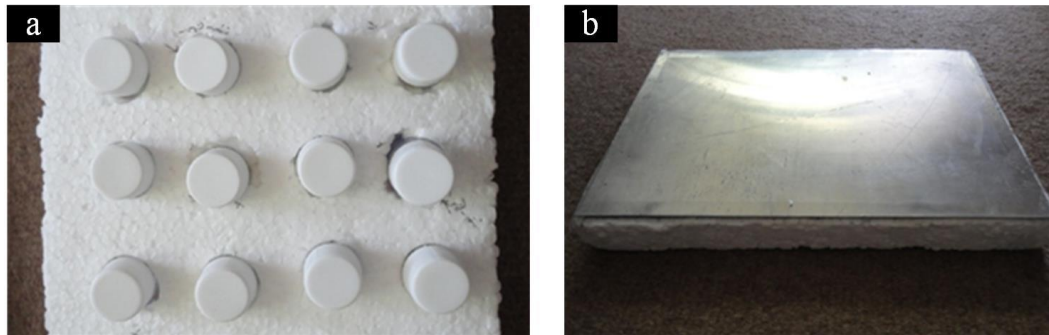


**Figure 8.** A system prepared from aluminum plate and foam in order to freeze the polymers solution in one direction (a) view from the foam side with the glass containers – (b) view from the aluminum plate side

After dissolving the polymers in a glass container (acetic acid + dH<sub>2</sub>O) at 40° C, KCl was added. KCl was added in amounts equivalent to 100%, 50% and 25% of the total polymer concentration. According to results of SEM, increase of porogen percentage, led to increase in pore diameters. Additionally, a more aligned and homogenous tubular structure was formed in the scaffolds prepared with the highest KCl amount. Increasing the freezing temperature also caused an increase in the mean diameter of the pores. That's why, in the studies, freezing temperature of -80°C and KCl as 100% of the total polymer concentration was used. The glass container was then placed in the system consisting of aluminum plate and foam, the mixture was frozen in one direction and freeze-dried for 72 hours. After cross-linking the scaffolds, KCl was allowed to leach for 12 hours at 37°C in distilled water and then freeze-dried. In bioglass containing groups, pure and borate modified BG-NPs were then added to the polymer solution at a concentration of 10% and 20% of total polymer weight and mixed for 45 minutes (50% CA, 15% PULL, 35% GEL, with total polymer concentration of 2.5%). Experiment scaffold groups prepared by this method are given in Table 11.

#### **2.4.4.2. Preparation of Three Dimensional Scaffolds by (FD/MMP) Method**

In order to obtain homogenous distribution of tubular structures in the scaffolds, a mold that has pins with 400  $\mu\text{m}$  diameter and with 400  $\mu\text{m}$  distance between them, was designed and produced by Hidronerji Company (Ostim, Ankara). In (Fig. 9a), schematic arrangement of pins on the mold is shown. The metal mold which consisted of pins with 400  $\mu\text{m}$  diameter and with 400  $\mu\text{m}$  distance between them is presented in Fig.9b&c. Homogenous distribution of tubular structures were not obtained in the prepared three-dimensional scaffolds using this mold due to closeness of the pins to each other on the mold and unequal distances between the pins. Then, a new mold that consisted of pins with 500  $\mu\text{m}$  diameter with 600  $\mu\text{m}$  distance between pins was made and all experiments were done using this new mold (Fig. 9d&e).The metal mold which consisted of pins with 400  $\mu\text{m}$  diameter and with 400  $\mu\text{m}$  distance between them is presented (Figure 9). In order to prepare the three dimensional scaffolds, firstly polymer solution was prepared in 58% acetic acid at 40°C. Pure and borate modified BG-NPs were then added to the polymer solution at a concentration of 10% and 20% of total polymer weight and mixed for 45 minutes (50% CA, 15% PULL, 35% GEL, with total polymer concentration of 5%). One experiment group, was prepared without bioglass as the control group. The mixtures were poured into petri dishes, awaited 3 hours at -80°C and freeze-dried for 40 hours (Mozafari et al., 2010). The mold was pressed onto dry scaffolds to obtain the tubular structures in the freeze-dried scaffolds.

**Table 11.** Experimental groups used for preparing the three dimensional scaffolds by using the (TIPS/PL) method.

Groups	Bioglass Percentage
Without bioglass	0
B0 - 10	10
B0 - 20	20
B7 - 10	10
B7 - 20	20
B14 - 10	10
B14 - 20	20
B21 - 10	10
B21 - 20	20

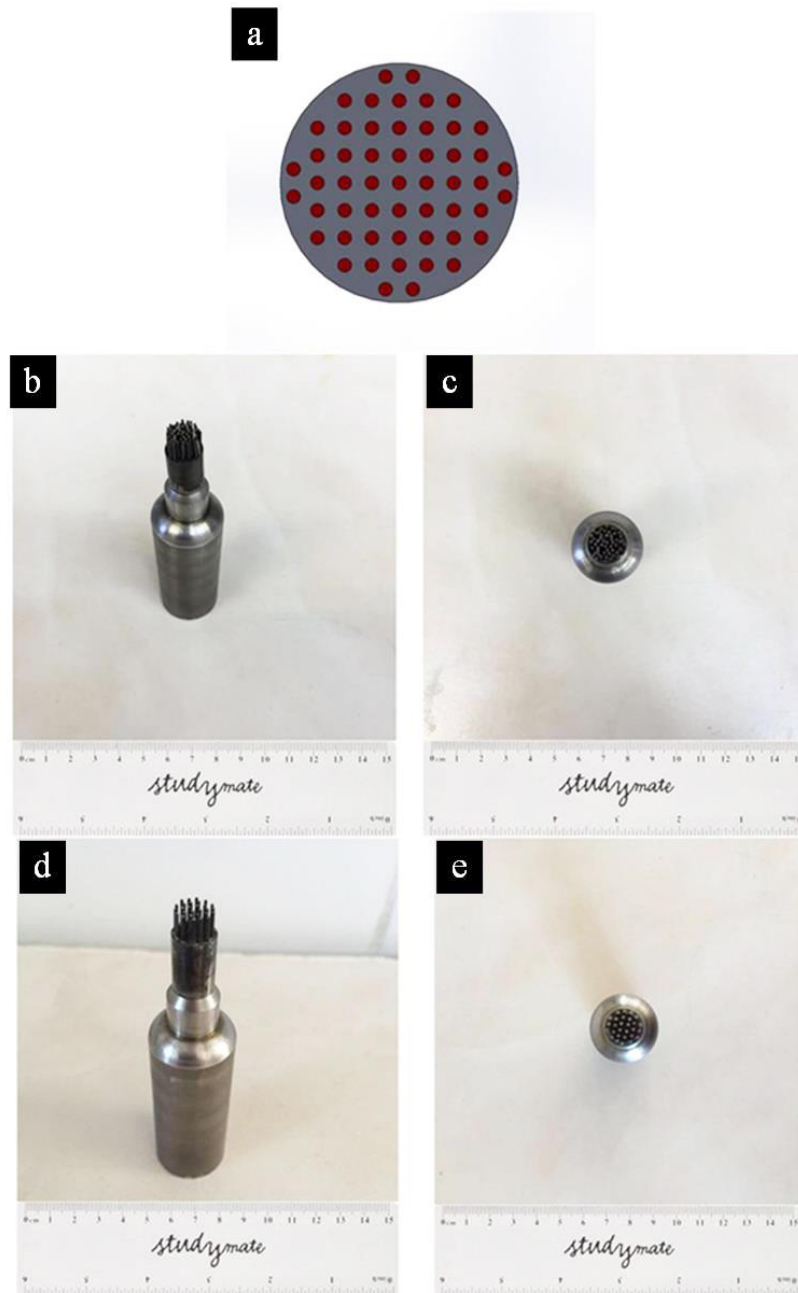


**Figure 9.** Schematic image of the metal mold consisting of pins with 400 μm diameter and distance of 400 μm between (a); Image of the designed and produced metal mold consisting of pins with 400 μm diameter and distance of 400 μm between them, side view (b); view from above (c); Image of the designed and produced metal mold consisting of pins with 500 μm diameter and distance of 600 μm between them, side view (d); view from above (e).

#### 2.4.5. Cross-linking of Three-Dimensional Scaffolds

The scaffolds prepared by the two methods were cross-linked in order to preserve their structural integrity. The CA/PULL/GEL and CA/Ox-PULL/GEL scaffolds prepared by the freeze-drying method were cross-linked by 5% glutaraldehyde solution for 25 and 50 minutes. Glutaraldehyde is used for cross-linking polymers containing hydroxyl or amine groups. The reason for the efficiency of glutaraldehyde is the high reactivity of the aldehyde groups, which form imine bonds (Schiff's base) with amino groups and acetal bonds with hydroxyl groups (Campos et al., 2013). The scaffolds prepared by the freeze-drying method and composed of CA/ Carboxyl-PULL/GEL were cross-linked with EDC/NHS by immersing in an ethanol-water mixture (8:2, v/v; pH 4.75) containing EDC 50 mmol/l and NHS 10 mmol/l for 2 and 7 hours (two groups). Then, the samples were washed with distilled water in order to remove unreacted EDC and then freeze-dried for 20 hours (Lai et al., 2012). EDC, is a carbodiimide cross-linking agent for amide bond formation between a carboxylate and an amine group. The most effective pH for carbodiimide-mediated amide formation is between pH 4.5 and 7.5. EDC is mostly used in combination with sulfo-NHS. Sulfo-NHS increase the stability of the active intermediate, which finally reacts with the amine group. Efficiency of NHS-coupled reactions is high and better yield of cross-linked product formation is obtained when comparing to EDC alone (Sinz, 2006).

Weight loss of scaffolds containing Ox-PULL and cross-linked by GTA after one month incubation was less than scaffolds containig PULL, cross-linked by GTA and Carboxyl-PULL and cross-linked with EDC/NHS in phosphate buffer solution (0.1 M, pH 7.4). Therefore, scaffolds composed of CA/Ox-PULL/GEL and prepared by the method of (TIPS/PL), were cross-linked by 5% GTA solution for 6 hours.

Scaffolds prepared by the method of (FD/MMP) were cross-linked by 5% GTA in different steps and immersed in phosphate buffer solution (0.1 M, pH 7.4) at 37°C.



According to in vitro degradation results, two steps cross-linking (before and after mold pressing) and for longer times, was more efficient for decreasing weight loss percentage of scaffolds and preserving their structural integrity. Therefore, scaffolds were immersed in 5% GTA solution for 30 minutes before mold pressing, then for 12 hours after mold pressing steps. All the time after immersion in GTA solution, in order to neutralize unreacted glutaraldehyde, the samples were immersed in the 0.2 M glycine solution for 30 minutes and then washed three times with distilled water and then, were freeze-dried for 20 hours.

#### **2.4.6. In Vitro Degradation Analysis**

The scaffolds were cut at certain sizes and weighed ( $n = 3$ ), then were placed in closed bottles. Phosphate buffer solution (PBS, pH 7.4) was then added to the bottles and incubated at 37°C in a shaking water bath. At certain time intervals, samples were taken from the bottles, excess water was removed by the help of the filter paper and their weights were recorded. After washing with distilled water, they were freeze-dried for 40 hours, weighed again and their weight loss percentage was measured according to the following formula. pH of the phosphate buffer for each measurement interval was also measured (Shahini et al., 2014).

$$\text{Weight loss (\%)} = \frac{\text{Initial dry weight} - \text{Dry weight at intervals}}{\text{Initial dry weight}} \times 100 \quad (3)$$

#### **2.4.7. Water Absorption Capacity Measurement of the Scaffolds**

Water absorption capacity of the scaffolds was measured using a general gravimetric method (Shahini et al., 2014). Samples were cut into certain sizes, weighed and

placed in closed bottles containing phosphate buffer solution (PBS; pH 7.4), and then were incubated at 37°C in a shaking water bath. At different time intervals, samples were taken from the bottles, water on the surface of scaffolds was removed by the help of the filter paper and the wet weights of scaffolds were recorded. Water absorption capacity (percentage) was determined using the following formula

$$\text{Water absorption capacity (\%)} = \frac{\text{Wet weight} - \text{Dry weight}}{\text{Dry weight}} \times 100 \quad (4)$$

#### **2.4.8. Scanning Electron Microscopy (SEM) Analysis**

Porosity and surface morphology of the scaffolds were investigated by scanning electron microscopy (SEM - Quanta 200 FEG, Netherlands) as described in Section 2.3.3.

#### **2.4.9. In Vitro Biomineralization Analysis**

The prepared scaffolds were cut into three samples with equal weights and shapes and were placed into falcon tubes containing Simulated Body Fluid (SBF) (Kokubo & Takadama, 2006) and incubated at 37°C for 14 days. Concentrations of ions present in SBF are listed in Table 12. After different incubation periods, samples were removed from SBF solution, washed 3 times with deionized water. They were then freeze-dried for 20 hours and weighed. Scaffolds were examined with SEM to investigate the apatite formation as described in Section 2.3.3.

**Table 12.** Ion concentrations in SBF solution

Ion	Ion Concentrations (mM)
Na <sup>+</sup>	142.0
K <sup>+</sup>	5.0
Mg <sup>2+</sup>	1.5
Ca <sup>2+</sup>	2.5
Cl <sup>-</sup>	147.8
HCO <sub>3</sub> <sup>-</sup>	4.2
HPO <sub>4</sub> <sup>2-</sup>	1.0

#### **2.4.10. Porosity Measurements**

The porosity of scaffolds was theoretically measured using the Archimede's principle (Tripathi & Melo, 2015). In this method, dry mass (Md) of the scaffold was recorded. The test sample was submerged under water and the submerged mass of the scaffold was recorded. The scaffold was then placed in a vacuum oven and the pressure was subjected to loading and unloading until the bubbles were removed from the samples. After removing the excess water on the surface of the wetted samples with filter paper, wet weight (Mw) of the scaffold was recorded. Triplicate samples were used for the study.

Porosity of the scaffolds was determined using the following formula:

$$\text{Porosity \%} = \frac{(M_w - M_d)}{(M_w - M_{sub})} \times 100 \quad (5)$$

where,  $M_w$  is the water saturated wet mass of the scaffold,  $M_d$  is the dry mass of the scaffold, and  $M_{sub}$  is the submerged mass of the scaffold. Mercury porosimetry was also used for porosity measurements of scaffolds that were prepared by (TIPS/PL) (Qunatochrome Cooperation, Coremaster 60). Shape of the pores were supposed to be cylindrical. Relationship between the pressure applied by the device and diameter of the pores was calculated by the Washburn equation:

$$D = (-4a \cos b) / P. \quad (6)$$

where  $P$  is the applied pressure,  $D$ : pore diameter,  $a$ : mercury surface tension (480 dyne /cm),  $b$ : contact angle between the pore wall and mercury (generally 140°) (Hu et al., 2011).

#### **2.4.11. Mechanical Tests**

Mechanical properties of the scaffolds prepared by (TIPS/PL) method. ( $n=3$ ) were studied by compression test using (Univert, Cellscale, Canada) instrument. Mechanical tests could not be performed on scaffolds prepared by the (FD/MMP) (diameter: approx. 0.6 mm) due to their small size. Stress and elastic modulus values were determined at 25% strain in the stress-strain curve (Grover et al., 2012).

## **2.5. Cell Culture Studies**

### **2.5.1. Isolation of hDPSCs**

Human third molars were collected from the patients (19–23 years of age) under the guidelines approved by the Ethic Committee of Middle East Technical University. After extraction, teeth were put into sterile chilled falcons containing 50 mL phosphate-buffered saline (PBS) and were transferred to the laboratory on ice. Teeth were first cleaned with alcohol-soaked sterile gauze and washed with sterile distilled water. Each tooth was cut around the cementum-enamel junction by using sterilized diamond disc to reveal the pulp chamber. The pulp tissue was gently separated from the crown and root with a sterile dentinal excavator and digested in a solution of collagenase type I (3 mg/ml) (Sigma) and dispase (4 mg/ml) (Sigma) for 60 minutes at 37°C. 4 ml DMEM (Gibco, Germany) supplemented with 15% (FBS, Gibco, Germany) was added to stop the enzymatic digestion and centrifuged at 1800 rpm for 5 minutes. Cells were washed twice with sterile PBS 1X and centrifuged again for 5 minutes at 1800 rpm. Cells were then cultured in 10% FBS containing DMEM at 37°C in a carbon dioxide incubator (Atari et al., 2011).

### **2.5.2. Characterization of Human DPSCs**

In order to verify mesenchymal stromal phenotype of the isolated stem cells from human third molar teeth, flow cytometry analysis was conducted at METU Biomaterials and Tissue Engineering Center of Excellence (BIOMATEN). For this purpose, third passage DPSCs were used. After trypsinization, cells were washed with FACS buffer and fixed by 4% paraformaldehyde for 15 minutes. Monoclonal antibodies against CD31, CD44, CD73, CD90, CD105 (mouse anti-human) and

CD45 (rabbit anti-human) were obtained from cell signaling (USA). Cells ( $1 \times 10^6$ ) were incubated with the mentioned primary antibodies and appropriate isotype controls in dark for 30 minutes as stated in the manufacturer's instructions. After washing with FACS buffer, cells were incubated with secondary antibodies (anti mouse Alexa Fluor® 488-conjugated, anti-rabbit Alexa Fluor® 647 conjugated) cell signaling (USA) for 30 minutes in dark. After washing, cells were suspended in 300  $\mu$ l PBS and then were analyzed using flow cytometry data acquisition and analysis software (Accuri™ C6, BD Biosciences, Germany) (Alipour et al., 2010).

### **2.5.3. In Vitro Cytotoxicity Assessment of Pure and Borate Modified BG-NPs**

In vitro cytotoxicity test of pure and borate modified BG-NPs was performed using DPSCs by indirect contact method according to (ISO/EN) 10993-5 guideline. Obtained materials were sterilized by dry heating sterilization at 200 °C for 2 h and extracts were prepared by incubating 50 mg of BG in 1 ml serum-free DMEM culture medium at 37 °C for 24h. The extract solution was further diluted to different concentrations (25, 12.5, 6.25 and 3.125 mg/ml) using same culture medium. DPSCs were cultured in 96 well plate at a density of  $5 \times 10^3$  cells/well. 24h post seeding, 100  $\mu$ l of diluted extracts and 100  $\mu$ l of DMEM (with 10% FBS) were added as culture media and cells were incubated at 37°C in a carbon dioxide incubator for one week. MTT assay was used to evaluate the metabolic activity of cells at different incubation periods. At each time point cells were incubated in a mixture containing 10  $\mu$ l MTT working solution (5 mg/ml in DMEM) and 90  $\mu$ l of DMEM without phenol red (n=4) at 37 °C for 4 h. At the end of incubation period supernatant was removed and replaced with 100  $\mu$ l dimethylsulphoxide (DMSO) (Merck) in order to dissolve formazan crystals formed inside cells. After 15 min of slow shaking, the optical density was measured at 570 nm. Stem cells cultured only with cell culture medium supplemented with 10% FBS were used as control group (Zheng et al., 2016).

#### **2.5.4. Evaluation of Effect of Pure and Borate Modified BG-NPs on Differentiation of Dental Pulp Stem Cells**

Effect of pure and borate modified BG-NPs on odontogenic differentiation of DPSCs was evaluated by measuring ALP enzyme activity test as an early marker of odontogenic differentiation and immunohistochemical staining for dentin sialoprotein (DSP), osteopontin ve collagen type I. Effect of different bioactive glasses on odontogenic differentiation was investigated using the bioglass concentration (6.25 mg/ml) determined by the cytotoxicity tests.

##### **2.5.4.1. Measurement of Alkaline Phosphatase (ALP) Enzyme Activity and Intracellular Calcium Amounts of DPSCs**

ALP activity and intracellular calcium amounts of DPSCs that were cultured with the BG extracts were measured to study the effect of pure and borate modified BG-NPs on odontogenic differentiation of these stem cells. DPSCs cells at passage 3 were seeded on 24-well plates at an initial density of  $7.5 \times 10^3$  cells/well. After 24 h of incubation, the medium was changed with extract medium obtained with 6.25 mg/ml pure and borate modified BG-NPs. Supplements were added to extract medium to have a final concentration of 10% FBS, 1% penicillin-streptomycin, 50  $\mu$ g/ml ascorbic acid, 10 mM  $\beta$ -glycerophosphate, and 10 nM dexamethasone. Addition of supplements was done to obtain an odontogenic differentiation medium (Taşlı et al., 2013). Cells were incubated in this medium for 14 days and each medium change was done with this modified extract medium. As control group, DPSCs cultured with only odontogenic medium were used. Cells were washed with PBS and were lysed by incubating in lysis buffer (0.1% Triton X-100, 0.1% (w/v) sodium azide, and  $10^{-4}$  M protease cocktail in PBS), at 37°C for 1 h while shaking at 150 rpm 7 and 14 days after incubation. 75  $\mu$ l of p-nitrophenyl phosphate (pNPP) substrate solution and 25

$\mu\text{l}$  of  $\text{MgCl}_2$  solution were added to 75  $\mu\text{l}$  of lysate in a 96 well-plate, and the plates were incubated at 37 °C for 1 h while shaking at 150 rpm. Absorbance was measured at 405 nm on a plate reader ( $\mu\text{Quant}^{\text{TM}}$  microplate spectrophotometer, Biotek Instruments Inc., USA). A calibration curve was constructed using p-nitrophenol to determine p-nitrophenol produced. Protein concentration of the cell lysates was measured by bicinchoninic acid (BCA) assay. A calibration curve constructed using different concentrations of bovine serum albumin (BSA) was used to determine the protein amount in the cell lysates. The enzyme activity was expressed in terms of specific enzyme activity ( $\mu\text{M}/\text{mg}$  protein/minute). For measurement of intracellular calcium amount, 25  $\mu\text{l}$  of the lysate was mixed with 225  $\mu\text{l}$  0.1 M HCl in eppendorfs and 25  $\mu\text{l}$  of the obtained mixture was added to 120  $\mu\text{l}$  o-cresolphalein complexone, 8-hydroxyquinone-5-sulfonic acid and 2-amino-2-methyl-1,3-prandiol in the wells of 96-well plate. After shaking at 100 rpm, the absorbance was read at 560 nm. Calcium chloride was used as standard to construct the calibration curve for determining intracellular calcium amounts. Intracellular calcium amount was expressed in terms of g Ca/g Protein.

### **2.5.5. Immunohistochemical Staining**

Dental Pulp Stem Cells (DPSCs) at passage 3 were seeded on 24-well plates. DPSCs were cultured with odontogenic differentiation medium (DMEM containing 10% FBS, 1% penicillin-streptomycin, 50  $\mu\text{g}/\text{ml}$  ascorbic acid, 10 mM  $\beta$  - glycerophosphate, and  $10^{-7}$  M dexamethasone) (Taşlı et al, 2013) prepared with DMEM extracts of 6.25 mg/ml of pure and borate modified BG-NPs, at 37°C for 14 days. BG extracts were used for all medium changes. As a control group, DPSCs cultured with odontogenic medium without addition of BG extracts were used. After 14 days of incubation, cells were fixed with paraformaldehyde (4%) for 10 min at room temperature. After fixation the cells were permeabilized with Triton X-100 (0.1% in PBS for 5 min) and saturated with blocking buffer (PBS containing 3%



BSA) for 30 min. Cells were incubated for 1 h at room temperature with different primary antibodies [Anti-Collagen I antibody (abcam, Britain), Anti-dentin sialophosphoprotein (DSPP) antibody (abcam, Britain), Anti-Osteopontin antibody (Abcam, England) followed by 1 h incubation with the secondary antibody [Donkey anti-Rabbit IgG H&L (DyLight® 488) (Abcam, Britain)] in the dark. Nuclei of the cells were stained for 5 minutes with 1 µg/ml 40-6-diamidino-2-phenylindole (DAPI; Sigma). Labelled cells were observed and photographed using a fluorescent microscope (Zeiss axio observer z1, Germany) (Navabazam et al., 2013).

#### **2.5.6. Cell Viability Assays**

For cell viability assessment on the scaffolds, they were sterilized with UV and hDPSCs were seeded on scaffolds at an initial seeding density of  $7.5 \times 10^3$ /scaffold. Viability of hDPSCs on the scaffolds was determined by Alamar Blue Assay (Invitrogen, USA) at the end of 1, 4, 7, and 14 days of incubations (Mishra et al., 2011). Alamar Blue, or 7-hydroxy-3H-phenoxazine-3-one 10-oxetine, is an indicator for showing cells viability as its chemical reduction occurs by inner metabolic activities of cells (O'brien et al., 2000). As the indicator dye is reduced, it changes from non-fluorescent blue to the fluorescent pink. For Alamar Blue assay, the medium was removed and the cells were washed with PBS (0.1 M, pH 7.22). 10% Alamar blue solution (10 % alamar blue & 90 % DMEM without phenol red) was added to each well and incubated at dark for 4 hours. The optical densities of reduced solutions were obtained at 570 nm and 600 nm via microplate spectrophotometer (µQuant™, Biotek Instruments Inc., USA) using the ELISA software programme (Atlanta, USA) and recorded (Li et al., 2005).

### **2.5.7. Measurement of ALP Activity and Intracellular Calcium Amounts of hDPSCs Seeded on Scaffolds**

After seeding  $4 \times 10^4$  hDPSCs on scaffolds prepared, cells were cultured in odontogenic differentiation medium (DMEM containing 10% FBS, 1% penicillin-streptomycin, 50  $\mu\text{g/ml}$  ascorbic acid, 10 mM  $\beta$ -glycerophosphate, and 10 nM dexamethasone) for 14 days. ALP activity of cells was measured after 7 and 14 days of incubation at 37°C in a carbon dioxide incubator. At each time, cells on scaffolds were lysed. Scaffolds were first kept for 10 minutes at -80°C and then for 10 minutes at 37°C. The same steps were repeated by adding PBS on the scaffolds. After this step, ALP activity of cells and intracellular calcium amounts were measured according to Section 2.5.4.1. The total DNA content of the cells was determined by Hoechst 33258 staining followed by fluorometric absorbance measurements. Before Hoechst 33258 staining, lysates were dispersed in a 1:5 volume ratio in: 10 mM Tris aminomethane, 1 mM ethylenediamine tetraacetic acid and 100 mM sodium chloride solution (TNE buffer solution, pH 7.5). Calibration curve for DNA determination was constructed with the bovine thymus DNA solution (0-500 ng DNA/ml) prepared in different concentrations in the TNE buffer solution. The enzyme activity of the cells was given as the specific enzyme activity (mol/g DNA/min).

### **2.5.8. Immunohistochemical and Histological Analysis of hDPSCs Seeded Scaffolds**

After seeding  $4 \times 10^4$  hDPSCs on scaffolds, cells were incubated for 14 days in odontogenic differentiation medium (DMEM containing 10% FBS, 1% penicillin-streptomycin, 50  $\mu\text{g/ml}$  ascorbic acid, 10 mM  $\beta$ -glycerophosphate, and 10 nM dexamethasone). After 7 and 14 days of incubation histological and immunohistochemical stainings were done to evaluate the odontogenic

differentiation of hDPSCs in scaffolds and formation of dentin-like hard tissue. For histological analysis, DPSCs seeded scaffolds were washed with PBS and fixed with 4% paraformaldehyde solution overnight. After fixation, cells on scaffolds were dehydrated in ethanol and then the scaffolds were embedded in paraffin. After obtaining 5  $\mu\text{m}$  thick sections from the paraffin blocks, Von Kossa staining was done to examine calcium deposition by the cells. After sections were deparaffinized, they were washed with distilled water, covered with 1% silver nitrate solution and exposed to ultraviolet light for 2 hours. The sections were then washed with distilled water, covered with 2.5% sodium thiosulphate and incubated for 5 min. After this step, sections were washed with distilled water again, counterstained with Nuclear Red Fast for 5 min. After counterstaining, sections were then washed with distilled water, dehydrated in alcohol series, immersed in xylene, and covered with coverslip. After deparaffinizing the sections, immunohistochemical staining was done for DSPP, osteopontin and collagen type I markers according to Section 2.5.5.

## **2.6. Statistical Analysis**

Statistical analysis of the data was done with one-way analysis of variance (ANOVA) with Tukey's post hoc test for multiple comparisons using SPSS software (ver. 23.0; IBM Corporation, NY, USA). Differences were considered significant at  $p \leq 0.05$ . The results were expressed as mean  $\pm$  standard deviation (Xynos et al., 2000).



## CHAPTER 3

### 3. RESULTS AND DISCUSSION

#### 3.1. Characterization of the Synthesized BG-NPs

##### 3.1.1. Scanning Electron Microscopy (SEM) Analysis

###### 3.1.1.1. Combination of Sol-Gel and Co-Precipitation Methods

The morphology and particle size of BG and borate modified BGs synthesized by combination of sol-gel and co-precipitation methods, were analyzed by SEM examination (Fig. 10). They all had spherical shape of similar size ranging from between 70 and 120 nm.

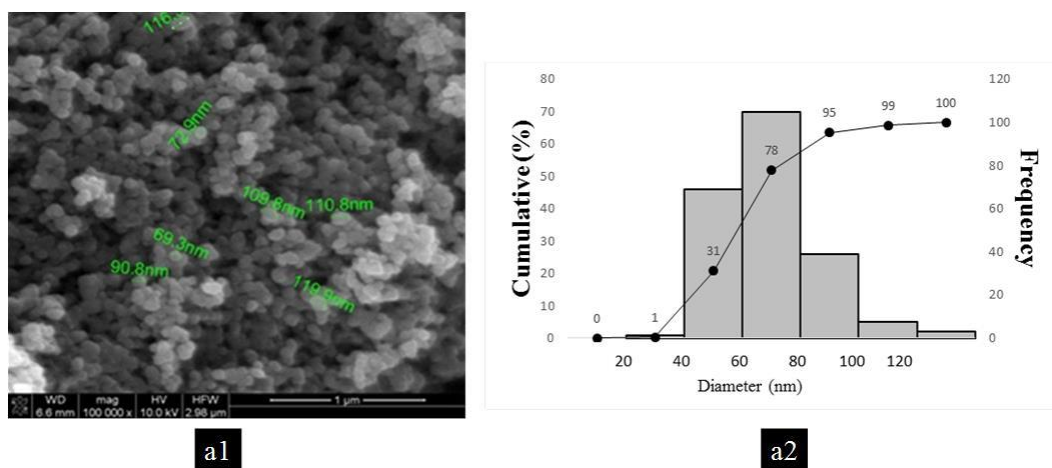


**Figure 10.** SEM image and particle size distribution curve of B0-BG synthesized by combination of sol-gel and co-precipitation methods.

### 3.1.1.2. Quick Alkali-Mediated Sol-Gel Method

Morphology and particle size of BG and borate modified BG materials synthesized by the quick alkali-mediated sol-gel method, were analyzed by SEM examination (Fig. 11a-d). All of the BG and modified BG particles were spherical or close to spherical shape with different sizes. Size of the BG particles became larger with the addition of borate. This expansion in particle size could be due to slower gelation rate for borate modified BG materials compared to bare BG. During synthesis of borate modified BG materials, boric acid addition resulted in more acidic pH and hence, gelation through ammonia addition into the acid sol took longer time compared to BG group. It was also reported that slower gelation rate enhanced growth of colloidal particles (El-Kady et al., 2010).

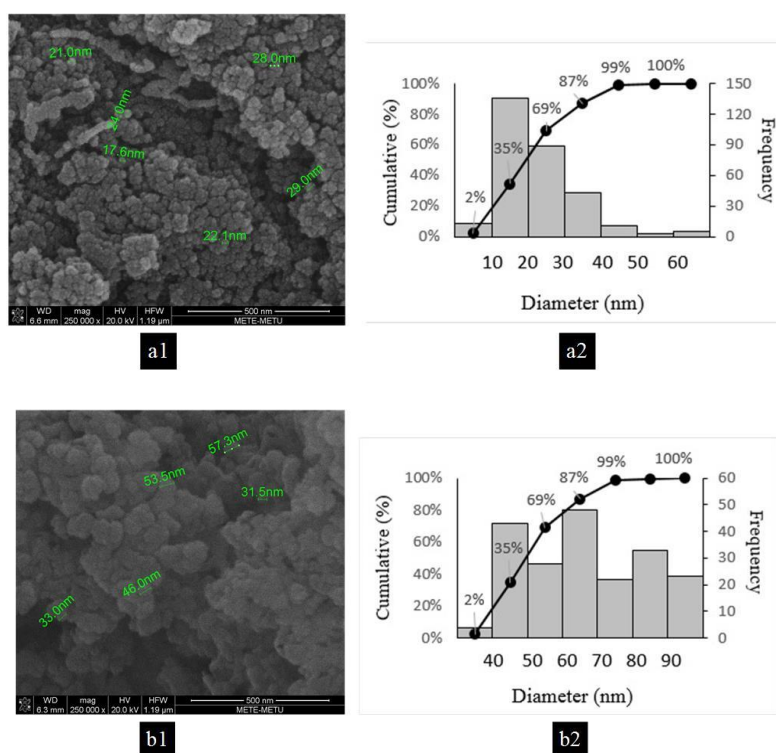
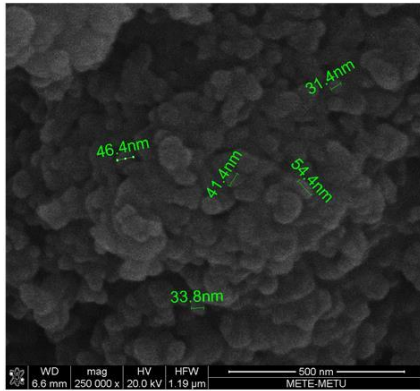
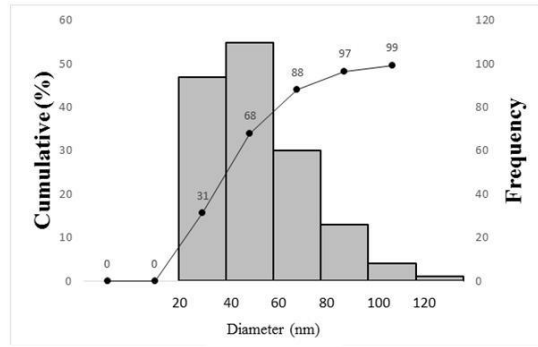


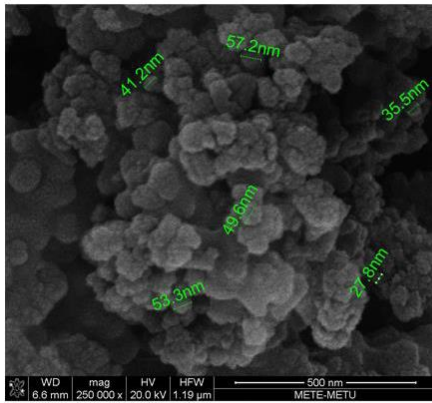
**Figure 11.** SEM images and particle size distribution curves of a) B0-BG, b) B7-BG, synthesized by the quick alkali-mediated sol-gel method.



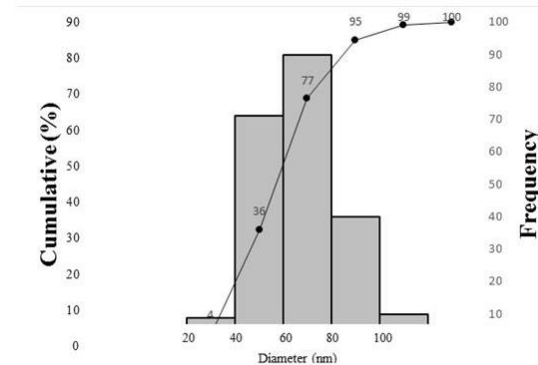
c1



c2



d1



d2

**Figure 11 - Continued.** SEM images and particle size distribution curves of c) B14-BG, d) B21-BG synthesized by the quick alkali-mediated sol-gel method.

### **3.1.2. X-Ray Diffraction (XRD) Analysis**

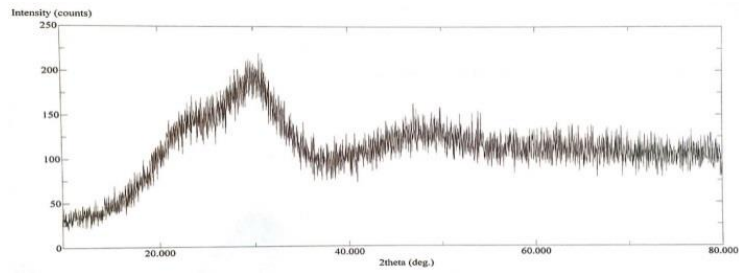
#### **3.1.2.1. Combination of Sol-Gel and Co-Precipitation Methods**

Phase analysis of synthesized B0-BG and borate modified glass nanoparticles synthesized by the combination of sol-gel and co-precipitation methods, was done by XRD analysis to reveal the amorphous/crystalline phases (Fig. 12a-c). A broad dispersive band was observed for the XRD spectra of B0-BG and B7-BG (Fig. 12a&b) indicating the amorphous nature of the synthesized bioactive glass. In Fig.12c XRD spectra of B14-BG nanoparticles, a broad dispersive band and some other peaks are seen. The broad dispersive band is related to the amorphous structure of bioactive glass, while the sharp peaks show crystalline regions in the structure (Luz & Mano, 2011). Bioactive glasses with higher crystallinity, degrade in body fluid slowly. Therefore this type of bioglass is less bioactive (Kongsuwan et al., 2015).

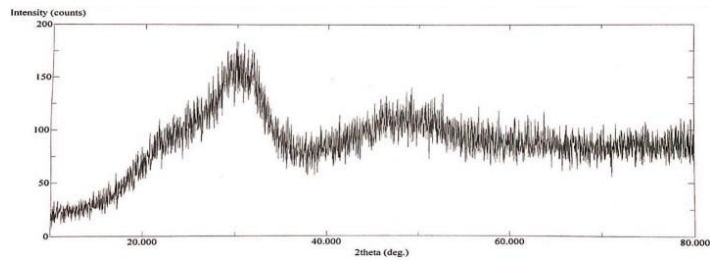
#### **3.1.2.2. Quick Alkali-Mediated Sol-Gel Method**

In order to assess the crystalline/amorphous structure of BG, XRD patterns of B0-BG and borate modified BGs synthesized by the quick alkali-mediated sol-gel method, were investigated (Fig. 13a-d). The spectra of BGs contained only a weak peak located at  $2\theta=31.75^\circ$  which was attributed to calcium silicate ( $\text{Ca}_2\text{SiO}_4$ ) (JCPDS # 29- 0369) and there were no distinct peaks demonstrating the presence of a crystalline phase, henceforth approving the amorphous nature of the prepared BGs. Furthermore, crystallization of BG is known to occur at a temperature around  $800^\circ\text{C}$  and above (Goh et al., 2014b). XRD patterns of all borate modified BG materials showed an increase in the broadening range of the main diffraction peak of BG,

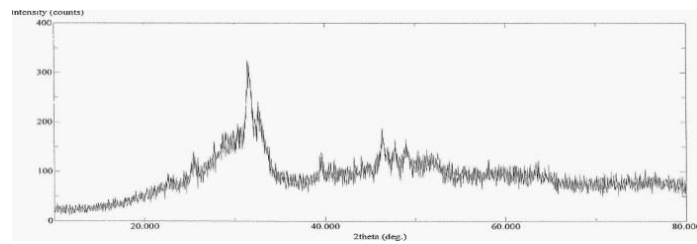




a)



b)



c)

**Figure 12.** XRD spectra of synthesized a) B0-BG, b) B7-BG, c) B14-BG synthesized by combination of sol-gel and co-precipitation methods.

Balasubramanian et al. (Balasubramanian et al., 2016). They synthesized two different BGs with five compositions. All compositions presented broad peaks and distinct peaks related to a crystalline phase were not detected. Gorustovich et al. prepared melt-derived glasses from a base 45S5 bioactive glass and added 2 wt% of boron oxide to obtain (45S5.2B) composition. Their XRD results showed the presence of amorphous structure in both 45S5 and (45S5.2B) bioactive glasses (Gorustovich et al., 2006). Laczka and colleagues modified bioactive glass-ceramic

material with a formula of 40% SiO<sub>2</sub>, 54% CaO, 6% mol P<sub>2</sub>O<sub>5</sub> by mole percentages by adding 5% mole boron using the sol-gel method. While unmodified bioactive glass had an amorphous structure, boron modification resulted in formation of a crystalline phase, but with a low degree of crystallization (Laczka et al., 2000). Yang and colleagues synthesized NBG with the formula of 60.68% SiO<sub>2</sub>, 38.83% CaO, 3.49% P<sub>2</sub>O<sub>5</sub> by mole percentages with 10% and 20% of boron modification through sol-gel process and calcined at 600°C. According to their XRD result, the group without incorporation of boron, represented amorphous phase, but groups with B<sub>2</sub>O<sub>3</sub> addition, showed minor crystallites (Yang et al., 2012).

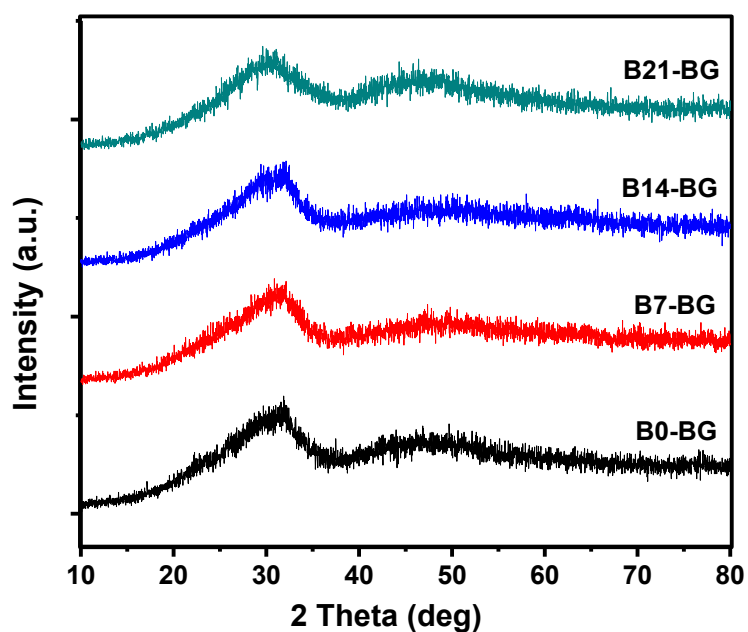


**Figure 13.** XRD spectra of synthesized B0-BG, B7-BG, B14-BG, B21-BG synthesized by the quick alkali-mediated sol-gel method.

### **3.1.3. Inductively Coupled Plasma Mass Spectrometry (ICP-MS) Analysis**

#### **3.1.3.1. Combination of Sol-Gel and Co-Precipitation Methods**

Chemical composition of BG and borate modified BGs synthesized by combination of sol-gel and co-precipitation methods, were obtained from ICP analysis and results are summarized in Table 13. According to the results of ICP-MS analysis, compositions of the BG nanoparticles were not very close to their theoretical compositions and only in B7-BG, mole percentages of SiO<sub>2</sub>, and CaO, were consistent with the theoretical compositions. B<sub>2</sub>O<sub>3</sub> mole percentage, in B7-BG composition was about half of the expected molar percentage, and in B14-BG its composition, was found to be lower than the expected mole percentage. As a result of the rapid gelation and precipitation, composition of multi-component glasses, may show differences from the designed composition (Roohani-Esfahani et al., 2012). Isaac and colleagues (2011), investigated the in vitro effect of a new Sr-doped bioactive glass manufactured by the sol-gel method on osteoblast viability and differentiation. According to result of ICP-AES analysis, composition of the as-prepared bioactive glass was very close to the theoretical composition (Isaac et al., 2011).

**Table 13.** Chemical composition of BG and borate modified BG materials obtained with ICP-MS.

Sample ID	Reactants (Mole %)			
	SiO <sub>2</sub>	CaO	P <sub>2</sub> O <sub>5</sub>	B <sub>2</sub> O <sub>3</sub>
B0-BG	62.2 (58)	30 (38)	7.9 (4)	0
B7-BG	50 (51)	37 (38)	9.7 (4)	3.1 (7)
B14-BG	36.2 (44)	54 (38)	9.1 (4)	0.6 (14)

Values in the parentheses, belong to the theoretical compositions of BGs

### 3.1.3.2. Quick Alkali-Mediated Sol-Gel Method

Chemical composition of BG and borate modified BG materials synthesized by the quick alkali-mediated sol-gel method, was obtained from ICP analysis, and results are summarized in Table 14. ICP-MS analysis of all samples exhibited that the borate doping was successful and the amount of B<sub>2</sub>O<sub>3</sub> present in the materials was in good agreement with the theoretical values.

**Table 14.** Chemical composition of BG and borate modified BG materials obtained with ICP-MS.

Sample ID	Reactants (Mole %)			
	SiO <sub>2</sub>	CaO	P <sub>2</sub> O <sub>5</sub>	B <sub>2</sub> O <sub>3</sub>
B0-BG	62.55 (58)	35.6 (38)	1.85 (4)	-
B7-BG	53.1 (51)	39.4 (38)	1.3 (4)	5.9 (7)
B14-BG	47.74 (44)	36.16 (38)	1.12 (4)	13 (14)
B21-BG	39.58 (37)	39.66 (38)	1.28 (4)	20.22 (21)

Values in the parentheses, belong to the theoretical compositions of BGs.

According to ICP-MS results, synthesis of BGs by the quick alkali-mediated sol-gel method, was more successful than the synthesis by the combination of sol-gel and co-precipitation methods. For this reason, quick alkali-mediated method was used for the synthesis of BGs for the rest of thesis.

#### 3.1.4. Fourier Transform Infrared Spectroscopy (FTIR) Analysis

FTIR spectra of BG and borate modified BG materials revealed characteristic peaks related to Si-O-Si (Fig. 14). These spectra exhibited broad absorption band located around 950-1100 cm<sup>-1</sup> assigned to the Si-O-Si asymmetric stretching (Goh et al., 2014b). The weak band at 925 cm<sup>-1</sup> was suggested to be due to either Si-O-Ca or non-bridging oxygen (NBO) (Aguiar et al., 2008, Goh et al., 2014a). The absorption

peak determined at  $473\text{ cm}^{-1}$  was attributed to O-P-O antisymmetric stretching. Other two absorption peaks observed at  $709$  and  $1358\text{ cm}^{-1}$  were related to the bending of B-O-B linkage and B-O stretching vibrations of  $\text{BO}_3$  units, respectively (Zhou et al., 2014, Pal et al., 2011). Besides this, the presence of absorption bands at  $1730\text{ cm}^{-1}$  in the FTIR spectra of all samples confirmed the hygroscopic nature of the silicate glass and this absorption band was related to the bending vibration modes of O-H groups (Goh et al., 2014b). Furthermore, absorption band related to carbonate group was also detected around  $1220\text{ cm}^{-1}$ , which might be due to the absorbed  $\text{CO}_2$  during the preparation process.

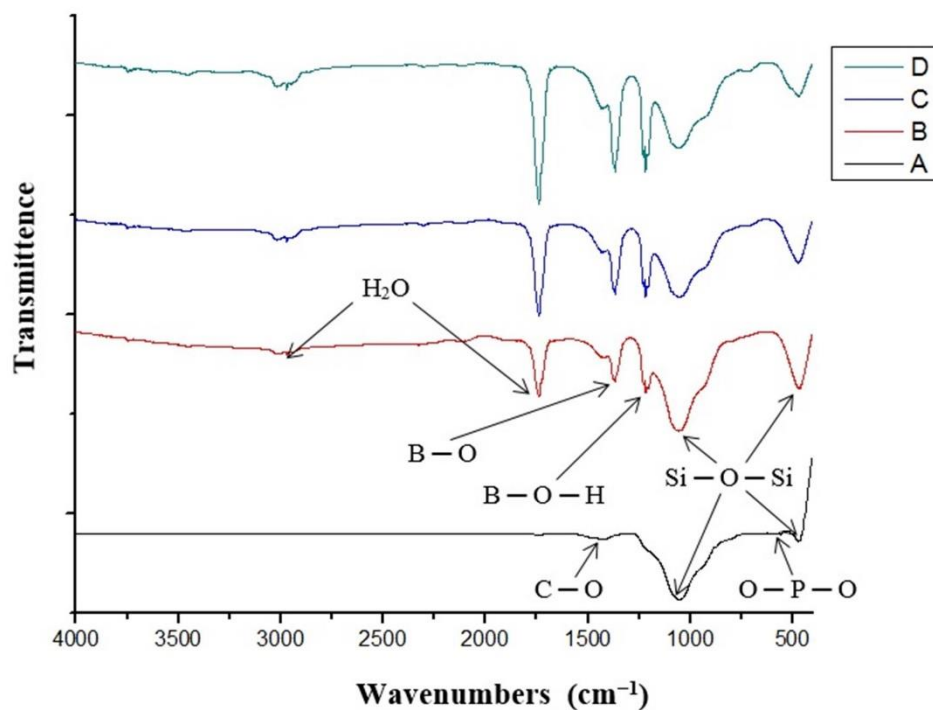


**Figure 14.** FTIR spectra of different compositions of BG-NPs, A) B0-BG, B) B7-BG, C) B14-BG, D) B21-BG, respectively. All samples were calcined at  $600^\circ\text{C}$  for 2 h.

### 3.1.5. Fourier Transform Raman (FT-Raman) Spectroscopy

FT-Raman analysis results of different compositions of BG-NPs are presented in (Fig. 15). FT-Raman spectrum of B0-BG showed a wide absorption band at about  $1087\text{ cm}^{-1}$ , which is related to the asymmetric stretching mode of Si-O-Si bonds (González et al., 2003). A characteristic peak of  $\text{SiO}_4^{4-}$  group was observed at  $850\text{ cm}^{-1}$ . In addition, the spectrum showed peaks of symmetric stretching of  $\text{PO}_4^{3-}$  groups at  $960\text{ cm}^{-1}$  (Tousi et al., 2013). The FT-Raman spectra of B7-BG, B14-BG, B21-BG also showed a peak at around  $1065\text{ cm}^{-1}$ , which was believed to be the result of overlapping of characteristic vibration of  $\text{B}_2\text{O}_3$  groups and asymmetric stretching mode of Si-O-Si bonds (Kamitsos et al., 1987). Overlapping of symmetric stretching of  $\text{PO}_4^{3-}$  groups and a bond of  $\text{BO}_3^{3-}$  group was also seen at  $960\text{ cm}^{-1}$  (He et al., 2014). This peak became more expanded as the borate amount in the composition increased. In comparison to FTIR results, peaks related to phosphate groups were evident in FT-Raman spectra of all compositions.

### 3.1.6. Porosimetry Analysis

Specific surface area, average pore diameter and total pore volume of samples measured by BET and BJH analyses are summarized in Table 15. Results suggested that pores were mesoporous (Wu & Chang, 2012). With increase of  $\text{B}_2\text{O}_3$  content from 0% to 21%, the specific surface area and pore volume decreased. This could be due to increase in BG particle size with borate incorporation (Lei et al., 2012). Bioactivity and cytocompatibility of BGs are greatly affected by decrease in the size or increase in specific surface area (Ostomel et al., 2006).  $\text{N}_2$  adsorption-desorption isotherms of the synthesized BG-NPs are presented in (Fig. 16). All of the isotherms

corresponded to type III isotherm curve and also indicated mesoporous structure of the samples (Manda et al., 2012).

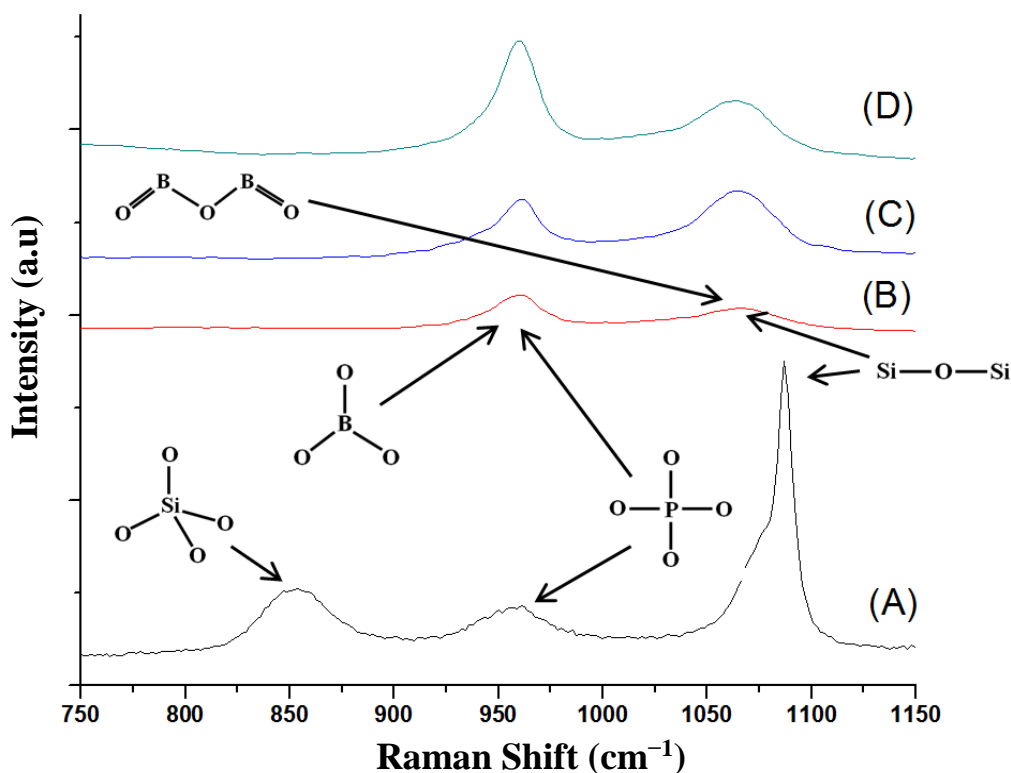


**Figure 15.** FT-Raman spectra of different compositions of BG-NPs, A) B0-BG, B) B7-BG, C) B14-BG, D) B21-BG, respectively. All samples were calcined at 600 °C for 2 h.

### 3.1.7. In Vitro Bioactivity Tests

After 14 days of immersion in SBF medium, release of Si, Ca<sup>2+</sup> and B ions from the BG and borate modified BG was measured, as shown in (Fig. 17a-c). Release profile of Si ion is considered as an indicator for the glass network dissolution. An initial burst release of Si ion was detected at day 1 followed by a sustained release until day 14. Observed release profile could be either due to precipitation of insoluble salts incorporating Si or attributed to the newly formed apatite that creates a diffusion



barrier, thus causing decrease in release of Si (Sarin et al., 2016). Same trend was observed with calcium ion release, as shown in (Fig. 17b). Generally, higher Si and Ca concentrations are expected to be released from borate modified BG materials when compared to pure BG which can be explained with the weaker glass structure caused through B<sub>2</sub>O<sub>3</sub> substitution (Lepry & Nazhat, 2015). (Fig. 17c) shows the release profile of B ion, the release of B ion increased gradually as immersion time increased. A maximum release of 249 mg/L was observed for B21-BG. The change in pH of SBF over 14 days upon immersion of B0-BG and borate modified BG samples is shown in (Fig. 17d). It was observed that pH of SBF in all groups increased gradually over 14 days of immersion which could be due to the ionic exchange between surface Ca<sup>2+</sup> ions with the H<sup>+</sup> ions from the SBF (Nandi et al., 2016a).

**Table 15.** BET and BJH analyses results of BG and B<sub>2</sub>O<sub>3</sub> modified BGs.

<b>Sample ID</b>	<b>Surface Area (m<sup>2</sup>/g)</b>	<b>Pore Volume (cc/g)</b>	<b>Pore Size (Å)</b>	<b>Average Nanoparticle Size (nm)</b>
B0-BG	197	0.529	66	23.6
B7-BG	83	0.299	14.7	44.3
B14-BG	46	0.369	14.8	41.5
B21-BG	42	0.141	22.4	44.1

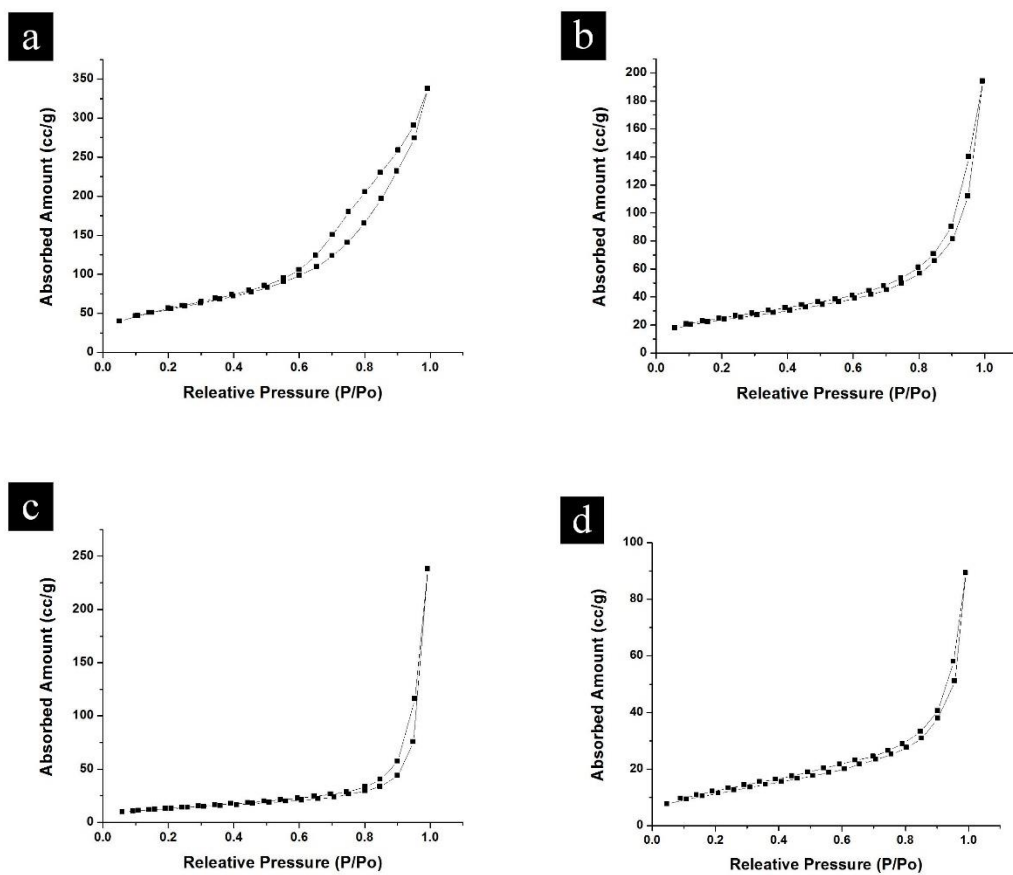


**Figure 16.**  $N_2$  adsorption-desorption isotherm of synthesized a) B0-BG, b) B7-BG, c) B14-BG, d) B21-BG synthesized by the quick alkali-mediated sol-gel method.

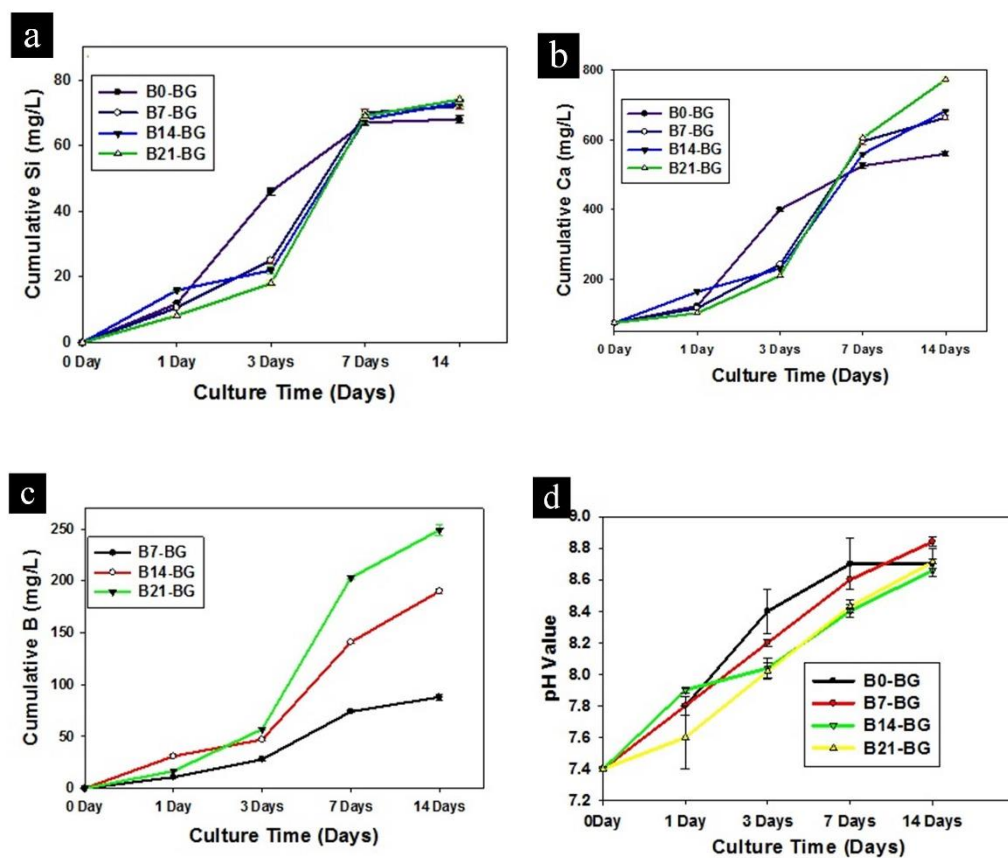


**Figure 17.** SBF incubation studies for B0-BG and borate modified BG; Release of a) Si ion, b)  $\text{Ca}^{+2}$  ion, c) B ion, and d) changes in pH of SBF with time groups.

Bioactivity test conducted in SBF is a known protocol for examining the ability of biomaterials to establish a bond with human hard tissue. The spontaneous growth of bone-like apatite nuclei on the surface of biomaterials upon immersion in SBF enables the material to make direct connection with living human bone cells. The surface morphology of borate modified BG nanoparticles after soaking in SBF for various days is shown in (Fig. 18). After 3 days of immersion in SBF, a few spherical particles were observed on some parts of the disc surfaces of all groups. Highest deposition was observed in the B21-BG group. Increase of  $\text{B}_2\text{O}_3$  content positively affected the bioactivity of BG where the composition was in the range of glass network modifier (Ciceo et al., 2014). When the incubation period was prolonged to

7 days, the surface of discs was completely covered with spherical apatite particles. After immersion of BG discs into SBF solution, firstly calcium ion undergoes ionic exchange with  $H^+$  of SBF leading to the formation of silanol ( $Si-OH$ ) on the surface of disc, followed by polymerization of silanol groups to produce amorphous silica gel. Calcium and phosphorous underwent ionic migration from SBF to discs' surface and they were transformed into amorphous calcium phosphate which act as a template for consequent precipitation of crystalline apatite (Goh et al., 2014b).

Chemical composition of formed apatite layer was analyzed via energy dispersive X-ray s (EDX) analysis and the results are given in (Table 16). Calcium, phosphate and oxygen were the main ions that were detected in the layer formed, which were calcium phosphate in nature. Ca/P ratios of the apatite layer formed by borate modified groups at day 3, and that of B21-BG group at day 14 were close to Ca/P ratio of stoichiometric hydroxyapatite (1.67) (Adams & Essien, 2015). Ca/P ratios of the precipitates observed in other groups were in the range of 1.83 to 1.92, which belong to other phases of calcium phosphates present in the body (Paiva et al., 2006). Positive effect of borate ions on the bioactivity of silicate BGs was achieved only by replacing an appropriate amount of  $SiO_2$  with  $B_2O_3$ , because of its function as glass network modifier (Maheswaran et al., 2014). As  $B_2O_3$  content increases in glasses, glass network weakens and opens easily, which results in higher ion exchange with SBF (Tainio et al., 2017).

## **3.2. Preparation of Three Dimensional CA/PULL/GEL Scaffolds**

### **3.2.1. Determination of Oxidation Degree of Oxidized PULL and Degree of Substitution of Carboxyl Groups of Carboxylated PULL**

PULL is highly soluble in water. For this reason, its cross-linking is necessary to maintain structural stability of the 3D scaffolds. Carbonyl groups in the chemical structure of PULL were formed by periodate oxidation in order to cross-link with gultaraldehyde. Measurement of oxidation degree of polymers is important in order to assess efficiency of cross-linking (Su et al., 2010). Oxidation degree of oxidized PULL was determined as  $56.45 \pm 1.85\%$  (n=2). This result is consistent with results of similarworks. In one study, sodium alginate was oxidized with different amounts of sodium metaperiodate and its oxidation degree was measured by the titration method. Oxidation degree was determined as  $57.5 \pm 0.2 \%$  (Balakrishnan et al., 2014). In another work, periodate-oxidization of sodium alginate was done in order to obtain oxidized sodium alginate and for evaluation of the degree of oxidation, iodometry method was used. Oxidation degree was measured as 54% (Wei et al., 2016). Higher degree of oxidation in periodate oxidized polysaccharides, leads to higher degrees of cross-linking (Durán et al., 2016). As a result, there will be a better control over degradation rate of the scaffolds incorporating oxidized polysaccharides (Bruneel & Schacht, 1995, Su et al., 2010). Degree of substitution of carboxylated PULL was measured as 0.13 by the titrimetric method. In one study, xanthan was carboxymethylated to obtain carboxymethyl xanthan and the degree of substitution was measured to be 0.35 and 4.38 in two different groups (Mendes et al., 2012).

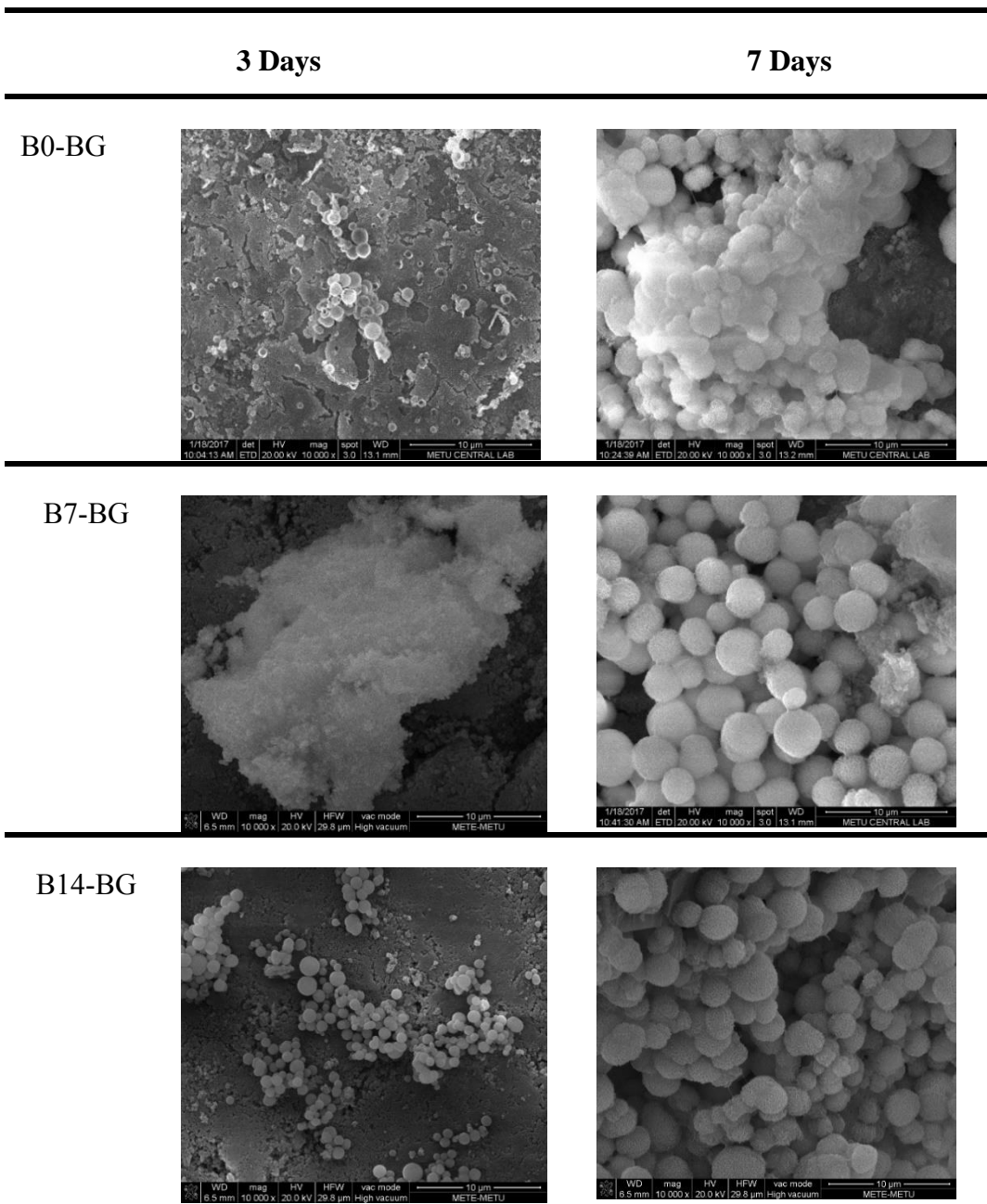


**Figure 18.** SEM images of B0-BG and borate modified BG samples after soaking in SBF for various periods of time.

B21-BG

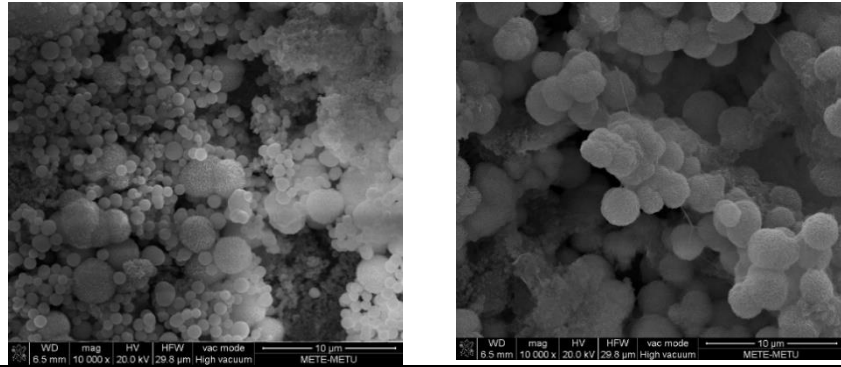


**Figure 18 - Continued.** SEM images of B0-BG and borate modified BG samples after soaking in SBF for various periods of time.

**Table 16.** Ca/P ratio of apatite layer formed after immersion of samples in SBF solution.

Sample ID	3 Days	14 Days
B0-BG	$1.92 \pm 0.04$	$1.89 \pm 0.13$
B7-BG	$1.67 \pm 0.02$	$1.94 \pm 0.06$
B14-BG	$1.64 \pm 0.20$	$1.83 \pm 0.02$
B21-BG	$1.65 \pm 0.06$	$1.62 \pm 0.03$

### 3.2.2. In Vitro Degradation Analysis

Degradation analysis results of GTA cross-linked CA/PULL/GEL, CA/Ox-PULL/GEL and EDC/NHS crosslinked CA/Carboxyl-PULL/GEL scaffolds are presented in Figures 19-21. For all incubation periods, the highest weight loss was

observed in the uncross-linked group. Similar weight loss was observed for scaffolds cross-linked with GTA for 25 minutes and 50 minutes.

The weight loss of the GTA cross-linked scaffolds containing Ox-PULL (Fig. 20) was found to be lower than the weight loss observed for GTA cross-linked scaffolds containing PULL (Fig. 19). The scaffolds containing Carboxyl-PULL were cross-linked with EDC/NHS for 2 h and 7 h. Weight loss observed for scaffolds crosslinked with EDC/NHS for 7h was lower than that observed in scaffolds crosslinked for 2h. In one study, gelatin scaffolds were cross-linked with EDC/NHS for different durations (1.5-96 hours). Prolonging cross-linking time increased the degree of cross-linking due to new cross-links (Lai et al., 2012). According to the degradation results, we obtained better results when GTA was used as the cross-linking agent for crosslinking the scaffolds containing Ox-PULL. Cross-linking for 25 minutes was found sufficient for efficient crosslinking.

Therefore, in rest of the studies, Ox-PULL was used.

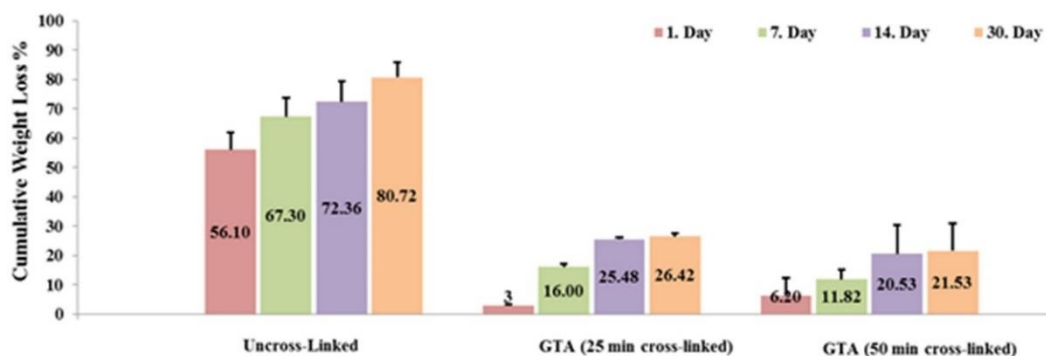


**Figure 19.** Weight loss of GTA cross-linked CA/PULL/GEL scaffold samples (%50 CA, %15 PULL, %35 GEL, with total polymer concentration of %2.5), in PBS (0.1 M, pH 7.4) at 37°C (n=3).



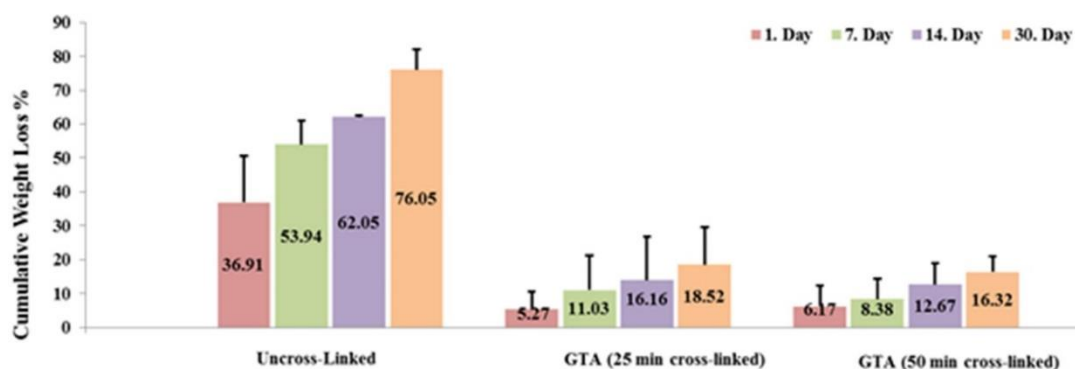


**Figure 20.** Weight loss of GTA cross-linked CA/Ox-PULL/GEL scaffold samples (%50 CA, %15 Ox-PULL, %35 GEL, with total polymer concentration of %2.5) in PBS (0.1 M, pH 7.4) at 37°C (n=3).

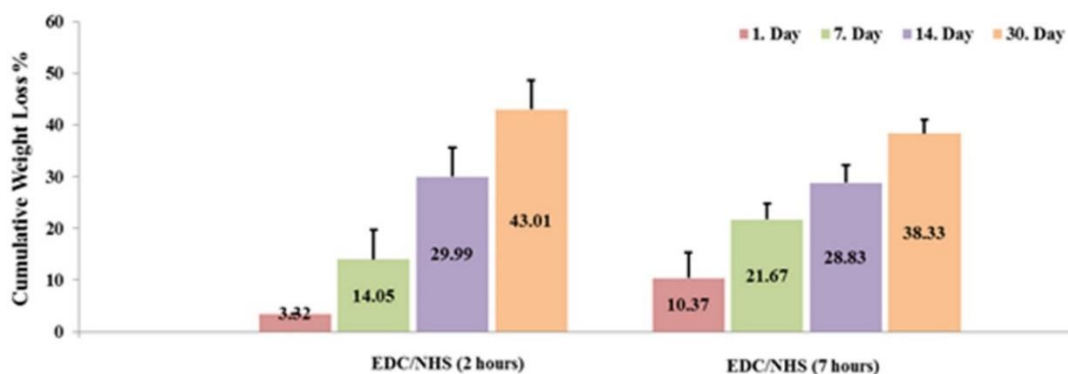


**Figure 21.** Weight loss of EDC/NHS cross-linked CA/Carboxyl-PULL/GEL scaffold samples (50% CA, 15% Carboxyl-PULL, 35% GEL, with total polymer concentration of %2.5) in PBS (0.1 M, pH 7.4) at 37°C (n=3).

### 3.2.2.1. Scaffolds Prepared by (TIPS/PL) Method

Degradation studies of different scaffold groups prepared by the (TIPS/PL) method which were cross-linked with GTA for 6 hours were conducted in PBS (0.1 M, pH

7.4) for 30 days (Fig. 22). Their pH values were also examined in PBS (0.1 M, pH 7.4) for 30 days (Table 17). As seen in Fig.22, the highest weight loss occurred in group B21-20 ( $3.8 \pm 3.4\%$ ), group without BG had ( $0.7 \pm 1.1\%$ ) weight loss 1 day after incubation, and the other groups possessed nearly similar and lower weight loss. In all groups, pH declined after 1 day of incubation. They all showed weight loss during the first day and degradation products of polymers (like broken PULL chains) might be the reason of observed pH decline (Souza et al., 2017). After 7 days of incubation, group without BG showed the highest weight loss percentage ( $16.3 \pm 4.0\%$ ). Borate incorporated BG containing scaffold groups had lower weight loss in comparison to groups without borate, except (B21-20) group. The lowest weight loss was observed in B7-10 ( $6.5 \pm 0.6\%$ ) and B21-10 ( $7.0 \pm 1.8\%$ ) groups at Day 7. After 7 days of incubation, pH values in most groups decreased, which was consistent with weight loss results, as weight loss continued in all groups. At day 14, weight loss also increased in all groups, but increase of weight loss percentage between days 7 and 14 was higher in B7-10, B7-20 and B14-10 groups. The lowest weight loss was seen in B21-10 group ( $19.8 \pm 2.5\%$ ). At day 14, pH of most groups with BG incorporation, increased. This is consistent with weight loss results, as most BG containing groups had higher weight loss between days 7 and 14. As a result of BG dissolution, alkaline and alkaline earth ions leached to the solution and made pH alkaline (Boccaccini et al., 2010). At this time point, pH of groups (without BG, B7-10, B21-10, and B21-20), did not change much. 22 days after incubation, pH values did not change much in BG added groups, which could be due to the decrease in dissolution rate of BGs. pH of group (without BG), increased due to less polymeric degradation. After 30 days of incubation, B7-10 group exhibited the lowest weight loss ( $28.5 \pm 1.6\%$ ), B0-20 group had the highest weight loss ( $37.2 \pm 3.3\%$ ), and group without BG showed moderate ( $32.8 \pm 3.6\%$ ) weight loss. After one month, in all groups, pH did not change much. This is consistent with weight loss results. Lower weight loss was observed between days 22 and 30 in all groups.

BG addition led to a lower weight loss in scaffolds till day 7. Incorporation of 10% borate modified BG in B7, B14, and B21 scaffold groups resulted in lower weight

loss than observed in 20% borate modified containing group, especially at day 7. Dissolution of alkali ions from BG-NPs, led to a neutralization of acidic degradation products of polymers (CA/Ox-PULL/GE) and thus degradability of the scaffolds has declined. Borate containing BGs, possessed increased rate of dissolution of ions, which makes them more biodegradable (Fig. 22). These groups in this study released higher amount of alkali ions that could neutralize the acidic products of polymers degradation (Fig. 22). This is the cause of lower weight loss in groups with addition of borate containing BGs. Decrease in glass network connectivity led to increase of its solubility (Nandi et al., 2011). In general, PBS change at different time points affected pH values by removing the polymeric chains. Also pH values always were between 7.0 and 7.4. Presence of borate modified BGs could result in higher increase in pH, but because of neutralization of alkaline ions from BGs with polymers acidic products, this effect was not observed. This is a desired effect, since pH change was in the range tolerated by the cells (Tainio et al., 2017).

Srinivasan et al. (2012), prepared scaffolds of alginate/nano BG for periodontal tissue engineering. According to results of in vitro degradation of alginate (control) and alginate/BG composite scaffolds, composite scaffolds showed a higher degradation than the control group up to day 14. This could be due to preferential dissolution of BG particles. Afterwards, there was not much difference in weight loss percentage of the groups. Overall, composite scaffolds were shown to be biodegradable (Srinivasan et al., 2012). Kolan et al. (2017), studied in vitro degradation of 3D printed poly-caprolactone (PCL)/bioactive borate glass (13-93B3) composite as a scaffolding material and Pluronic F127 hydrogel was used as a cell suspension medium in scaffolds. Test groups were prepared with and without presence of the hydrogel. Weight loss of PCL+13-93B3 glass scaffolds after one week was about 11%. The reason for the observed weight loss is release of ionic dissolution products from borate BG, since PCL needed a longer time for degradation. PCL+13-93B3 glass scaffolds fabricated with hydrogel, showed 16% weight loss after one week. The difference between results of two test groups was reasoned to be due to unstable nature of hydrogel. As a result, incorporation of borate

BG increased degradability of the scaffolds in a controlled manner (Murphy et al., 2016).

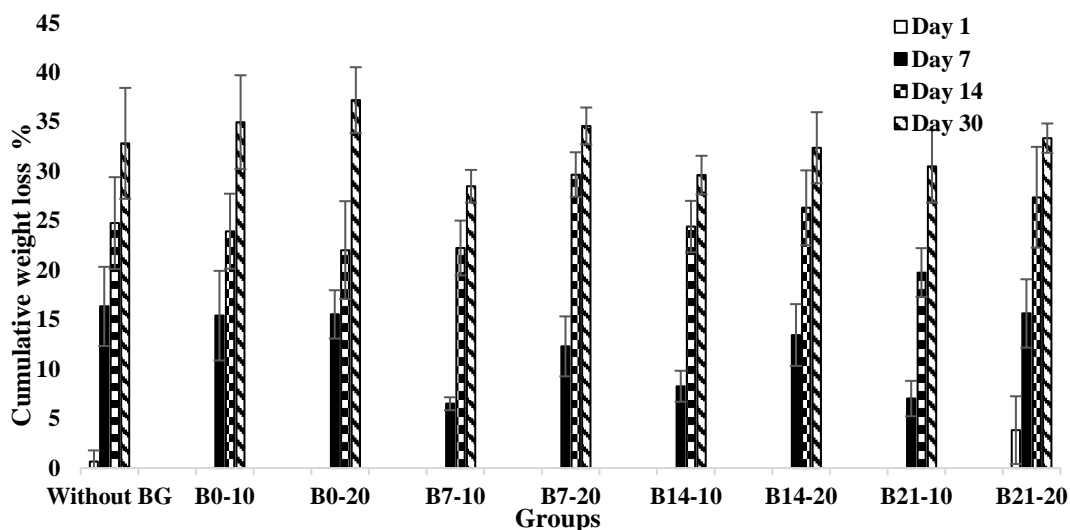


**Figure 22.** Weight loss of GTA cross-linked (6 hours) CA/Ox-PULL/GEL scaffolds in PBS (0.1 M, pH 7.4) at 37°C (n=3). Scaffolds were prepared by (TIPS/PL) method (50% CA, 15% PULL, 35% GEL, with total polymer concentration of 2.5%).

### 3.2.2.2. Scaffolds Prepared by (FD/MMP) Method

Degradation studies of different scaffold groups prepared by (FD/MMP) method that were cross-linked with 5% GTA solution for 30 minutes before mold pressing and for 12 hours after mold pressing, were conducted in PBS (0.1 M, pH 7.4) for 30 days. Weight loss was observed in all groups after 1 day of incubation and the group without BG showed the highest weight loss ( $9.0 \pm 0.8\%$ ) (Fig. 23) and the lowest weight loss was observed in B21-10 ( $4.0 \pm 3.6\%$ ). After 7 days of incubation, weight loss percentage in all groups except B7-10, B14-10, B14-20 and B21-10 scaffold group was higher than observed in scaffold group without BG incorporation ( $15.0 \pm 3.9\%$ ). Similar to day 1, B21-10 group showed the lowest weight loss ( $9.7 \pm 0.9\%$ ) at

**Table 17.** pH of PBS (0.1 M, pH 7.4) in which 6 hours GTA cross-linked CA/Ox-PULL/GEL scaffolds incubated at 37°C for different periods (n=3). Scaffolds were prepared by (TIPS/PL) method.

	<b>Day1</b>	<b>Day7</b>	<b>Day14</b>	<b>Day22</b>	<b>Day30</b>
<b>Without BG</b>	7.23 ± 0.01	7.19 ± 0.04	7.13 ± 0.05	7.29 ± 0.04	7.25 ± 0.03
<b>B0 – 10</b>	7.18 ± 0.02	6.98 ± 0.10	7.18 ± 0.03	7.20 ± 0.03	7.25 ± 0.02
<b>B0 – 20</b>	7.18 ± 0.02	7.00 ± 0.06	7.18 ± 0.02	7.19 ± 0.03	7.26 ± 0.03
<b>B7 – 10</b>	7.18 ± 0.00	7.17 ± 0.03	7.19 ± 0.02	7.16± 0.04	7.27 ± 0.03
<b>B7 – 20</b>	7.17 ± 0.01	7.03 ± 0.03	7.19 ± 0.03	7.19 ± 0.01	7.27 ± 0.02
<b>B14 – 10</b>	7.30 ± 0.02	7.13 ± 0.04	7.26 ± 0.01	7.27 ± 0.01	7.32 ± 0.04
<b>B14 – 20</b>	7.28 ± 0.02	7.08 ± 0.05	7.25 ± 0.01	7.27 ± 0.01	7.30 ± 0.01
<b>B21 – 10</b>	7.27 ± 0.03	7.16 ± 0.05	7.16 ± 0.02	7.23 ± 0.02	7.23 ± 0.02
<b>B21 – 20</b>	7.25 ± 0.02	7.11 ± 0.01	7.15 ± 0.00	7.20 ± 0.03	7.21 ± 0.03

day 7. After 14 days of incubation, weight loss continued in all groups, but increase of weight loss percentage between days 7 and 14 was pronounced in B0-20, B7-20, B14-20 and B21-10 scaffold groups. After one month, the lowest weight loss was observed in B7-10 scaffold group ( $22.8 \pm 5.4\%$ ), while B0-20 and B7-20 groups were the two groups with the highest weight loss percentages ( $32.2 \pm 3.8\%$  and  $31.6 \pm 3.0\%$ , respectively). In general, till day 1, nearly in all groups and till day 7, in some groups (most apparently B21-10), BG addition had resulted in a lower weight loss. In scaffolds with BG, neutralization of acidic degradation products of polymers (CA/Ox-PULL/GE as a result of dissolution of alkali ions from BG-NPs) might have led to a decrease in degradation of scaffolds (Srinivasan et al., 2012). It was observed that incorporation of borate into BGs, resulted in increased rate of dissolution of ions and BG degradation. Lower weight loss in borate modified BG incorporated scaffolds could be due to neutralization of acidic products released with the degradation of the polymers by increased release rate of alkali ions from BGs. Solubility of bioactive glasses is dependent on their network connectivity (Nandi et al., 2011).  $B_2O_3$  is a glass network modifier at low concentrations (Maheswaran et al., 2014). In groups containing  $B_2O_3$ , with increase of  $B_2O_3$  content, glass network connectivity decreased, which led to increased solubility of the glass. In the work done by Maji et al. (2016), 3D porous scaffolds composed of gelatin, chitosan and 58S BG nanoparticles were prepared for bone tissue engineering. In vitro degradation study showed that scaffold groups with higher BG content, showed lower weight loss during 14 days. It was suggested that in order to control degradation rate of the scaffolds, incorporated BG amount could be optimized (Maji et al., 2016). Murphy et al. (2017), bioprinted human adipose stem cells (ASCs) on a polycaprolactone (PCL)/bioactive borate glass composite. Concentration of borate glass (13-93B3) was 10 to 50 weight % of the extrudable paste. Weight loss percentage of the scaffold after two weeks of incubation in cell culture medium was about 35%. This weight loss was mainly due to controlled release of borate BG, since degradation of PCL needs longer time. In general, incorporation of borate BG

led to controlled degradation of scaffold over time which is necessary for some tissue engineering purposes (Murphy et al., 2017).

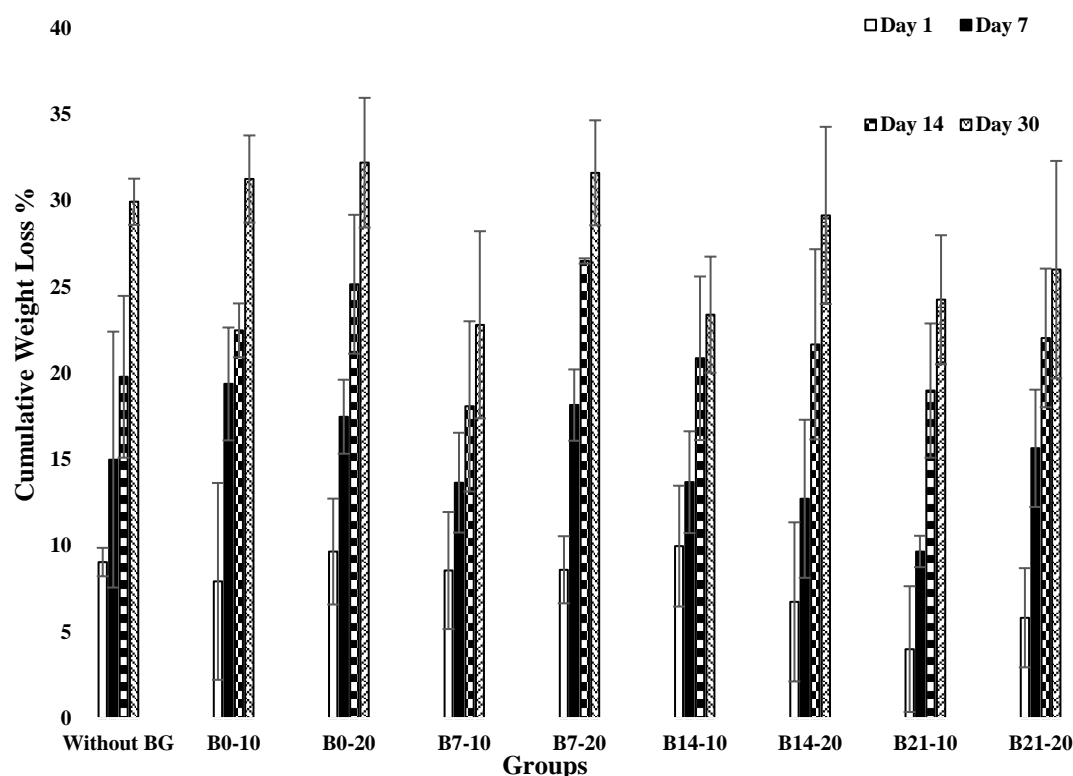


**Figure 23.** Weight loss of GTA cross-linked (30 minutes before mold pressing and for 12 hours after mold pressing) CA/Ox-PULL/GEL scaffolds in PBS (0.1 M, pH 7.4) at 37°C (n=3). Scaffolds were prepared by the (FD/MMP) method (50% CA, 15% PULL, 35% GEL, with total polymer concentration of 5%).

pH values of different scaffold groups prepared by (FD/MMP) method that were crosslinked were examined in PBS (0.1 M, pH 7.4) for 30 days (Table 18). In all groups, pH declined after 1 day of incubation. This is because that all groups started losing weight at this time point. Degradation product of polymers (broken PULL chains), are acidic and this is the reason for pH decrease (Liang et al., 2010). There

was not much change in pH of different groups after 7 and 14 days of incubation. pH of groups was nearly the same compared to day 7, only there was a little decrease in pH of group (without BG) and a small increase in pH of groups (B0-20, and B7-10). In BG containing scaffolds, as BG degraded, alkaline ions were released and their exchange with hydrogen ions ( $H^+$ ), could cause an increase in pH (Luo et al., 2017). In this work, till day 14, this effect was not seen, which could be due to neutralization of acidification made by polymeric degradation products and the alkalinity caused by BG dissolution. Decrease in pH of scaffold group without BG at day 14, was consistent with weight loss results. However, 22 days after incubation, pH increased in all groups. In BG containing groups, this increase was higher in borate incorporated groups. Degradation rate of borosilicate glasses was higher than silicate glasses and they could affect pH rise much due to the dissolution of the network modifiers (Turk & Deliormanlı, 2017). At day 22, pH of group (without BG), increased due to less polymeric degradation. After one month, pH values in all groups, slightly decreased. This is consistent with weight loss results as lower weight loss occurred between days 22 and 30 in all groups. Slight variation in pH is favorable, since this pH range could be tolerated by the cells (Tainio et al., 2017).



**Table 18.** pH of PBS (0.1 M, pH 7.4) in which CA/Ox-PULL/GEL scaffolds cross-linked with 5% GTA solution for 30 minutes before mold pressing and for 12 hours after mold pressing, were incubated at 37°C for different periods (n=3). Scaffolds were prepared by (FD/MMP) method.

	<b>Day 1</b>	<b>Day 7</b>	<b>Day 14</b>	<b>Day 22</b>	<b>Day 30</b>
<b>Without BG</b>	7.23 ± 0.01	7.19 ± 0.04	7.13 ± 0.05	7.29 ± 0.04	7.25 ± 0.03
<b>B0 – 10</b>	7.20 ± 0.05	7.19 ± 0.05	7.17 ± 0.04	7.23 ± 0.02	7.21 ± 0.00
<b>B0 – 20</b>	7.15 ± 0.05	7.17 ± 0.02	7.22 ± 0.03	7.24 ± 0.01	7.21 ± 0.00
<b>B7 – 10</b>	7.16 ± 0.01	7.14 ± 0.02	7.19 ± 0.02	7.25 ± 0.00	7.21 ± 0.02
<b>B7 – 20</b>	7.15 ± 0.00	7.15 ± 0.01	7.15 ± 0.00	7.24 ± 0.00	7.21 ± 0.01
<b>B14 – 10</b>	7.13 ± 0.01	7.17 ± 0.00	7.17 ± 0.02	7.22 ± 0.03	7.18 ± 0.03
<b>B14 – 20</b>	7.14 ± 0.00	7.15 ± 0.01	7.15 ± 0.02	7.22 ± 0.02	7.17 ± 0.03
<b>B21 – 10</b>	7.16 ± 0.02	7.17 ± 0.02	7.19 ± 0.01	7.22 ± 0.01	7.17 ± 0.01
<b>B21 – 20</b>	7.17 ± 0.01	7.15 ± 0.01	7.17 ± 0.00	7.22 ± 0.02	7.18 ± 0.03

### **3.2.3. Water Absorption Capacity of the Scaffolds**

#### **3.2.3.1. Scaffolds Prepared by (TIPS/PL) Method**

Scaffolds prepared by the (TIPS/PL) method were cross-linked with GTA for 6 hours and these scaffolds were kept in PBS (0.1 M, pH 7.4) for 30 days. Their water absorption (WA) capacities were measured at different time points (Table 19). One day after immersion in PBS, WA% of all groups reached the highest value since water entered the pores. B7-10, had the highest WA% at day1. In all groups, WA capacity in PBS decreased with time during 1 month of incubation. This decrease was in accordance with weight loss of the scaffolds. BG containing groups had higher WA percentages than scaffold without BG. Increase of BG content from 10% to 20%, led to an increase in WA capacity. Enhancement of WA with inclusion of BG was due to large specific area of BG (Wu et al., 2017), its hydrophilicity (Lei et al., 2013) and also weak interlocking between BG and polymer matrix (Ghimire, 2016). Similar results were reported in the literature (Ghimire, 2016, Pourhaghgouy & Zamanian, 2014). B21-10 and B21-20 scaffolds had lower WA percentages than scaffold group without BG. Porosity percentages of these two groups were lower than scaffolds without BG, and less water could infiltrate into them. 20% BG, addition resulted in a decrease of WA%. B7-20, and B14-20 groups also had higher weight loss in all time intervals, compared to their 10% BG groups. B14-10, was one of the groups having the lowest weight loss percentage at the end of one month. It also had the highest water absorption percentage nearly at that time points. In most of the groups, WA% decrease was gradual during one month. a high WA% difference was observed at two time points (for example, in B7-20, between days 7 and 14), weight loss increased in that period. Altering BG content and composition incorporated in scaffolds, is a way for controlling their WA capacity which would improve cell growth (Li et al., 2016).

**Table 19.** Water absorption results of GTA cross-linked (6 hours) CA/Ox-PULL/GEL scaffolds in PBS (0.1 M, pH 7.4) at 37°C that were prepared by the method of (TIPS/PL) (n=3).

	<b>Day1 (%)</b>	<b>Day7 (%)</b>	<b>Day14 (%)</b>	<b>Day30 (%)</b>
<b>Without BG</b>	649.75 ± 71.98	631.15 ± 67.73	590.73 ± 88.92	497.16 ± 50.48
<b>B0 – 10</b>	681.33 ± 91.60	654.19 ± 66.04	551.82 ± 70.30	480.44 ± 36.64
<b>B0 – 20</b>	691.65 ± 17.45	673.29 ± 49.36	638.07 ± 24.70	494.87 ± 63.79
<b>B7 – 10</b>	697.55 ± 79.59	652.24 ± 84.62	577.70 ± 46.15	501.56 ± 33.15
<b>B7 – 20</b>	675.63 ± 71.44	623.82 ± 19.08	541.92 ± 83.87	474.46 ± 57.80
<b>B14 – 10</b>	690.85 ± 73.58	629.52 ± 88.44	591.74 ± 77.49	519.78 ± 64.92
<b>B14 – 20</b>	685.71 ± 71.43	563.09 ± 65.50	488.09 ± 62.40	457.14 ± 51.50
<b>B21 – 10</b>	608.14 ± 44.24	578.23 ± 69.094	544.95 ± 45.46	445.63 ± 23.29
<b>B21 – 20</b>	616.40 ± 169.52	601.84 ± 149.95	538.27 ± 138.03	455.97 ± 119.86

### 3.2.3.2. Scaffolds Prepared by (FD/MMP) Method

Scaffolds prepared by the (FD/MMP) method that were cross-linked with GTA for 30 minutes before mold pressing and for 12 hours after mold pressing, were kept in

PBS (0.1 M, pH 7.4) for 30 days. Their water absorption (WA) capacities were measured at different time points (Table 20). One day after immersion, all scaffold groups had high WA%. WA capacity of the scaffolds ranged from 160% (without BG) to 350% in (B0-20). In all groups, WA capacity decreased gradually with time during one month of incubation. This decrease was compatible with the increase in weight loss of the scaffolds. Scaffolds with BG had significantly higher WA percentages than scaffold without BG. WA increased with the increased amount of BG from 10% to 20%. BG is hydrophilic in nature and its inclusion to composites improved the WA% (Hafezi et al., 2016). Samples with higher BG content, possess larger glass/polymer interface, and weaker mechanical interlocking between BG and the polymer matrix (Ghimire, 2016), which enhanced the entrapment of water into the composite scaffolds (Ghimire, 2016, El-Kady et al., 2012). Our results were in agreement with literature. Scaffolds without BG had the lowest water absorption percentage at the end of one month. Among BG incorporated scaffolds B0-10 incorporated group had the highest WA. WA capability of composites could be modulated by changing their BG content and scaffolds with favorable WA capability, are needed for improving the interactions between the cells and biomaterials (Hou et al., 2016). According to this thesis results, inclusion of borate modified BG to scaffolds, resulted in a controlled trend in their WA capacity.

**Table 20.** Water absorption measurement results of GTA cross-linked (30 minutes before mold pressing and for 12 hours after mold pressing) CA/Ox-PULL/GEL scaffolds in PBS (0.1 M, pH 7.4) at 37°C that were prepared by the method of (FD/MMP) (n=3).

	<b>Day 1 (%)</b>	<b>Day 7 (%)</b>	<b>Day 14 (%)</b>	<b>Day 30 (%)</b>
<b>Without BG</b>	158.7 ± 7.6*	152.5 ± 38.4*	163.6 ± 11.8*	136.4 ± 25.2*
<b>B0 – 10</b>	344.4 ± 9.6	323.8 ± 21.8	330.9 ± 45.3	322.5 ± 29.6
<b>B0 – 20</b>	352.5 ± 31.2	321.2 ± 19.1	288.9 ± 16.6	308.8 ± 24.6
<b>B7 – 10</b>	319.0 ± 28.8	323.8 ± 11.1	312.2 ± 26.7	291.8 ± 35.7
<b>B7 – 20</b>	308.8 ± 30.3	329.3 ± 29.1	291.5 ± 10.9	280.0 ± 7.14
<b>B14 – 10</b>	310.6 ± 73.6	298.0 ± 24.4	288.4 ± 38.2	302.7 ± 39.2

**Table 20 - Continued.** Water absorption measurement results of GTA cross-linked (30 minutes before mold pressing and for 12 hours after mold pressing) CA/Ox-PULL/GEL scaffolds in PBS (0.1 M, pH 7.4) at 37°C that were prepared by the method of (FD/MMP) (n=3).

<b>B14 – 20</b>	320.9 ± 18.6	322.1 ± 35.6	300.1 ± 29.6	286.0 ± 37.4
<b>B21 – 10</b>	330.4 ± 13.2	338.7 ± 19.5	327.7 ± 19.7	310.9 ± 14.7
<b>B21 – 20</b>	332.7 ± 9.3	320.3 ± 11.3	324.6 ± 16.9	315.2 ± 28.3

\* denotes the lowest statistical difference between control group (without BG) and other groups at all time points ( $p < 0.05$ ).

### 3.2.4. Scanning Electron Microscopy (SEM) Results

#### 3.2.4.1. Scaffolds Prepared by TIPS/PL Method

In order to induce phase separation, freezing temperatures of -196°C and -80°C were used. When -196°C was used as the freezing temperature for preparing CA/Ox-PULL/GEL scaffolds (Fig. 24), aligned and tubular structures were formed in the scaffolds and mean diameter of the pores was found as 4.45 μm. When -80°C was used as the freezing temperature, KCl was also added as porogen in different amounts to polymer solution (100%, 50% and 25% of the total polymer weight) in order to obtain larger macropores, as it is seen in (Fig. 25a-c), aligned and tubular structures were formed in the scaffolds successfully. When KCl was added in

amounts equivalent to 100%, 50% and 25% of the total polymer concentration, the mean diameters of the pores were found as 10.8  $\mu\text{m}$ , 8.7  $\mu\text{m}$  and 6.7  $\mu\text{m}$ , respectively. Increase of porogen percentage, led to increase in pore diameter. A more aligned and homogenous tubular structures were formed in the scaffolds prepared with highest porogen concentration (Fig. 25a). These results were consistent with the similar works in the literature (Wang et al., 2010, Mounesi Rad et al., 2016). Increasing the freezing temperature and using porogen increased the mean diameter of the pores. Freezing temperature of  $-80^{\circ}\text{C}$  and KCl as 100% of the total polymer concentration were used for preparing scaffolds for the rest of the studies conducted in the thesis.

Cross-sections of the scaffolds prepared by using  $-80^{\circ}\text{C}$  as the freezing temperature and KCl as the porogen (100% of the total polymer weight) with particle sizes in the range of (180-212  $\mu\text{m}$ ), were analyzed by SEM (Fig. 25a). As it is seen, aligned and tubular structures were formed. Mean diameter of the pores in scaffolds without BG, was 10.80  $\mu\text{m}$ . Examination of cross-sections B0-10, B14-20 scaffolds with SEM (Fig. 26a&b) revealed that incorporation of BG, did not cause an evident change in the mean diameter of the pores. Presence of micropores (diameter  $<10\ \mu\text{m}$ ) in the scaffolds is essential for body fluid circulation, vascularity restoration and for controlled delivery of drugs (Jasadee & Lupong, 2010), while macropores (diameter  $>100\ \mu\text{m}$ ) facilitate cell attachment, migration, colonization and tissue formation (Abdurrahim & Sopyan, 2008, AbdulQader et al., 2013). Diameter of dentinal tubules in the natural tissue differs according to its location from 2.5  $\mu\text{m}$  near the pulp to 0.9  $\mu\text{m}$  near the dentin–enamel junction (Shalaby & Salz, 2006). Results indicated that scaffold structure was successful in mimicking tubular structure of natural dentin. The obtained structure could be suitable for settlement of odontoblastic prolongations in order to provide alignment against the existing dentin surface when implanted in vivo. Lluch et al. (2009), prepared scaffolds of poly (ethyl methacrylate-co-hydroxyethyl acrylate) [P(EMAcO-HEA)] with different amounts of silica by the fiber-templating method for dentin regeneration. Hybrid organic–inorganic nanocomposite consisted of homogeneously distributed aligned tubular

pores with diameter of 8  $\mu\text{m}$ . According to the microscope images, scaffolds looked alike natural dentin regarding structure and distribution of the pores (Vallés Lluch et al., 2009). In another work for dentine/pulp-like tissue regeneration, poly (lactic-co-glycolic) acid scaffolds were prepared by the solvent-casting/particulate leaching method. NaCl was used as the porogen with two different size ranges. In scaffolds prepared by using NaCl with particle size of (150–180  $\mu\text{m}$ ), pores were in the range of 8 to 250  $\mu\text{m}$ , and in those using porogen particle size of 180–300  $\mu\text{m}$ , pores were in the range of 30 to more than 300  $\mu\text{m}$  (El-Backly et al., 2008).

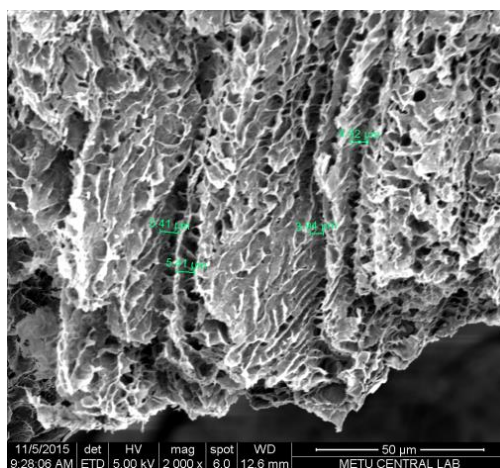


**Figure 24.** Cross-sectional SEM images of the scaffolds composed of CA/Ox-PULL/GEL prepared by the (TIPS/PL) method (Freezing temperatures:  $-196^{\circ}\text{C}$ ).



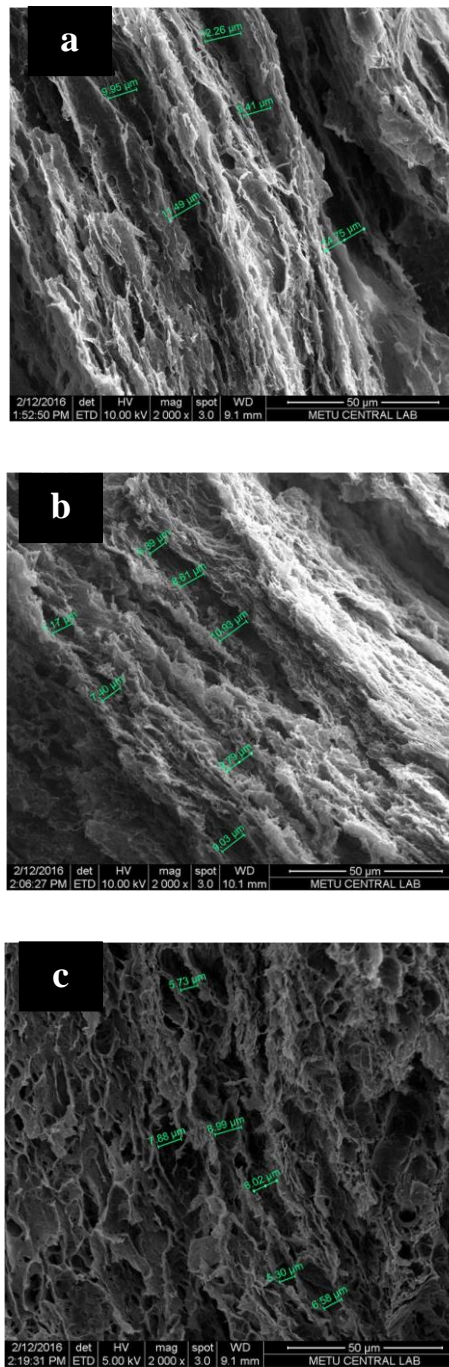


**Figure 25.** Cross-sectional SEM images of the CA/Ox-PULL/GEL scaffolds prepared by the TIPS/PL method and using KCl as porogen at different amounts (a) 100% (b) 50% (c) 25% of the total polymer concentration. (Freezing temperatures: -80°C).

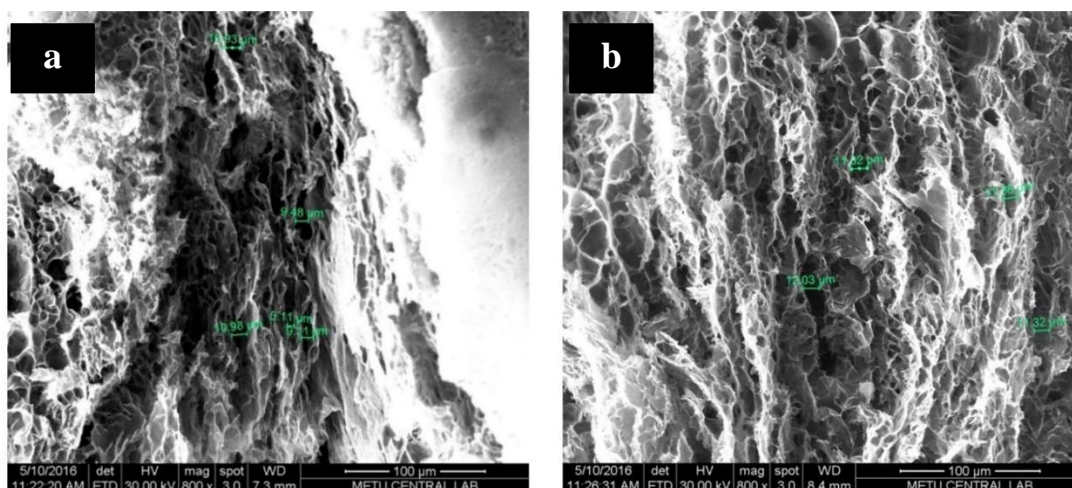


**Figure 26.** Cross-sectional SEM images of the CA/Ox-PULL/GEL scaffolds prepared by the TIPS/PL method using KCl as %100 of the total polymer weight, (a) B0-10 group (b) B14-20 group. (Freezing temperatures:  $-80^{\circ}\text{C}$ ).

### 3.2.4.2. Scaffolds Prepared by (FD/MMP) Method

Surface morphology of the prepared scaffolds, was evaluated by SEM (Fig. 27). In all groups, homogenously distributed tubular structures were successfully formed. Mean diameter of the tubular structures (macropores) was about  $420\ \mu\text{m}$  and the distance between walls of the tubules was around  $560.3\ \mu\text{m}$ . SEM images of macropores walls are presented in (Fig. 28a&b) and images revealed the presence of open small pores in walls of the macropores. Presence of macropores in the scaffolds, enhances gas diffusion, nutrient supply, and waste removal, and as a result vascularization and tissue ingrowth promotes (Van Tienen et al., 2002, Loh & Choong, 2013). For dentin regeneration, pore size should be suitable for alignment of polarized odontoblast cells on the surface of the matrix or against the existing dentin surface (AbdulQader et al., 2013). Results are consistent with results of other studies, which shows our success for obtaining aligned macropores with homogenous distribution throughout the scaffold. Macropore size in the range of 250 to  $500\ \mu\text{m}$

has been shown to be suitable for dentin regeneration purposes (El-Backly et al., 2008, Wang et al., 2011, Yun et al., 2015). For growth of blood vessels, scaffolds with pore diameters larger than 400  $\mu\text{m}$ , are beneficial (Feng et al., 2011). According to in vivo test results by different groups, it was shown that porcine dental pulp-derived cells were able to align on the surface of the regenerating tissue when cultured on the scaffolds with 300  $\mu\text{m}$  pore size (Ando et al., 2009, Tonomura et al., 2010). Abdul Qader et al. (2016), prepared calcium phosphate (BCP) scaffolds composed of hydroxyapatite/beta tricalcium phosphate (20/80) with different porosities by the wet precipitation method for dentin tissue regeneration. Mean pore size of the macropores of the scaffolds was measured as  $308 \pm 12 \mu\text{m}$  (AbdulQader et al., 2016). Qu et al. (2015) prepared 3D nanofibrous gelatin (NF-gelatin) scaffolds by TIPS/PL method for regeneration of the dental pulp-dentin complex. Structure of the scaffolds consisted of macropores with diameters in the range of 250-420  $\mu\text{m}$  and walls of macropores had a nanofibrous structure (Qu et al., 2015).

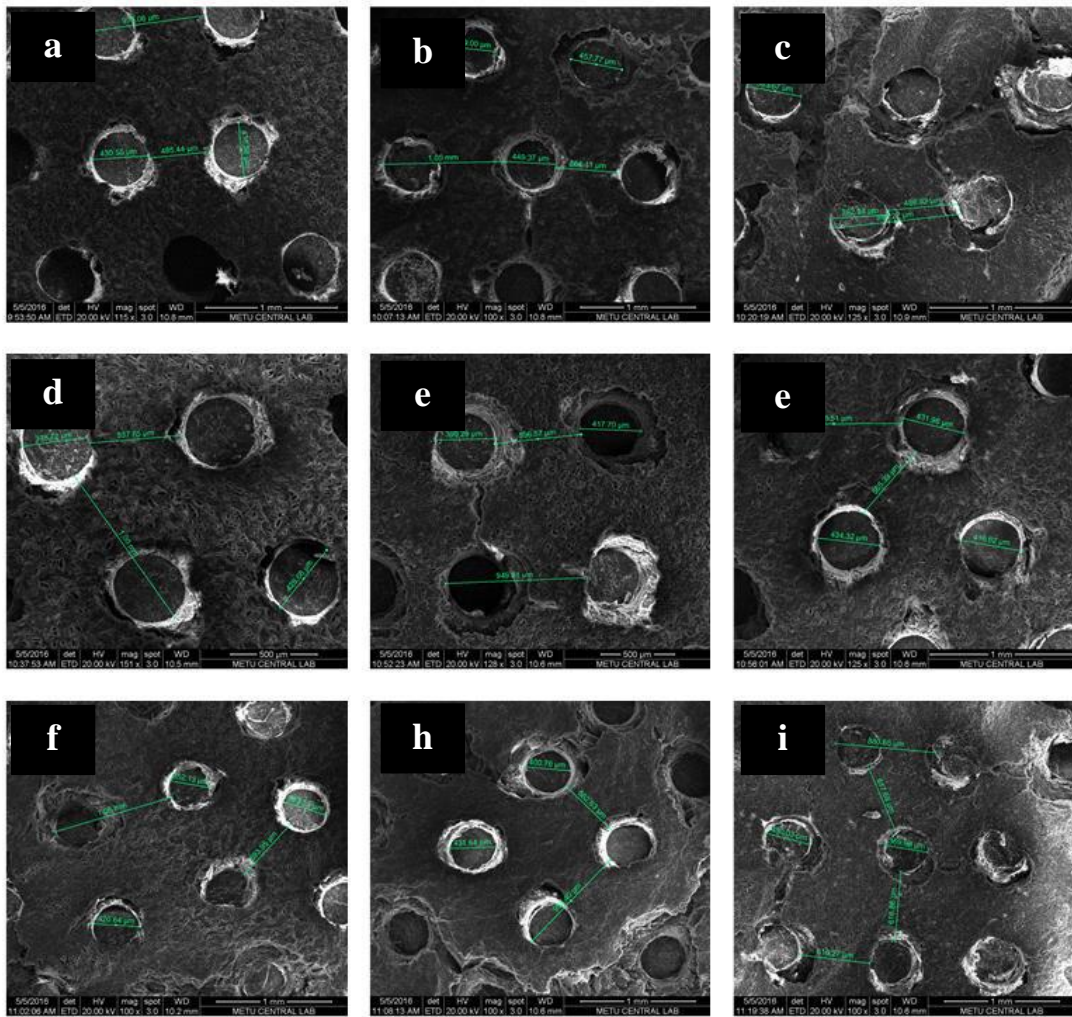


**Figure 27.** SEM images of the scaffolds prepared by the FD/MMP method, a) without BG, b) B0 – 10, c) B0 – 20, d) B7 – 10, e) B7 – 20, f) B14 – 10, g) B14 – 20, h) B21 – 10, and i) B21 – 20.

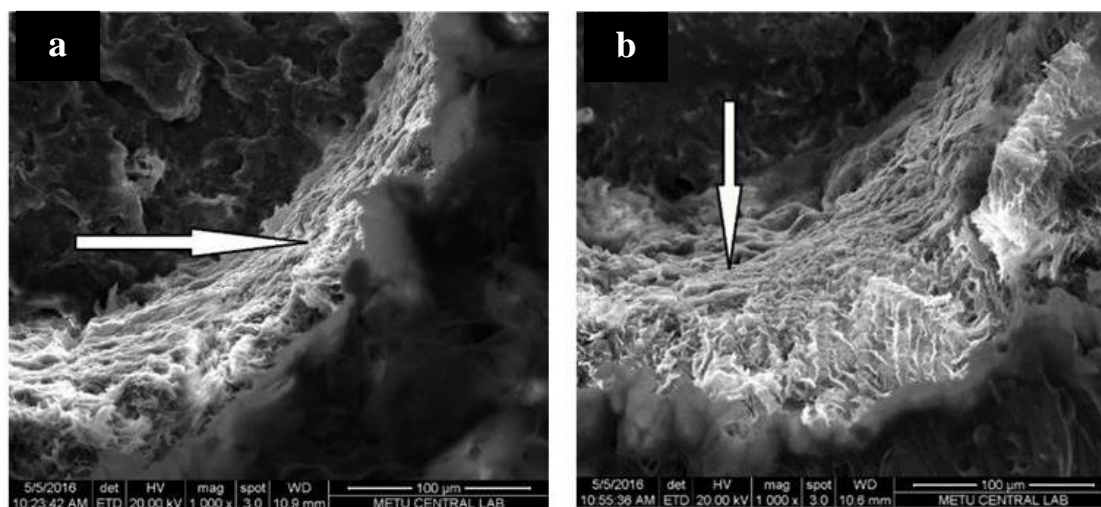


**Figure 28.** SEM images of macropores walls of the scaffolds prepared by the FD/MMP method, a) without BG, and b) 14B – 10, (arrow shows wall of the macropore).

### 3.2.5. In Vitro Bioactivity Tests

#### 3.2.5.1. Scaffolds Prepared by TIPS/PL Method

Different scaffold groups prepared by the TIPS/PL method were examined by SEM after 7 and 14 days of incubation in SBF (Fig. 29). SEM images indicated full coverage of the scaffolds compositions was confirmed by EDS analysis. Ca-P layer was detected on scaffolds without BG 14 days after SBF incubation, but in BG containing groups, at both time points, layers rich in Ca-P were present and with increasing immersion time, deposition became homogenous and thicker. According to EDS analysis, Ca/P ratio in the deposits observed on B0-10 group that were incubated in SBF for 7 days was 1.55. Ca/P ratios of the deposits formed on B14-10 (on day 14) and B14-20 (day 7) were 1.56 and 1.53), respectively. These ratios are lower than Ca/P ratio for stoichiometric hydroxyapatite (1.67), but are near to that of hydroxycarbonate apatite (HCA) (1.5) (Talebian et al., 2014). In other words, it is

similar to human bone apatite composition rather than pure hydroxyapatite. Ca/P ratios of deposits of the other groups were in the range of 1.0 to 2.0, which are characteristic for other phases of calcium phosphates found in the body (Paiva et al., 2006). BG nanoparticles are negatively charged and their silicate ions provide nucleation initiation sites for formation of apatite on scaffolds surfaces, during immersion in SBF. Deposited calcium phosphates are amorphous first, which then crystallize to form hydroxycarbonate apatite (HCA) (Araújo et al., 2016). As a result of SiO<sub>2</sub> substitution with B<sub>2</sub>O<sub>3</sub> in bioactive glasses, glass network structure opens and thus ion exchange with SBF solution enhances, which results in higher quantity of apatite deposition (Tainio et al., 2017). In total, we can say that BG added groups, showed profound bioactivity, and (10-20)% borate modification has positively affected the bioactivity.

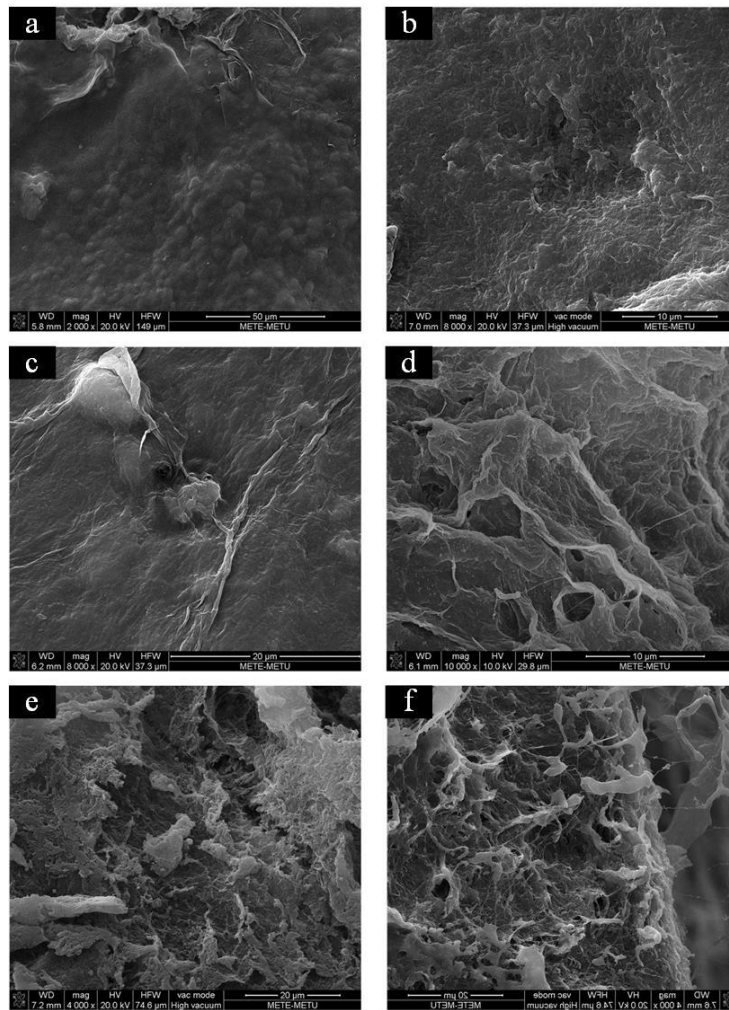


**Figure 29.** SEM images of the scaffolds prepared by the TIPS/PL method, and kept in SBF for 7 and 14 days: a) without BG, day 7; b) without BG, day 14; c) B0-10, day 7; d) B0-10, day 14; e) B0-20, day 7; f) B0-20, day 14.

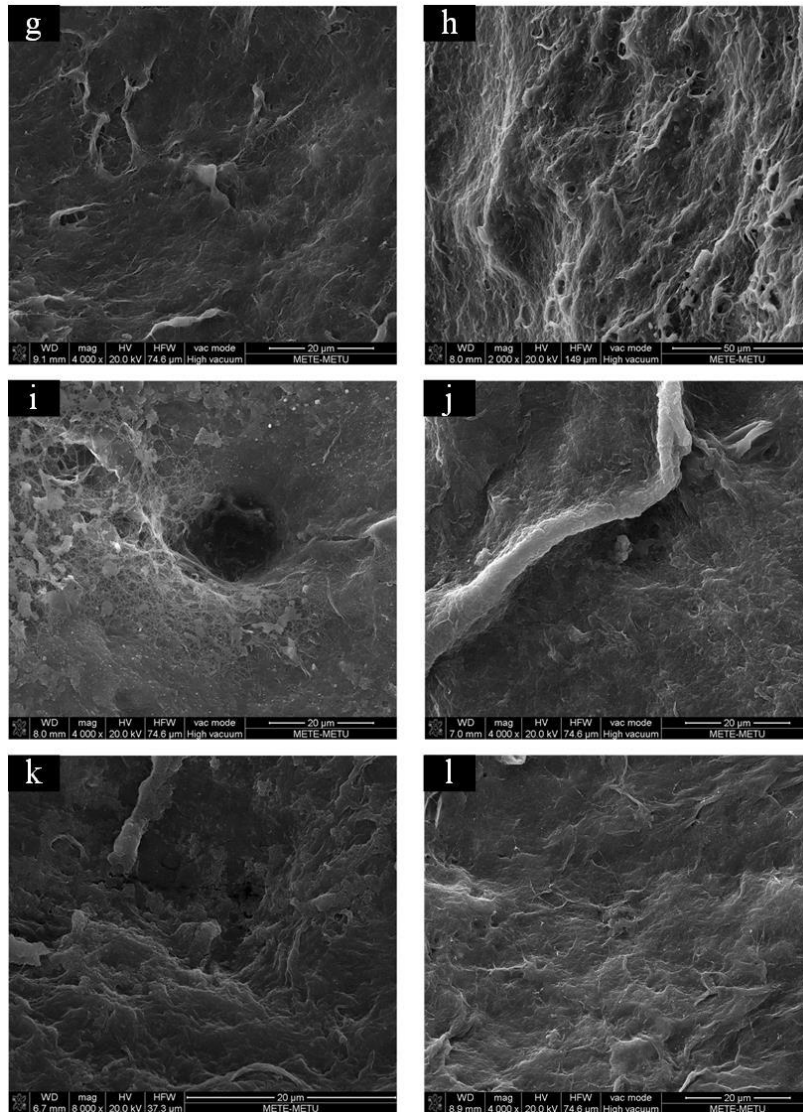


**Figure 29 - Continued.** SEM images of the scaffolds prepared by the TIPS/PL method, and kept in SBF for 7 and 14 days: g) B7-10, day 7; h) B7-10, day 14; i) B7-20, day 7; j) B7-20, day 7; k) B14-10, day 7; l) B14-10, day 14.



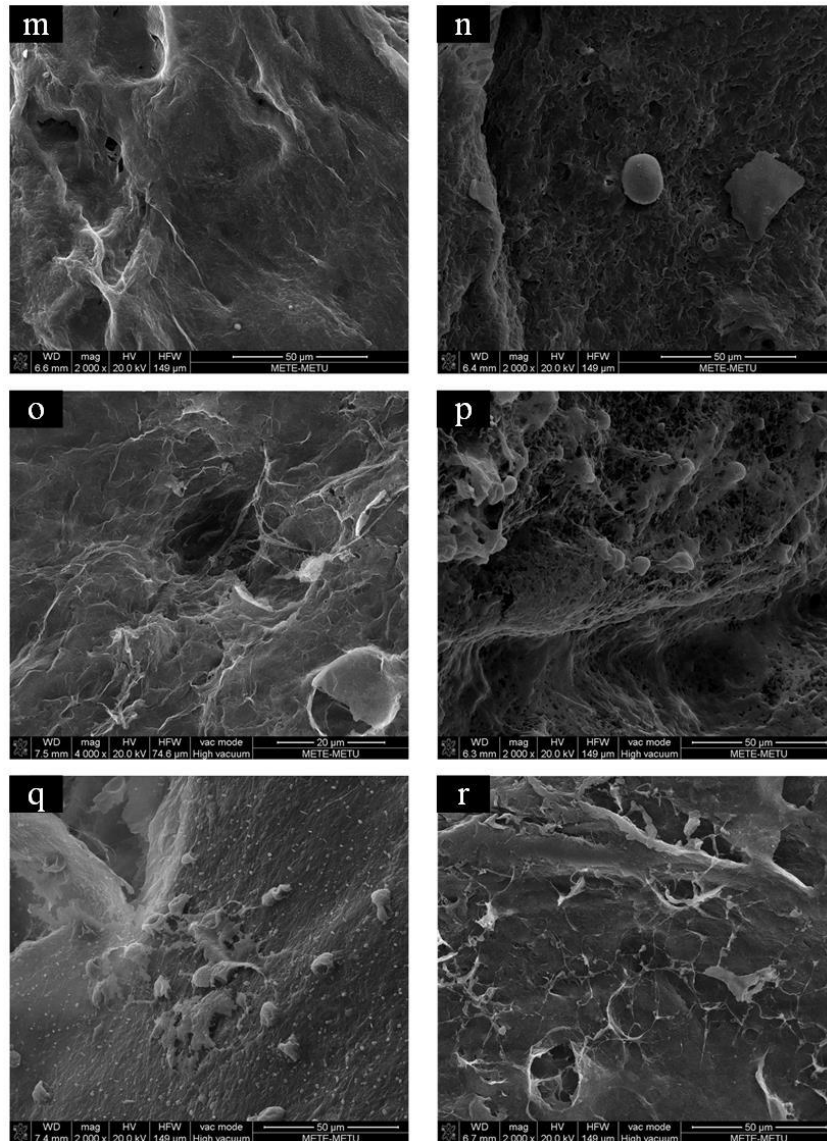


**Figure 29 - Continued.** SEM images of the scaffolds prepared by the TIPS/PL method, and kept in SBF for 7 and 14 days: m) B14-20, day 7; n) B14-20), day 14; o) B21-10, day 7; p) B21-10, day 14; q) B21-20, day 7; r) B21-20, day 14.

### 3.2.5.2. Scaffolds Prepared by FD/MMP Method

Different scaffold groups prepared by the FD/MMP method were first cross-linked with 5% GTA solution for 30 minutes before mold pressing and for 12 hours after mold pressing. These scaffolds were placed into SBF solution for 14 days and they were examined by SEM, after 7 and 14 days of incubation (Fig. 30). According to SEM images, calcium phosphate (Ca-P) precipitates formed on scaffolds surfaces which was confirmed by EDS analysis. After 7 days of incubation in SBF Ca-P layer was detected on scaffolds except scaffolds without BG, at both time points, showing the positive effect of BG incorporation on formation of the Ca-P rich layer. In all BG incorporated groups, precipitation became homogenous and its thickness increased with time. Ca/P ratios of deposits on B0-10 scaffolds at days 7, and 14 were 1.47 and 1.52, respectively. In borate modified BG added groups, Ca/P ratio of deposits on B21-20 scaffolds at days 7, and 14 were 1.55 and 1.60, which the latter was closer to Ca/P ratio of stoichiometric hydroxyapatite (1.67) (Adams & Essien, 2015). Ca/P ratios of the precipitates observed in other groups were in the range of 1.0 to 1.99, which belong to other phases of calcium phosphates present in the body (Paiva et al., 2006). For apatite formation in SBF, ions exchange from glass and from the solution in order to form silanols (SiOH) on the glass surface. As time passes, silanols formation increases, followed by their condensation to create a SiO<sub>2</sub>-rich layer. This layer acts as the nucleation initiation site for deposition of Ca-P coating, which finally crystallizes to form hydroxycarbonate apatite (HCA) (Maçon et al., 2015). Degradation rate of B<sub>2</sub>O<sub>3</sub> containing bioactive glasses in SBF, is higher than silicate glasses, which possess a strong and chemically stable network due to presence of SiO<sub>2</sub>. With increase of B<sub>2</sub>O<sub>3</sub> content in glasses, their bioactivity increases as a result of their weaker network (Stanić, 2017). In general, BG addition facilitated the bioactivity of the scaffolds.

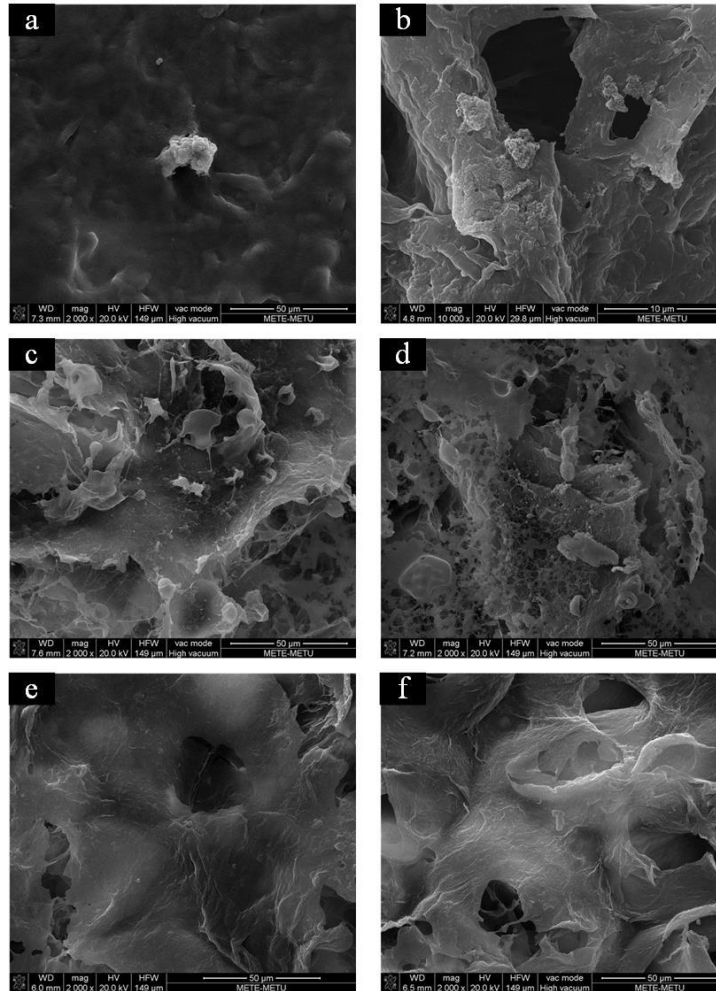


**Figure 30.** SEM images of the scaffolds prepared by the FD/MMP method, and kept in SBF for 7 and 14 days: a) withoutBG, day 7; b) without BG, day 14; c) B0-10, day 7; d) B0-10, day 14; e) B0-20, day 7; f) B0-20, day 14.

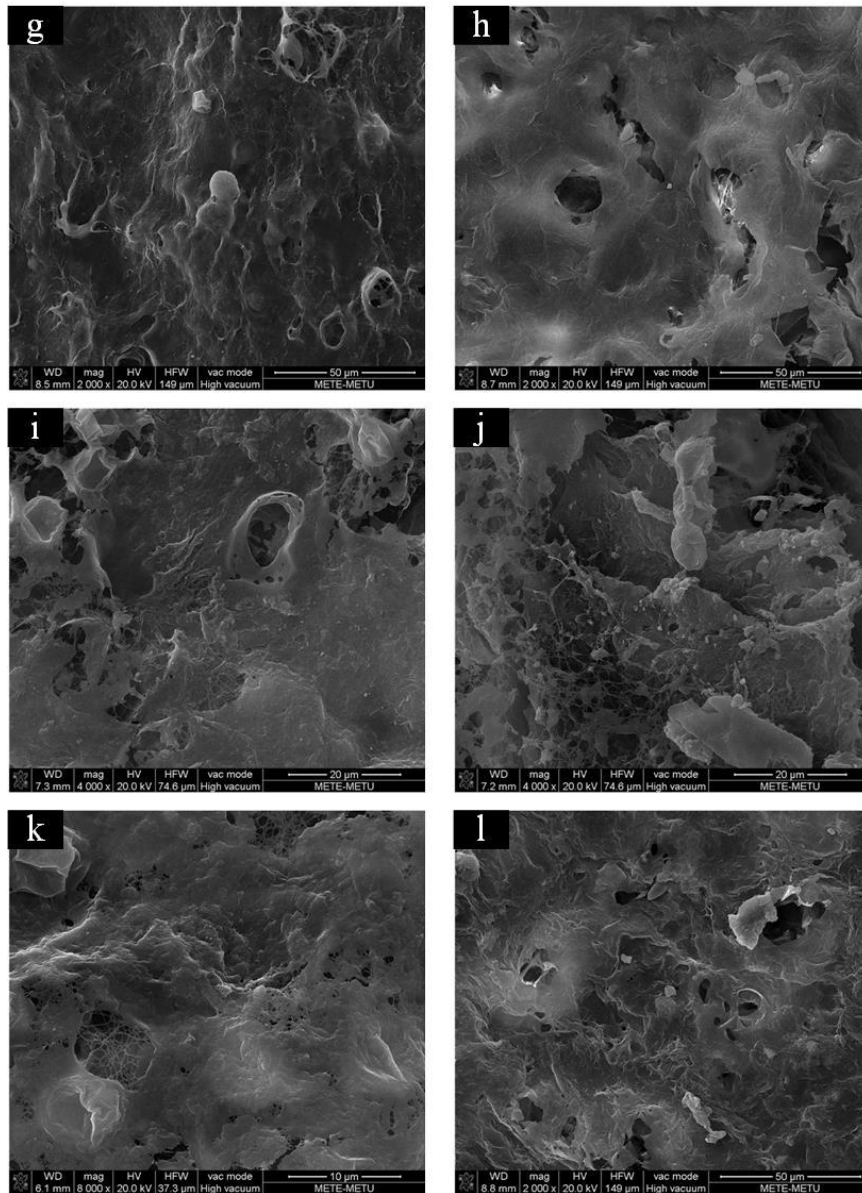


**Figure 30 - Continued.** SEM images of the scaffolds prepared by the FD/MMP method, and kept in SBF for 7 and 14 days: g) B7-10, day 7; h) B7-10, day 14; i) B7-20, day 7; j) B7-20, day 7; k) B14-10, day 7; l) B14-10, day 14.

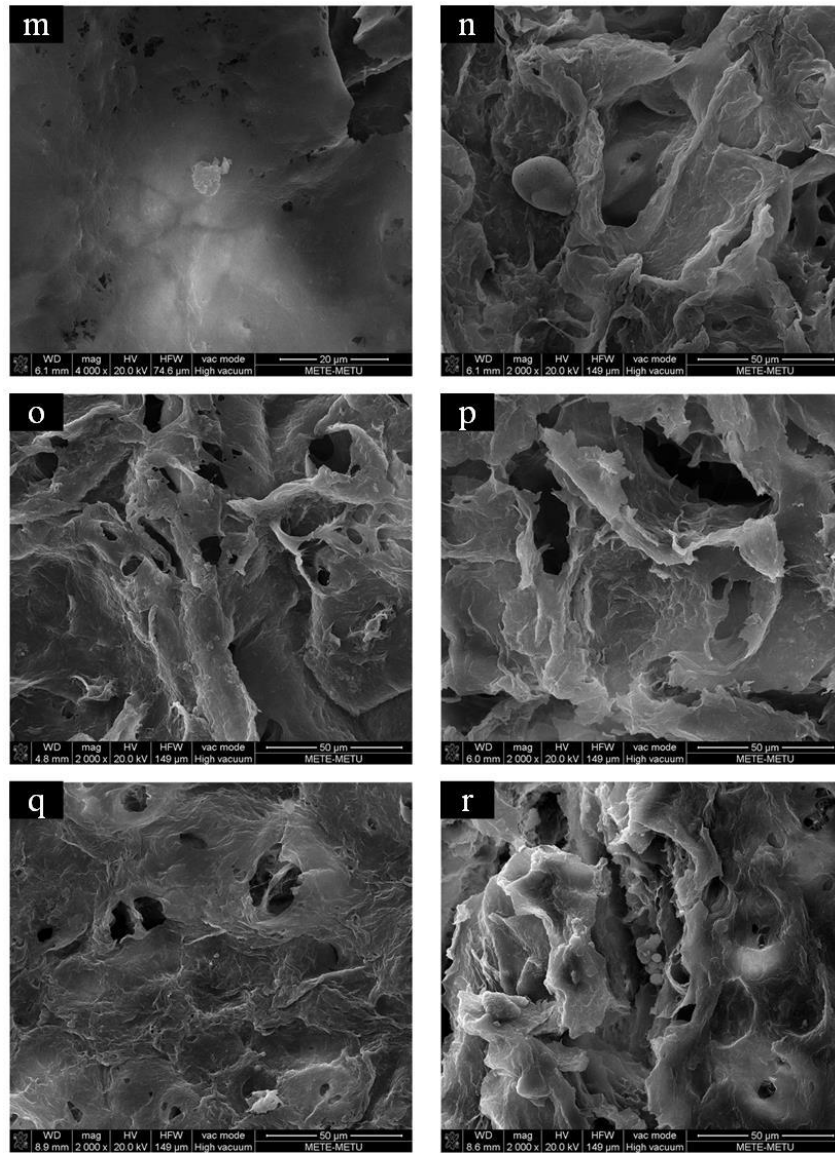


**Figure 30 - Continued.** SEM images of the scaffolds prepared by the FD/MMP method, and kept in SBF for 7 and 14 days: m) B14-20, day 7; n) B14-20), day 14; o) B21-10, day 7; p) B21-10, day 14; q) B21-20, day 7; r) B21-20, day 14.

### **3.2.6. Porosity Measurements**

#### **3.2.6.1. Porosity Results of Scaffolds Prepared by TIPS/PL Method**

Results of porosity measurement analysis by mercury porosimetry device for the scaffolds composed of CA/Ox/PULL/GEL prepared by the (TIPS/PL) method are given in (Fig. 31). Pore sizes ranged between 5 to 200  $\mu\text{m}$  and pore size distribution was mainly in the range of 10 to 50  $\mu\text{m}$ . The minimum pore size required to allow the ingrowth of mineralized tissue seems to be in the order of 50  $\mu\text{m}$ : larger pore sizes seem to improve speed and depth of penetration of mineralized tissues into the biomaterial, but on the other hand impair the mechanical properties (Mour et al, 2010). Greater porosities with more macropores could support the formation of an osteodentine-like matrix, while scaffolds with less porosity and much more micropores could support the formation of more organized matrix deposition more similar to dentine (El-Backly et al, 2008).

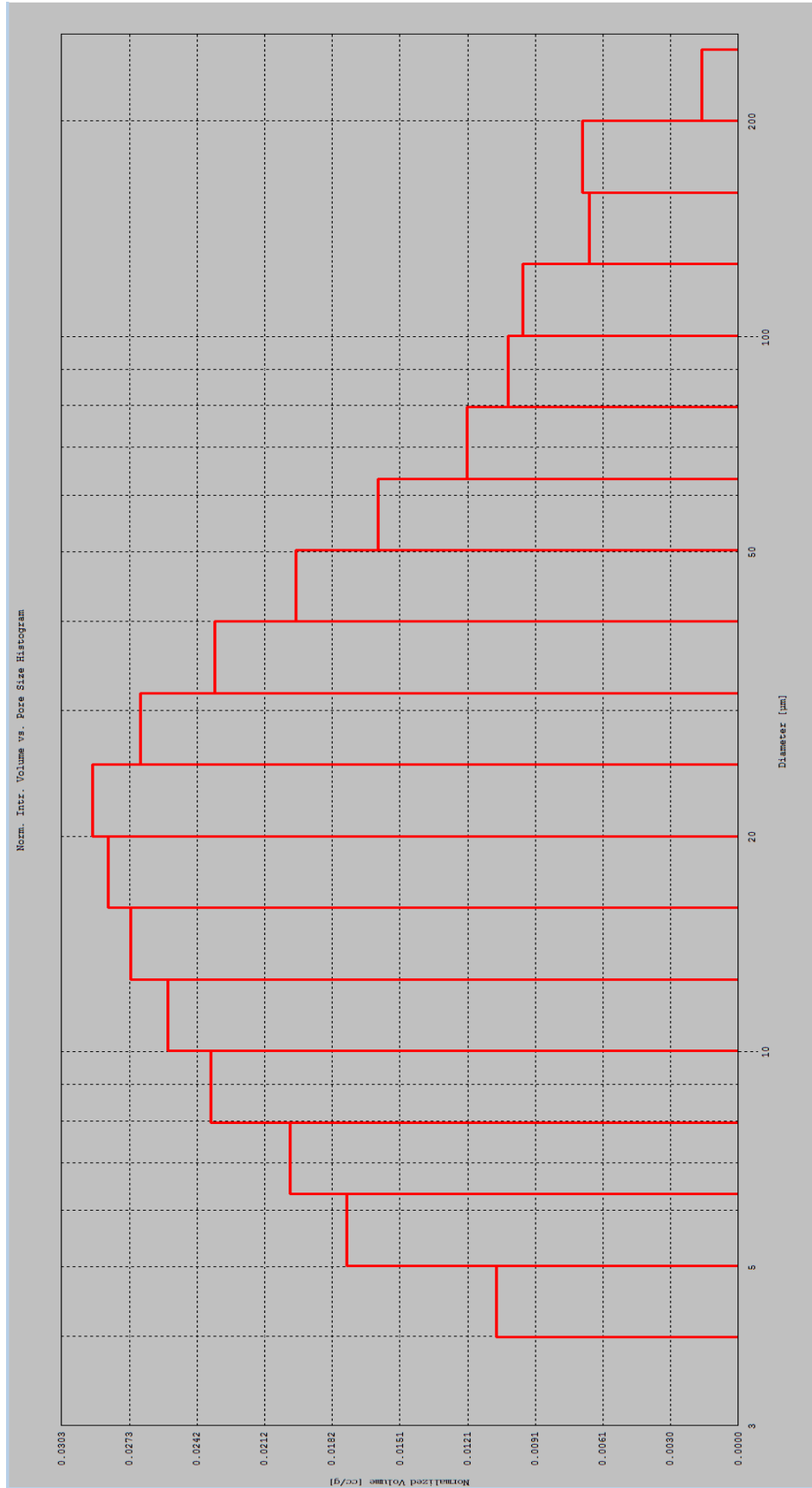


**Figure 31.** Pore size distribution of CA/Ox-PULL/GEL scaffold prepared by the TIPS/PL) method, measured by the mercury porosimetry device

Porosity of scaffolds was theoretically measured by the Archimede's principle. Average porosity percentage in the scaffolds made by the TIPS/PL method was measured to be around 91.6% (Table 21). The two highest porosity percentages were observed in scaffolds without BG ( $94.3 \pm 1.5\%$ ) and B14-10 scaffolds ( $94.5 \pm 0.8\%$ ) and the lowest porosity percentage was observed in B14-20 group ( $87.5 \pm 3.0\%$ ). Increasing BG content from 10% to 20%, caused a decrease in the porosity percentage in B7, and B14 scaffold groups, especially in B14. In B0 group, there was not pronounced difference in the porosity percentages of two groups, and in B21, a slight increase of porosity percentage occurred in B21-20 group. The reason for higher porosity in groups without BG could be due to higher amount of liquid present in the scaffolds (Lemos et al., 2016). Results are consistent with results of similar works. In one study for bone tissue engineering in 2016, highly porous scaffolds were prepared by the freeze-drying method using nano-sized 58S bioactive glass/chitosan/gelatin (BG was added as 0, 10, 20 and 30 wt % of the scaffold). According to porosity measurement results, the group without incorporation of BG had the highest porosity (about 89%), and with increase in BG content, porosity percentage decreased (about 81% in group with 30% BG addition). Porosity percentage difference between the groups was not significant ( $p > 0.05$ ), which showed the independence of the scaffolds porosity from their composition (Maji et al., 2016). Faghiri et al. (2017), prepared composite scaffolds composed of S53P4 bioactive glass and chitosan for bone regeneration purposes and investigated the effect of bioglass content of scaffolds on their porosity percentage. As a result, with increase of BG content in the experimental groups named (chitosan-BG 24 wt%, 29 wt%, and chitosan-BG 49 wt%), overall porosity decreased (Faghiri, 2017).

Porosity is one of the factors determining the success of regeneration by the mesenchymal stem cells/scaffold constructs (Kasten et al., 2008). Organization of dental stem cells, neurogenesis, angiogenesis and also nutritional diffusion depend on adequate porosity and pore size in dentin-pulp complex tissue engineering (Murray et al., 2007). There are a few studies in the literature that investigated the effect of porosity percentage of scaffolds on proliferation and differentiation of



dental pulp cells. AbdulQader et al. (2013), prepared biphasic calcium phosphate scaffold of hydroxyapatite/beta-tricalcium phosphate in a ratio of 20/80 by the wet precipitation method for dentin regeneration. Porosity measurements revealed presence of 65% porosity in the scaffolds. It was suggested that the mean size of 300  $\mu\text{m}$  would be beneficial for the alignment of hDPSCs and their odontoblastic differentiation. (AbdulQader et al., 2013). Zhang et al. (2006), evaluated the performance of hDPSCs on 3-dimensional HA/TCP ceramic discs with a HA/TCP ratio of (60/40), and a titanium fiber mesh consisting of two layers with different fiber diameters. Volumetric porosity measurements revealed 90% porosity in ceramic discs and 86% porosity in the fibrous titanium mesh. According to in vitro tests, both scaffolds enhanced proliferation and differentiation of hDPSCs and after in vivo implantation in mice, well-vascularized tissues that were positive for DSPP (immunohistochemistry and RT-PCR) were formed (Zhang et al., 2006). Wang et al. (2011) investigated the effect of scaffold structure on odontogenic differentiation of hDPSCs by developing nanofibrous (NF) and solid-walled (SW) poly (L-lactic acid) (PLLA) scaffold. Similar porosities of about 96% was measured in both the NF-PLLA and SW-PLLA scaffolds. In vitro and in vivo studies demonstrated promotion of odontogenic differentiation of hDPSCs and mineralization on NF-PLLA scaffolds. (Wang et al., 2011). As compared to these dentin regeneration studies, high porosity of our scaffolds is beneficial for ingrowth and survival of DPSCs (Table 21).

**Table 21.** Porosity percentages of the scaffolds prepared by the TIPS/PL method (n=3)

<b>Groups</b>	<b>Porosity Percentage</b>
Without BG	94.3 ± 1.5
B0 - 10	92.8 ± 0.7
B0 - 20	93.1 ± 1.1
B7 - 10	92.1 ± 1.0
B7 - 20	91.8 ± 0.2
B14 - 10	94.5 ± 0.8
B14 - 20	87.5 ± 3.0 *
B21 - 10	88.7 ± 1.2
B21 - 20	89.6 ± 1.2

B14-20 possessed the lowest porosity percentage among all groups ( $p < 0.05$ ).

### **3.2.6.2. Porosity Results of Scaffolds Prepared by FD/MMP Method**

For measuring porosity of the scaffolds, Archimedes principle was used. Average of porosity percentage in the scaffolds made by the FD/MMP method was measured to be around %88.5 (Table 22). Scaffolds without BG showed the highest porosity percentage ( $90.5 \pm 0.8\%$ ), and B14-20 scaffolds had the lowest porosity percentage ( $87.0 \pm 0.5\%$ ). Increasing BG content from 10% to 20%, decreased the porosity in

B0, B7, and B14 scaffold groups. Higher porosity scaffolds without BG could be due to presence of high volume of liquid in their structure (Maji et al., 2016). These results are comparable with similar studies. Lemos and colleagues (2016), prepared 3D nanocomposite chitosan/bioactive glass scaffolds and evaluated their porosity. 58S bioactive glass (BG) was used in the studies and there were two kinds of experimental groups: with addition of (0% BG, 10% BG, 20% BG, 30% BG) (wt%), and also with incorporation of BG nanoparticles (BGNP) as (0% BGNP, 3% BGNP, 5% BGNP, 10% BGNP (wt%). Porosity decreased from 72% in (0% BG), to 48% in (30% BG) and also from 72.1% in (0% BGNP), to 62.3% in (10% BGNP) (Lemos et al., 2016). Xiong et al. (2014), prepared collagen/hyaluronic acid (HA) composite scaffolds containing nano-bioactive glass (NBAG) by the freeze-drying method for bone tissue engineering. NBAG was added as (0, 5, 10 wt%) of the polymers. Porosity percentage of all groups was higher than 75% and increase in NBAG content, led to a decrease in porosity percentage with no significant difference between the groups ( $p > 0.05$ ). The reason was explained as scaffolds becoming denser as a result of NBAG addition (Xiong & He, 2014).

In regenerative endodontics, scaffolds with high porosity and proper pore size, are required in order to facilitate migration and organization of dental stem cells and diffusion of nutrients throughout the structure (Leong et al., 2016). Effect of porosity percentage of scaffolds on proliferation and differentiation of dental pulp cells has not been studied well (AbdulQader et al., 2016). Tonomura et al. (2010), used a composite of hydroxyapatite/beta-tricalcium phosphate (HAP/b-TCP), with ratio of (2:8) in their in vivo study for investigating the regeneration of dentin-like tissue using porcine dental pulp-derived cells. According to transmission electron microscopy (TEM) results, they had 60% in porosity (Tonomura et al., 2010). Zhang et al. (2006), evaluated in vitro behavior of hDPSCs on 3-dimensional ceramic disks and a fibrous titanium mesh. Sintered HA/TCP ceramic discs with a HA/TCP ratio of 60/40 used in this study, had the volumetric porosity of 90% and the titanium fiber mesh which consisted of two layers (with different fiber diameters), possessed 86% of volumetric porosity (Zhang et al., 2006). In the work by Qu and colleagues

(2015), TIPS/PL method was used for preparing 3D NF-gelatin scaffolds for dental pulp-dentin complex regeneration, and porosity percentage of the scaffolds was found as 96.5% (Qu et al., 2015). If we compare our results with these works, we can see that our scaffolds were porous enough in order to fulfill requirements of dentin tissue engineering.

### **3.2.7. Mechanical Tests**

Compressive strength and elastic moduli values of different groups of scaffolds made by the (TIPS/PL) method were measured at 25% of strain in the stress-strain curve. The highest compressive strength was measured for group B14-10 ( $0.40 \pm 0.03$ ) MPa (Table 23). All BG containing groups except B0-20, possessed higher compressive strength and elastic modulus than the scaffolds without BG. BG incorporation enhanced the mechanical properties. With increase of BG content, compressive strength and elastic moduli values decreased. This shows uniform distribution of BG nanoparticles within the polymer matrix and strong interfacial bonding between inorganic particles and organic matrix in scaffolds (Gao et al., 2009). Increase of BG content to 20%, led to a decrease of mechanical strength in different groups. In the literature it was shown that BG incorporation could improve the mechanical properties of nanocomposites with certain amount of BG addition (Tavakoli et al., 2015, Otadi & Mohebbi-Kalhari, 2015). Lower filler content and nanoparticle size (higher surface area), could increase bonding between the filler and polymers, leading to enhancement of the strength and the ability to resist deformation (Lemos et al., 2016, Abdal-hay et al., 2017). Xiong et al. (2014), prepared composite collagen/hyaluronic acid (HA)/nano-bioactive glass (NBAG) scaffolds for bone regeneration. NBAG was added as (0, 5, 10 wt%) of the polymers. With increase of NBAG content, compressive strength of the scaffolds increased, from 0.31 MPa in group (0 wt% NBAG), to 0.43 MPa in group (10 wt% NBAG), and differences

**Table 22.** Results of porosity measurements of the scaffolds prepared by the FD/MMP method (n=3).

<b>Groups</b>	<b>Porosity Percentage</b>
Without BG	90.5 ± 0.8
B0 - 10	89.2 ± 0.5
B0 - 20	88.6 ± 0.6 *
B7 - 10	89.5 ± 0.4
B7 - 20	88.2 ± 0.8
B14 - 10	87.0 ± 0.5
B14 - 20	85.1 ± 0.7 *
B21 - 10	88.7 ± 1.2
B21 - 20	89.6 ± 1.2

B0-20 and B14-20 possessed the lowest porosity percentages ( $p < 0.05$ ).

Luo et al. (2017), prepared 13-93 bioactive glass/sodium alginate (SA) composite scaffolds by 3D printing method for bone regeneration. BG was added to SA, in mass ratios of 0 : 4, 1 : 4, 2 : 4 and 4 : 4. According to mechanical test (at 70%

deformation), pure SA scaffolds possessed the lowest values (compressive strength: 9.08 MPa, and modulus: 42.62 MPa). BG addition led to an increase in the mechanical properties of BG/SA 1 : 4 group (compressive strength: 10.87 MPa, modulus: 52.49 MPa). BG/SA 2 : 4 group had the highest mechanical properties (compressive strength: 16.47 MPa, modulus: 79.49 MPa), where mechanical properties decreased in BG/SA 4 : 4 group (compressive strength: 10.94 MPa, modulus: 53.07 MPa) (Luo et al., 2017).

In polymeric scaffolds, increase of pore size and porosity, decreases the compressive properties. In our work, this effect is seen in scaffold group without BG, which possessed the highest porosity percentage and its compressive modulus was the lowest among all groups. Although porosity of B14-10 was similar to scaffold group without BG, it possessed the highest compressive modulus among all groups. Increase of compressive modulus in B14-10, shows good distribution of BG nanoparticles in this group. Elastic moduli of all borate modified BG containing groups (except B7-20) were higher than elastic modulus of B0-10 group. In B14 and B21 groups and mechanical strength with 20% BG incorporation has decreased less in comparison to groups B0 and B7. In general, positive effect of borate modified BG incorporation on mechanical properties, especially with 14B-BG and 21B-BG addition was observed. Chen et al. (2015), prepared p(N-isopropylacrylamide-co-butyl methylacrylate) nanogels and added boron-containing mesoporous bioactive glass (B-MBG) to obtain composite scaffolds for bone tissue engineering. Mechanical strength of PIB nanogels was measured by a stress-controlled rheometer. Mechanical strength of the nanogels improved as a result of B-MBG incorporation. When 6.0 wt% B-MBG was added to 5.0 wt% PIB nanogels dispersion, mechanical strength was higher in comparison to 8.0 wt% PIB nanogels dispersion, and with increase in B-MBG content (10.0 wt%), mechanical strength further increased (Chen et al., 2015).

Compressive strength and elastic moduli values of our BG incorporated scaffolds were in the range reported in the literature. Kwon et al. (2017), prepared a collagen

hydrogel scaffold and cross-linked it with cinnamaldehyde (CA) for regenerative endodontic purposes. Mechanical test of hydrogels treated with CA (0, 0.1, 0.5 and 1  $\mu\text{mol l}^{-1}$ ), showed increase in compressive strength of the scaffolds with increase in CA dose, which was from around 0.1 MPa in untreated control group to around 0.5 MPa in (1  $\mu\text{mol l}^{-1}$  CA) group (statistically significant,  $p < 0.05$ ) (Kwon et al., 2017). Qu and colleagues (2014), prepared 3D nanofibrous gelatin/magnesium phosphate (NF-gelatin/MgP) hybrid scaffolds for dentin regeneration. MgP was incorporated as 0%, 5%, 10%, and 20% wt/wt of NF-gelatin. With increase of MgP, up to 10% (wt/wt), the compressive modulus significantly increased ( $\sim 0.5$  MPa), compared to NF-gelatin control ( $\sim 0.4$  MPa) ( $p < 0.05$ ), but higher MgP concentration, led to decrease in the mechanical strength of scaffolds (Qu et al., 2014). Qu et al. (2015), combined low and high-stiffness nanofibrous gelatin (NF-gelatin) matrices into a single scaffold for dentin-pulp complex tissue engineering. According to mechanical test results of cross-linked scaffolds, cross-linking duration affected the compressive modulus of the NF-gelatin under wet conditions, which was 0.23 kPa for 15 min duration and became 24.25 kPa for 24 h duration (Qu et al., 2015).

### **3.3. Cell Culture Studies**

#### **3.3.1. Isolation of hDPSCs**

Dental pulp stem cells (DPSCs) were successfully isolated from human teeth using the enzymatic method. Figure 32 shows phase contrast microscopy images of isolated DPSCs. They had fibroblast-like morphology as reported in previous studies (Eslaminejad et al., 2009, Chen et al., 2012).

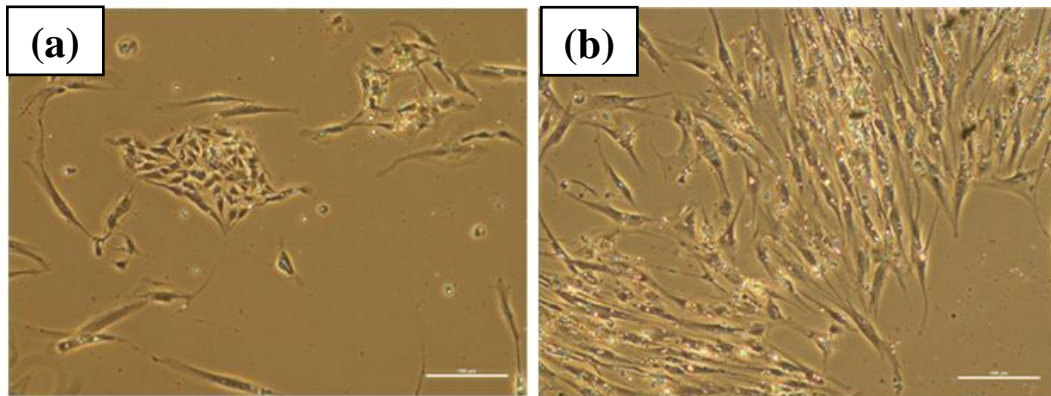


**Figure 32.** Phase contrast microscopy images of the isolated hDPSCs (a) 3 days and (b) 5 days after isolation

### 3.3.2. Characterization of hDPSCs

Flow cytometry analysis was done to confirm mesenchymal stromal phenotype of the isolated stem cells from human third molar teeth. Table 24 shows the percentage of CD positive and CD negative markers expressed by hDPSCs (n=2). Fig.33 shows flow cytometry histograms of hDPSCs of different surface markers. hDPSCs showed high positivity for mesenchymal stem cells markers as CD73 (96.08%), CD44 (85.07%), CD90 (95.9%), CD105 (98.74%) and high negativity for the endothelial stem cells marker of CD31 (78.89%) and hematopoietic stem cells marker of CD45 (76.06%). hDPSCs possessed surface receptors of the mesenchymal stem cells, therefore we can suggest that they were mesenchymal stem cells.



**Table 23.** Compression test results of the scaffolds prepared by the (TIPS/PL) method (n=3).

<b>Groups</b>	<b>Compressive Strength (MPa)</b>	<b>Elastic Modulus (MPa)</b>
Without BG	0.18 ± 0.01	0.72 ± 0.06
B0 - 10	0.33 ± 0.09	1.04 ± 0.17
B0 - 20	0.18 ± 0.07	0.75 ± 0.18
B7 - 10	0.35 ± 0.05	1.25 ± 0.25
B7 - 20	0.19 ± 0.06	0.84 ± 0.12
B14 - 10	0.40 ± 0.03 *	1.57 ± 0.09
B14 - 20	0.34 ± 0.03	1.16 ± 0.05
B21 - 10	0.35 ± 0.07	1.54 ± 0.27
B21 - 20	0.28 ± 0.04	1.20 ± 0.16

\* denotes for the highest statistical difference between group B14-10 and other groups ( $p < 0.05$ ).

**Table 24.** Immunophenotypic properties of hDPSCs cells (n=2). Numbers in the table indicate the percentages of CD positive and CD negative cells.

Percentage of CD positive hDPSCs		Percentage of CD negative hDPSCs	
Markers	hDPSCs	Markers	hDPSCs
CD73	96.08 ± 1.23	CD45	76.06± 1.17
CD105	98.74 ± 0.06	CD31	78.89 ± 7.80
CD90	95.90 ± 1.50		
CD44	85.07 ± 4.47		

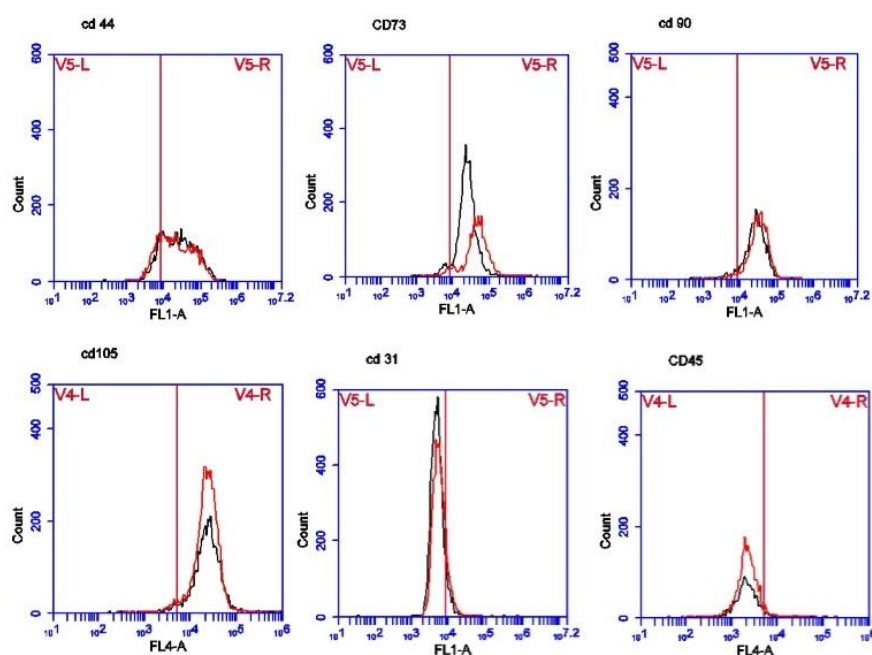


**Figure 33.** Flow cytometry analysis results for expression of surface markers by hDPSCs for mesenchymal stem cells markers (CD44, CD 73, CD90, CD105), endothelial stem cells marker (CD31) and hematopoietic stem cells marker (CD45).

### 3.3.3. In Vitro Cytotoxicity Assessment of BG and Borate Modified BG

For B0-BG group, no toxic effect was observed for all doses at all time points. Higher cell viability relative to control group was observed on days; 1 (except 25 mg/ml), 3 (for 6.25 and 12.5 mg/ml) and 7 (for 3.125 and 6.25 mg/ml) (Fig. 34a-c). For B7-BG group, cell viability decreased to around 60% for 25 mg/ml after 1 day of incubation (Fig. 34a). However, same toxic effect was not observed for 50 mg/ml. After 3 days of incubation, cell viability increased in all groups showing that cells proliferated. At day 7, viability of stem cells treated with 50 mg/ml B7-BG was higher than the control group, which suggested that ions released might have a positive effect on the cell viability. For B14-BG, cytotoxic effect was seen for 25 ve 50 mg/ml concentrations after 3 days of incubation (Fig. 34b). Dose dependent cell viability results of highest B containing group, B21-BG was similar to group B14-BG (Fig. 34). After 3 days of incubation, the lowest concentration had positive effect on proliferation of cells and the highest concentration showed toxic effect. After 7 days of incubation, only 6.25 and 12.5 mg/ml concentrations caused viability higher than 85% relative to the control group and in the other groups, viability was less than 85%. One point that needs to be also considered is that although there was positive effect of ions released on cell viability, a decrease in the cell viability could be observed with time due to confluency reached. Similarly, in a study, a decrease in cell viability was reported after 21 days of incubation of cells derived from human follicular liquid on Bioglass coated Titanium scaffold (Bioglass-Ti), compared to day 7 due to confluency of cells on the biomaterial (Omes & Riva, 2014)

Gong et al. (Gong et al., 2014) studied the effect of extracts of a novel nano-sized 58S BG on proliferation, odontogenic differentiation and mineralization of cells (hDPCs). Proliferation of cells in BG groups was lower than control groups at different time points which could be due to inhibitory effect of high ionic concentrations of Si and Ca. In another study, the effect of ionic dissolution products of 45S5 BG enriched with 2% B<sub>2</sub>O<sub>3</sub> (45S5.2B) on proliferation of human umbilical

vein endothelial cell (HUVEC) was evaluated. According to the results, treatment with (45S5.2B) caused higher cell proliferation. This could be because of concentration of boron in medium being below the toxic level (Durand et al., 2014). In another study, different concentrations of sodium pentaborate pentahydrate (NaB) were used for evaluation of dose dependent effect of cytotoxicity and differentiation on human tooth germ stem cells (hTGSCs). High concentrations of NaB caused toxicity on hTGSCs . On the other hand, viability of cells increased when 10- and 20- $\mu\text{g/ml}$  concentrations were used (Taşlı et al., 2013). According to the cytotoxicity test results, 6.25 mg/ml concentration did not show cytotoxic effect in all BG compositions [B0-BG, B7-BG, B14-BG and B21-BG] during all incubation periods and even caused an increase in cell viability.

For this reason, this concentration was chosen as the optimum concentration for further cell culture studies.

### **3.3.4. Evaluation of Effect of BG Nanoparticles on Differentiation of Dental Pulp Stem Cells**

#### **3.3.4.1. Measurement of Alkaline Phosphatase (ALP) Enzyme Activity and Intracellular Calcium amounts of DPSCs**

Odontogenic differentiation is indicated by alkaline phosphatase activity and calcium uptake increase by the odontogenically committed cells followed by mineralization around the differentiating cells. ALP is an enzyme responsible for production of orthophosphate species inside the cells. In the meantime, osteogenically committed cells start uptake of calcium ions and store. In the end, orthophosphates and calcium ions are released to extracellular environment where mineralization occurs during

osteogenic differentiation. Here, hDPSCs were selected as odontogenic progenitor cells.

Figure 35a shows the results of ALP enzyme activity of DPSCs treated with extracts obtained from 6.25 mg/ml BG NPs. For all groups, ALP enzyme activity of cells at 14-day time point, was higher (nearly 20 times) than the activity observed on day 7. There was not much difference in ALP enzyme activity of cells among BG groups at this time point. ALP is an early biochemical marker of odontogenic differentiation and in some studies its peak has been shown at the end of first week of incubation (Gong et al., 2014) and in some studies at the end of second or third weeks of incubation (Jun et al., 2017).

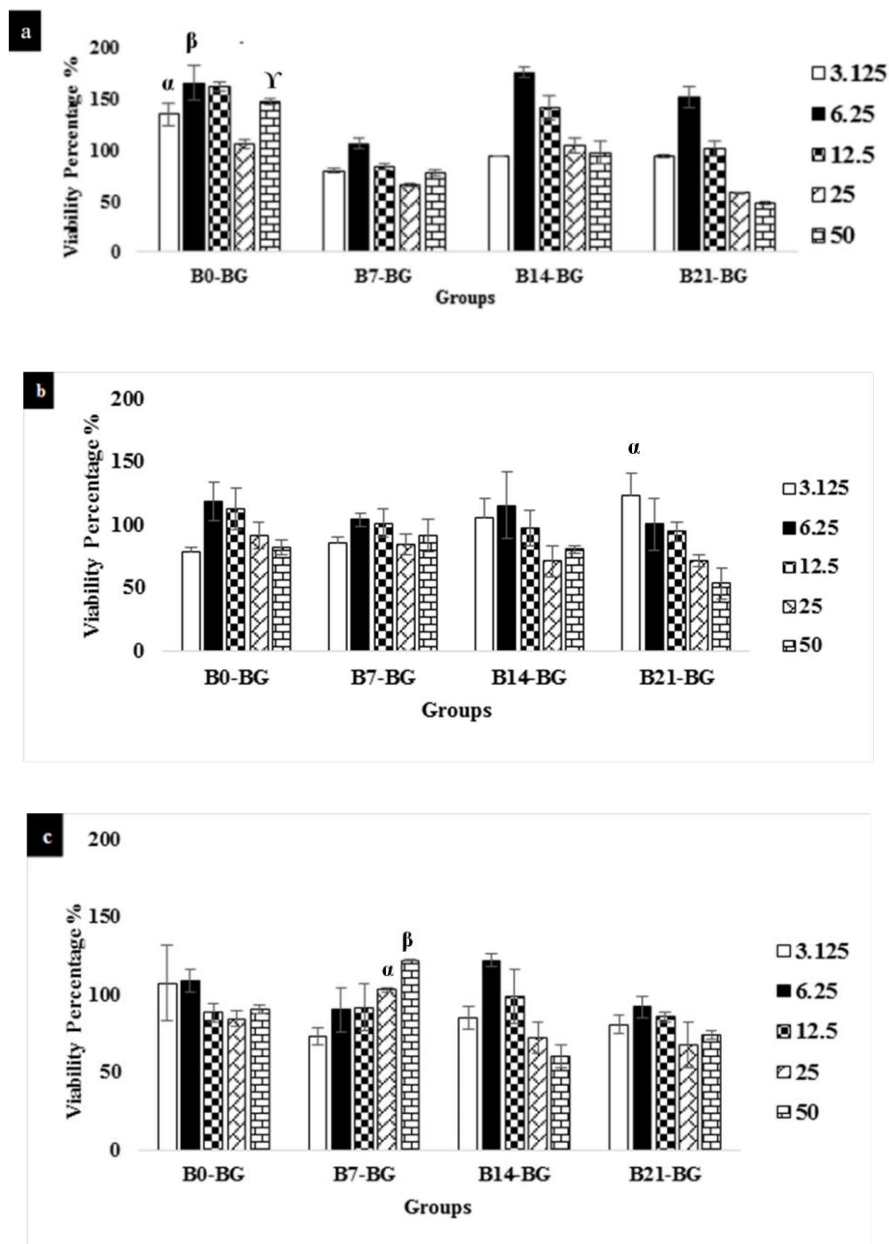


**Figure 34.** Effect of extracts of BG-NPs prepared with different concentrations on the viability of DPSCs (n=4) 1, 3, and 7 days after incubation. Cell viability is given as relative cell viability where viability of untreated DPSCs was taken as 100%. ( $\alpha$ ,  $\beta$ , and  $\gamma$ : denote the statistically highest groups among all BG compositions at day 1.  $\alpha$ : denotes the statistically highest group among all BG compositions at day 3.  $\alpha$ , and  $\beta$ : denote the statistically highest groups among all BG compositions at day 7,  $p < 0.05$ ).

For providing optimum conditions for growth and differentiation of cells, a threshold of BG and inorganic material in the medium is required (Lu et al., 2005). Lee et al. (Lee et al., 2016) prepared aminated mesoporous bioactive nanoparticles (MBNs-NH<sub>2</sub>) and investigated their effect on odontogenic differentiation of rat dental pulp stem cells (rDPSCs). ALP activity of cells was highest at day 14 and elevated concentrations of Ca and Si ions in MBNs-NH<sub>2</sub> treated cells were observed at different incubation periods confirming the odontoblastic differentiation. Sharmin et al. (Sharmin et al., 2013) investigated the effect of B<sub>2</sub>O<sub>3</sub> addition on phosphate-based BG compositions. ALP activity of cells increased with 0–5 mol % B<sub>2</sub>O<sub>3</sub> content, but ALP activity of cells was adversely affected when cells were exposed to a B<sub>2</sub>O<sub>3</sub> content higher than 10%,

Figure 35b shows intracellular calcium amounts of DPSCs treated with extracts obtained from 6.25 mg/ml BG-NPs. At day 7, intracellular calcium amounts in all groups were higher than observed on day 14. The amount of intracellular calcium in TCPS (control) group was statistically lower than all BG treated groups and highest intracellular calcium amount was observed in B21- BG group ( $p < 0.05$ ) at day 7. Positive effect of extracellular Ca<sup>2+</sup> and Si<sup>4+</sup> on osteogenic and odontogenic differentiation is known, but the role of intracellular levels or effects of Ca<sup>2+</sup> and Si<sup>4+</sup> on odontoblast differentiation have not been well studied (Tousi et al., 2013, Li et al., 2015). In the study conducted by Li et al. (Li et al., 2015) it was shown that Ca<sup>2+</sup> positively affects odontoblastic differentiation of DPSCs by increasing the endogenous BMP2 expression level and enhancing expression of dentin sialophosphoprotein (DSPP), but inhibits ALP activity. As a result of high ALP activity, high concentrations of phosphate are provided at the site of mineral deposition. At day 14, intracellular calcium has been consumed with phosphate to form hard tissue. Dentin which is composed of calcium and phosphate, is formed by differentiated odontoblasts from DPSCs (Lee et al., 2016). Overall, ALP activity is also considered as a marker for odontoblastic differentiation of hDPSCs (Han et al., 2014). Zhang et al. prepared bioactive calcium phosphate cements incorporating zinc-bioglass (ZnBG). Adding Zn-BGN enhanced odontogenic differentiation of

DPSCs and mineralized nodule formation significantly increased with increase in amount of Zn-BGN added (Zhang et al., 2015).

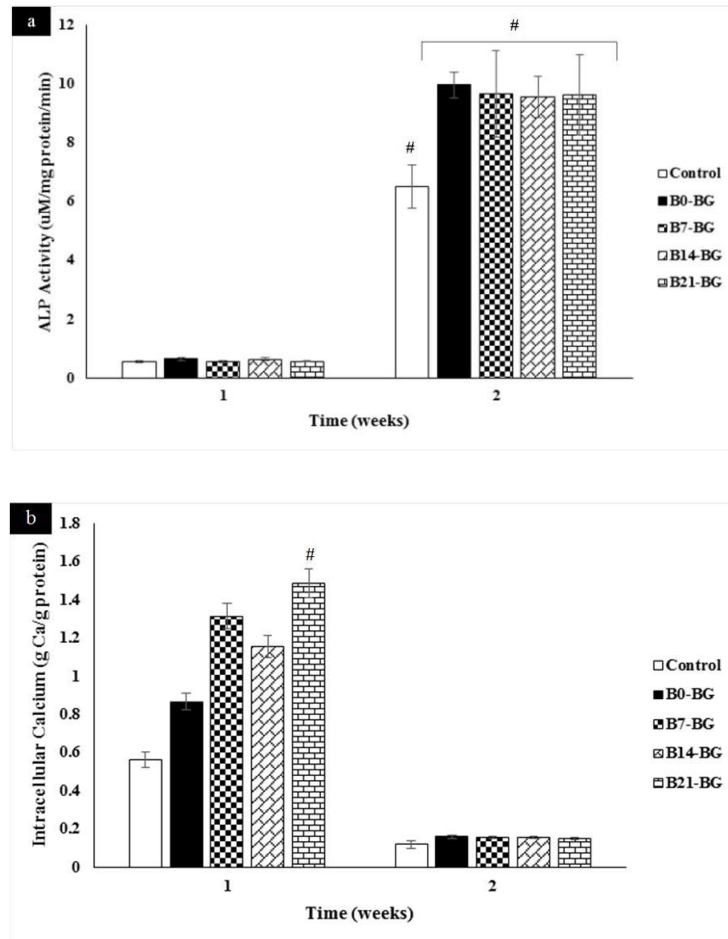


**Figure 35.** (a) ALP activity and (b) intracellular calcium amounts of DPSCs cells treated with extracts obtained with 6.25 mg/ml in odontogenic differentiation medium (DMEM containing 10% FBS, 1% penicillin-streptomycin, 50  $\mu$ g/ml ascorbic acid, 10 mM  $\beta$ -glycerophosphate, and 10 nM dexamethasone) at different incubation periods (n=4). For ALP activity, # denotes the statistical difference between groups at week 2 and for intracellular calcium amounts, # denotes the statistical difference between group B21-BG and groups (without BG, and B0-BG) at week 1 (p<0.05).



### 3.3.4.2. Immunohistochemical Staining

To evaluate the effect of borate modification of BG on odontoblast differentiation immunocytochemical staining for DSPP, osteopontin, collagen type I was conducted on DPSCs treated with extracts of boron modified BG and BG nanoparticles. DSPP is a well-known marker of odontoblasts and plays important roles in early odontoblast differentiation and late dentin mineralization of dental pulp cells (Wei et al., 2007, Feng et al., 1998). Osteopontin is a significant osteoblast-related gene product and mature osteoblasts, odontoblasts, and cementoblasts could synthesize it (Morinobu et al., 2003, Narayanan et al., 2001, Yamamoto et al., 2016). Collagen type I is synthesized during functional differentiation of odontoblasts (Narayanan et al., 2001, Sato et al., 2009). Positive staining for DSPP (Fig. 36a-d), osteopontin (Fig. 36e-h) and collagen type I (Fig. 36i-l) proteins in the cytoplasm of the hDPSCs was observed in all of the BG groups after culturing in media containing 6.25 mg/ml BG extracts of different BG groups for 7 days. Staining results on day 7 were moderate for all groups and with increase of borate content in BGs, reaction was more pronounced. Positive staining for DSPP (Fig. 37a-d), osteopontin (Fig. 37e-h) and collagen type I (Fig. 37i-l) proteins in the cytoplasm of the hDPSCs was also observed in all of the BG groups, when culture continued for 14 days. Staining results on day 14 were intense for all groups and with increase of borate content in BGs, reaction was more pronounced which showed the positive effect of borate addition for odontogenic differentiation of DPSCs. Similarly, Taşlı et al., showed the positive effect of boron on odontogenic differentiation of stem cells. In this study, they prepared different concentrations of sodium pentaborate pentahydrate (NaB) and assessed effect of boron on osteogenic and odontogenic differentiation of Human Tooth Germ Stem Cells (hTGSCs). As a result of immunocytochemical stainings, expression of osteogenic markers (OCN and COL1A) was confirmed (Taşlı et al., 2013). In one study, Gong and colleagues evaluated the effect of a novel nano-sized

58S bioactive glass (nano-58S BG) on odontogenic differentiation of hDPSCs in vitro. After exposing hDPSCs to nano-58S BG, 45S5 BG, and 58S BG extractions, immunocytochemical assay of DSPP on day 7 and OCN on day 14 revealed positive staining of both markers in the BG groups. Staining was most intense in the nano-58S group, but 58S, 45S5 group, and control groups, showed moderate, light, and negative staining, respectively. As a result, it was shown that nano-sized 58S BG could enhance the odontogenic differentiation of hDPSCs (Gong et al., 2014).

### **3.3.5. Cell Viability Assays for the 3-Dimensional Scaffolds**

#### **3.3.5.1. Scaffolds Prepared by TIPS/PL Method**

Viability of hDPSCs on the scaffolds was determined by Alamar Blue Assay (Fig. 38). In all groups, reduction percentage of Alamar blue has increased with time and this shows that hDPSCs proliferated on the scaffolds. Among the BG incorporated groups, viability of cells on B0-20 and B14-10 was higher than observed on scaffolds without BG. Increase in BG content of scaffolds resulted in an increase of cell viability, except B14 incorporated group. Incorporation of borate has caused increase in cell viability, in other words cell proliferation at day 3 in comparison to B0 group. In Group B14-10 cell proliferation was slightly higher than observed in scaffold group without BG after 7 days of incubation. In one study, biocompatibility of glutamine-based segmented polyurethanes including 1 to 25 wt.% BG-NPs was evaluated in vitro with DPSCs. Enhanced proliferation of DPSCs, was observed at

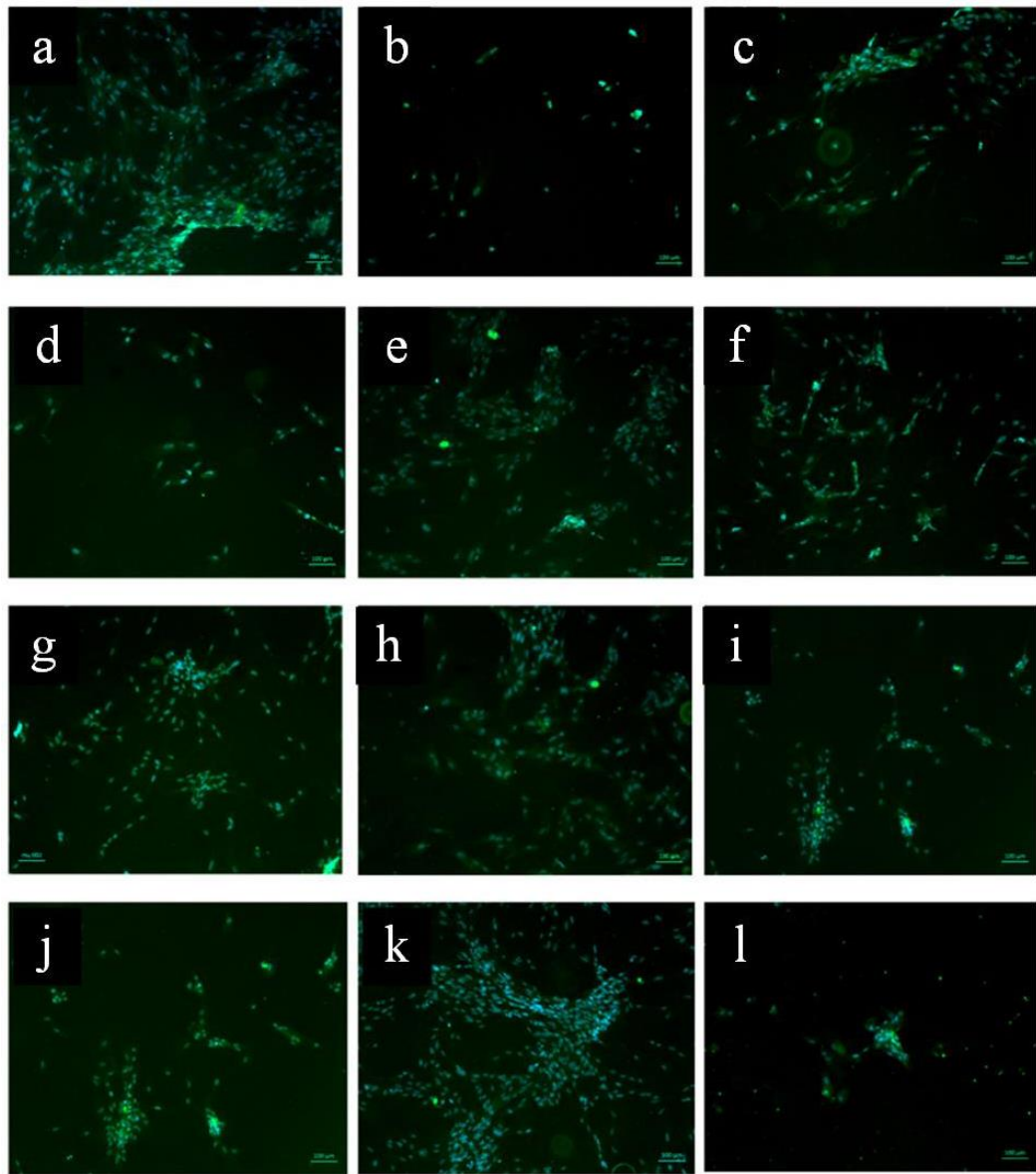


**Figure 36.** Results of immunocytochemical staining of DPSCs incubated in medium containing 6.25 mg/ml BG extracts after 7 days, (a, b, c, d) [DSPP (green) and DAPI (blue) staining for group B0-BG, group B7-BG, group B14-BG, group B21-BG; (e, f, g, h) [Osteopontin (green) and DAPI (blue) staining for group B0-BG, group B7-BG, group B14-BG, group B21-BG; (i, j, k, l) [Collagen type I (green) and DAPI (blue) staining for group B0-BG, group B7-BG, group B14-BG, group B21-BG; (scale bar: 100  $\mu$ m).

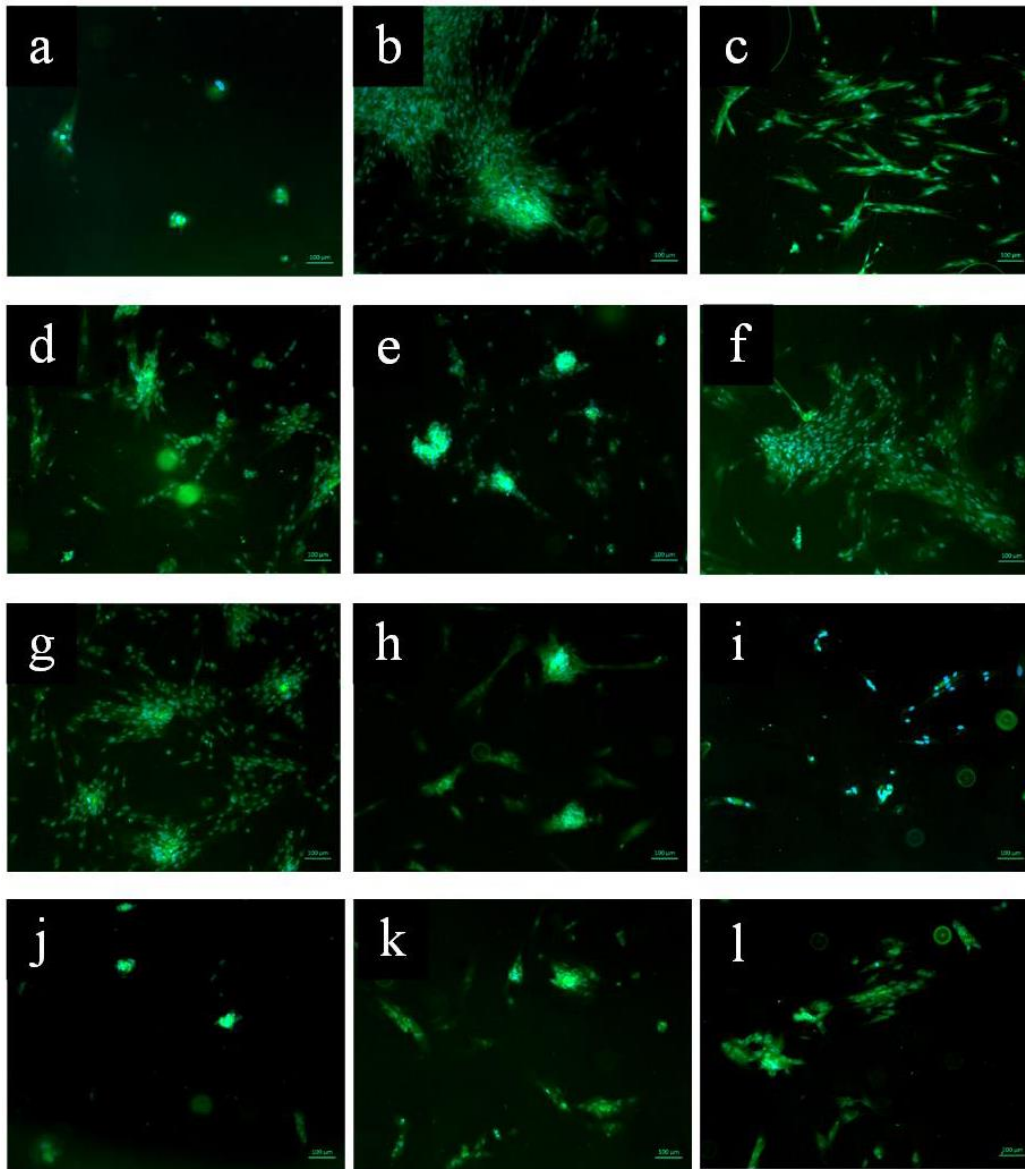


**Figure 37.** Results of immunocytochemical staining of DPSCs incubated in medium containing 6.25 mg/ml BG extracts after 14 days, (a, b, c, d) [DSPP (green) and DAPI (blue) staining for group B0-BG, group B7-BG, group B14-BG, group B21-BG; (e, f, g, h) [Osteopontin (green) and DAPI (blue) staining for group B0-BG, group B7-BG, group B14-BG, group B21-BG; (i, j, k, l) [Collagen type I (green) and DAPI (blue) staining for group B0-BG, group B7-BG, group B14-BG, group B21-BG; (scale bar: 100  $\mu$ m).

day 5 after incubation in composites with (1–2.5 wt.%) BG-NPs, and composites with (5, 15, 25 wt.%) filler, adversely affected the proliferation at day 9 (Aguilar-Pérez et al., 2016). Demirci and colleagues (2015) prepared dental composites having different amount of sodium pentaborate pentahydrate. hDPSCs were used for osteogenic and odontogenic differentiation experiments to test the biocompatibility of the materials. Boron-containing dental composites promoted osteogenic and odontogenic capabilities of hDPSCs, while being non-toxic (Demirci et al., 2015).

It has been shown that boron increases osteoblast cells proliferation and mineralization via regulating expression of messenger RNA (mRNA) of proteins involved in mineralization, such as collagen type 1 (COL1), osteopontin (OPN), bone sialoprotein (BSP), and osteocalcin (OCN) (Hakki et al., 2010). Effect of boron on hBMSCs differentiation is due to increased level of mRNA expression related to alkaline phosphatase and bone morphogenetic proteins (BMPs) (Ying et al., 2011, Salazar, 2016).

Morphology of cells on scaffolds was studied by SEM at different incubation periods (Fig.39). One day after incubation, hDPSCs attached on scaffolds and spread (Fig. 39-a,c,e,g,i,k,m,o). On day 7, consistent with Alamar blue test result, proliferation of hDPSCs on the scaffolds increased. They spread along the pore surfaces and filled the scaffolds surfaces (Fig 39-b,d,f,h,j,l,n,p). According to these results, it was observed that the prepared scaffolds supported adhesion and spread of hDPSC cells. In all groups, on day 1, cells began spreading after adherence and appeared to spread more on day 7. In the scaffold group without BG, on the 7th day, the cells spread well over the scaffold and covered the surface. In BG containing groups, when the amount of BG was increased from 10% to 20%, adhesion and spread of the cells increased and among the borate incorporated groups, hDPSCs on B7 and B14 spread more on day 7. Wu vd. (2011) prepared boron-containing, dexamethasone (DEX) loaded mesopore bioactive glass (MBG) scaffolds to investigate the biological properties of the scaffolds. On day 1, they observed that a few number of osteoblasts

adhered on the surface of the pore walls and on day 7, cells spread on the pore walls and populated the pores (Wu et al., 2011).

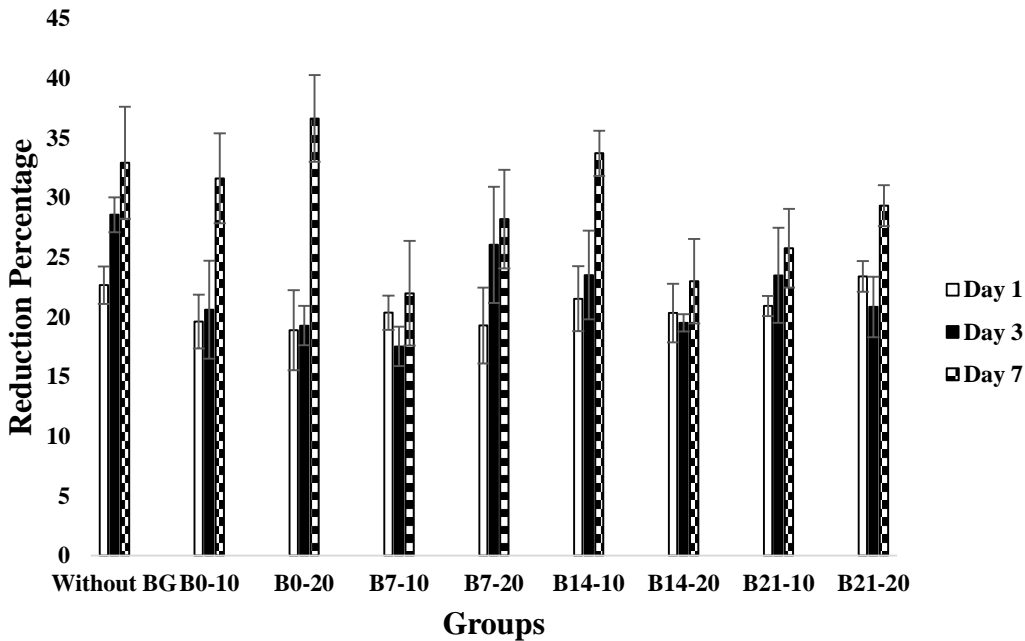


**Figure 38.** Result of proliferation assay of hDPSCs cultured on scaffolds prepared by the TIPS/PL method with Alamar blue assay for 7 days (n=3).

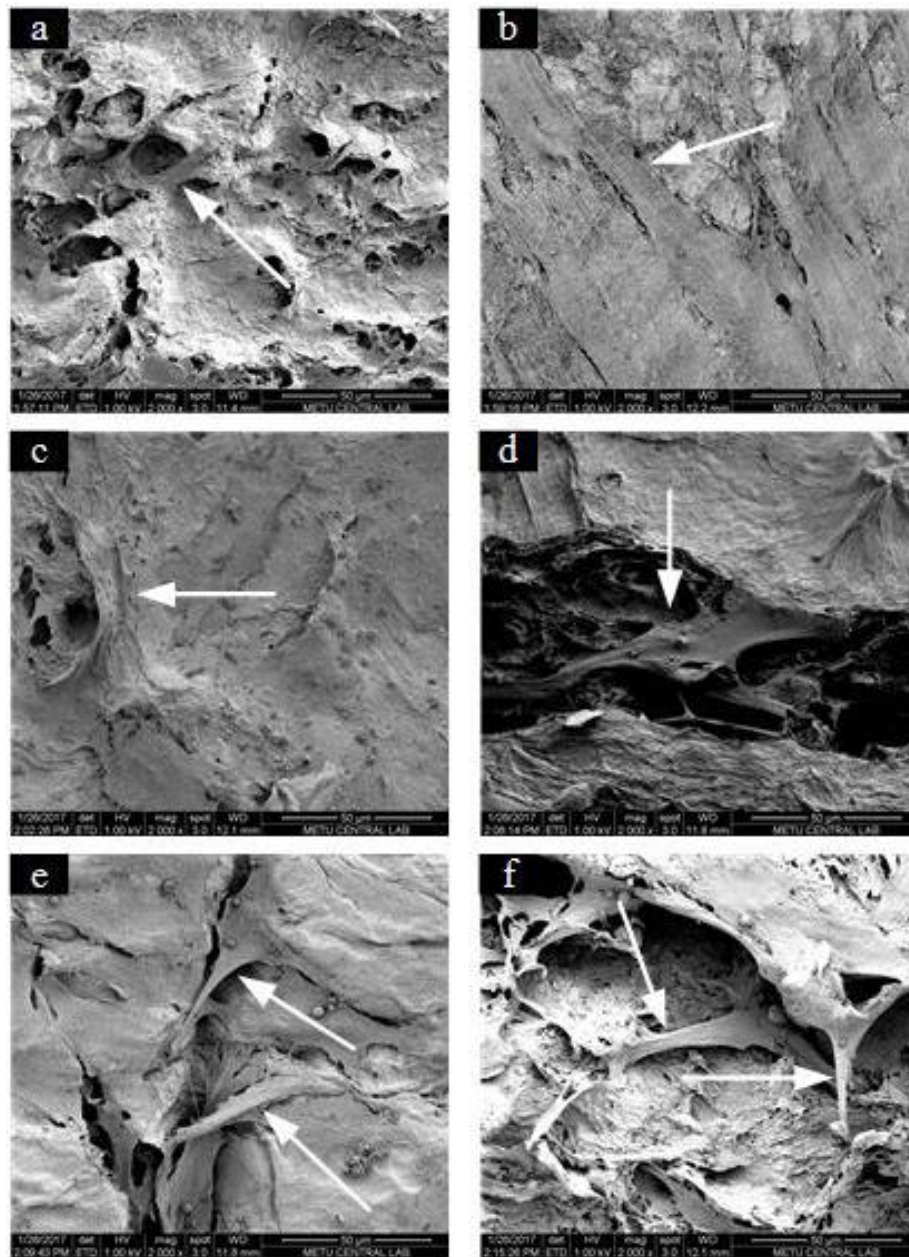


**Figure 39.** SEM images of hDPSCs seeded on the scaffolds prepared by the TIPS/PL method: a) without BG, day 1; b) without BG, day 7; c) B0-10, day 1; d) B0-10, day 7; e) B0-20, day 1; f) B0-20, day 7 (scale bar: 50  $\mu$ m).

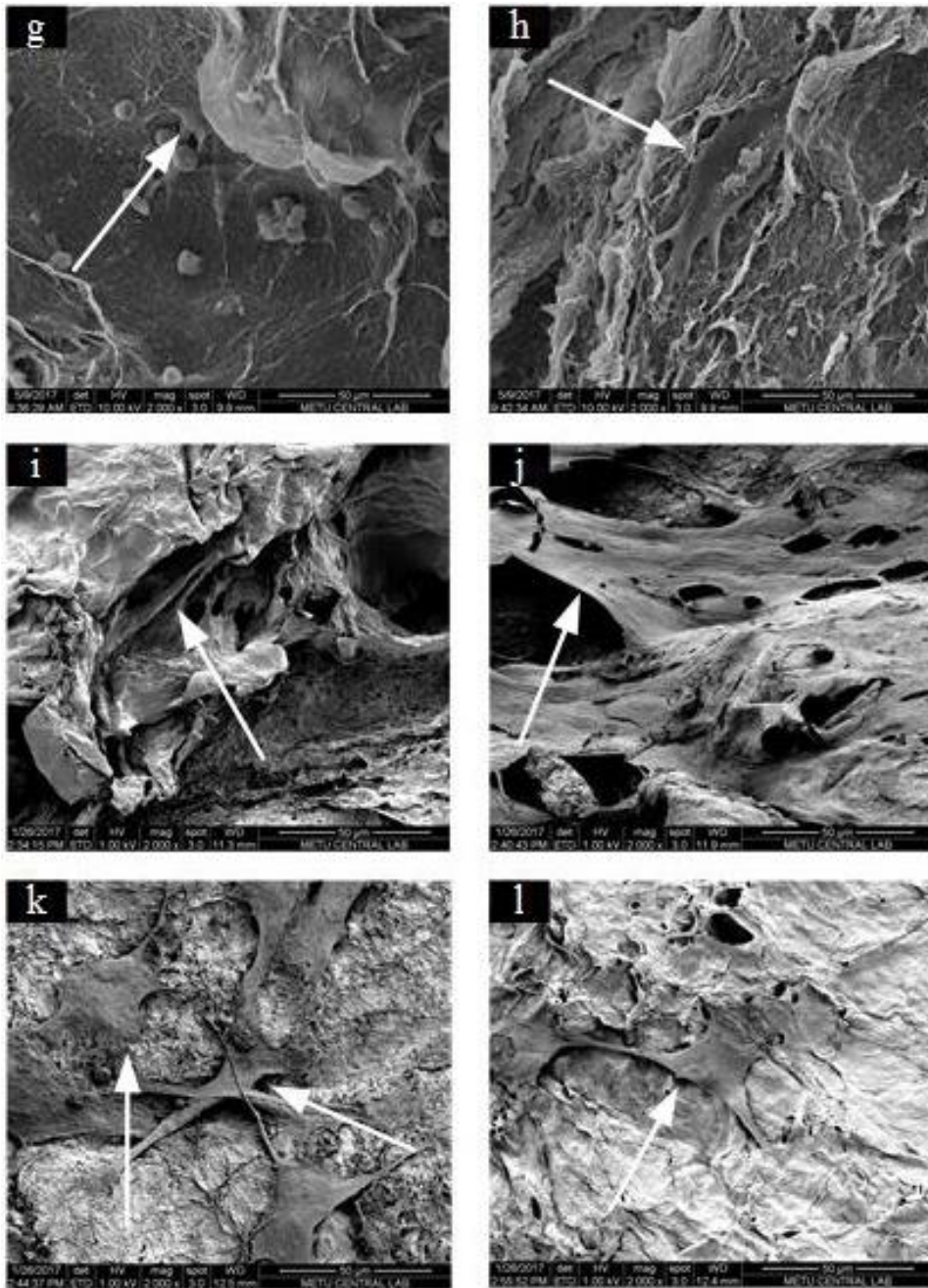


**Figure 39 - Continued.** SEM images of hDPSCs seCeded on the scaffolds prepared by TIPS/PL method: g) B7-10, day 1; h) B7-10, day 7; i) B7-20, day 1; j) B7-20, day 7; k) B14-10, day 1; l) B14-10, day 7 (scale bar: 50 µm).



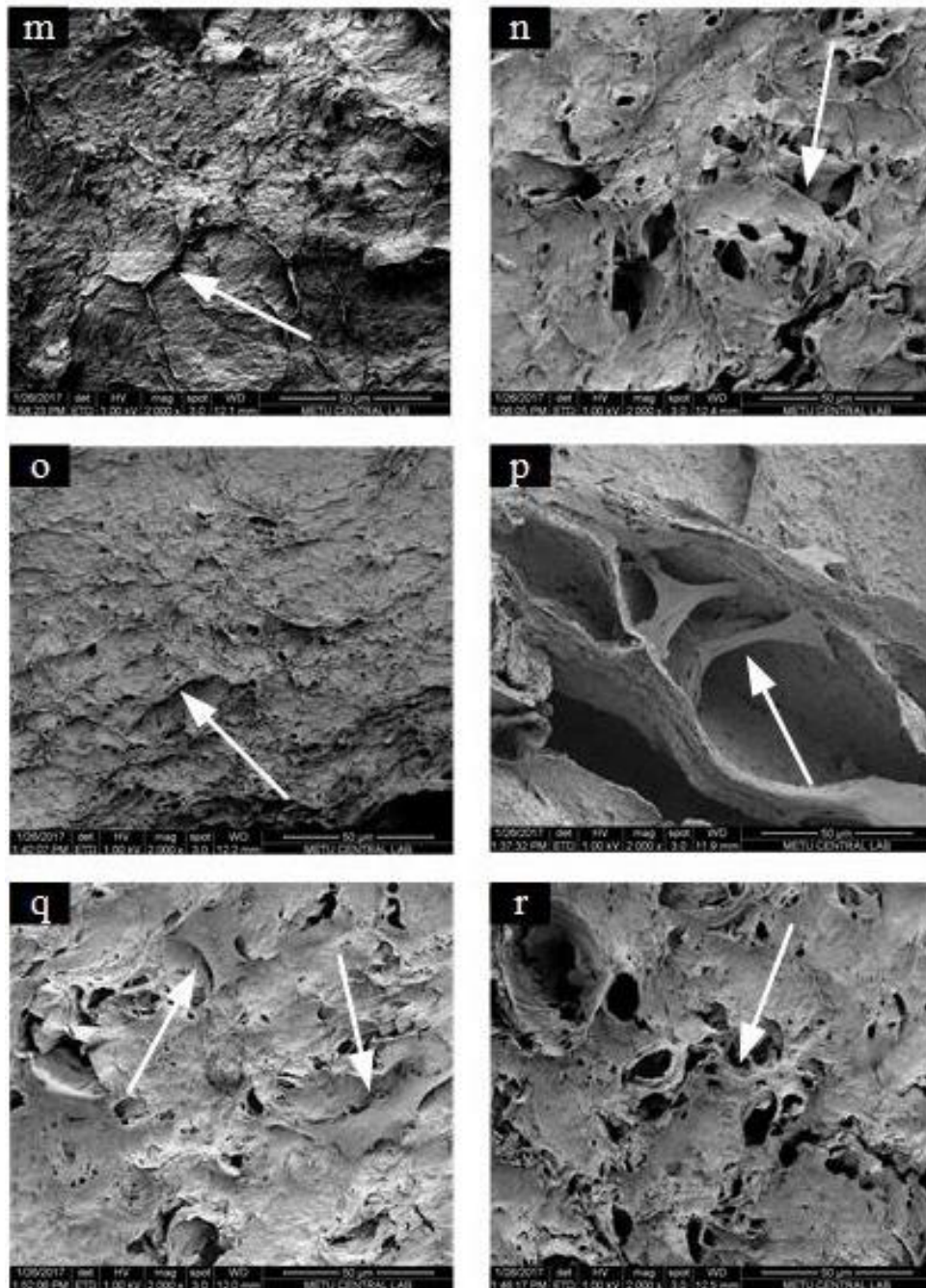


**Figure 39 - Continued.** SEM images of hDPSCs seeded on the scaffolds prepared by the TIPS/PL method: m) B14-20, day 1; n) B14-20, day 7; o) B21-10, day 1; p) B21-10, day7; q) B21-20, day 1; r) B21-20, day 7 (scale bar: 50  $\mu$ m).

### 3.3.5.2. Scaffolds Prepared by FD/MMP Method

Viability of hDPSCs on the scaffolds was determined by Alamar Blue Assay (Fig. 40). According to results obtained for cellular viability analysis at the end of day 1, all scaffolds displayed equally favorable properties in terms of cellular attachment. However, B0-10 samples presented a significantly lowest number of cells attached ( $p < 0.05$ , Fig. 40). Since we observed cells in the macropores 1 day after seeding for all scaffolds regardless of the presence of pure and borate modified BG-NPs, lower attachment on B0-10 containing scaffolds could be as a result of loss of cells from scaffolds during seeding step but not due to cytotoxicity (Fig. 41). Additionally, a significant increase in cell viability was observed from day 1 to day 7 for all groups (Fig. 40). Owing to highest hDPSCs viability on B7-20 scaffolds, the presence of borate as a dopant in BG species was not only found to be non-cytotoxic but also prompted to support a more suitable environment for hDPSCs proliferation (Fig. 40). Although a higher cell viability was observed on scaffolds containing borate modified BG, cell viability on B14 and B21 scaffolds was lower than observed B7 containing scaffolds on day 7 (Fig. 40). A study on the effect of B on the human tooth germ cells (hTGC) by Taşlı et al. (2015) showed that in spite of an initial increment in cellular viability of hTGCs was observed, increase in boron concentration resulted in dose dependent decrease in hTGC viability (Taşlı et al., 2013). Consequently, B7, B14 and B21 scaffolds can be regarded as non-cytotoxic, and improved cell adhesion and proliferation. Among these groups B7 containing scaffolds scaffolds appeared to be more robust for cellular attachment and proliferation.

Furthermore, SEM images showed that cells could migrate into macropores and proliferate without any sign of cytotoxicity (Fig. 41). No significant morphological difference was observed for cells observed in all scaffold groups on days 1 and 7. Moreover, hDPSCs were found to form a confluent layer of cells in macropores and continue to proliferate on day 7 (Fig. 41). The confluent layer of hDPSCs and protrusions from proliferating cells (white arrow) suggested that a dynamic

environment that mimicks natural dental extracellular matrix with BG reinforcements was present that resulted in odontoblastic differentiation of hDPSCs in macropores. In a similar study, Wu et al. studied silk-based 3D scaffolds for dentin tissue engineering and claimed that silk scaffolds having 550  $\mu\text{m}$  pores led to extensive dentin tissue formation after implanted in rat omentum for 20 weeks due to macroporous structure (Xu et al., 2008).

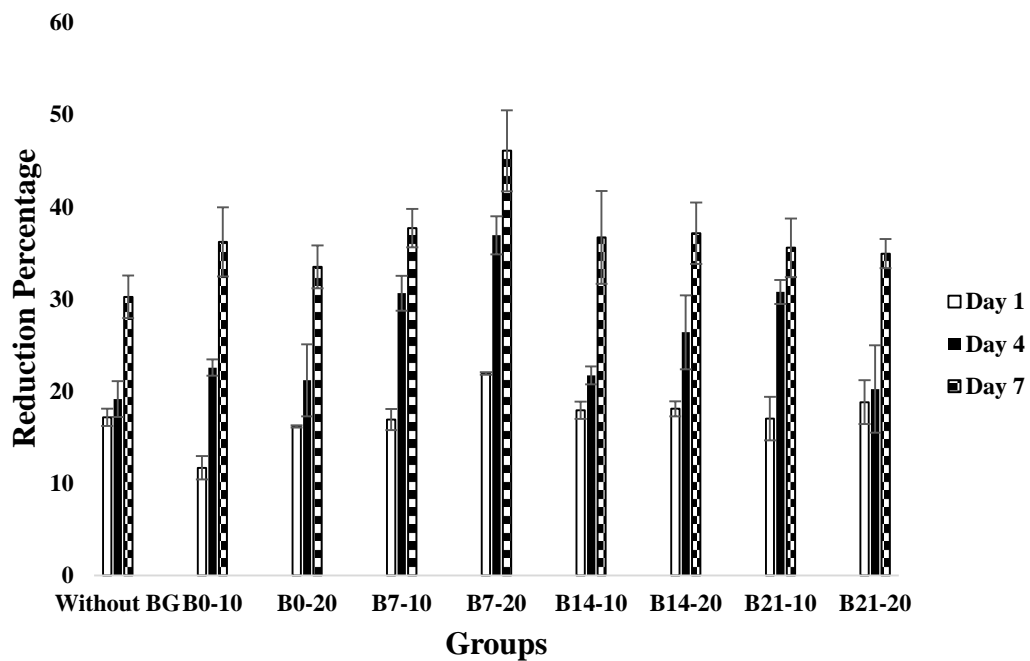


**Figure 40.** Result of proliferation assay of hDPSCs cultured on scaffolds prepared by the FD/MMP method with Alamar blue assay for 7 days (n=3).

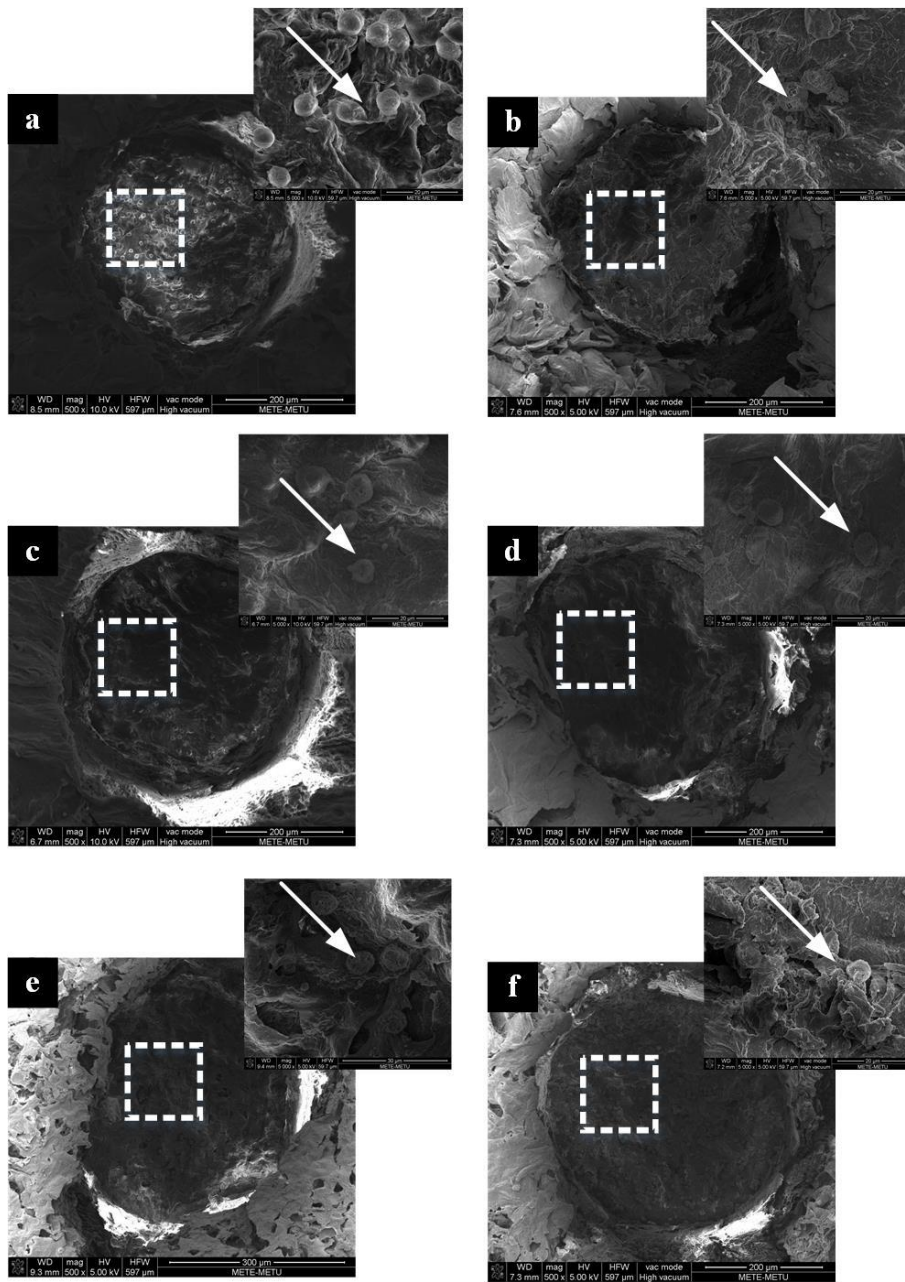


**Figure 41.** SEM images of hDPSCs seeded on the scaffolds prepared by the FD/MMP method a) without BG, day 1; b) without BG, day 7; c) B0-10, day 1; d) B0-10, day 7; e) B0-20, day 1; f) B0-20, day 7 (scale bar: 200 μm, inserts: 20 μm), white arrows show cells.

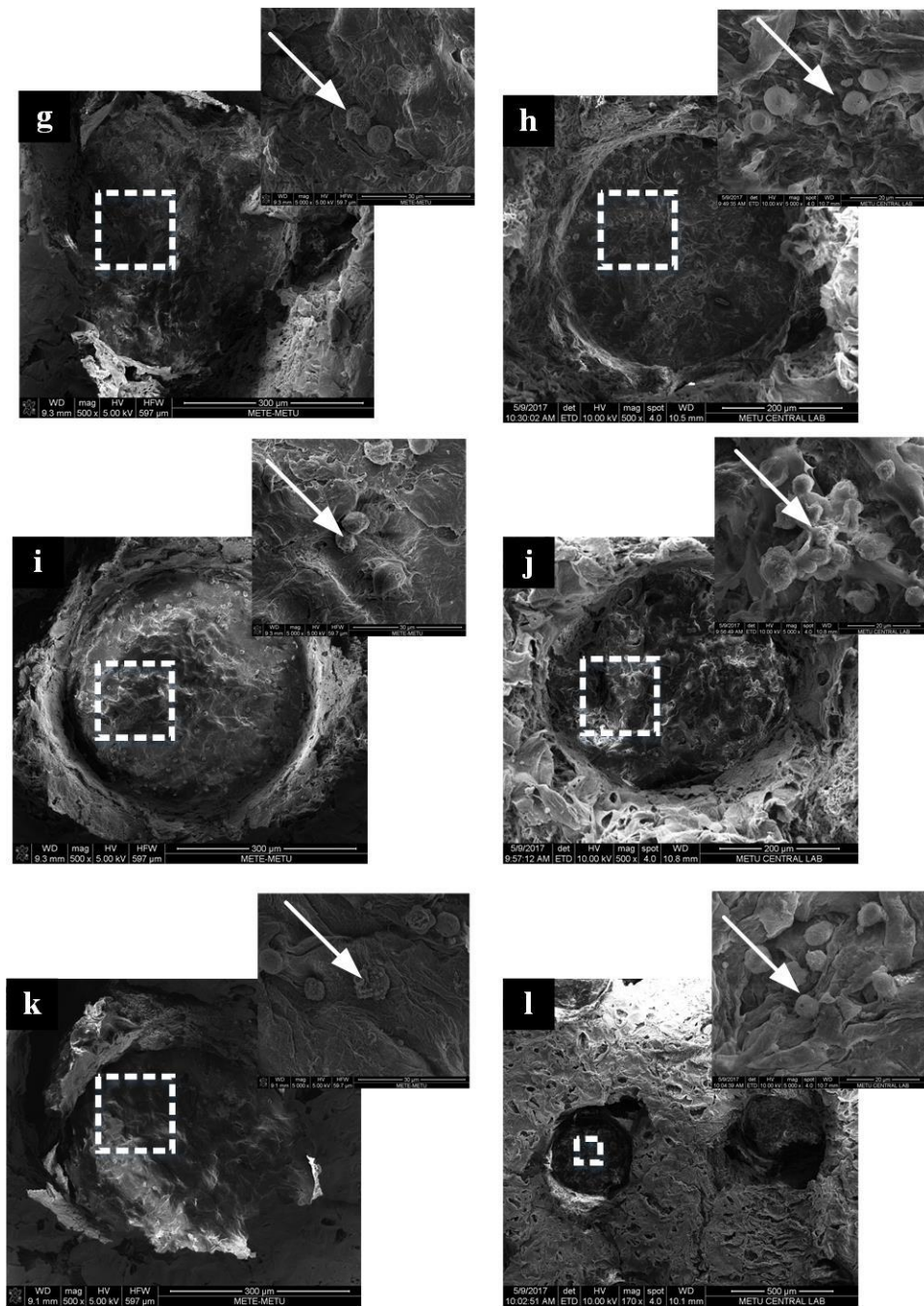


**Figure 41 - Continued.** SEM images of hDPSCs seeded on the scaffolds prepared by the FD/MMP method: g) B7-10, day 1; h) B7-10, day 7; i) B7-20, day 1; j) B7-20, day 7; k) B14-10, day 1; l) B14-10, day 7 (scale bar: 200  $\mu\text{m}$ , inserts: 20  $\mu\text{m}$ ), white arrows show cells.

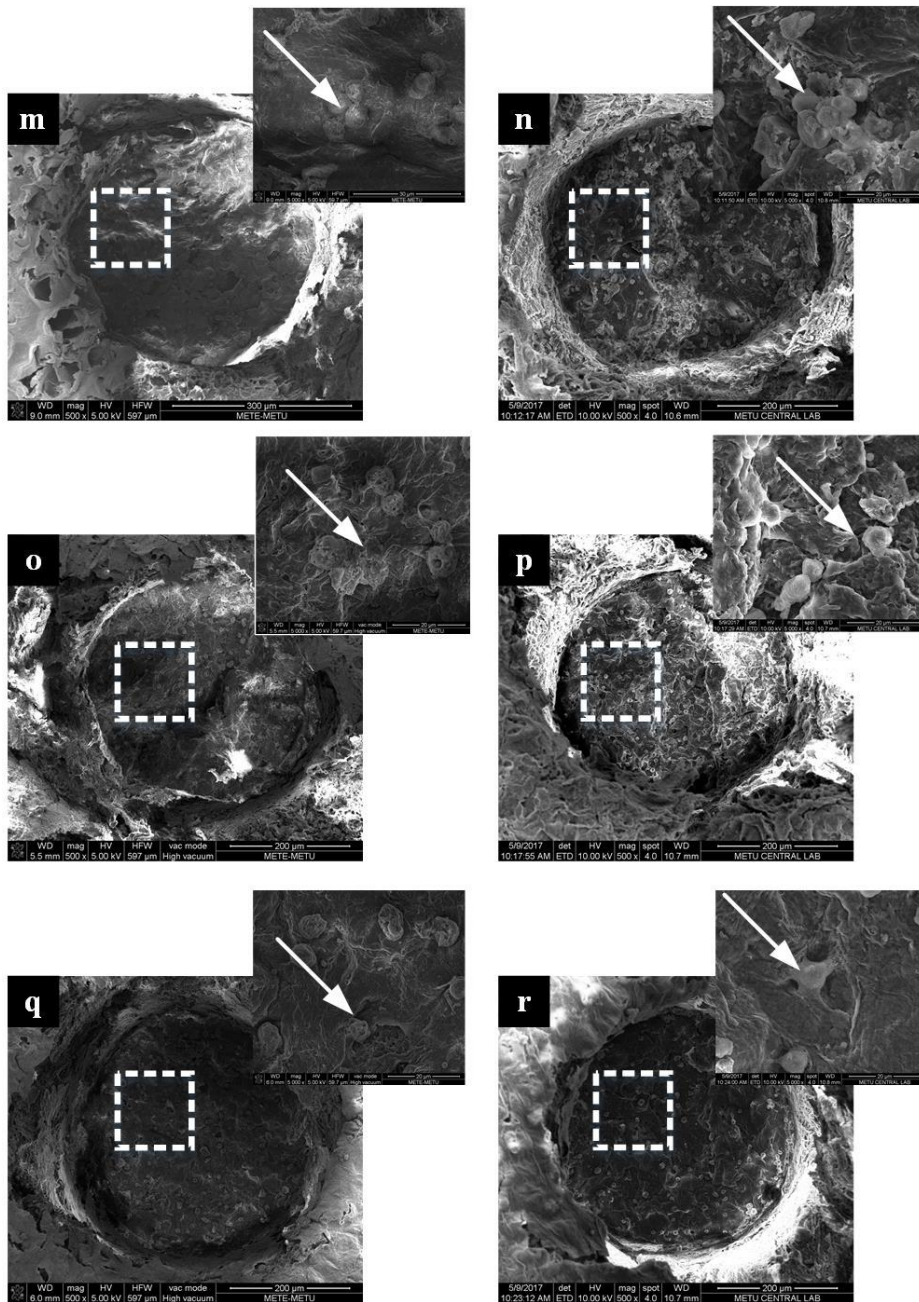


**Figure 41 - Continued.** SEM images of hDPSCs seeded on the scaffolds prepared by the FD/MMP method: m) B14-20, day 1; n) B14-20, day 7; o) B21-10, day 1; p) B21-10, day 7; q) B21-20, day 1; r) B21-20, day 7 (scale bar: 200  $\mu\text{m}$ , inserts: 20  $\mu\text{m}$ ), white arrows show cells.

### **3.3.6. Evaluation of Differentiation of hDPSCs Seeded on Three Dimensional Scaffolds**

#### **3.3.6.1. Measurement of ALP Activity and Intracellular Calcium Amounts of hDPSCs Seeded on Three Dimensional Scaffolds**

##### **3.3.6.1.1. Scaffolds Prepared by TIPS/PL Method**

ALP activity and intracellular calcium amounts of hDPSCs seeded on the scaffolds prepared by the TIPS/PL method, were measured after 7 and 14 days of culture (Fig. 42&43). The highest ALP enzyme activity in all groups was observed after 14 days of incubation. At day 14, ALP enzyme activity of all groups was about 10-fold higher than that observed at the end of the 7-day incubation. No significant difference was observed in ALP enzyme activity of cells seeded onto different scaffold groups. However, on the 14th day, ALP enzyme activity of cells on scaffolds without BG was significantly lower than all groups. Cells in B14-10 and B14-20 groups had higher ALP enzyme activity than groups (B0-10, and B21-10) at this time point ( $p < 0.05$ ). ALP activity results indicated that hDPSCs differentiated into odontoblasts (Lee et al., 2016), and incorporation of borate modified BG, promoted the differentiation profoundly.

In one study, a composite nanofibrous matrix made of biopolymer blend polycaprolactone-gelatin (BP) and mesoporous bioactive glass nanoparticles (BGNs) was prepared and odontogenic differentiation of hDPSCs seeded on BGNs was assessed. Addition of BGNs promoted ALP activity levels and increase of BG amount from 10% to 20% in scaffolds resulted in increased levels of ALP activity of cells. (Kim et al., 2015). In another study, the effect of different concentrations of sodium pentaborate pentahydrate (NaB) on odontogenic differentiation of human tooth germ

stem cells (hTGSCs) was investigated. ALP activity of stem cells, which were treated with NaB for 14 days, was statistically significantly higher than the control group (Taşlı et al., 2013).

Intracellular calcium amounts of all groups on day 14 after incubation, were higher than their amounts on day 7 (Fig. 43). There was no significant difference in intracellular calcium levels of different groups at time point 7 day. However, on the 14th day, intracellular calcium amounts measured in B14-10 and B14-20 scaffold groups were significantly higher than other groups ( $p < 0.05$ ). These results were consistent with the results of ALP activity, which showed the positive effect of borate modified BG presence for stimulating odontogenic differentiation of hDPSCs in scaffolds.

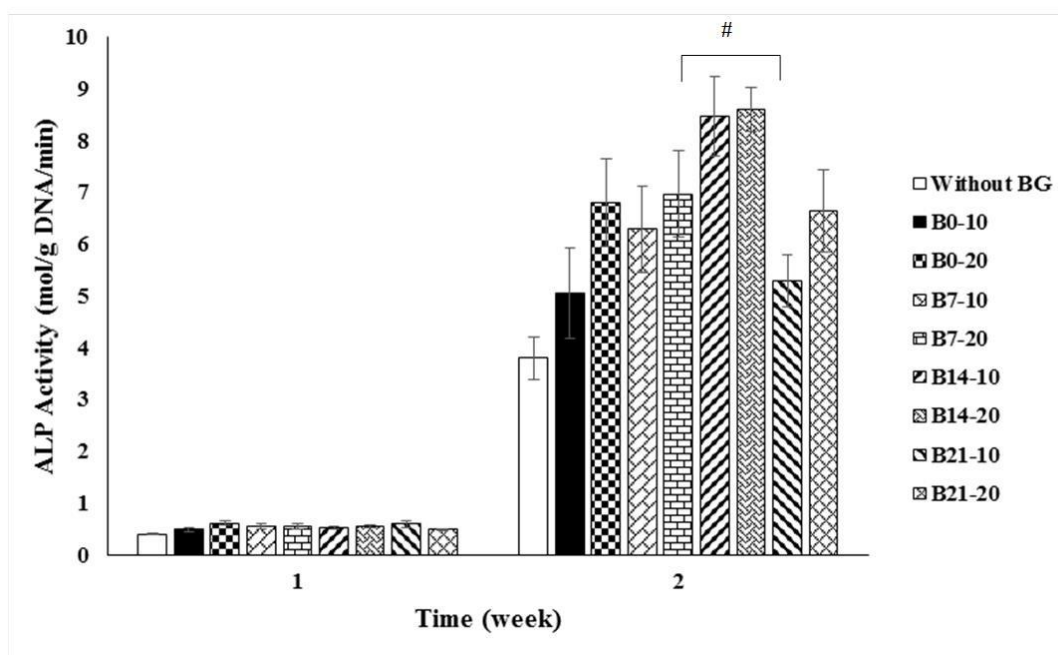


**Figure 42.** ALP enzyme activity of hDPSCs seeded on scaffolds prepared by the (TIPS/PL) method ( $n=4$ ). # designates the groups that are significantly different than groups (without BG, B0-10, and B21-10) at week 2 ( $p < 0.05$ ).



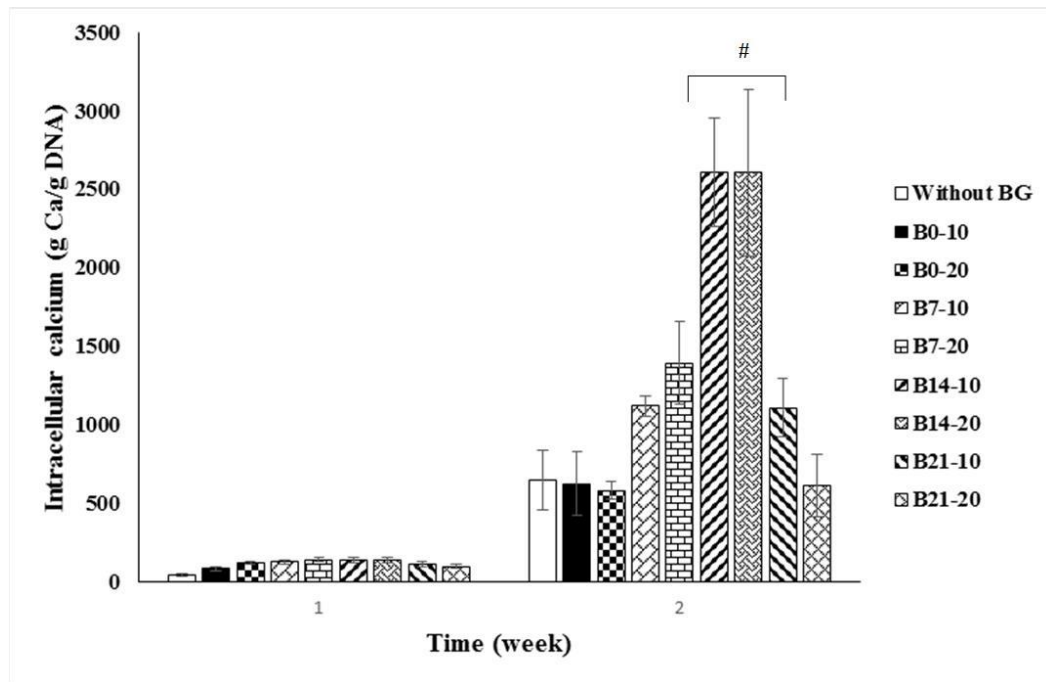


**Figure 43.** Intracellular calcium amounts of hDPSCs seeded on scaffolds prepared by the (TIPS/PL) method (n=4). # designates the groups that were significantly different than all groups at week 2 (p<0.05).

### 3.3.6.1.2. Scaffolds Prepared by FD/MMP Method

Odontogenic differentiation was analyzed by determining alkaline phosphatase activity and intracellular calcium concentration per total DNA of the hDPSCs cultivated on different scaffold groups. DPSC seeded on the scaffolds primarily showed non-odontogenic nature with very low ALP activity and intracellular calcium concentration at the end of 1<sup>st</sup> week (Fig. 44&45). However, an increase was observed for both ALP activity of cells seeded on scaffolds with pure BG (B0-20) and on scaffolds having borate modified BG (B14-10). Cells cultivated on B14-10 scaffolds had significantly highest ALP activity while cells on scaffolds without BG showed the lowest ALP activity (Fig. 44). Additionally, intracellular calcium amounts were in agreement with ALP activity results (Fig. 45). Calcium ions were

began to be taken up by DPSCs as early as 2<sup>nd</sup> week. From 1<sup>st</sup> to 2<sup>nd</sup> week, an immense increase in calcium storage for scaffolds with pure BG (B0-20) and for the scaffolds having borate modified BG (B14-10) was seen (Fig. 45).

B is an essential trace metal for wide range of anabolic activities such as mineral deposition and maintenance of tooth (Toker et al., 2016). Gümüşderelioğlu et al. (2015) analyzed the effect of B on osteogenic differentiation through its release from chitosan nanoparticles (Gümüşderelioğlu et al., 2015). They observed that local increment in B concentration upon release brought about higher ALP activity, upregulation of bone-related genes such as Collagen I, Osteopontin and Osteocalcin. Moreover, Abo-Aziza and Zaki (2017) demonstrated that cellular differentiation towards osteogenic phenotype may be enhanced for highly confluent cells having mesenchymal phenotype (Abo-Aziza & Zaki, 2017). They also stated that confluent bone marrow mesenchymal stem cells displayed higher ALP activity and calcium deposition per total protein produced in the cells. For these reasons, we suggest that DPSCs differentiated into odontogenic lineage owing to presence of pure BG, borate modified BG groups and possibly cellular confluency in the macropores. On the other hand, a significant decrease in the ALP activity was also observed for cells in B14 and B21 scaffold groups that contained higher amount of borate modified BG (Figure M and N). This could be a consequence of higher borate ions release from the samples. As observed by Hakki et al. (2010), high B release might have led to decrease in the rate of osteogenic differentiation (Hakki et al., 2010). They observed that over 100 ng/ml local concentration of B such as 1000 ng/ml suppressed release of osteogenic factors from MC3T3-E1 pre-osteoblastic cell line such as Collagen I and BMP-7. Collectively, borate doped BG species as reinforcements, were shown to improve biological properties in the odontogenic direction. B14-10 scaffolds displayed significantly highest differentiation rate of DPSC towards odontogenic phenotype as determined through quantification of ALP activity and intracellular calcium concentration (Fig. 44&45).

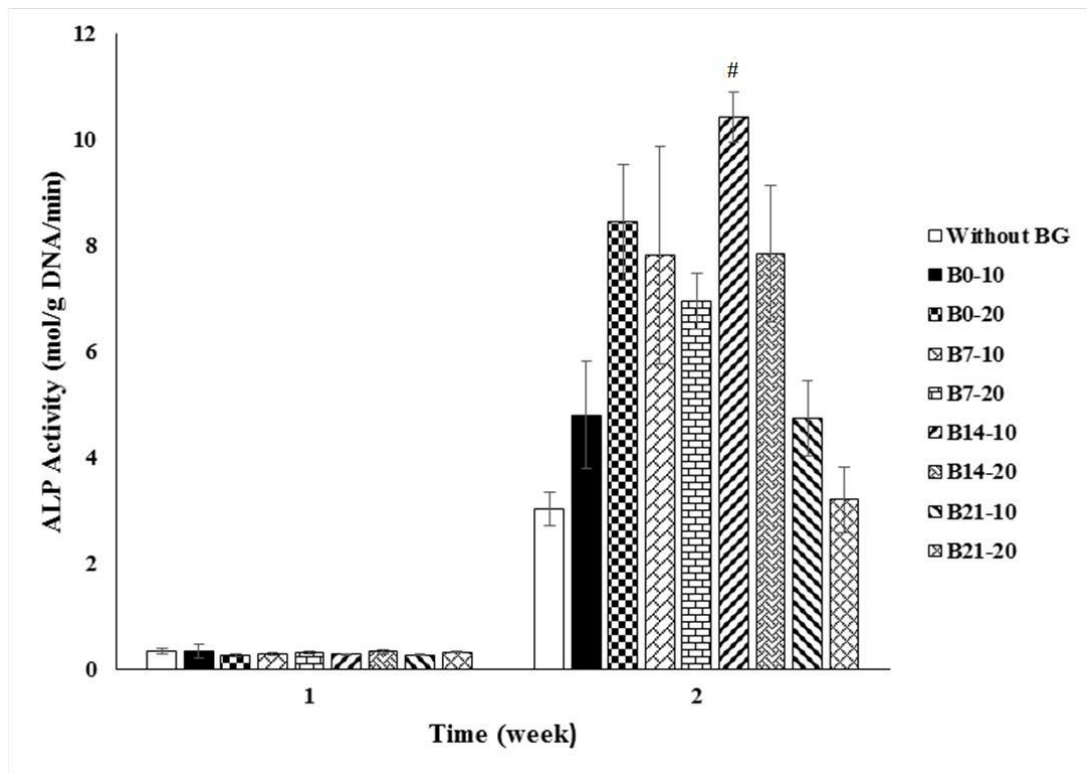


**Figure 44.** ALP enzyme activity of hDPSCs seeded on scaffolds prepared by the FD/MMP method (n=4). # designates the group significantly different than all groups (except B0-20, and B7-10) at week 2 ( $p < 0.05$ ).

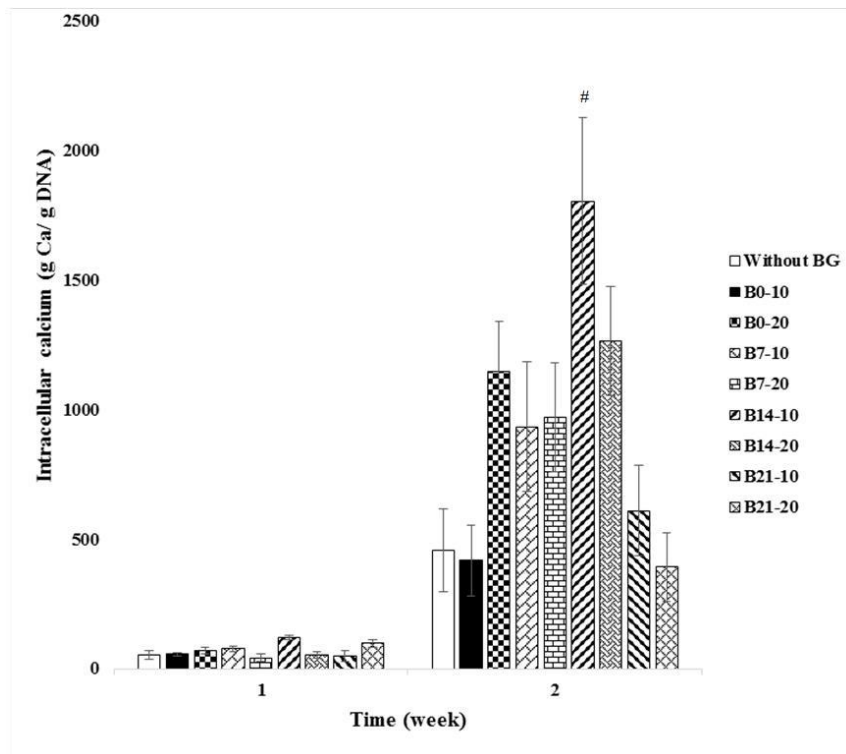


**Figure 45.** Intracellular calcium amounts of hDPSCs that were seeded on scaffolds prepared by the FD/MMP method (n=4). # designates the group significantly different than all groups (except: B14-20) at week 2 ( $p < 0.05$ ).

### 3.3.6.2. Immunohistochemical and Histological Analysis of hDPSCs Seeded Scaffolds

#### 3.3.6.2.1. Scaffold Prepared by TIPS/PL Method

Expression of the odontoblastic differentiation markers DSPP, OPN and Col I was examined by immunohistochemical staining of cell-seeded scaffolds after 14 and 21 days after incubation (Fig. 46-48). DSPP is one of the major dentinal non-collagenous proteins and plays a key role in odontoblast maturation and dentin mineralization (Deshpande et al., 2011, Tada et al., 2010). Osteopontin (OPN), is a

late-mineralization marker, which plays a role in the differentiation of odontoblast-like cells and also reparative dentinogenesis (Choi et al., 2014, Saito et al., 2016). Type I collagen is the main extracellular matrix protein in dentin, which is involved in odontoblastic differentiation (Linde, 1985, Abrahão et al., 2006). It is also needed for calcification and crystal formation in dental pulp (Huang & Thesleff, 2013). In all groups, positive staining of these proteins was observed 14 days after incubation, which became stronger 21 days after incubation. 21 days after incubation, expression of these proteins in cells that were cultivated on scaffolds containing pure BG (B0-10), was stronger than observed in scaffold group (without BG) and expression became much stronger in borate modified BG containing groups. Distance of all stained sections from the scaffold surface was 150  $\mu\text{m}$ . Immunohistochemical staining of hDPSCs seeded on the scaffolds for DSPP, OPN, COL I, revealed presence of the highest number of cells in B14-10 group, 21 days after incubation with much pronounced staining than all groups. Higher expression of odontoblastic markers in borate modified BG containing groups, is indicative of positive role of borate modified BGs in odontogenic differentiation of hDPSCs on the scaffolds.

In order to evaluate calcium deposition on the cell-scaffold constructs, Von Kossa staining was performed 7 and 14 days after incubation (Fig. 49a-j). Results revealed the start of mineral deposition (black color) 7 days after incubation in different groups (Fig. 49a, c, e, g, and i), and higher levels of deposition were observed, 14 days after incubation (Fig. 49b, d, f, h, and j). At time point 7 days, higher deposition in B7-10 and B14-10 scaffold groups was noticed, while at time point 14 days, deposition in B0-10 scaffolds was higher than scaffolds without BG and cells cultivated on B14-10 scaffold showed the highest deposition among all groups. In total, higher mineralization in borate modified BG containing groups indicated that this biomaterial facilitated odontogenic differentiation. Qu et al. (2013), prepared 3D nano-fibrous gelatin/silica bioactive glass (NF-gelatin/SBG) hybrid scaffolds and assessed expression of marker genes for odontogenic differentiation (Col I, ALP, OCN, DSPP and DMP-1) by RT-PCR after 4 weeks of incubation. According to the results, significantly higher expression of all the marker genes in hybrid scaffolds

than NF-gelatin group was observed. Von Kossa staining at this time point, presented higher mineral deposition in scaffolds containing SBG than the control group. All these results indicated odontogenic differentiation of hDPSCs in SBG added NF-gelatin scaffolds was increased (Qu & Liu, 2013). In one study, dental composites incorporating 1%, 5%, and 10% (w/w) sodium pentaborate pentahdrate were prepared. Immunocytochemical staining for DSPP after 10 days of incubation in odontogenic medium with hDPSCs, revealed higher levels of protein expression in boron added groups (especially 1% boron added group). According to RT-PCR analysis, osteocalcin gene levels increased more in boron-containing composites, but DMP1 gene levels were not significantly different in all groups. Higher mineral deposition was detected in boron-containing composites after Von-Kossa staining. In total, boron-containing dental composites enhanced odontogenic potential of hDPSCs (Demirci et al., 2015).

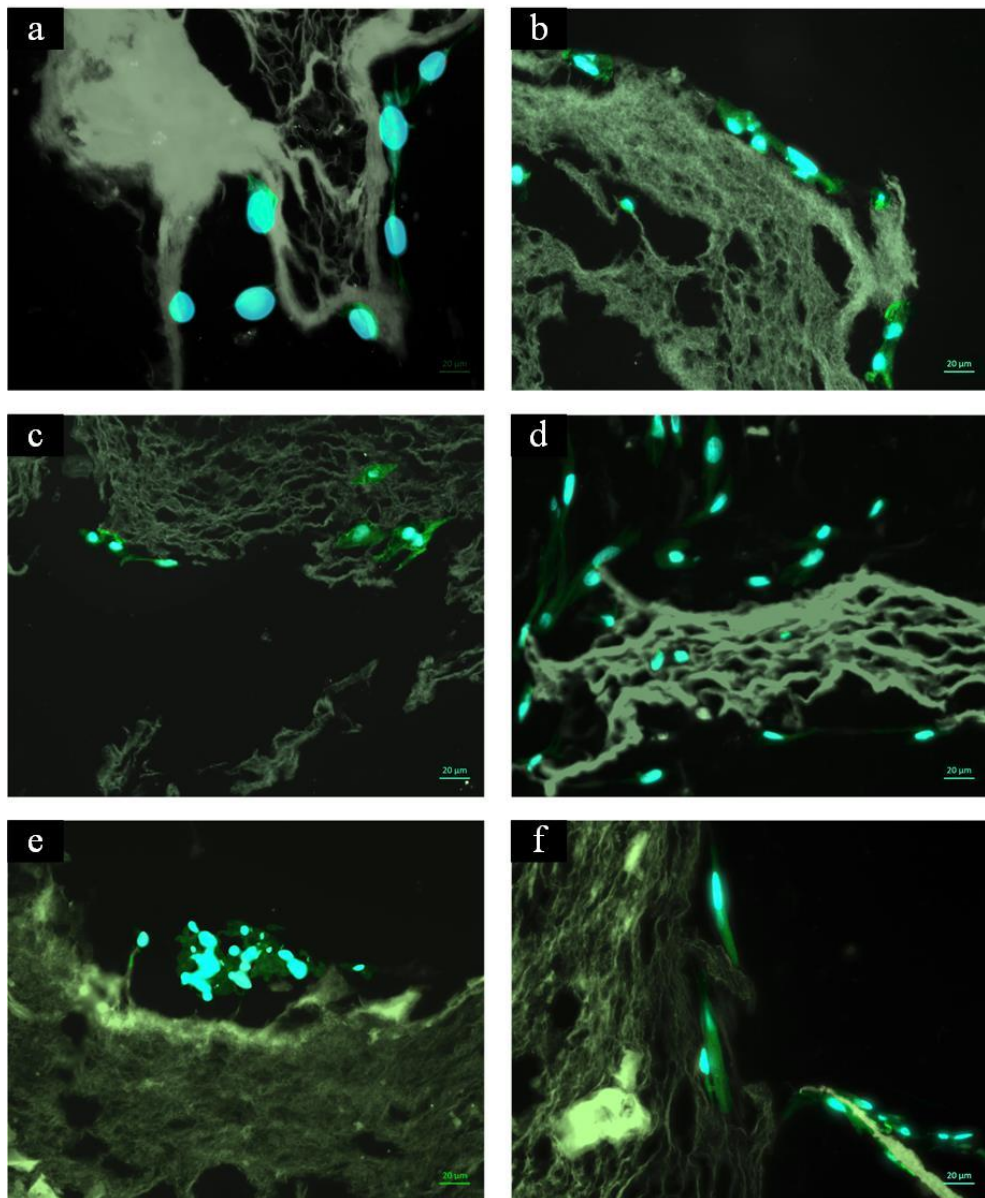


**Figure 46.** Results of immunohistochemical staining of DPSCs seeded on the scaffolds prepared by the TIPS/PL method, [DSPP (green) and DAPI (blue)], a) without BG, day 14; b) without BG, day 21; c) B0-10, day 14; d) B0-10, day 21; e) B7-10, day 14; f) B7-10, day 21, (distance of stained sections from the scaffold surface was 150  $\mu\text{m}$ ) (scale bar: 20  $\mu\text{m}$ ).

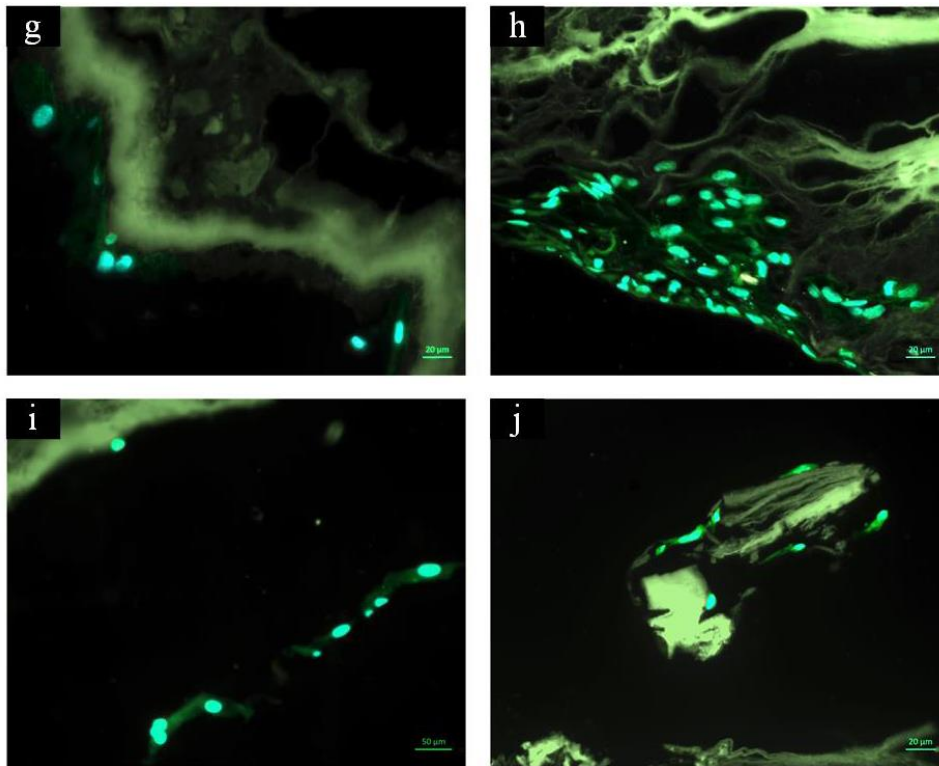


**Figure 46 - Continued.** Results of immunohistochemical staining of DPSCs seeded on the scaffolds prepared by the TIPS/PL method, [DSPP (green) and DAPI (blue)], g) B14-10, day 14; h) B14-10, day 21; i) B21-10, day 14; j) B21-10, day 21, distance of stained sections from the scaffold surface was 150  $\mu\text{m}$ ) (scale bar: 20  $\mu\text{m}$ ).



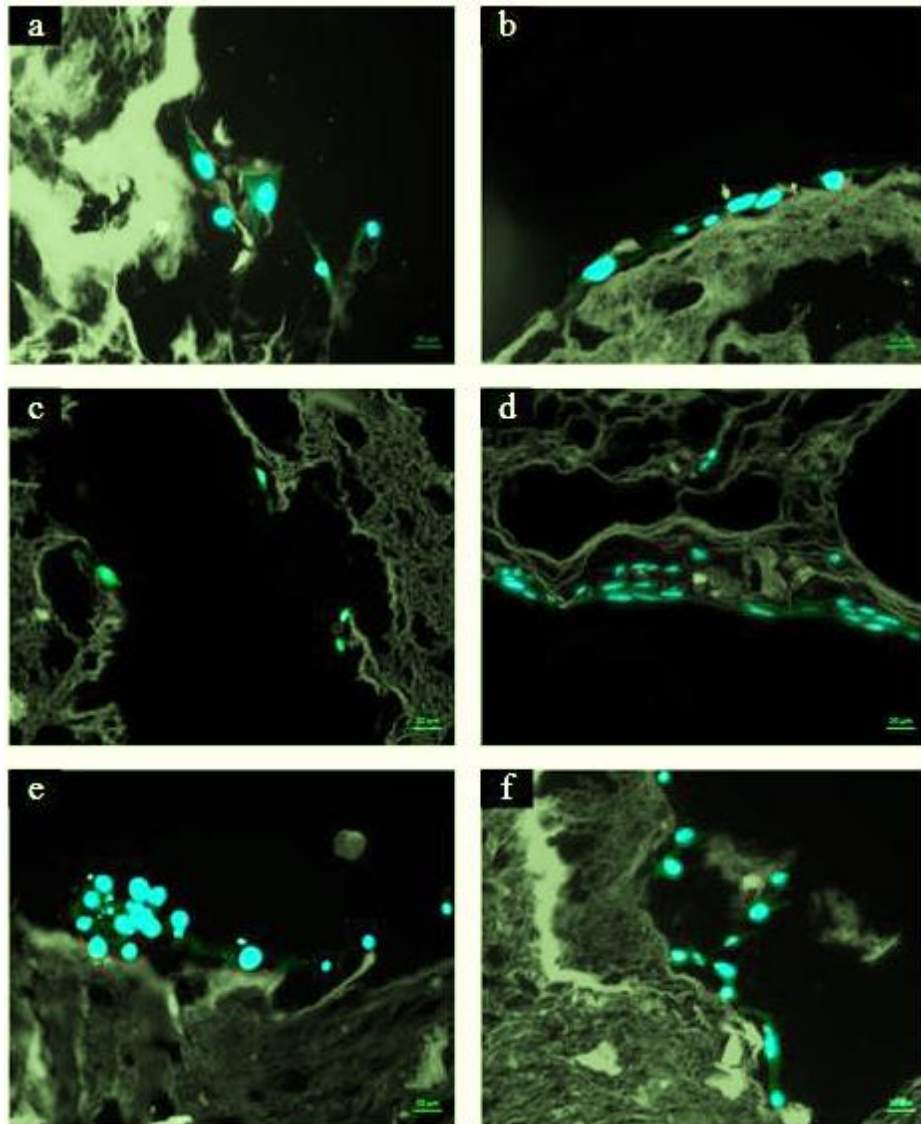


**Figure 47.** Results of immunohistochemical staining of DPSCs seeded on the scaffolds prepared by the TIPS/PL method, [OPN (green) and DAPI (blue)], a) without BG, day 14; b) without BG, day 21; c) B0-10, day 14; d) B0-10, day 21; e) B7-10, day 14; f) B7-10, day 21, distance of stained sections from the scaffold surface was 150  $\mu\text{m}$ ) (scale bar: 20  $\mu\text{m}$ ).

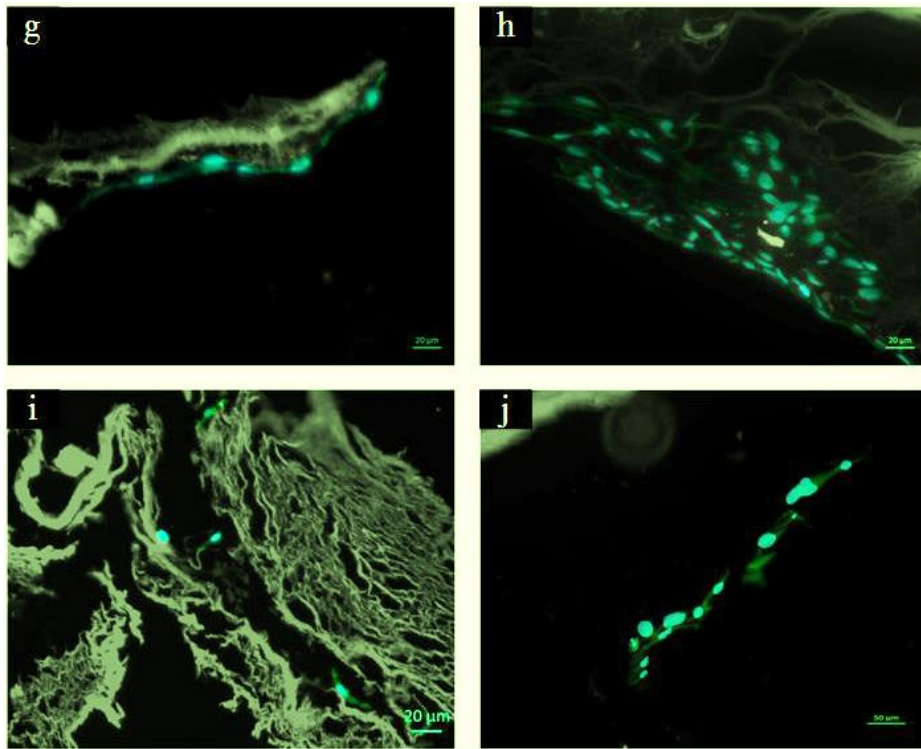


**Figure 47 - Continued.** Results of immunohistochemical staining of DPSCs seeded on the scaffolds prepared by the TIPS/PL method, [OPN (green) and DAPI (blue)] g) B14-10, day 14; h) B14-10, day 21; i) B21-10, day 14; j) B21-10, day 21, distance of stained sections from the scaffold surface was 150 μm) (scale bar: 20 μm).

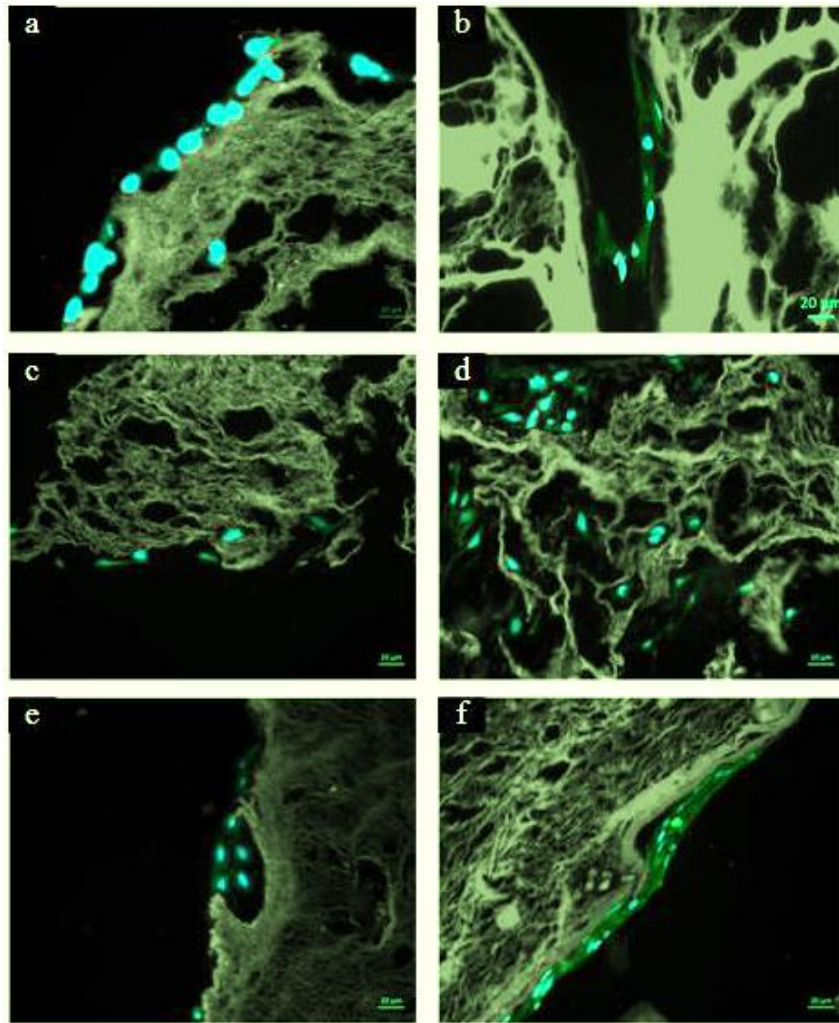


**Figure 48.** Results of immunohistochemical staining of DPSCs seeded on the scaffolds prepared by the TIPS/PL method, [COLI (green) and DAPI (blue)], a) without BG, day 14; b) without BG, day 21; c) B0-10, day 14; d) B0-10, day 21; e) B7-10, day 14; f) B7-10, day 21 distance of stained sections from the scaffold surface was 150  $\mu\text{m}$ ) (scale bar: 20  $\mu\text{m}$ ).

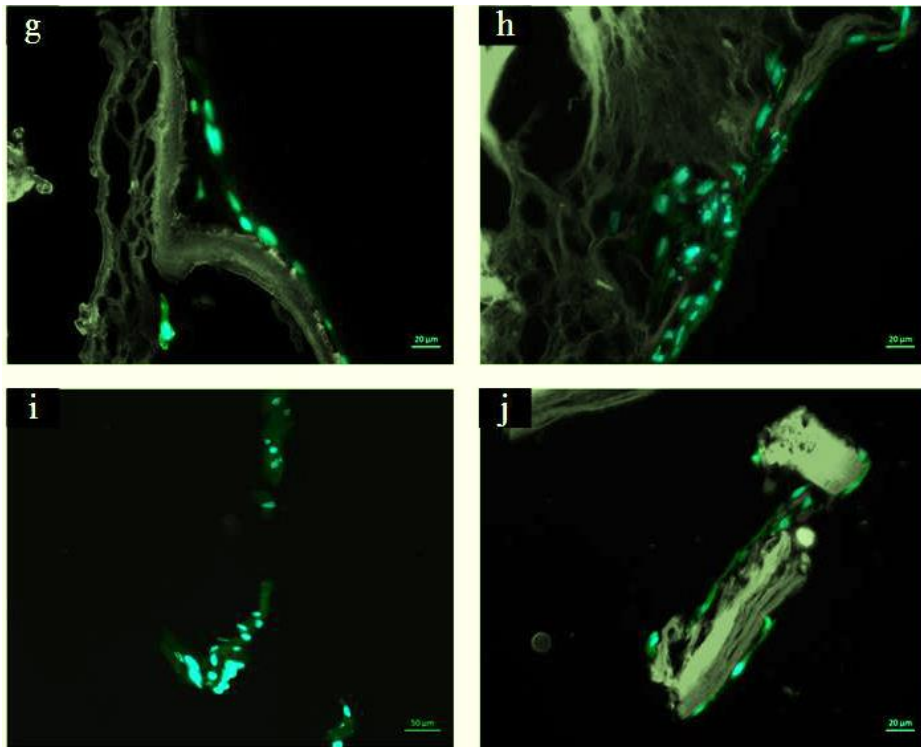


**Figure 48 - Continued.** Results of immunohistochemical staining of DPSCs seeded on the scaffolds prepared by the TIPS/PL method, [COLI (green) and DAPI (blue)], g) B14-10, day 14; h) B14-10, day 21; i) B21-10, day 14; j) B21-10, day 21 distance of stained sections from the scaffold surface was 150 µm) (scale bar: 20 µm).

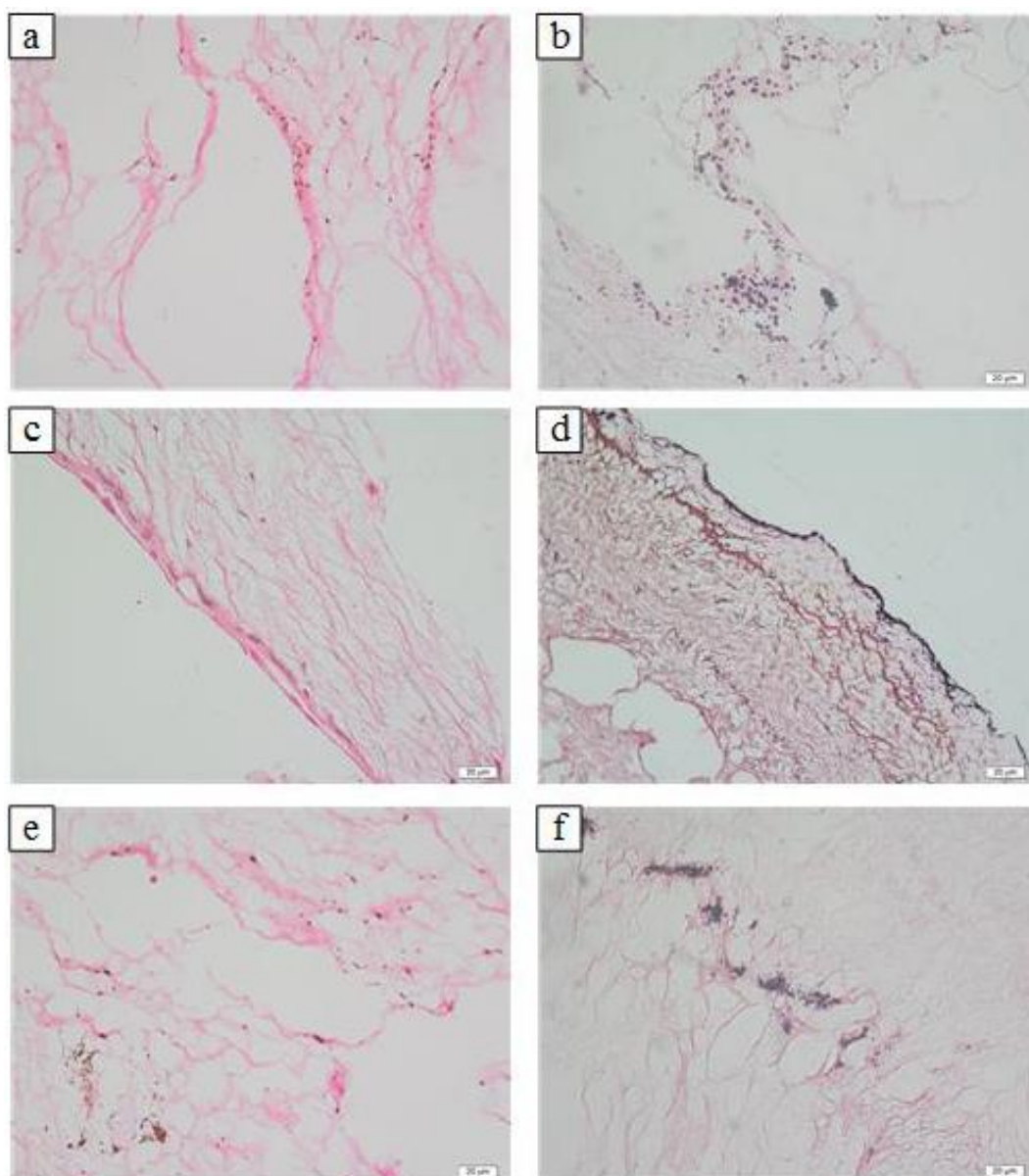


**Figure 49.** Results of Von Kossa staining of DPSCs seeded on the scaffolds prepared by the TIPS/PL method, a) without BG, day 14; b) without BG, day 21; c) B0-10, day 14; d) B0-10, day 21; e) B7-10, day 14; f) B7-10, day 21, distance of stained sections from the scaffold surface was 150  $\mu\text{m}$ ) (scale bar: 20  $\mu\text{m}$ ).

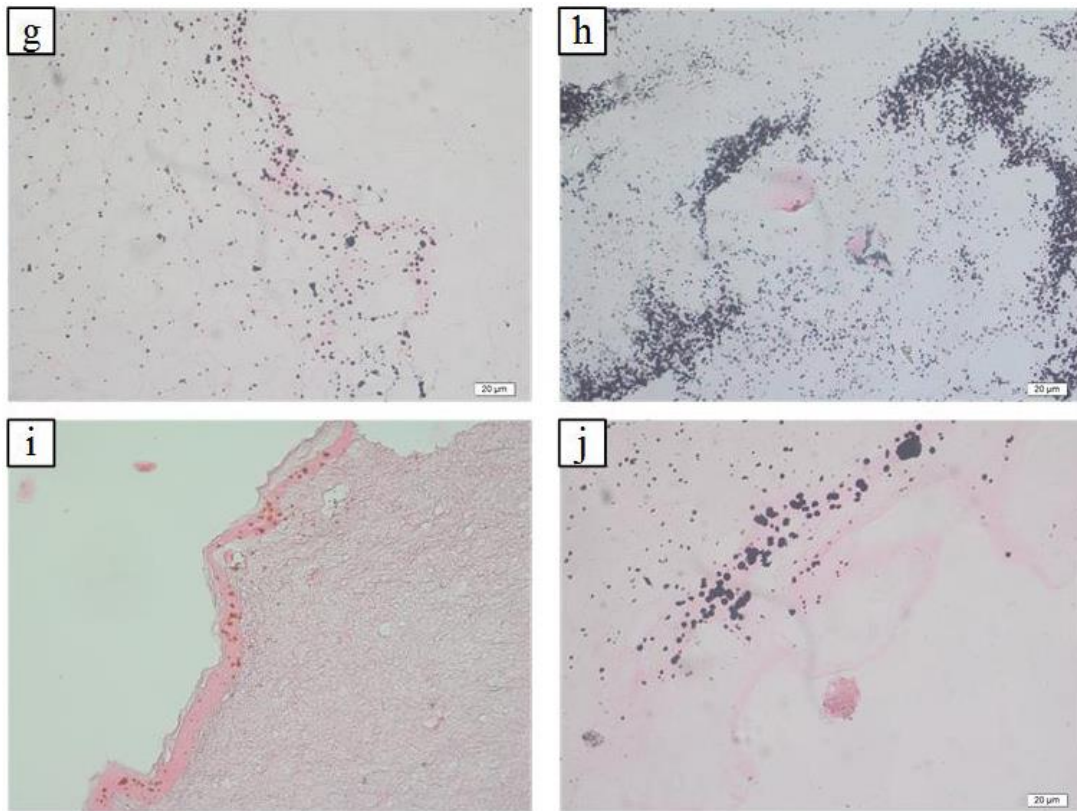


**Figure 49 - Continued.** Results of Von Kossa staining of DPSCs seeded on the scaffolds prepared by the TIPS/PL method, g) B14-10, day 14; h) B14-10, day 21; i) B21-10, day 14; j) B21-10, day 21, distance of stained sections from the scaffold surface was 150  $\mu\text{m}$ ) (scale bar: 20  $\mu\text{m}$ ).

### 3.3.6.2.2. Scaffolds Prepared by FD/MMP Method

Expression of the odontoblastic differentiation markers DSPP, OPN and Col I was examined by immunohistochemical staining 14 and 21 days after incubation of cell-seeded scaffolds with the odontogenic medium (Fig. 50-52). Dentin sialophosphoprotein (DSPP) is a unique marker of late odontoblast differentiation and is essential for dentin mineralization (Suzuki et al., 2012, Li et al., 2011c). Osteopontin (OPN) is a non-collagenous protein usually present in the reparative

dentin. It plays a role in the differentiation of odontoblast-like cells and regulation of matrix mineralization (Saito et al., 2016, Cajazeira Aguiar & Arana-Chavez, 2007). Type I collagen is one of dentin matrix proteins, secreted by the differentiating odontoblasts and modulates odontogenic differentiation and mineralization (Iwamoto et al., 2017, Wiesmann et al., 2004). In all groups, positive staining of the proteins was observed 14 days after incubation, which became stronger 21 days after incubation. At this time point, expression of all three odontoblastic markers in group (B0-10, B0-20) was higher than group (without BG). In borate modified BG containing groups expression of the markers was intense in comparison to groups with incorporation of pure BG. Distance of all stained sections from the scaffold surface was 150  $\mu\text{m}$ . Staining of DPSCs seeded on the scaffolds, revealed presence of the highest number of cells in B14-10 group for DSPP, in B7-10, and B14-10 groups for OPN, in B14-20, and B21-10 groups for COL I, 21 days after incubation with much pronounced staining than all groups. Enhancement of the proteins expression as a result of borate introduction into the scaffolds, indicates positive effect of borate modified BGs in odontogenic differentiation of hDPSCs on the scaffolds.

In order to evaluate *in vitro* mineralization on the cell-scaffold constructs, Von Kossa staining was done 7 and 14 days after incubation (Fig. 53a-i). Calcium deposition (black color) was observed 7 days after incubation (Fig. 53a, c, e, g, i, k, m, o and q), and higher levels of deposition were observed, 14 days after incubation (Fig. 53b, d, f, h, j, l, n, p, and r). After 7 days of incubation, groups B14-10, B21-10, and B21-20 groups revealed higher mineralization than the other groups and at day 14 days enhanced mineralization was observed in B14-10 and B14-20 groups in comparison to all groups. As a result, borate modified BG containing scaffold groups promoted mineralization and thus odontogenic differentiation of seeded hDPSCs.

In one study, mineral trioxide aggregate was mixed with different additives of distilled water, 2.5% ( $\text{Na}_2\text{HPO}_4$ ) and 5% ( $\text{CaCl}_2$ ) and hDPSCs were cultured on them (aggregated powders) in odontogenic medium. According to RT-PCR analysis of

odontoblastic differentiation markers (DSPP, COL I) 14 and 21 days after incubation, DSPP on MTA mixed with 2.5% Na<sub>2</sub>HPO<sub>4</sub> showed significantly higher expression than groups with other additives on both time points (P < 0.05). There was no difference between expression levels of COL1 in MTA mixed with 5% CaCl<sub>2</sub> and 2.5% Na<sub>2</sub>HPO<sub>4</sub> and pure MTA on day 14, while on MTA mixed with 5% CaCl<sub>2</sub> and 2.5% Na<sub>2</sub>HPO<sub>4</sub>, cells showed significantly higher expression of COL1 than on MTA mixed with distilled water day 21 after incubation (P < 0.05). Von Kossa staining on day 21, presented highest mineral deposition on MTA groups with additives with not much difference between the groups. In conclusion, positive effect of MTA mixed with 5% CaCl<sub>2</sub> or 2.5% Na<sub>2</sub>HPO<sub>4</sub>, was detected for odontoblastic differentiation and mineralization of hDPSCs (Kulan et al., 2017). Demirci et al. (2015), prepared dental composites including 1%, 5%, and 10% (w/w) sodium pentaborate pentahdrate. 10 days after incubation of hDPSCs seeded composites in odontogenic medium, higher levels of DSPP protein was observed (especially 1% boron added group), and elevated levels of calcium deposition in all boron containing composites were also observed. RT-PCR analysis also revealed significantly higher gene levels for DMP1 gene, but not significant increase of DMP1 gene levels in groups with boron addition. In general, facilitated odontogenic differentiation of hDPSCs was confirmed in presence of boron containing composites (Demirci et al., 2015).



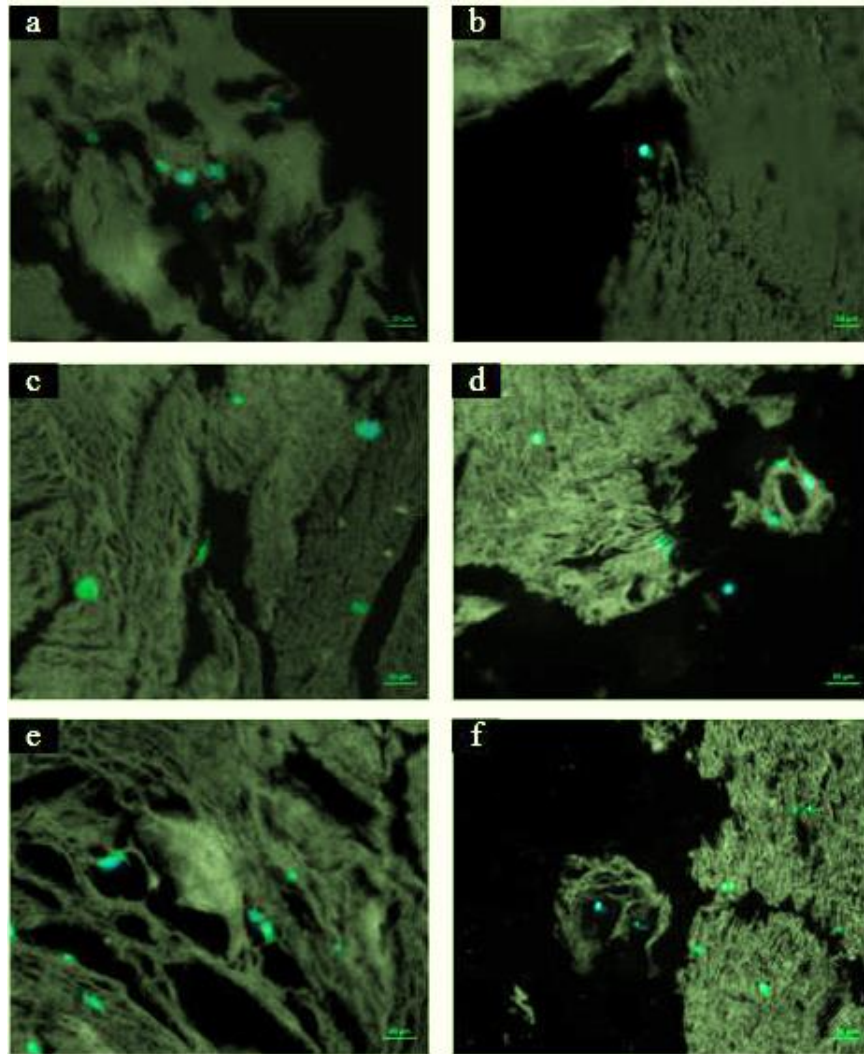


**Figure 50.** Results of immunocytochemical staining of DPSCs seeded on the scaffolds prepared by the FD/MMP method [DSPP (green) and DAPI (blue)], a) without BG, day 14; b) without BG, day 21; c) B0-10, day 14; d) B0-10, day 21; e) B0-20, day 14; f) B0-20, day 21, distance of stained sections from the scaffold surface was 150  $\mu\text{m}$ ) (scale bar: 20  $\mu\text{m}$ ).

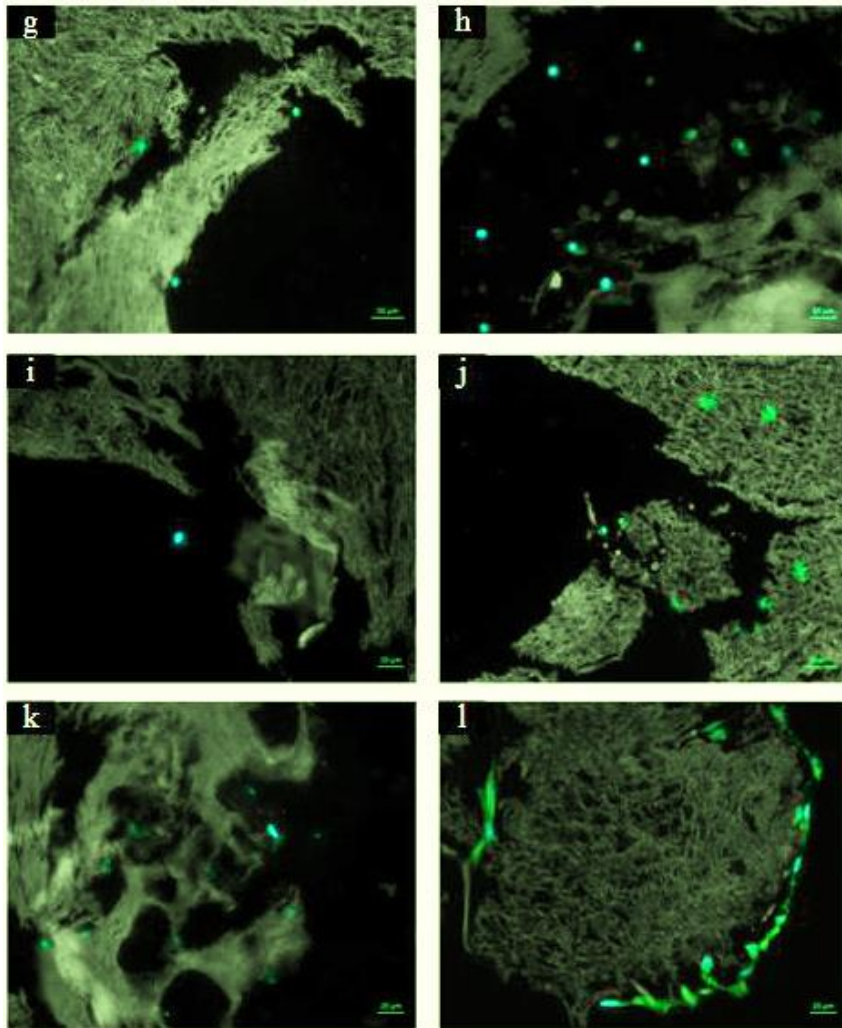


**Figure 50 - Continued.** Results of immunocytochemical staining of DPSCs seeded on the scaffolds prepared by the FD/MMP method [DSPP (green) and DAPI (blue)], g) B7-10, day 14; h) B7-10, day 21; i) B7-20, day 14; j) B7-20, day 21; k) B14-10, day 14; l) B14-10, day 21, distance of stained sections from the scaffold surface was 150  $\mu\text{m}$ ) (scale bar: 20  $\mu\text{m}$ ).

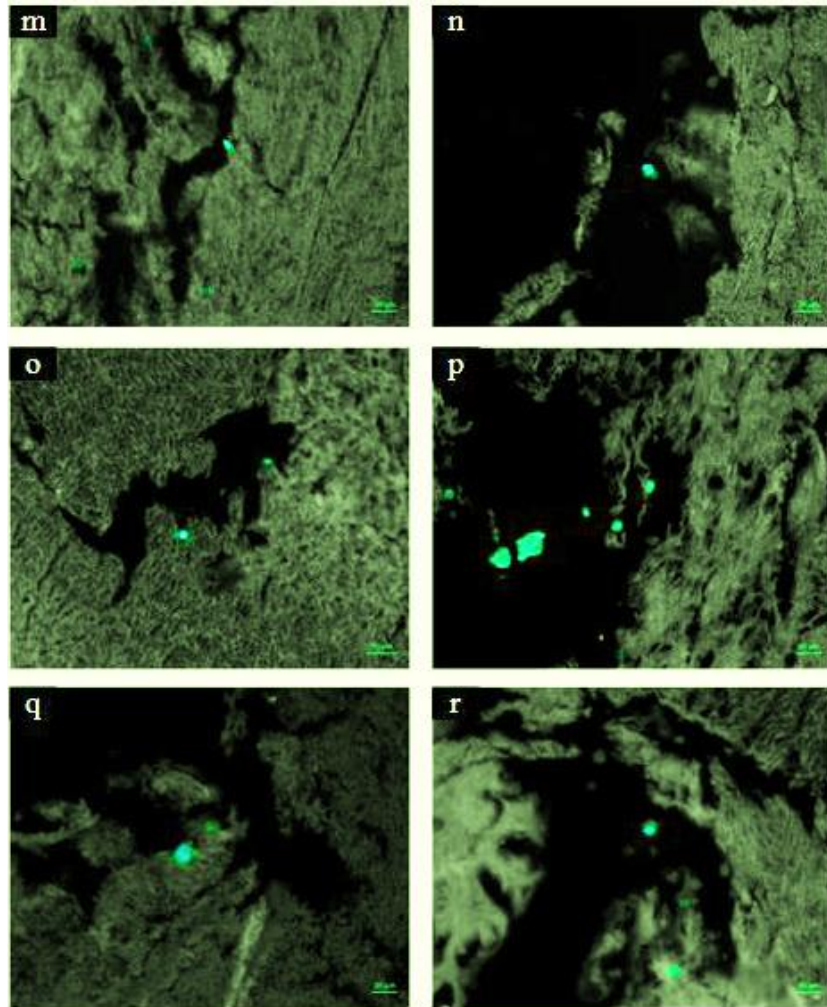


**Figure 50 - Continued.** Results of immunocytochemical staining of DPSCs seeded on the scaffolds prepared by the FD/MMP method [DSPP (green) and DAPI (blue)], m) B14-20, day 14; n) B14-20, day 21; o) B21-10, day 14; p) B21-10, day 21; q) B21-20, day 14; r) B21-20, day 21, (distance of stained sections from the scaffold surface was 150  $\mu\text{m}$ ) (scale bar: 20  $\mu\text{m}$ ).

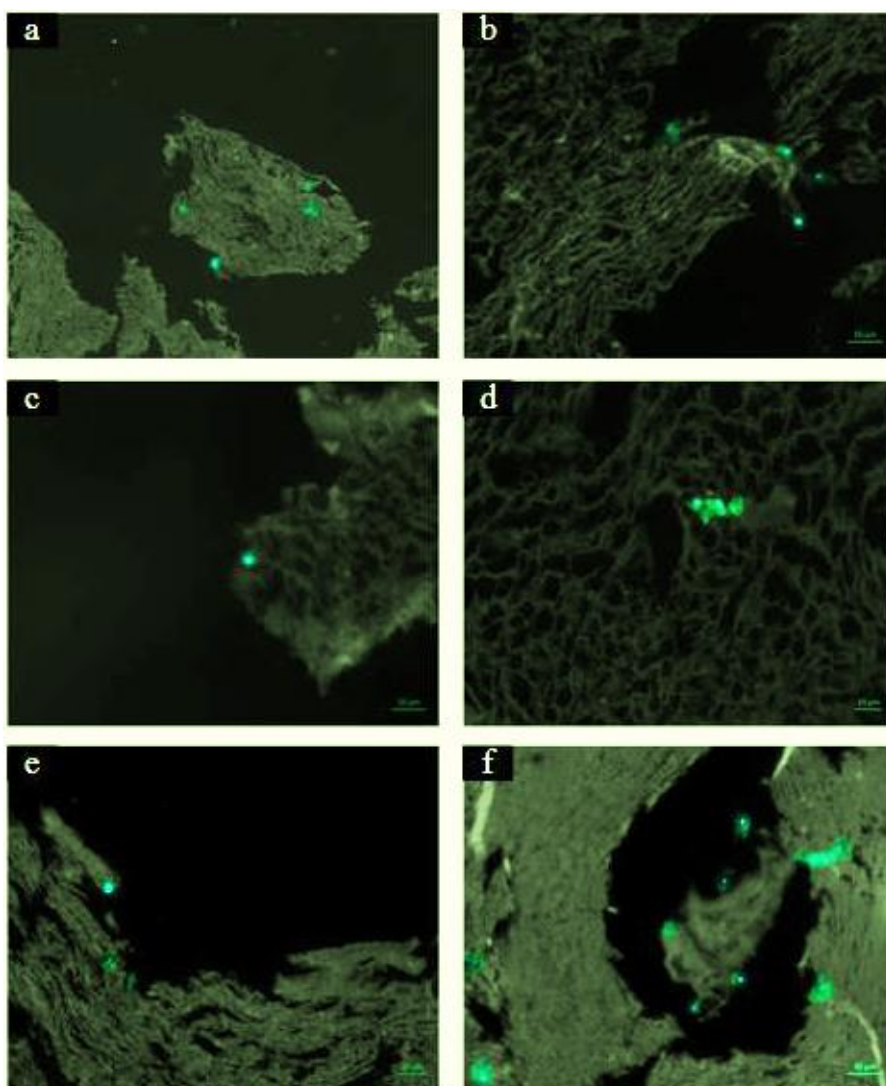


**Figure 51.** Results of immunocytochemical staining of DPSCs seeded on the scaffolds prepared by the FD/MMP method [OPN (green) and DAPI (blue)], a) without BG, day 14; b) without BG, day 21; c) B0-10, day 14; d) B0-10, day 21; e) B0-20, day 14; f) B0-20, day 21, distance of stained sections from the scaffold surface was 150  $\mu\text{m}$ ) (scale bar: 20  $\mu\text{m}$ ).

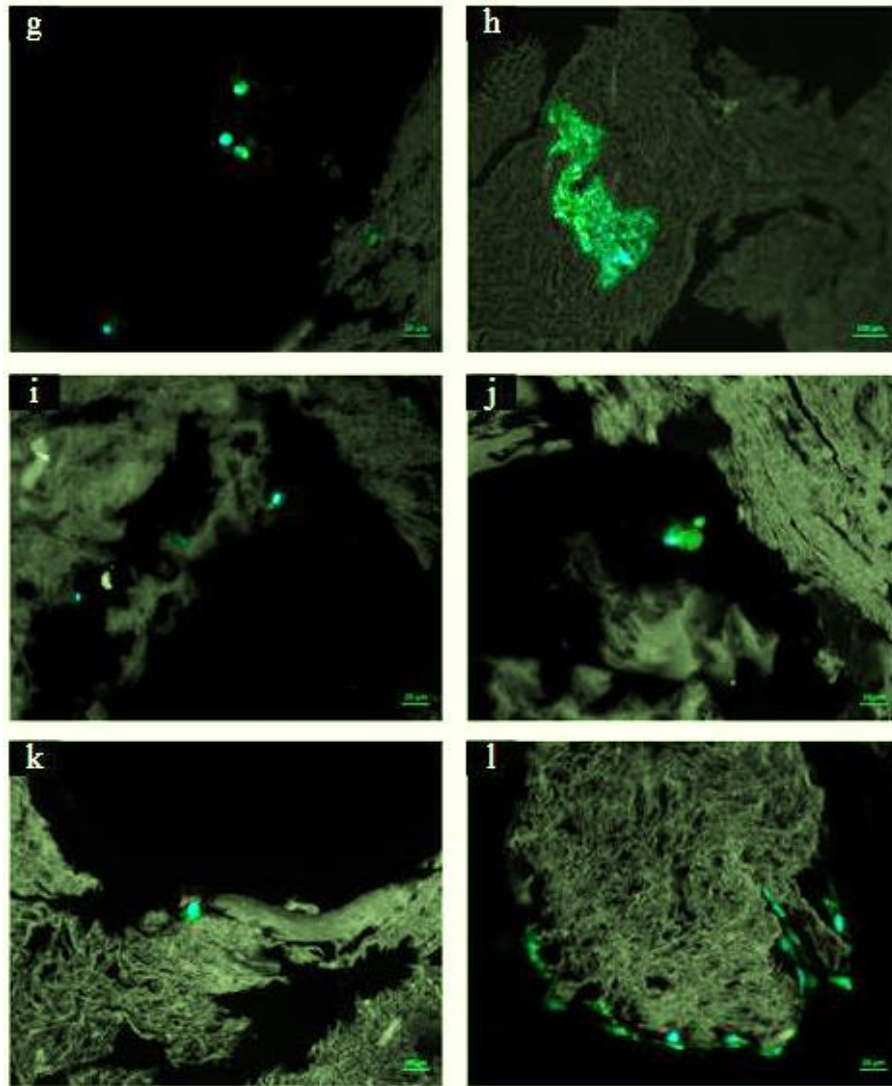


**Figure 51 - Continued.** Results of immunocytochemical staining of DPSCs seeded on the scaffolds prepared by the FD/MMP method [OPN (green) and DAPI (blue)], g) B7-10, day 14; h) B7-10, day 21; i) B7-20, day 14; j) B7-20, day 21; k) B14-10, day 14; l) B14-10, day 21, (distance of stained sections from the scaffold surface was 150 µm) (scale bar: 20 µm).

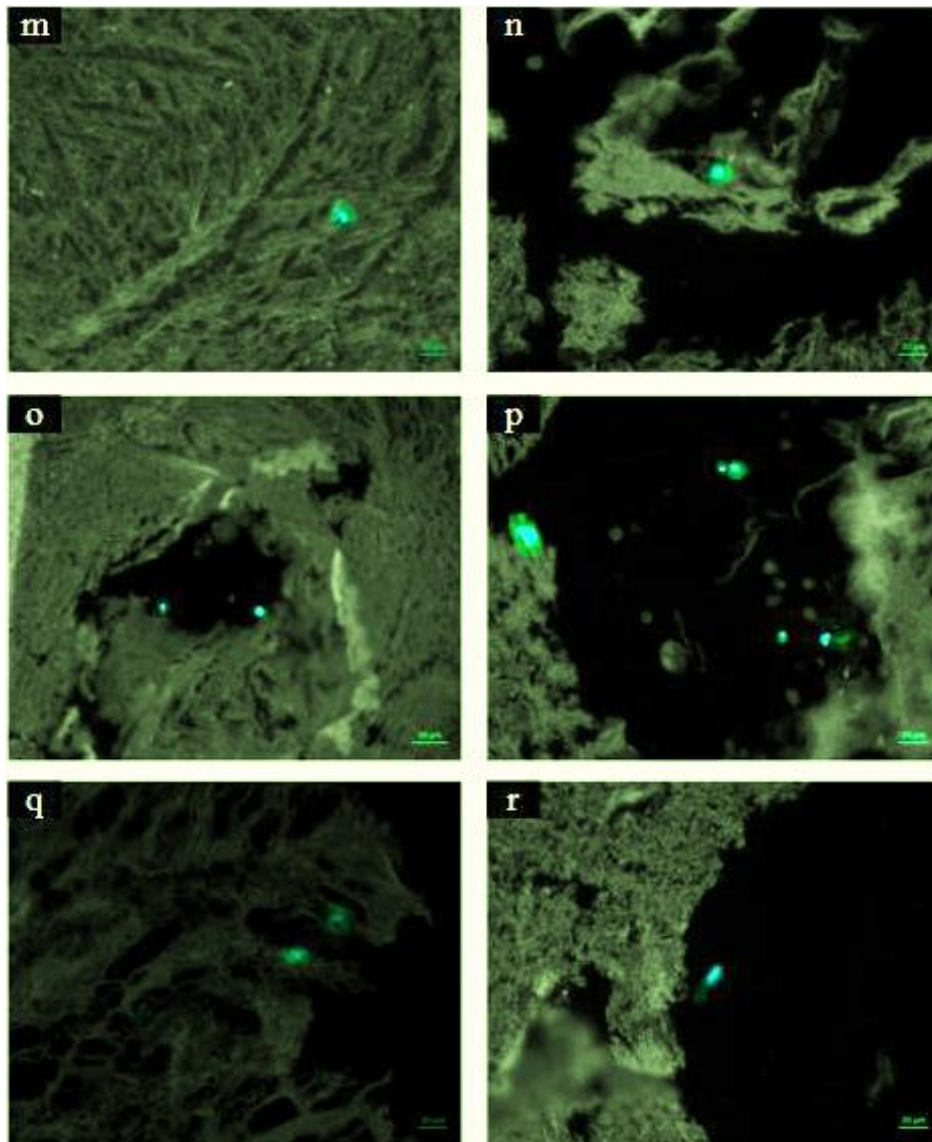


**Figure 51 - Continued.** Results of immunocytochemical staining of DPSCs seeded on the scaffolds prepared by the FD/MMP method [OPN (green) and DAPI (blue)], m) B14-20, day 14; n) B14-20, day 21; o) B21-10, day 14; p) B21-10, day 21; q) B21-20, day 14; r) B21-20, day 21, distance of stained sections from the scaffold surface was 150  $\mu\text{m}$ ) (scale bar: 20  $\mu\text{m}$ ).

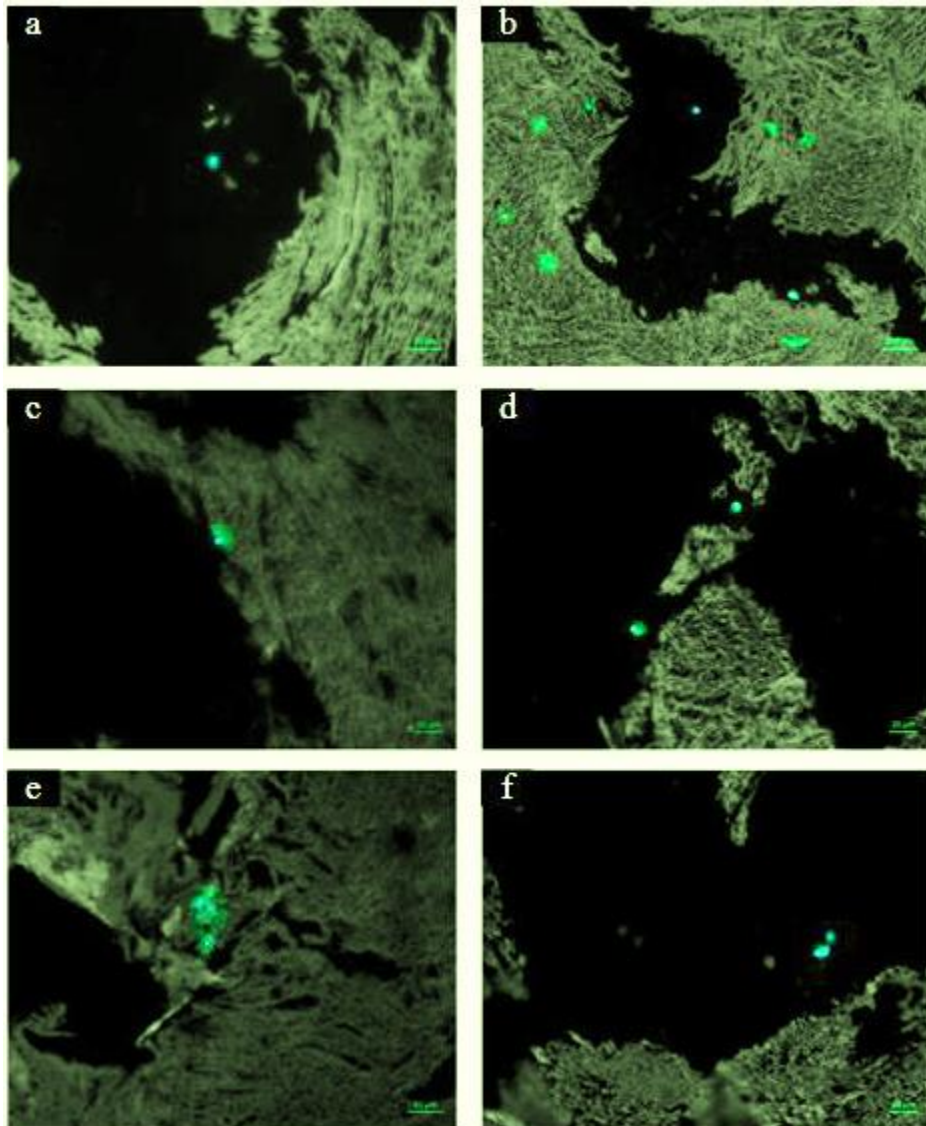


**Figure 52.** Results of immunocytochemical staining of DPSCs seeded on the scaffolds prepared by the FD/MMP method [COLI (green) and DAPI (blue)], a) without BG, day 14; b) without BG, day 21; c) B0-10, day 14; d) B0-10, day 21; e) B0-20, day 14; f) B0-20, day 21, distance of stained sections from the scaffold surface was 150  $\mu\text{m}$ ) (scale bar: 20  $\mu\text{m}$ ).

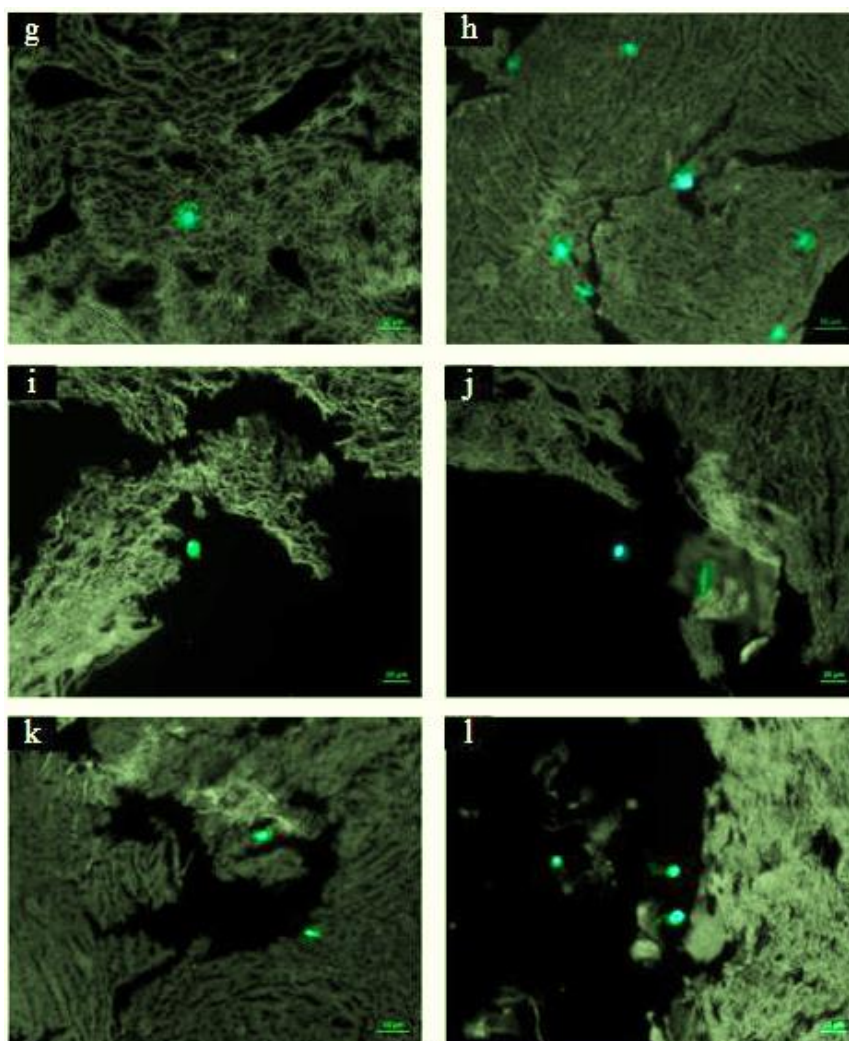


**Figure 52 - Continued.** Results of immunocytochemical staining of DPSCs seeded on the scaffolds prepared by the FD/MMP method [COLI (green) and DAPI (blue)], g) B7-10, day 14; h) B7-10, day 21; i) B7-20, day 14; j) B7-20, day 21; k) B14-10, day 14; l) B14-10, day 21 distance of stained sections from the scaffold surface was 150  $\mu\text{m}$ ) (scale bar: 20  $\mu\text{m}$ ).



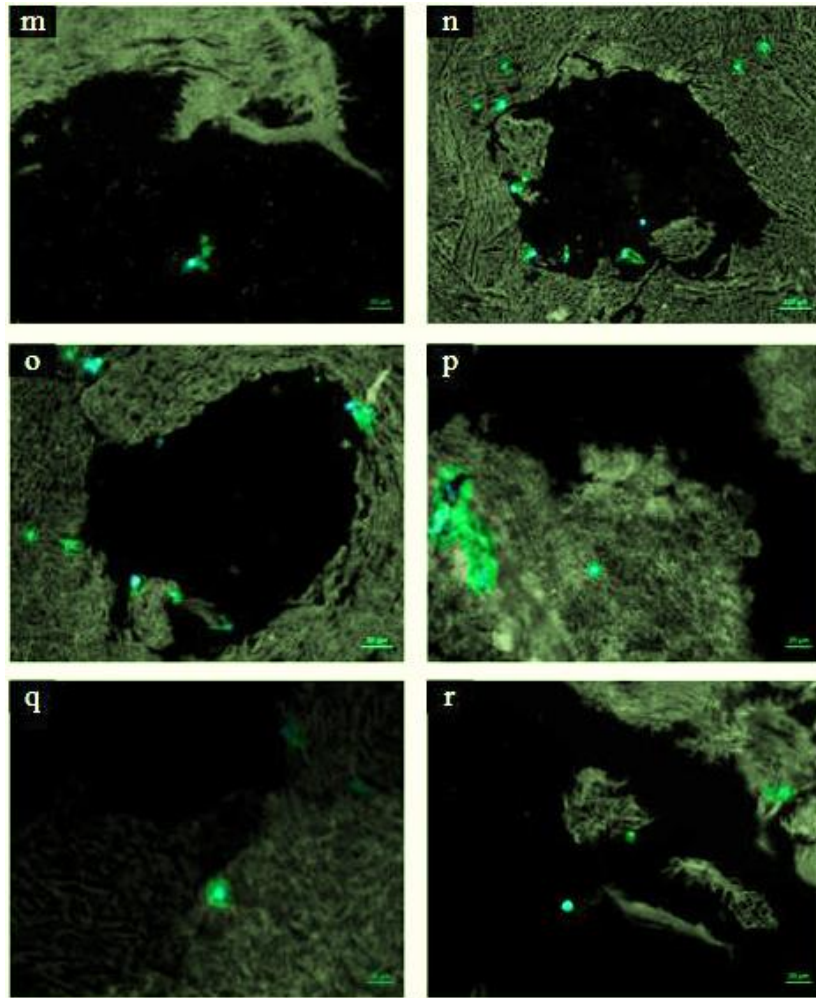


**Figure 52 - Continued.** Results of immunocytochemical staining of DPSCs seeded on the scaffolds prepared by the FD/MMP method [COLI (green) and DAPI (blue)], m) B14-20, day 14; n) B14-20, day 21; o) B21-10, day 14; p) B21-10, day 21; q) B21-20, day 14; r) B21-20, day 21, (distance of stained sections from the scaffold surface was 150  $\mu\text{m}$ ) (scale bar: 20  $\mu\text{m}$ ).

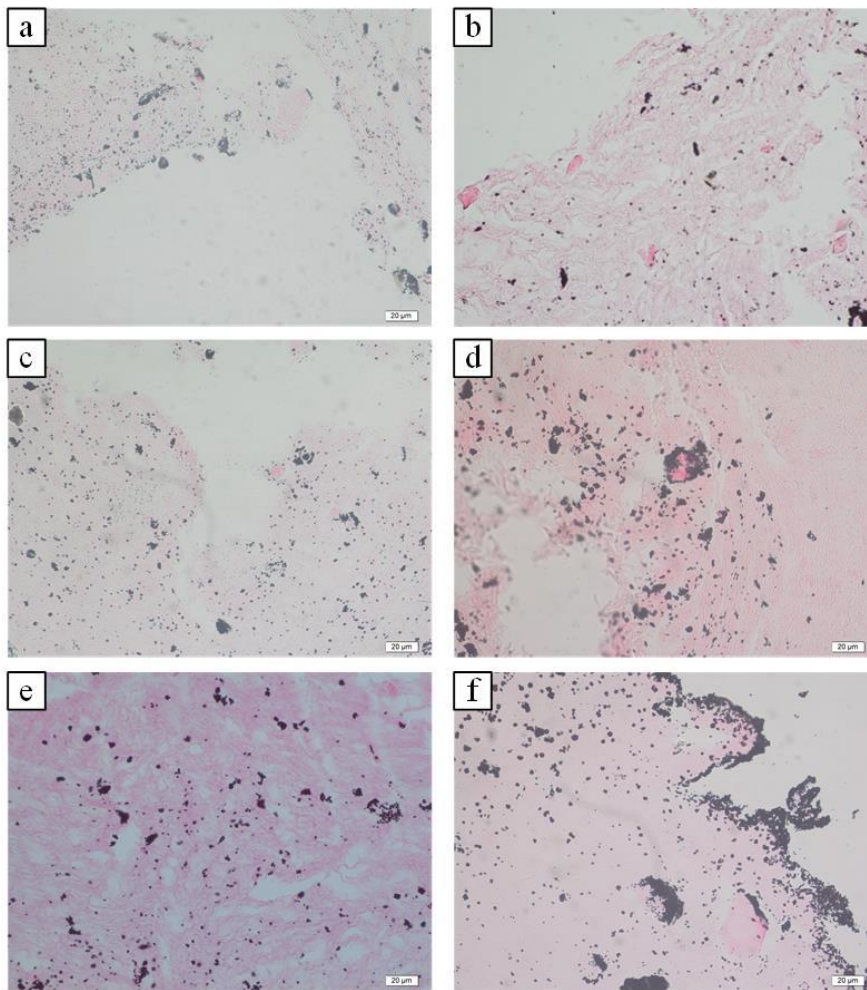


**Figure 53.** Results of Von Kossa staining of DPSCs seeded on the scaffolds prepared by the FD/MMP method, a) without BG, day 7; b) without BG, day 14; c) B0-10, day 7; d) B0-10, day 14; e) B0-20, day 7; f) B0-20, day 14, (distance of stained sections from the scaffold surface was 150  $\mu\text{m}$ ) (scale bar: 20  $\mu\text{m}$ ).

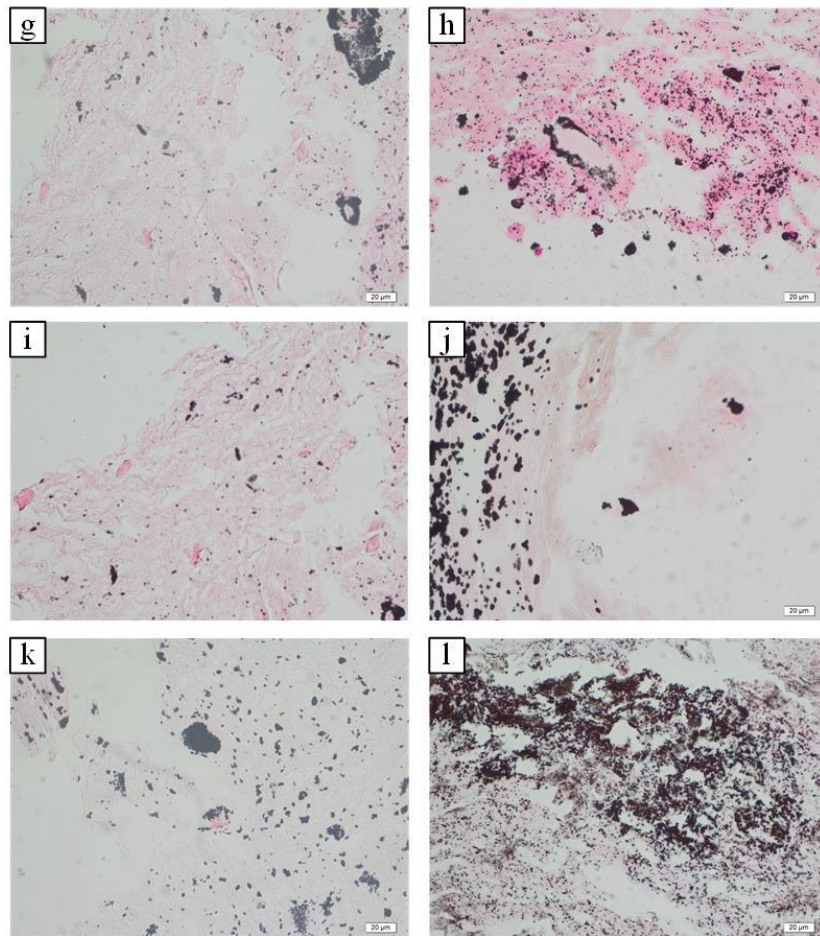


**Figure 53- Continued.** Results of Von Kossa staining of DPSCs seeded on the scaffolds prepared by the FD/MMP method, g) B7-10, day 7; h) B7-10, day 14; i) B7-20, day 7; j) B7-20, day 7; k) B14-10, day 7; l) B14-10, day 14, (distance of stained sections from the scaffold surface was 150 µm) (scale bar: 20 µm).

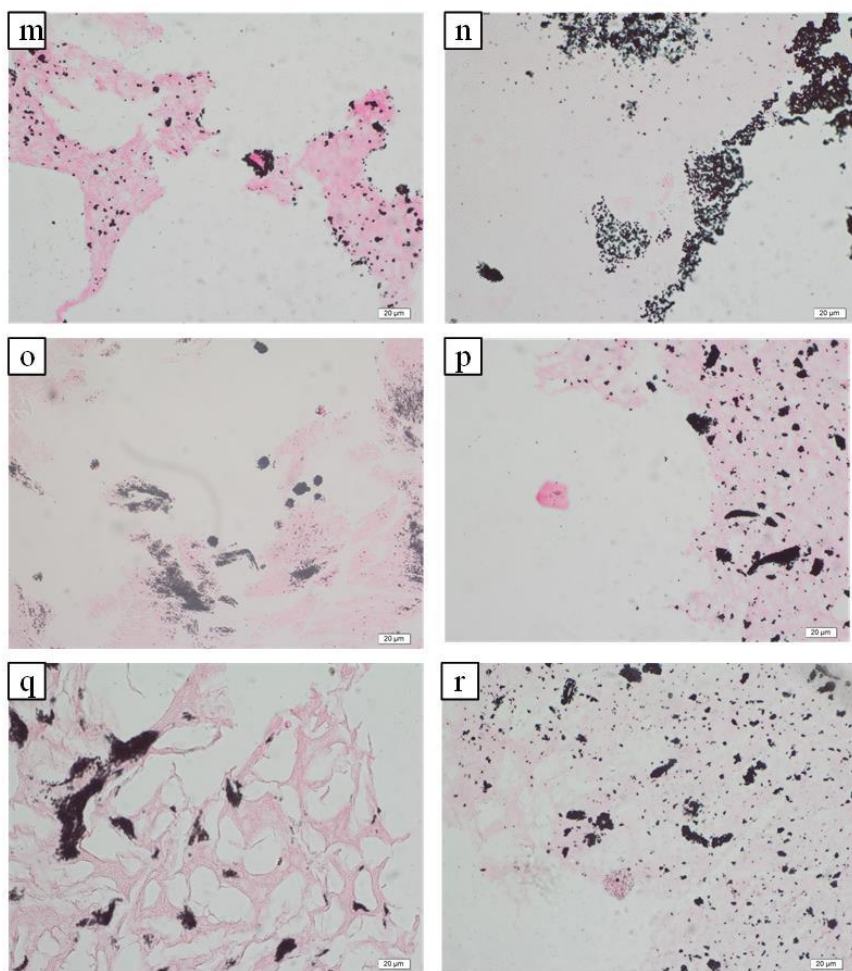


**Figure 53 - Continued.** Results of Von Kossa staining of DPSCs seeded on the scaffolds prepared by the FD/MMP method, m) B14-20, day 7; n) B14-20, day 14; o) B21-10, day 7; p) B21-10, day 14; q) B21-20, day 7; r) B21-20, day 14, (distance of stained sections from the scaffold surface was 150 µm) (scale bar: 20 µm).

## CHAPTER 4

### CONCLUSION

In this thesis, pure and borate modified BG-NPs with different ratios of modification (7, 14 and 21%) were characterized and their effects on dental pulp derived stem cells were examined. In addition, boron modified BG-NPs were added to cellulose acetate/pullulan/gelatin (CA/PULL/GEL) at 10% and 20% weight percentages and potential use of three-dimensional dentin-like constructs were investigated for dentin regeneration. Amorphous and nano-sized B0-BG, B7-BG, B14-BG, and B21-BG, with compositions almost consistent with the theoretical ones were successfully synthesized by the quick alkali-mediated sol-gel method. All BG groups possessed the characteristic functional groups and with increase of borate in bioglass composition, specific surface area, average pore diameter and total pore volume of the BG particles decreased. Increase of  $B_2O_3$  content, resulted in enhanced bioactivity of BGs. Cell culture studies conducted with hDPSCs showed that 6.25 mg/ml bioglass concentration was the optimum concentration. Synthesized BG-NPs increased proliferation of hDPSCs. Borate incorporation increased intracellular calcium amounts and the highest intracellular calcium amount was observed in B21-BG group. Immunocytochemical analysis showed expression of DSPP, osteopontin and collagen type I in BG groups with higher expression in groups containing borate. Dentin constructs composed of borate modified BG-NPs and (CA/ox-PULL/GEL) polymers were successfully developed by (TIPS/PL) and (FD/MMP) methods. Scaffolds possessed tubular pore structures and presented improved biodegradability and water absorption properties during one month. High porosity of the scaffolds was suitable for dentin regeneration purpose, and scaffolds prepared by the (TIPS/PL) method provided enough mechanical strength. Incorporation of borate modified BGs, enhanced deposition of Ca-P containing minerals on the scaffolds. Cell culture

studies with hDPSCs showed positive effects of borate modified BG incorporation for cells attachment, proliferation, and odontogenic differentiation. This study showed that borate modified BG-NPs can be suggested as biomaterial for dental tissue engineering applications and prepared dentin constructs with addition of borate modified BG-NPs are promising to be used in regenerative dentistry. In vivo studies are needed for investigating the potential use of the prepared constructs for dentin regeneration in clinic.

## REFERENCES

- Abbasi Z, Bahrololoom M, Shariat M and Bagheri R (2015). Bioactive glasses in dentistry: a review. *Journal of Dental Biomaterials* **2**: 1-9.
- Abdal-hay A, Khalil KA, Hamdy AS and Al-Jassir FF (2017). Fabrication of highly porous biodegradable biomimetic nanocomposite as advanced bone tissue scaffold. *Arabian Journal of Chemistry* **10**: 240-252.
- AbdulQader ST, Ab Rahman I, Ismail H, Kannan TP and Mahmood Z (2013). A simple pathway in preparation of controlled porosity of biphasic calcium phosphate scaffold for dentin regeneration. *Ceramics International* **39**: 2375-2381.
- AbdulQader ST, Rahman IA, Thirumulu KP, Ismail H and Mahmood Z (2016). Effect of biphasic calcium phosphate scaffold porosities on odontogenic differentiation of human dental pulp cells. *Journal of Biomaterials Applications* **30**: 1300-1311.
- Abdurrahim T and Sopyan I (2008). Recent progress on the development of porous bioactive calcium phosphate for biomedical applications. *Recent Patents on Biomedical Engineering* **1**: 213-229.
- Abo-Aziza FA and Zaki A (2017). The Impact of Confluence on Bone Marrow Mesenchymal Stem (BMMSC) Proliferation and Osteogenic Differentiation. *International Journal of Hematology-Oncology and Stem Cell Research* **11**: 121-132.
- Abrahão IJ, Martins MD, Katayama E, Antoniazzi JH, Segmentilli A and Marques MM (2006). Collagen analysis in human tooth germ papillae. *Brazilian Dental Journal* **17**: 208-212.
- Adams LA and Essien ER (2015). In Vitro Transformation of Sol-gel Derived Bioactive Glass from Sand. *American Journal of Biomedical Sciences* **7**: 218-228.
- Aguiar H, Solla EL, Serra J, González P, León B, Almeida N, Cachinho S, Davim EJC, Correia R, Oliveira JM and Fernandes MHV (2008). Orthophosphate

nanostructures in SiO<sub>2</sub>–P<sub>2</sub>O<sub>5</sub>–CaO–Na<sub>2</sub>O–MgO bioactive glasses. *Journal of Non-Crystalline Solids* **354**: 4075-4080.

Aguilar-Pérez FJ, Vargas-Coronado RF, Cervantes-Uc JM, Cauch-Rodríguez JV, Covarrubias C and Pedram-Yazdani M (2016). Preparation and bioactive properties of nano bioactive glass and segmented polyurethane composites. *Journal of Biomaterials Applications* **30**: 1362-1372.

Albrektsson T and Johansson C (2001). Osteoinduction, osteoconduction and osseointegration. *European Spine Journal* **10**: S96-S101.

Alipour R, Sadeghi F, Hashemi-Beni B, Zarkesh-Esfahani SH, Heydari F, Mousavi SB, Adib M, Narimani M and Esmaeili N (2010). Phenotypic characterizations and comparison of adult dental stem cells with adipose-derived stem cells. *International Journal of Preventive Medicine* **1**:164–171.

Ando Y, Honda MJ, Ohshima H, Tonomura A, Ohara T, Itaya T, Kagami H and Ueda M (2009). The induction of dentin bridge-like structures by constructs of subcultured dental pulp-derived cells and porous HA/TCP in porcine teeth. *Nagoya Journal of Medical Science* **71**: 51-62.

Anil S, Anand P, Alghamdi H and Jansen J (2011). Dental implant surface enhancement and osseointegration. *Implant Dentistry-A Rapidly Evolving Practice. Rijeka InTech* 86–90.

Arana-Chavez VE and Massa LF (2004). Odontoblasts: the cells forming and maintaining dentine. *The International Journal of Biochemistry & Cell Biology* **36**: 1367-1373.

Araújo M, Miola M, Baldi G, Perez J and Verné E (2016). Bioactive glasses with low Ca/P ratio and enhanced bioactivity. *Materials* **9**: 226.

Arora A, Sharma P and Katti DS (2015). Pullulan-based composite scaffolds for bone tissue engineering: Improved osteoconductivity by pore wall mineralization. *Carbohydrate Polymers* **123**: 180-189.

Asma C, Meriem E, Mahmoud B and Djafer B (2014). Physicochemical characterization of gelatin-cmc composite edibles films from polyion-complex hydrogels. *Journal of the Chilean Chemical Society* **59**: 2279-2283.



- Atari M, Barajas M, Hernández-Alfaro F, Gil C, Fabregat M, Ferrés Padró E, Giner L and Casals N (2011). Isolation of pluripotent stem cells from human third molar dental pulp. *Histology and Histopathology* **26**: 1057 -1070.
- Atila D, Keskin D and Tezcaner A (2015). Cellulose acetate based 3-dimensional electrospun scaffolds for skin tissue engineering applications. *Carbohydrate Polymers* **133**: 251-261.
- Atila D, Keskin D and Tezcaner A (2016). Crosslinked pullulan/cellulose acetate fibrous scaffolds for bone tissue engineering. *Materials Science and Engineering: C* **69**: 1103-1115.
- Aydogdu H, Keskin D, Baran ET and Tezcaner A (2016). Pullulan microcarriers for bone tissue regeneration. *Materials Science and Engineering: C* **63**: 439-449.
- Bae W-J, Min K-S, Kim J-J, Kim J-J, Kim H-W and Kim E-C (2012). Odontogenic responses of human dental pulp cells to collagen/nanobioactive glass nanocomposites. *Dental Materials* **28**: 1271-1279.
- Bakopoulou A, Leyhausen G, Volk J, Tsiftoglou A, Garefis P, Koidis P and Geurtsen W (2011). Comparative analysis of in vitro osteo/odontogenic differentiation potential of human dental pulp stem cells (DPSCs) and stem cells from the apical papilla (SCAP). *Archives of Oral Biology* **56**: 709-721.
- Balakrishnan B, Joshi N, Jayakrishnan A and Banerjee R (2014). Self-crosslinked oxidized alginate/gelatin hydrogel as injectable, adhesive biomimetic scaffolds for cartilage regeneration. *Acta Biomaterialia* **10**: 3650-3663.
- Balasubramanian P, Grünwald A, Detsch R, Hupa L, Jokic B, Tallia F, Solanki AK, Jones JR and Boccaccini AR (2016). Ion Release, Hydroxyapatite Conversion, and Cytotoxicity of Boron-Containing Bioactive Glass Scaffolds. *International Journal of Applied Glass Science* **7**: 206-215.
- Balmayor ER, Baran E, Azevedo HS and Reis R (2012). Injectable biodegradable starch/chitosan delivery system for the sustained release of gentamicin to treat bone infections. *Carbohydrate Polymers* **87**: 32-39.

- Baudry A, Uzunoglu E, Schneider B, Kellermann O and Goldberg M (2016). From pulpal stem cells to tooth repair: an emerging field for dental tissue engineering. *Evidence-Based Endodontics* **1**: 2.
- Boccaccini AR, Erol M, Stark WJ, Mohn D, Hong Z and Mano JF (2010). Polymer/bioactive glass nanocomposites for biomedical applications: a review. *Composites Science and Technology* **70**: 1764-1776.
- Boynueğri D, Özcan G, Şenel S, Uç D, Uraz A, Ögüş E, Çakılcı B and Karaduman B (2009). Clinical and radiographic evaluations of chitosan gel in periodontal intraosseous defects: a pilot study. *Journal of Biomedical Materials Research Part B: Applied Biomaterials* **90**: 461-466.
- Bruneel D and Schacht E (1993). Chemical modification of pullulan: 1. Periodate oxidation. *Polymer* **34**: 2628-2632.
- Bruneel D and Schacht E (1995). Enzymatic degradation of pullulan and pullulan derivatives. *Journal of Bioactive and Compatible Polymers* **10**: 299-312.
- Cai J, Zhang Y, Liu P, Chen S, Wu X, Sun Y, Li A, Huang K, Luo R and Wang L (2013). Generation of tooth-like structures from integration-free human urine induced pluripotent stem cells. *Cell Regeneration* **2**: 6.
- Cajazeira Aguiar M and Arana-Chavez VE (2007). Ultrastructural and immunocytochemical analyses of osteopontin in reactionary and reparative dentine formed after extrusion of upper rat incisors. *Journal of Anatomy* **210**: 418-427.
- Campos E, Coimbra P and Gil M (2013). An improved method for preparing glutaraldehyde cross-linked chitosan–poly (vinyl alcohol) microparticles. *Polymer bulletin* **70**: 549-561.
- Casagrande L, Demarco F, Zhang Z, Araujo F, Shi S and Nör J (2010). Dentin-derived BMP-2 and odontoblast differentiation. *Journal of Dental Research* **89**: 603-608.
- Ceyhan T, Günay V, Çapoğlu A, Sayrak H and Karaca Ç (2007). Production and characterization of a glass-ceramic biomaterial and in vitro and in vivo evaluation of its biological effects. *Acta Orthop Traumatol Turc* **41**: 307-313.

- Chainoglou E, Karagkiozaki V, Choli-Papadopoulou T, Mavromanolis C, Laskarakis A and Logothetidis S (2016). Development of Biofunctionalized Cellulose Acetate Nanoscaffolds for Heart Valve Tissue Engineering. *World Journal of Nano Science and Engineering* **6**: 129–152.
- Chandrasekar RS, Lavu V, Kumar K and Rao SR (2015). Evaluation of antimicrobial properties of bioactive glass used in regenerative periodontal therapy. *Journal of Indian Society of Periodontology* **19**: 516-519.
- Chen B, Sun H-H, Wang H-G, Kong H, Chen F-M and Yu Q (2012). The effects of human platelet lysate on dental pulp stem cells derived from impacted human third molars. *Biomaterials* **33**: 5023-5035.
- Chen X, Zhao Y, Geng S, Miron RJ, Zhang Q, Wu C and Zhang Y (2015). In vivo experimental study on bone regeneration in critical bone defects using PIB nanogels/boron-containing mesoporous bioactive glass composite scaffold. *International Journal of Nanomedicine* **10**: 839-846.
- Choi Y-A, Seol M-Y, Shin H-I and Park EK (2014). Bobby Sox homology regulates odontoblast differentiation of human dental pulp stem cells/progenitors. *Cell Communication and Signaling* **12**: 35.
- Ciceo RL, Trandafir D-L, Radu T, Ponta O and Simon V (2014). Synthesis, characterisation and in vitro evaluation of sol–gel derived  $\text{SiO}_2\text{-P}_2\text{O}_5\text{-CaO-B}_2\text{O}_3$  bioactive system. *Ceramics International* **40**: 9517-9524.
- Demirci S, Kaya MS, Doğan A, Kalay Ş, Altın NÖ, Yarat A, Akyüz SH and Şahin F (2015). Antibacterial and cytotoxic properties of boron-containing dental composite. *Turkish Journal of Biology* **39**: 417-426.
- Deshpande AS, Fang P-A, Zhang X, Jayaraman T, Sfeir C and Beniash E (2011). Primary structure and phosphorylation of dentin matrix protein 1 (DMP1) and dentin phosphophoryn (DPP) uniquely determine their role in biomineralization. *Biomacromolecules* **12**: 2933-2945.
- Devirian TA and Volpe SL (2003). The physiological effects of dietary boron. *Critical Reviews in Food Science and Nutrition* **43**:219–231

- Du J, Tan E, Kim HJ, Zhang A, Bhattacharya R and Yarema KJ (2014). Comparative evaluation of chitosan, cellulose acetate, and polyethersulfone nanofiber scaffolds for neural differentiation. *Carbohydrate Polymers* **99**: 483-490.
- Dulong V, Forbice R, Condamine E, Le Cerf D and Picton L (2011). Pullulan–STMP hydrogels: a way to correlate crosslinking mechanism, structure and physicochemical properties. *Polymer Bulletin* **67**: 455-466.
- Durán VL, Larsson PA and Wågberg L (2016). On the relationship between fibre composition and material properties following periodate oxidation and borohydride reduction of lignocellulosic fibres. *Cellulose* **23**: 3495-3510.
- Durand LAH, Góngora A, López JMP, Boccaccini AR, Zago MP, Baldi A and Gorustovich A (2014). In vitro endothelial cell response to ionic dissolution products from boron-doped bioactive glass in the SiO<sub>2</sub>–CaO–P<sub>2</sub>O<sub>5</sub>–Na<sub>2</sub>O system. *Journal of Materials Chemistry B* **2**: 7620-7630.
- Dzondo-Gadet M, Mayap-Nzietchueng R, Hess K, Nabet P, Belleville F and Dousset B (2002). Action of boron at the molecular level. *Biological Trace Element Research* **85**: 23-33.
- El-Kady AM, Ali AF and Farag MM (2010). Development, characterization, and in vitro bioactivity studies of sol–gel bioactive glass/poly (L-lactide) nanocomposite scaffolds. *Materials Science and Engineering: C* **30**: 120-131.
- El-Kady AM, Rizk RA, El-Hady BMA, Shafaa MW and Ahmed MM (2012). Characterization, and antibacterial properties of novel silver releasing nanocomposite scaffolds fabricated by the gas foaming/salt-leaching technique. *Journal of Genetic Engineering and Biotechnology* **10**: 229-238.
- El-Backly RM, Massoud AG, El-Badry AM, Sherif RA and Marei MK (2008). Regeneration of dentine/pulp-like tissue using a dental pulp stem cell/poly (lactic-co-glycolic) acid scaffold construct in New Zealand white rabbits. *Australian Endodontic Journal* **34**: 52-67.
- Erdemli O, Captug O, Bilgili H, Orhan D, Tezcaner A and Keskin D (2010). In vitro and in vivo evaluation of the effects of demineralized bone matrix or calcium sulfate

addition to polycaprolactone–bioglass composites. *Journal of Materials Science: Materials in Medicine* **21**: 295-308.

Eslaminejad MB, Nazarian H, Shariati M and Vahabi S (2009). Human dental pulp stem cells: the culture optimization for increased growth. *International Journal of Hematology-Oncology and Stem Cell Research* **3**: 5-13.

Fadzli SSN, Roslinda S, Zainuddin F and Ismail H (2016). Synthesis of sol-gel derived glass powder and in vitro bioactivity property tested in simulated body fluid. *AIP Conference Proceedings*. AIP Publishing, p. 040033.

Fagerholm P, Lagali NS, Merrett K, Jackson WB, Munger R, Liu Y, Polarek JW, Söderqvist M and Griffith M (2010). A biosynthetic alternative to human donor tissue for inducing corneal regeneration: 24-month follow-up of a phase 1 clinical study. *Science Translational Medicine* **2**: 46ra61-46ra61.

Faqhiri H (2017). Chitosan and Silica Bioactive Glass 3D Porous Composite for Tissue Engineering. (M.Sc Thesis). Tampere University of Technology, Tampere, Finland.

Featherstone J (2008). Dental caries: a dynamic disease process. *Australian Dental Journal* **53**: 286-291.

Feng B, Jinkang Z, Zhen W, Jianxi L, Jiang C, Jian L, Guolin M and Xin D (2011). The effect of pore size on tissue ingrowth and neovascularization in porous bioceramics of controlled architecture in vivo. *Biomedical Materials* **6**: 015007.

Feng JQ, Luan X, Wallace J, Jing D, Ohshima T, Kulkarni AB, D'Souza RN, Kozak CA and MacDougall M (1998). Genomic organization, chromosomal mapping, and promoter analysis of the mouse dentin sialophosphoprotein (Dspp) gene, which codes for both dentin sialoprotein and dentin phosphoprotein. *Journal of Biological Chemistry* **273**: 9457-9464.

Fricain JC, Schlaubitz S, Le Visage C, Arnault I, Derkaoui SM, Siadous R, Catros S, Lalande C, Bareille R and Renard M (2013). A nano-hydroxyapatite–pullulan/dextran polysaccharide composite macroporous material for bone tissue engineering. *Biomaterials* **34**: 2947-2959.

Gala-Garcia A, Teixeira KIR, Wykrota FHL, Sinisterra RD and Cortés ME (2010). Bioceramic/poly (glycolic)-poly (lactic acid) composite induces mineralized barrier after direct capping of rat tooth pulp tissue. *Brazilian Oral Research* **24**: 08-14.

Gao H, Li B, Zhao L and Jin Y (2015). Influence of nanotopography on periodontal ligament stem cell functions and cell sheet based periodontal regeneration. *International journal of Nanomedicine* **10**: 400–4027.

Gao Y, Liu L and Zhang Z (2009). Mechanical performance of nano-CaCO<sub>3</sub> filled polystyrene composites. *Acta Mechanica Solida Sinica* **22**: 555-562.

Ge Y, Wang J, Shi Z and Yin J (2012). Gelatin-assisted fabrication of water-dispersible graphene and its inorganic analogues. *Journal of Materials Chemistry* **22**: 17619-17624.

Gerhardt L-C and Boccaccini AR (2010). Bioactive glass and glass-ceramic scaffolds for bone tissue engineering. *Materials* **3**: 3867-3910.

Gerhardt L-C, Widdows KL, Erol MM, Burch CW, Sanz-Herrera JA, Ochoa I, Stämpfli R, Roqan IS, Gabe S and Ansari T (2011). The pro-angiogenic properties of multi-functional bioactive glass composite scaffolds. *Biomaterials* **32**: 4096-4108.

Ghimire S (2016). In vitro and Mechanical Properties of Bioactive-Glass/polymer Composites.

Goh Y-F, Alshemary AZ, Akram M, Abdul Kadir MR and Hussain R (2014a). In-vitro characterization of antibacterial bioactive glass containing ceria. *Ceramics International* **40**: 729-737.

Goh YF, Alshemary AZ, Akram M, Kadir A, Rafiq M and Hussain R (2014b). Bioactive Glass: An In-Vitro Comparative Study of Doping with Nanoscale Copper and Silver Particles. *International Journal of Applied Glass Science* **5**: 255-266.

Gong W, Huang Z, Dong Y, Gan Y, Li S, Gao X and Chen X (2014). Ionic extraction of a novel nano-sized bioactive glass enhances differentiation and mineralization of human dental pulp cells. *Journal of Endodontics* **40**: 83-88.

González P, Serra J, Liste S, Chiussi S, León B and Pérez-Amor M (2003). Raman spectroscopic study of bioactive silica based glasses. *Journal of Non-crystalline Solids* **320**: 92-99.

- Gorustovich AA, López JMP, Guglielmotti MB and Cabrini RL (2006). Biological performance of boron-modified bioactive glass particles implanted in rat tibia bone marrow. *Biomedical Materials* **1**: 100-105.
- Gouma P, Xue R, Goldbeck C, Perrotta P and Balázs C (2012). Nano-hydroxyapatite—Cellulose acetate composites for growing of bone cells. *Materials Science and Engineering: C* **32**: 607-612.
- Grover CN, Cameron RE and Best SM (2012). Investigating the morphological, mechanical and degradation properties of scaffolds comprising collagen, gelatin and elastin for use in soft tissue engineering. *Journal of the Mechanical Behavior of Biomedical Materials* **10**: 62-74.
- Gümüşderelioğlu M, Tunçay EÖ, Kaynak G, Demirtaş TT, Aydın ST and Hakkı SS (2015). Encapsulated boron as an osteoinductive agent for bone scaffolds. *Journal of Trace Elements in Medicine and Biology* **31**: 120-128.
- Hafezi F, Hosseinejad F, Fooladi AAI, Mafi SM, Amiri A and Nourani MR (2012). Transplantation of nano-bioglass/gelatin scaffold in a non-autogenous setting for bone regeneration in a rabbit ulna. *Journal of Materials Science: Materials in Medicine* **23**: 2783-2792.
- Hafezi M, Safarian S, Khorasani MT and Osman NAA (2016). Polyurethane/58S bioglass nanofibers: synthesis, characterization, and in vitro evaluation. *RSC Advances* **6**: 35815-35824.
- Hakkı SS, Bozkurt BS and Hakkı EE (2010). Boron regulates mineralized tissue-associated proteins in osteoblasts (MC3T3-E1). *Journal of Trace Elements in Medicine and Biology* **24**: 243-250.
- Han N, Zheng Y, Li R, Li X, Zhou M, Niu Y and Zhang Q (2014).  $\beta$ -catenin enhances odontoblastic differentiation of dental pulp cells through activation of Runx2. *PloS one* **9**: e88890.
- Haro Durand LA, Vargas GE, Vera-Mesones R, Baldi A, Zago MP, Fanovich MA, Boccaccini AR and Gorustovich A (2017). In Vitro Human Umbilical Vein Endothelial Cells Response to Ionic Dissolution Products from Lithium-Containing 45S5 Bioactive Glass. *Materials* **10**: 740.

- Hashmi B, Mammoto T, Weaver J, Ferrante T, Jiang A, Jiang E, Feliz J and Ingber DE (2017). Mechanical induction of dentin-like differentiation by adult mouse bone marrow stromal cells using compressive scaffolds. *Stem Cell Research* **24**: 55-60.
- He F, He Z, Xie J and Li Y (2014). IR and Raman Spectra Properties of Bi<sub>2</sub>O<sub>3</sub>-ZnO-B<sub>2</sub>O<sub>3</sub>-BaO Quaternary Glass System. *American Journal of Analytical Chemistry* **5**: 1142.
- Helenius G, Bäckdahl H, Bodin A, Nannmark U, Gatenholm P and Risberg B (2006). In vivo biocompatibility of bacterial cellulose. *Journal of Biomedical Materials Research Part A* **76**: 431-438.
- Hench LL (2006). The story of Bioglass®. *Journal of Materials Science: Materials in Medicine* **17**: 967-978.
- Hench LL and Wilson J (1993). *An introduction to bioceramics*, World scientific, London.
- Hong Z, Liu A, Chen L, Chen X and Jing X (2009). Preparation of bioactive glass ceramic nanoparticles by combination of sol-gel and coprecipitation method. *Journal of Non-crystalline Solids* **355**: 368-372.
- Hou J, Fan D, Zhao L, Yu B, Su J, Wei J and Shin J-W (2016). Degradability, cytocompatibility, and osteogenesis of porous scaffolds of nanobredigite and PCL-PEG-PCL composite. *International Journal of Nanomedicine* **11**: 3545-3555.
- Hu W, Chen S, Xu Q and Wang H (2011). Solvent-free acetylation of bacterial cellulose under moderate conditions. *Carbohydrate Polymers* **83**: 1575-1581.
- Huang GT-J, Yamaza T, Shea LD, Djouad F, Kuhn NZ, Tuan RS and Shi S (2009). Stem/progenitor cell-mediated de novo regeneration of dental pulp with newly deposited continuous layer of dentin in an in vivo model. *Tissue Engineering Part A* **16**: 605-615.
- Huang JTG, Thesleff I (2013) Stem cells in craniofacial development and regeneration. Wiley-Blackwell, New Jersey. p. 153-177.
- Huang W, Day DE, Kittiratanapiboon K and Rahaman MN (2006). Kinetics and mechanisms of the conversion of silicate (45S5), borate, and borosilicate glasses to



hydroxyapatite in dilute phosphate solutions. *Journal of Materials Science: Materials in Medicine* **17**: 583-596.

Hunt CD (1998). Regulation of enzymatic activity. *Biological Trace Element Research* **66**: 205-225.

Inuyama Y, Kitamura C, Nishihara T, Morotomi T, Nagayoshi M, Tabata Y, Matsuo K, Chen KK and Terashita M (2010). Effects of hyaluronic acid sponge as a scaffold on odontoblastic cell line and amputated dental pulp. *Journal of Biomedical Materials Research Part B: Applied Biomaterials* **92**: 120-128.

Isaac J, Nohra J, Lao J, Jallot E, Nedelec J-M, Berdal A and Sautier J-M (2011). Effects of strontium-doped bioactive glass on the differentiation of cultured osteogenic cells. *European Cells & Materials* **21**: 130-43.

Iwamoto T, Nakamura T, Ishikawa M, Yoshizaki K, Sugimoto A, Ida-Yonemochi H, Ohshima H, Saito M, Yamada Y and Fukumoto S (2017). Pannexin 3 regulates proliferation and differentiation of odontoblasts via its hemichannel activities. *PLoS one* **12**: e0177557.

Jasadee K and Lupong K (2010). Properly engineered ceramic scaffolds for sustained drug delivery. *Journal of Materials Science and Engineering* **4**: 77-82.

Jones JR, Ehrenfried LM and Hench LL (2006). Optimising bioactive glass scaffolds for bone tissue engineering. *Biomaterials* **27**: 964-973.

Jun S-K, Lee J-H and Lee H-H (2017). The biomineralization of a bioactive glass-incorporated light-curable pulp capping material using human dental pulp stem cells. *BioMed Research International* **2017**, 2495282.

Kabashima H, Sakai T, Mizobe K, Nakamuta H, Kurita K and Terada Y (2013). The usefulness of an autologous blood clot combined with gelatin for regeneration of periodontal tissue. *Journal of Oral Science* **55**: 363-366.

Kamitsos E, Karakassides M and Chryssikos GD (1987). A vibrational study of lithium borate glasses with high Li<sub>2</sub>O content. *Physics and Chemistry of Glasses* **28**: 203-209.

Kasten P, Beyen I, Niemeyer P, Luginbühl R, Bohner M and Richter W (2008). Porosity and pore size of  $\beta$ -tricalcium phosphate scaffold can influence protein

production and osteogenic differentiation of human mesenchymal stem cells: an in vitro and in vivo study. *Acta Biomaterialia* **4**: 1904-1915.

Khazaei M, Bozorgi A, Khazaei S and Khademi A (2016). Stem cells in dentistry, sources, and applications. *Dental Hypotheses* **7**: 42-52.

Kim G-H, Park Y-D, Lee S-Y, El-Fiqi A, Kim J-J, Lee E-J, Kim H-W and Kim E-C (2015). Odontogenic stimulation of human dental pulp cells with bioactive nanocomposite fiber. *Journal of Biomaterials Applications* **29**: 854-866.

Kokubo T and Takadama H (2006). How useful is SBF in predicting in vivo bone bioactivity? *Biomaterials* **27**: 2907-2915.

Kongsuwan P, Brandal G and Yao YL (2015). Laser Induced Porosity and Crystallinity Modification of a Bioactive Glass Coating on Titanium Substrates. *Journal of Manufacturing Science and Engineering* **137**: 031004.

Kuijpers AJ, Engbers GH, Krijgsveld J, Zaat SA, Dankert J and Feijen J (2000). Cross-linking and characterisation of gelatin matrices for biomedical applications. *Journal of Biomaterials Science, Polymer Edition* **11**: 225-243.

Kükürtcü B (2015). Biyoaktif cam ve cam-seramik malzemelerin üretimi ve yapay vücut sıvısı içerisindeki davranımlarının incelenmesi. (Yüksek Lisans Tezi), İstanbul Teknik Üniversitesi Fen Bilimleri Enstitüsü, İstanbul.

Kulan P, Karabiyik O, Kose G and Kargul B (2017). The effect of accelerated mineral trioxide aggregate on odontoblastic differentiation in dental pulp stem cell niches. *International Endodontic Journal*.

Kulikowska A, Wasiak I and Ciach T (2013). Carboxymethyl Cellulose Oxidation to Form Aldehyde Group. *Challenges of Modern Technology* **4**: 11-18

Kumar A, Singh S, Thumar G and Mengji A (2015). Bioactive glass nanoparticles (NovaMin®) for applications in dentistry. *Journal of Medical and Dental Sciences* **14**: 30-35.

Kumar C (2009). Nanoscale bioactive silicate glasses in biomedical applications in: Nanostructured Oxides. Wiley–VCH 203-216.

- Kushwaha M, Pan X, Holloway JA and Denry IL (2012). Differentiation of human mesenchymal stem cells on niobium-doped fluorapatite glass-ceramics. *Dental Materials* **28**: 252-260.
- Kwon Y, Lee S, Hwang Y, Rosa V, Lee K and Min K (2017). Behaviour of human dental pulp cells cultured in a collagen hydrogel scaffold cross-linked with cinnamaldehyde. *International Endodontic Journal* **50**: 58-66.
- Laczka M, Cholewa-Kowalska K, Laczka-Osyczka A, Tworzydło M and Turyna B (2000). Gel-derived materials of a CaO-P<sub>2</sub>O<sub>5</sub>-SiO<sub>2</sub> system modified by boron, sodium, magnesium, aluminum, and fluorine compounds. *Journal of Biomedical Materials Research* **52**: 601-612.
- Lai J-Y, Li Y-T, Cho C-H and Yu T-C (2012). Nanoscale modification of porous gelatin scaffolds with chondroitin sulfate for corneal stromal tissue engineering. *International Journal of Nanomedicine* **7**: 1101–1114.
- Lee EJ, Kwak DH and Kim DJ (2015). Mechanical properties of cellulose acetate/hydroxyapatite nanoparticle composite fiber by electro-spinning process. *Journal of Ceramic Processing Research* **16**: 330-334.
- Lee J-H, Kang M-S, Mahapatra C and Kim H-W (2016). Effect of aminated mesoporous bioactive glass nanoparticles on the differentiation of dental pulp stem cells. *PloS one* **11**: e0150727.
- Lei B, Chen X, Han X and Zhou J (2012). Versatile fabrication of nanoscale sol–gel bioactive glass particles for efficient bone tissue regeneration. *Journal of Materials Chemistry* **22**: 16906-16913.
- Lei B, Shin K-H, Noh D-Y, Jo I-H, Koh Y-H, Kim H-E and Kim SE (2013). Sol–gel derived nanoscale bioactive glass (NBG) particles reinforced poly ( $\epsilon$ -caprolactone) composites for bone tissue engineering. *Materials Science and Engineering: C* **33**: 1102-1108.
- Lemos EM, Patrício PS and Pereira MM (2016). 3D nanocomposite chitosan/bioactive glass scaffolds obtained using two different routes: an evaluation of the porous structure and mechanical properties. *Química Nova* **39**: 462-466.

- Leong DJX, Setzer FC, Trope M and Karabucak B (2016). Biocompatibility of two experimental scaffolds for regenerative endodontics. *Restorative Dentistry & Endodontics* **41**: 98-105.
- Lepry WC and Nazhat SN (2015). Highly Bioactive Sol-Gel-Derived Borate Glasses. *Chemistry of Materials* **27**: 4821-4831.
- Li D, Jiao G, Zhang W, Chen X, Ning R and Du C (2016). Hybrid scaffolding strategy for dermal tissue reconstruction: a bioactive glass/chitosan/silk fibroin composite. *RSC Advances* **6**: 19887-19896.
- Li H, Yang J, Hu X, Liang J, Fan Y and Zhang X (2011a). Superabsorbent polysaccharide hydrogels based on pullulan derivate as antibacterial release wound dressing. *Journal of Biomedical Materials Research Part A* **98**: 31-39.
- Li J-H, Liu D-Y, Zhang F-M, Wang F, Zhang W-K and Zhang Z-T (2011b). Human dental pulp stem cell is a promising autologous seed cell for bone tissue engineering. *Chinese Medical Journal* **124**: 4022-4028.
- Li S, Hu J, Zhang G, Qi W, Zhang P, Li P, Zeng Y, Zhao W and Tan Y (2015). Extracellular Ca<sup>2+</sup> Promotes Odontoblastic Differentiation of Dental Pulp Stem Cells via BMP2-Mediated Smad1/5/8 and Erk1/2 Pathways. *Journal of Cellular Physiology* **230**: 2164-2173.
- Li W, Li X, Wang T, Li X, Pan S and Deng H (2012). Nanofibrous mats layer-by-layer assembled via electrospun cellulose acetate and electrospayed chitosan for cell culture. *European Polymer Journal* **48**: 1846-1853.
- Li X, Zhang C, Wang L, Ma C, Yang W and Li M (2013). Acylation Modification of *Antheraea pernyi* Silk Fibroin Using Succinic Anhydride and Its Effects on Enzymatic Degradation Behavior. *Journal of Chemistry* **2013**, 640913.
- Li Y, Lu Y, Maciejewska I, Galler KM, Cavender A and D'Souza R (2011c). TWIST1 promotes the odontoblast-like differentiation of dental stem cells. *Advances in Dental Research* **23**: 280-284.
- Li Z, Ramay HR, Hauch KD, Xiao D and Zhang M (2005). Chitosan–alginate hybrid scaffolds for bone tissue engineering. *Biomaterials* **26**: 3919-3928.

- Liang S-L, Cook WD, Thouas GA and Chen Q-Z (2010). The mechanical characteristics and in vitro biocompatibility of poly (glycerol sebacate)-Bioglass® elastomeric composites. *Biomaterials* **31**: 8516-8529.
- Lim H-C, Nam OH, Kim M-j, El-Fiqi A, Yun H-M, Lee Y-M, Jin G-Z, Lee H-H, Kim H-W and Kim E-C (2016). Delivery of dexamethasone from bioactive nanofiber matrices stimulates odontogenesis of human dental pulp cells through integrin/BMP/mTOR signaling pathways. *International Journal of Nanomedicine* **11**: 2557-2567.
- Linde A (1985). Session II: Cells and Extracellular Matrices of the Dental Pulp—CT Hanks, Chairman: The Extracellular Matrix of the Dental Pulp and Dentin. *Journal of Dental Research* **64**: 523-529.
- Liu J, Yu F, Sun Y, Jiang B, Zhang W, Yang J, Xu GT, Liang A and Liu S (2015). Concise Reviews: Characteristics and Potential Applications of Human Dental Tissue-Derived Mesenchymal Stem Cells. *Stem Cells* **33**: 627-638.
- Loh QL and Choong C (2013). Three-dimensional scaffolds for tissue engineering applications: role of porosity and pore size. *Tissue Engineering Part B: Reviews* **19**: 485-502.
- Lombardi M, Gremillard L, Chevalier J, Lefebvre L, Cacciotti I, Bianco A and Montanaro L (2013). A comparative study between melt-derived and sol-gel synthesized 45S5 bioactive glasses. *Key Engineering Materials*. Trans Tech Publ, pp. 15-30.
- Lu HH, Tang A, Oh SC, Spalazzi JP and Dionisio K (2005). Compositional effects on the formation of a calcium phosphate layer and the response of osteoblast-like cells on polymer-bioactive glass composites. *Biomaterials* **26**: 6323-6334.
- Lu Q, Pandya M, Rufaihah AJ, Rosa V, Tong HJ, Seliktar D and Toh WS (2015). Modulation of dental pulp stem cell odontogenesis in a tunable PEG-fibrinogen hydrogel system. *Stem Cells International* **2015**: 525367.
- Luo G, Ma Y, Cui X, Jiang L, Wu M, Hu Y, Luo Y, Pan H and Ruan C (2017). 13-93 bioactive glass/alginate composite scaffolds 3D printed under mild conditions for bone regeneration. *RSC Advances* **7**: 11880-11889.

- Luz GM and Mano JF (2011). Preparation and characterization of bioactive glass nanoparticles prepared by sol–gel for biomedical applications. *Nanotechnology* **22**: 494014.
- M. Mukundan L, Nirmal R, Vaikkath D and Nair PD (2013). A new synthesis route to high surface area sol gel bioactive glass through alcohol washing: A preliminary study. *Biomatter* **3**: e24288.
- Maçon AL, Kim TB, Valliant EM, Goetschius K, Brow RK, Day DE, Hoppe A, Boccaccini AR, Kim IY and Ohtsuki C (2015). A unified in vitro evaluation for apatite-forming ability of bioactive glasses and their variants. *Journal of Materials Science: Materials in Medicine* **26**: 115-125.
- Maheswaran A, Hirankumar G, Heller N, Karthickprabhu S and Kawamura J (2014). Structure, dielectric and bioactivity of P2O5–CaO–Na2O–B2O3 bioactive glass. *Applied Physics A* **117**: 1323-1327.
- Maji K, Dasgupta S, Pramanik K and Bissoyi A (2016). Preparation and evaluation of gelatin-chitosan-nanobioglass 3D porous scaffold for bone tissue engineering. *International Journal of Biomaterials* **2016**, 183–187.
- Manda M, Goudouri O-M, Papadopoulou L, Kantiranis N, Christofilos D, Triantafyllidis K, Chrissafis K, Paraskevopoulos KM and Koidis P (2012). The effect of high tempered firing cycle on the bioactive behavior of sol–gel derived dental porcelain modified by bioactive glass. *Journal of Sol-gel Science and Technology* **63**: 481-494.
- Mishra B, Vuppu S and Rath K (2011). The role of microbial pullulan, a biopolymer in pharmaceutical approaches: A review. *Journal of Applied Pharmaceutical Sciences*, 1 (6): 45-50.
- Mendes AC, Baran ET, Pereira RC, Azevedo HS and Reis RL (2012). Encapsulation and survival of a chondrocyte cell line within xanthan gum derivative. *Macromolecular Bioscience* **12**: 350-359.
- Migneault I, Dartiguenave C, Bertrand MJ and Waldron KC (2004). Glutaraldehyde: behavior in aqueous solution, reaction with proteins, and application to enzyme crosslinking. *Biotechniques* **37**: 790-806.

- Mishra B, Vuppu S and Rath K (2011). The role of microbial pullulan, a biopolymer in pharmaceutical approaches: A review. *Journal of Applied Pharmaceutical Sciences*, 1(6), 45–50.
- Mocanu G, Mihaï D, Dulong V, Picton L and Le Cerf D (2012). New anionic crosslinked multi-responsive pullulan hydrogels. *Carbohydrate Polymers* **87**: 1440-1446.
- Montazerian M and Dutra Zanotto E (2016). History and trends of bioactive glass-ceramics. *Journal of Biomedical Materials Research Part A* **104**: 1231-1249.
- Morinobu M, Ishijima M, Rittling SR, Tsuji K, Yamamoto H, Nifuji A, Denhardt DT and Noda M (2003). Osteopontin expression in osteoblasts and osteocytes during bone formation under mechanical stress in the calvarial suture in vivo. *Journal of Bone and Mineral Research* **18**: 1706-1715.
- Mounesi Rad S, Khorasani MT and Daliri Joupari M (2016). Preparation of HMWCNT/PLLA nanocomposite scaffolds for application in nerve tissue engineering and evaluation of their physical, mechanical and cellular activity properties. *Polymers for Advanced Technologies* **27**: 325-338.
- Mozafari M, Moztarzadeh F, Rabiee M, Azami M, Maleknia S, Tahriri M, Moztarzadeh Z and Nezafati N (2010). Development of macroporous nanocomposite scaffolds of gelatin/bioactive glass prepared through layer solvent casting combined with lamination technique for bone tissue engineering. *Ceramics International* **36**: 2431-2439.
- Murphy C, Kolan K, Li W, Semon J, Day D and Leu M (2017). 3D bioprinting of stem cells and polymer/bioactive glass composite scaffolds for bone tissue engineering. *International Journal of Bioprinting* **3**: 1-11.
- Murphy C, Kolan K, Long M, Li W, Leu M, Semon J and Day D (2016). 3d printing of a polymer bioactive glass composite for bone repair. *27th Annual International Solid Freeform Fabrication Symposium. Austin*. pp. 1718-31.
- Murray PE, Garcia-Godoy F and Hargreaves KM (2007). Regenerative endodontics: a review of current status and a call for action. *Journal of Endodontics* **33**: 377-390.

- Na K, Shin D, Yun K, Park K-H and Lee KC (2003). Conjugation of heparin into carboxylated pullulan derivatives as an extracellular matrix for endothelial cell culture. *Biotechnology Letters* **25**: 381-385.
- Nandi SK, Kundu B and Datta S (2011). Development and applications of varieties of bioactive glass compositions in dental surgery, third generation tissue engineering, orthopaedic surgery and as drug delivery system. *Biomaterials Applications for Nanomedicine*. InTech 2011, 69-116.
- Nandi SK, Mahato A, Kundu B and Mukherjee P (2016a). Doped Bioactive Glass Materials in Bone Regeneration. *Advanced Techniques in Bone Regeneration*. InTech 2016, 275–328
- Nandi SK, Mahato A, Kundu B and Mukherjee P (2016b). *Doped Bioactive Glass Materials in Bone Regeneration*. *Advanced Techniques in Bone Regeneration*. InTech, Rijeka, 275-328.
- Narayanan K, Srinivas R, Ramachandran A, Hao J, Quinn B and George A (2001). Differentiation of embryonic mesenchymal cells to odontoblast-like cells by overexpression of dentin matrix protein 1. *Proceedings of the National Academy of Sciences* **98**: 4516-4521.
- Navabazam AR, Nodoshan FS, Sheikhha MH, Miresmaeili SM, Soleimani M and Fesahat F (2013). Characterization of mesenchymal stem cells from human dental pulp, preapical follicle and periodontal ligament. *Iranian Journal of Reproductive Medicine* **11**: 235-242.
- Nielsen FH (1994). Biochemical and physiologic consequences of boron deprivation in humans. *Environmental Health Perspectives* **102**: 59-63.
- Nielsen FH (2004). Dietary fat composition modifies the effect of boron on bone characteristics and plasma lipids in rats. *Biofactors* **20**: 161-171.
- Ning F, Guo Y, Tang J, Zhou J, Zhang H, Lu W, Gao Y, Wang L, Pei D and Duan Y (2010). Differentiation of mouse embryonic stem cells into dental epithelial-like cells induced by ameloblasts serum-free conditioned medium. *Biochemical and Biophysical Research Communications* **394**: 342-347.



- O'Brien J, Wilson I, Orton T and Pognan F (2000). Investigation of the Alamar Blue (resazurin) fluorescent dye for the assessment of mammalian cell cytotoxicity. *The FEBS Journal* **267**: 5421-5426.
- Omes C and Riva F (2014). New Experimental Model for Basic Research in Stem Cell Field. *Austin Therapeutics* **1**: 3.
- Ostomel TA, Shi Q, Tsung CK, Liang H and Stucky GD (2006). Spherical bioactive glass with enhanced rates of hydroxyapatite deposition and hemostatic activity. *Small* **2**: 1261-1265.
- Otadi M and Mohebbi-Kalhari D (2015). Evaluate of different bioactive glass on mechanical properties of nanocomposites prepared using electrospinning method. *Procedia Materials Science* **11**: 196-201.
- Paduano F, Marrelli M, White LJ, Shakesheff KM and Tatullo M (2016). Odontogenic differentiation of human dental pulp stem cells on hydrogel scaffolds derived from decellularized bone extracellular matrix and collagen type I. *PloS one* **11**: e0148225.
- Paiva AO, Duarte MG, Fernandes MHV, Gil MH and Costa NG (2006). In vitro studies of bioactive glass/polyhydroxybutyrate composites. *Materials Research* **9**: 417-423.
- Pal M, Roy B and Pal M (2011). Structural characterization of borate glasses containing zinc and manganese oxides. *Journal of Modern Physics* **2011**.
- Park CH, Rios HF, Jin Q, Bland ME, Flanagan CL, Hollister SJ and Giannobile WV (2010). Biomimetic hybrid scaffolds for engineering human tooth-ligament interfaces. *Biomaterials* **31**: 5945-5952.
- Pereira JM (2013). Synthesis of new pullulan derivatives for drug delivery. (Ph.D. thesis), Virginia Polytechnic Institute and State University, Virginia.
- Petrauskaite O, Juodzbaly G, Viskelis P and Liesiene J (2016). Control of the porous structure of cellulose-based tissue engineering scaffolds by means of lyophilization. *Cellulose Chemistry and Technology* **50**: 23-30.
- Pizzorno L (2015). Nothing boring about boron. *Integrative Medicine: A Clinician's Journal* **14**: 35-48.

- Polini A, Bai H and Tomsia AP (2013). Dental applications of nanostructured bioactive glass and its composites. *Wiley Interdisciplinary Reviews: Nanomedicine and Nanobiotechnology* **5**: 399-410.
- Pourhaghgouy M and Zamanian A (2014). Ice-templated scaffolds of bioglass nanoparticles reinforced-chitosan. *Biomedical Engineering (ICBME), 2014 21<sup>th</sup> Iranian Conference on*. IEEE, pp. 48-52.
- Prescott RS, Alsanea R, Fayad MI, Johnson BR, Wenckus CS, Hao J, John AS and George A (2008). In vivo generation of dental pulp-like tissue by using dental pulp stem cells, a collagen scaffold, and dentin matrix protein 1 after subcutaneous transplantation in mice. *Journal of Endodontics* **34**: 421-426.
- Qian Y-F, Zhang K-H, Chen F, Ke Q-F and Mo X-M (2011). Cross-linking of gelatin and chitosan complex nanofibers for tissue-engineering scaffolds. *Journal of Biomaterials Science, Polymer Edition* **22**: 1099-1113.
- Qu T, Jing J, Jiang Y, Taylor RJ, Feng JQ, Geiger B and Liu X (2014). Magnesium-containing nanostructured hybrid scaffolds for enhanced dentin regeneration. *Tissue Engineering Part A* **20**: 2422-2433.
- Qu T, Jing J, Ren Y, Ma C, Feng JQ, Yu Q and Liu X (2015). Complete pulpodentin complex regeneration by modulating the stiffness of biomimetic matrix. *Acta biomaterialia* **16**: 60-70.
- Qu T and Liu X (2013). Nano-structured gelatin/bioactive glass hybrid scaffolds for the enhancement of odontogenic differentiation of human dental pulp stem cells. *Journal of Materials Chemistry B* **1**: 4764-4772.
- Ravi PR, Vats R, Balija J, Adapa SPN and Aditya N (2014). Modified pullulan nanoparticles for oral delivery of lopinavir: Formulation and pharmacokinetic evaluation. *Carbohydrate Polymers* **110**: 320-328.
- Ravindran S, Zhang Y, Huang C-C and George A (2013). Odontogenic induction of dental stem cells by extracellular matrix-inspired three-dimensional scaffold. *Tissue Engineering Part A* **20**: 92-102.
- Rekha M and Sharma CP (2007). Pullulan as a promising biomaterial for biomedical applications: a perspective. *Trends in Biomaterials & Artificial Organs* **20**: 116-121.

Richaud R, Lachas H, Healey A, Reed G, Haines J, Jarvis K, Herod A, Dugwell D and Kandiyoti R (2000). Trace element analysis of gasification plant samples by icp–ms: validation by comparison of results from two laboratories. *Fuel* **79**: 1077-1087.

Roohani-Esfahani S, Nouri-Khorasani S, Lu Z, Fathi M, Razavi M, Appleyard R and Zreiqat H (2012). Modification of porous calcium phosphate surfaces with different geometries of bioactive glass nanoparticles. *Materials Science and Engineering: C* **32**: 830-839.

Rosa V, Dubey N, Islam I, Min K-S and Nör JE (2016). Pluripotency of stem cells from human exfoliated deciduous teeth for tissue engineering. *Stem Cells International* **2016**:5957806.

Rose JB, Pacelli S, Haj AJE, Dua HS, Hopkinson A, White LJ and Rose FR (2014). Gelatin-based materials in ocular tissue engineering. *Materials* **7**: 3106-3135.

Saito K, Nakatomi M, Ida-Yonemochi H and Ohshima H (2016). Osteopontin is essential for type I collagen secretion in reparative dentin. *Journal of Dental Research* **95**: 1034-1041.

Sakai V, Zhang Z, Dong Z, Neiva K, Machado M, Shi S, Santos C and Nör J (2010). SHED differentiate into functional odontoblasts and endothelium. *Journal of Dental Research* **89**: 791-796.

Sarin J, Björkvik L, Hiltunen M, Hupa L, Pulkkinen J and Vallittu PK (2016). The effect of fibrin sealant on bioactive glass S53P4 particles – pH impact and dissolution characteristics in vitro. *Journal of Science: Advanced Materials and Devices* **1**: 482-487.

Sato S, Tsuchiya M, Komaki K-i, Kusunoki S-i, Tsuchiya S, Haruyama N, Takahashi I, Sasano Y and Watanabe M (2009). Synthesis and intracellular transportation of type I procollagen during functional differentiation of odontoblasts. *Histochemistry and cell biology* **131**: 583-591.

Schrieber R and Gareis H (2007). *Gelatine handbook: theory and industrial practice*, John Wiley & Sons.

Shahini A, Yazdimamaghani M, Walker KJ, Eastman MA, Hatami-Marbini H, Smith BJ, Ricci JL, Madihally SV, Vashae D and Tayebi L (2014). 3D conductive

nanocomposite scaffold for bone tissue engineering. *International Journal of Nanomedicine* **9**: 167.

Shalaby SW and Salz U (2006). *Polymers for dental and orthopedic applications*, CRC Press.

Sharma S, Srivastava D, Grover S and Sharma V (2014). Biomaterials in tooth tissue engineering: a review. *Journal of Clinical and Diagnostic Research: JCDR* **8**: 309-315.

Sharmin N, Hasan MS, Parsons AJ, Furniss D, Scotchford CA, Ahmed I and Rudd CD (2013). Effect of boron addition on the thermal, degradation, and cytocompatibility properties of phosphate-based glasses. *BioMed Research International* **2013**, 1-12.

Shingel KI (2004). Current knowledge on biosynthesis, biological activity, and chemical modification of the exopolysaccharide, pullulan. *Carbohydrate Research* **339**: 447-460.

Singh RS, Saini GK and Kennedy JF (2008). Pullulan: microbial sources, production and applications. *Carbohydrate Polymers* **73**: 515-531.

Sinz A (2006). Chemical cross-linking and mass spectrometry to map three-dimensional protein structures and protein–protein interactions. *Mass Spectrometry Reviews* **25**: 663-682.

Sowmya S, Kumar PS, Chennazhi K, Nair S, Tamura H and Rangasamy J (2011). Biocompatible  $\beta$ -chitin hydrogel/nanobioactive glass ceramic nanocomposite scaffolds for periodontal bone regeneration. *Artif. Organs* **25**: 1-11.

Srinivasan S, Jayasree R, Chennazhi K, Nair S and Jayakumar R (2012). Biocompatible alginate/nano bioactive glass ceramic composite scaffolds for periodontal tissue regeneration. *Carbohydrate Polymers* **87**: 274-283.

Stanić V (2017). Variation in Properties of Bioactive Glasses After Surface Modification. *Clinical Applications of Biomaterials*. Springer, pp. 35-63.

Su W-Y, Chen Y-C and Lin F-H (2010). Injectable oxidized hyaluronic acid/adipic acid dihydrazide hydrogel for nucleus pulposus regeneration. *Acta Biomaterialia* **6**: 3044-3055.

- Suzuki S, Haruyama N, Nishimura F and Kulkarni AB (2012). Dentin sialophosphoprotein and dentin matrix protein-1: two highly phosphorylated proteins in mineralized tissues. *Archives of Oral Biology* **57**: 1165-1175.
- Tada H, Nemoto E, Kanaya S, Hamaji N, Sato H and Shimauchi H (2010). Elevated extracellular calcium increases expression of bone morphogenetic protein-2 gene via a calcium channel and ERK pathway in human dental pulp cells. *Biochemical and Biophysical Research Communications* **394**: 1093-1097.
- Tainio J, Paakinaho K, Ahola N, Hannula M, Hyttinen J, Kellomäki M and Massera J (2017). In Vitro Degradation of Borosilicate Bioactive Glass and Poly (l-lactide-co- $\epsilon$ -caprolactone) Composite Scaffolds. *Materials* **10**: 1274.
- Takahata T, Okihara T, Yoshida Y, Yoshihara K, Shiozaki Y, Yoshida A, Yamane K, Watanabe N, Yoshimura M and Nakamura M (2015). Bone engineering by phosphorylated-pullulan and  $\beta$ -TCP composite. *Biomedical Materials* **10**: 065009.
- Talebian S, Mehrali M, Mohan S, Mehrali M, Khanlou HM, Kamarul T, Afifi AM and Abass AA (2014). Chitosan (PEO)/bioactive glass hybrid nanofibers for bone tissue engineering. *Rsc Advances* **4**: 49144-49152.
- Taşlı PN, Doğan A, Demirci S and Şahin F (2013). Boron enhances odontogenic and osteogenic differentiation of human tooth germ stem cells (hTGSCs) in vitro. *Biological Trace Element Research* **153**: 419-427.
- Tavakoli E, Mehdikhani-Nahrkhalaji M, Hashemi-Beni B, Zargar-Kharazi A and Kharaziha M (2015). Preparation, characterization and mechanical assessment of poly (lactide-co-glycolide)/hyaluronic acid/fibrin/bioactive glass nano-composite scaffolds for cartilage tissue engineering applications. *Procedia Materials Science* **11**: 124-130.
- Teti G, Salvatore V, Focaroli S, Durante S, Mazzotti A, Dicarlo M, Mattioli-Belmonte M and Orsini G (2015). In vitro osteogenic and odontogenic differentiation of human dental pulp stem cells seeded on carboxymethyl cellulose-hydroxyapatite hybrid hydrogel. *Frontiers in Physiology* **6**.
- Toker H, Ozdemir H, Yuce HB and Goze F (2016). The effect of boron on alveolar bone loss in osteoporotic rats. *Journal of Dental Sciences* **11**: 331-337.

- Tonomura A, Mizuno D, Hisada A, Kuno N, Ando Y, Sumita Y, Honda MJ, Satomura K, Sakurai H and Ueda M (2010). Differential effect of scaffold shape on dentin regeneration. *Annals of Biomedical Engineering* **38**: 1664-1671.
- Tousi NS, Velten MF, Bishop TJ, Leong KK, Barkhordar NS, Marshall GW, Loomer PM, Aswath PB and Varanasi VG (2013). Combinatorial effect of Si<sup>4+</sup>, Ca<sup>2+</sup>, and Mg<sup>2+</sup> released from bioactive glasses on osteoblast osteocalcin expression and biomineralization. *Materials Science and Engineering: C* **33**: 2757-2765.
- Tripathi A and Melo JS (2015). Preparation of a sponge-like biocomposite agarose–chitosan scaffold with primary hepatocytes for establishing an in vitro 3D liver tissue model. *RSC Advances* **5**: 30701-30710.
- Turk M and Deliormanlı AM (2017). Electrically conductive borate-based bioactive glass scaffolds for bone tissue engineering applications. *Journal of Biomaterials Applications*: 32(1) 28–39
- Vallés Lluch A, Campillo Fernández A, Gallego Ferrer G and Monleón Pradas M (2009). Bioactive scaffolds mimicking natural dentin structure. *Journal of Biomedical Materials Research Part B: Applied Biomaterials* **90**: 182-194.
- Valliant EM, Romer F, Wang D, McPhail DS, Smith ME, Hanna JV and Jones JR (2013). Bioactivity in silica/poly ( $\gamma$ -glutamic acid) sol–gel hybrids through calcium chelation. *Acta Biomaterialia* **9**: 7662-7671.
- Van Tienen TG, Heijkants RG, Buma P, de Groot JH, Pennings AJ and Veth RP (2002). Tissue ingrowth and degradation of two biodegradable porous polymers with different porosities and pore sizes. *Biomaterials* **23**: 1731-1738.
- Vichery C and Nedelec J-M (2016). Bioactive glass nanoparticles: from synthesis to materials design for biomedical applications. *Materials* **9**: 288–304.
- Vollenweider M, Brunner TJ, Knecht S, Grass RN, Zehnder M, Imfeld T and Stark WJ (2007). Remineralization of human dentin using ultrafine bioactive glass particles. *Acta Biomaterialia* **3**: 936-943.
- Wang J, Liu X, Jin X, Ma H, Hu J, Ni L and Ma PX (2010). The odontogenic differentiation of human dental pulp stem cells on nanofibrous poly (L-lactic acid) scaffolds in vitro and in vivo. *Acta Biomaterialia* **6**: 3856-3863.

- Wang J, Ma H, Jin X, Hu J, Liu X, Ni L and Ma PX (2011). The effect of scaffold architecture on odontogenic differentiation of human dental pulp stem cells. *Biomaterials* **32**: 7822-7830.
- Wang Z-S, Feng Z-H, Wu G-F, Bai S-Z, Dong Y, Chen F-M and Zhao Y-M (2016). The use of platelet-rich fibrin combined with periodontal ligament and jaw bone mesenchymal stem cell sheets for periodontal tissue engineering. *Scientific Reports* **6**, 28126.
- Wei X, Ling J, Wu L, Liu L and Xiao Y (2007). Expression of mineralization markers in dental pulp cells. *Journal of Endodontics* **33**: 703-708.
- Wei Z, Zhao J, Chen YM, Zhang P and Zhang Q (2016). Self-healing polysaccharide-based hydrogels as injectable carriers for neural stem cells. *Scientific Reports* **6**: 37841.
- Wiesmann H, Meyer U, Plate U and Höhling H (2004). Aspects of collagen mineralization in hard tissue formation. *International Review of Cytology* **242**: 121-156.
- Wilson J and Low SB (1992). Bioactive ceramics for periodontal treatment: comparative studies in the Patas monkey. *Journal of Applied Biomaterials* **3**: 123-129.
- Wolff MS and Larson C (2009). The cariogenic dental biofilm: good, bad or just something to control? *Brazilian Oral Research* **23**: 31-38.
- Wong VW, Rustad KC, Galvez MG, Neofytou E, Glotzbach JP, Januszyk M, Major MR, Sorkin M, Longaker MT and Rajadas J (2010). Engineered pullulan–collagen composite dermal hydrogels improve early cutaneous wound healing. *Tissue Engineering Part A* **17**: 631-644.
- Wu C and Chang J (2012). Mesoporous bioactive glasses: structure characteristics, drug/growth factor delivery and bone regeneration application. *Interface Focus*: rsfs20110121.
- Wu C, Miron R, Sculean A, Kaskel S, Doert T, Schulze R and Zhang Y (2011). Proliferation, differentiation and gene expression of osteoblasts in boron-containing

associated with dexamethasone deliver from mesoporous bioactive glass scaffolds. *Biomaterials* **32**: 7068-7078.

Wu Z, Li Q, Pan Y, Yao Y, Tang S, Su J, Shin J-W, Wei J and Zhao J (2017). Nanoporosity improved water absorption, in vitro degradability, mineralization, osteoblast responses and drug release of poly (butylene succinate)-based composite scaffolds containing nanoporous magnesium silicate compared with magnesium silicate. *International Journal of Nanomedicine* **12**: 3637-3651.

Xia W and Chang J (2007). Preparation and characterization of nano-bioactive-glasses (NBG) by a quick alkali-mediated sol–gel method. *Materials Letters* **61**: 3251-3253.

Xie X-H, Yu X-W, Zeng S-X, Du R-L, Hu Y-H, Yuan Z, Lu E-Y, Dai K-R and Tang T-T (2010). Enhanced osteointegration of orthopaedic implant gradient coating composed of bioactive glass and nanohydroxyapatite. *Journal of Materials Science: Materials in Medicine* **21**: 2165-2173.

Xiong L and He Z (2014). Fabrication and properties of porous collagen/hyaluronic composite scaffolds containing nano-bioactive glass for tissue engineering. *Journal of Macromolecular Science, Part A* **51**: 891-897.

Xu F, Weng B, Gilkerson R, Materon LA and Lozano K (2015). Development of tannic acid/chitosan/pullulan composite nanofibers from aqueous solution for potential applications as wound dressing. *Carbohydrate Polymers* **115**: 16-24.

Xu W-P, Zhang W, Asrican R, Kim H-J, Kaplan DL and Yelick PC (2008). Accurately shaped tooth bud cell–derived mineralized tissue formation on silk scaffolds. *Tissue Engineering Part A* **14**: 549-557.

Xynos ID, Edgar AJ, Bותרy LD, Hench LL and Polak JM (2000). Ionic products of bioactive glass dissolution increase proliferation of human osteoblasts and induce insulin-like growth factor II mRNA expression and protein synthesis. *Biochemical and Biophysical Research Communications* **276**: 461-465.

Yamamoto T, Hasegawa T, Yamamoto T, Hongo H and Amizuka N (2016). Histology of human cementum: Its structure, function, and development. *Japanese Dental Science Review* **52**: 63-74.



- Yang X, Zhang L, Chen X, Sun X, Yang G, Guo X, Yang H, Gao C and Gou Z (2012). Incorporation of B<sub>2</sub>O<sub>3</sub> in CaO-SiO<sub>2</sub>-P<sub>2</sub>O<sub>5</sub> bioactive glass system for improving strength of low-temperature co-fired porous glass ceramics. *Journal of Non-Crystalline Solids* **358**: 1171-1179.
- Yao R, He J, Meng G, Jiang B and Wu F (2016). Electrospun PCL/Gelatin composite fibrous scaffolds: mechanical properties and cellular responses. *Journal of Biomaterials Science, Polymer Edition* **27**: 824-838.
- Yokoi T, Saito M, Kiyono T, Iseki S, Kosaka K, Nishida E, Tsubakimoto T, Harada H, Eto K and Noguchi T (2007). Establishment of immortalized dental follicle cells for generating periodontal ligament in vivo. *Cell and Tissue Research* **327**: 301-311.
- Yun H-M, Lee E-S, Kim M-j, Kim J-J, Lee J-H, Lee H-H, Park K-R, Yi J-K, Kim H-W and Kim E-c (2015). Magnetic nanocomposite scaffold-induced stimulation of migration and odontogenesis of human dental pulp cells through integrin signaling pathways. *PloS one* **10**: e0138614.
- Zhang J, Park Y-D, Bae W-J, El-Fiqi A, Shin S-H, Lee E-J, Kim H-W and Kim E-C (2015). Effects of bioactive cements incorporating zinc-bioglass nanoparticles on odontogenic and angiogenic potential of human dental pulp cells. *Journal of Biomaterials Applications* **29**: 954-964.
- Zhang W, Ahluwalia IP, Literman R, Kaplan DL and Yelick PC (2011). Human dental pulp progenitor cell behavior on aqueous and hexafluoroisopropanol based silk scaffolds. *Journal of Biomedical Materials Research Part A* **97**: 414-422.
- Zhang W, Walboomers XF, van Kuppevelt TH, Daamen WF, Bian Z and Jansen JA (2006). The performance of human dental pulp stem cells on different three-dimensional scaffold materials. *Biomaterials* **27**: 5658-5668.
- Zhang X, Jia W, Gu Y, Xiao W, Liu X, Wang D, Zhang C, Huang W, Rahaman MN and Day DE (2010). Teicoplanin-loaded borate bioactive glass implants for treating chronic bone infection in a rabbit tibia osteomyelitis model. *Biomaterials* **31**: 5865-5874.

Zhang X, Zeng D, Li N, Wen J, Jiang X, Liu C and Li Y (2016). Functionalized mesoporous bioactive glass scaffolds for enhanced bone tissue regeneration. *Scientific Reports* **6**: 19361.

Zheng K, Lu M, Rutkowski B, Dai X, Yang Y, Taccardi N, Stachewicz U, Czyska-Filemonowicz A, Hüser N and Boccaccini AR (2016). ZnO quantum dots modified bioactive glass nanoparticles with pH-sensitive release of Zn ions, fluorescence, antibacterial and osteogenic properties. *Journal of Materials Chemistry B* **4**: 7936-7949.

Zhijiang C, Yi X, Haizheng Y, Jia J and Liu Y (2016). Poly (hydroxybutyrate)/cellulose acetate blend nanofiber scaffolds: Preparation, characterization and cytocompatibility. *Materials Science and Engineering: C* **58**: 757-767.

Zhou Y, Yang Y, Huang F, Ren J, Yuan S and Chen G (2014). Characterization of new tellurite glasses and crystalline phases in the  $\text{TeO}_2\text{-PbO-Bi}_2\text{O}_3\text{-B}_2\text{O}_3$  system. *Journal of Non-Crystalline Solids* **386**: 90-94.

Zhou Z, Ou B, Huang T, Zeng W, Liu L, Liu Q, Chen J, Zhao Y, Yang Z and Cao D (2013). Biocompatibility In-vitro of Gel/HA Composite Scaffolds Containing Nano-Bioactive Glass for Tissue Engineering. *Journal of Macromolecular Science, Part A* **50**: 1048-1053.

Zhu W and Liang M (2015). Periodontal ligament stem cells: current status, concerns, and future prospects. *Stem Cells International* **2015**, 972313.

## APPENDIX A

### ETHICS COMMITTEE REPORT

UYGULAMALI ETİK ARAŞTIRMA MERKEZİ  
APPLIED ETHICS RESEARCH CENTER



DUMLUPINAR BULVARI 06800  
ÇANKAYA ANKARA/TURKEY  
T: +90 312 210 22 91  
F: +90 312 210 79 59  
ueam@metu.edu.tr  
www.ueam.metu.edu.tr

Sayı: 28620816/135-632

11 Mart 2014

Gönderilen: : Doç. Dr. Ayşen Tezcaner  
Mühendislik Bilimleri

Gönderen : Prof. Dr. Canan Özgen   
Uygulamalı Etik Araştırma Merkezi Başkanı

İlgi : Etik Onayı.

Etik Kurul izni için sunmuş olduğunuz " Dentin Rejenerasyonuna Yönelik Bor ile Modifiye Edilmiş Nanobiyocam İçeren Taşıyıcılar Geliştirilmesi ve Karakterizasyonu " isimli Tübitak projesi başvurunuz ODTÜ "İnsan Araştırmaları Etik Komitesi" tarafından uygun görülerek etik onayı verilmiştir.

Bilgilerinize saygılarımla sunarım.



Prof. Dr. Canan Özgen  
UEAM Başkanı  
(IAK Başkanı)



Prof. Dr. Canan Sümer  
IA Komitesi Üyesi



Prof. Dr. Mehmet Utku  
IA Komitesi Üyesi



Prof. Dr. Aydan Balamir  
IA Komitesi Üyesi



Prof. Dr. Ayhan Sol  
IA Komitesi Üyesi



## APPENDIX B

### CALIBRATION CURVE FOR ALP ASSAY

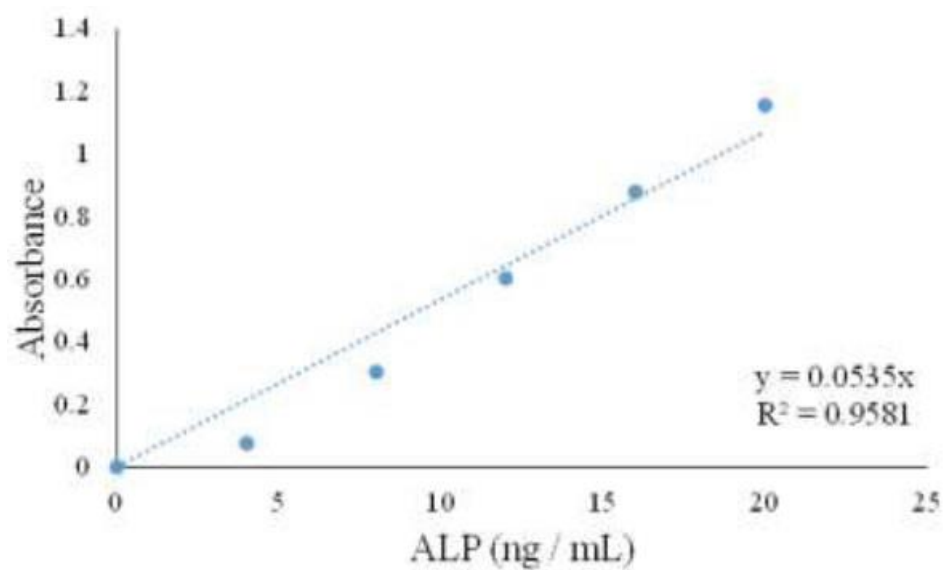


**Figure 54.** Calibration curve for ALP assay constructed with para-nitrophenol as standard.



## APPENDIX C

### CALIBRATION CURVE FOR DETERMINATION OF INTRACELLULAR CALCIUM

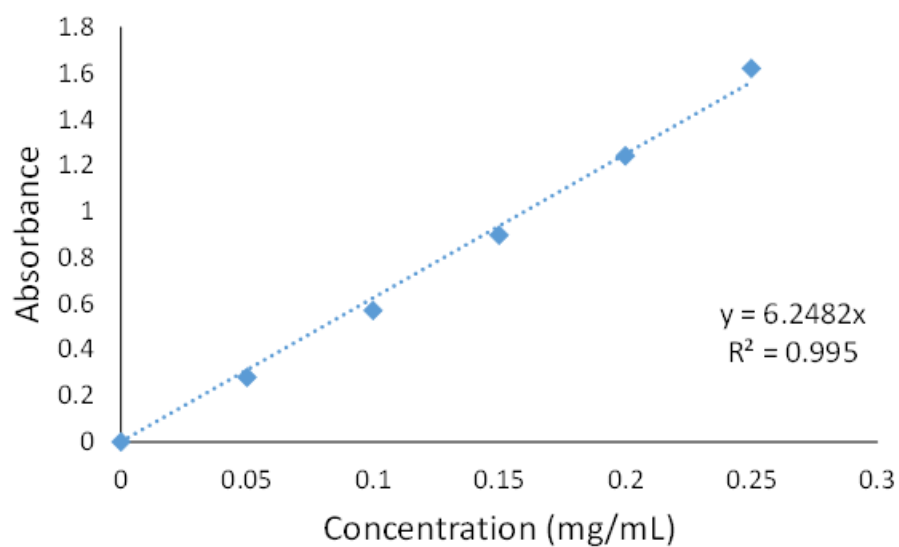


**Figure 55.** Calibration curve of calcium using various  $\text{CaCl}_2$  concentrations as standard (n=5).





## APPENDIX D

### CALIBRATION CURVE FOR DETERMINATION OF DNA CONTENT

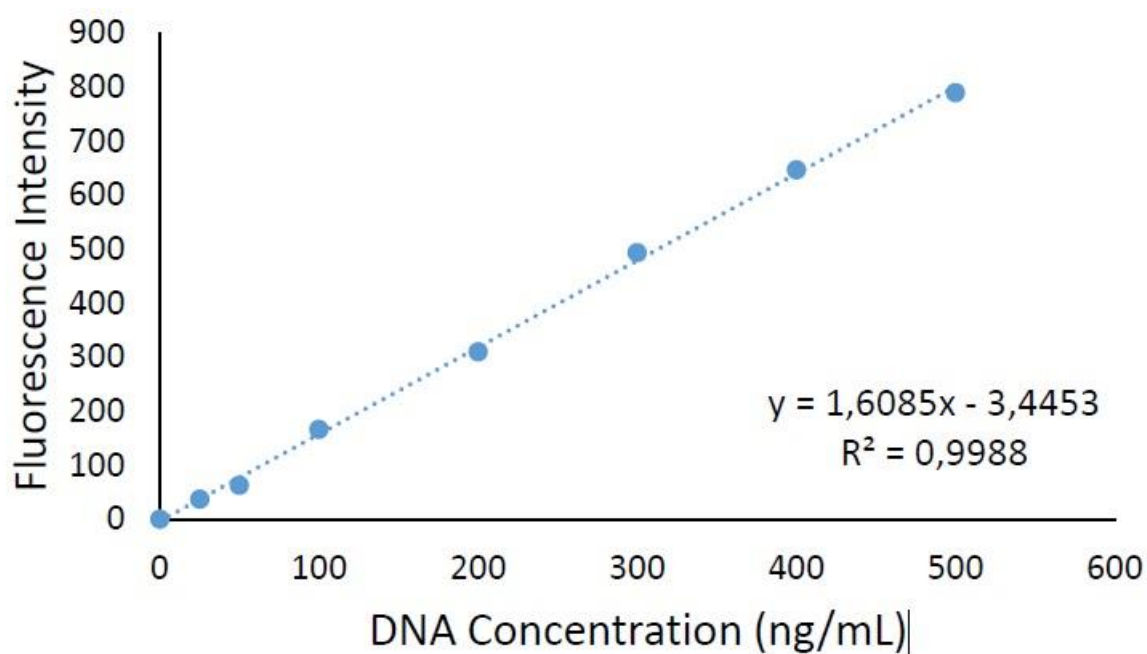


**Figure 56.** Calibration curve of DNA constructed with different concentrations of calf thymus DNA as standard for the determination of total DNA content in cell lysates in ALP assay (n=3).



## CURRICULUM VITAE

### PERSONAL INFORMATION

Surname, Name: Moonesi Rad, Reza  
Nationality: IRAN  
Date and Place of Birth: 13 June 1977 , Oroumieh  
Marital Status: Single  
Phone: +90 537 286 6991  
email: reza.rad@metu.edu.tr

### EDUCATION

Degree	Institution	Year of Graduation
MS	Urmia Azad University, Doctor of Veterinary Medicine	2002
High School	Soroush High School, Oroumieh	1995

### WORK EXPERIENCE

Year	Place	Enrollment
2004- 2010	Urmia University of Medical Sciences	Lecturere in General English Courses

### FOREIGN LANGUAGES

English (Fluent), Turkish (Fluent),

### REFEREED JOURNALS

1. E. Pourreza, A. Z. Alshemary, B. Yilmaz, **R. Moonesi Rad**, A. Tezcaner, Z. Evis. "Strontium and fluorine co-doped biphasic calcium phosphate: characterization and in vitro cytocompatibility analysis." *Biomedical Physics & Engineering Express* 3, no. 4 (2017): 045004.
2. **R. Moonesi Rad**, A. Z. Alshemary, D. Keskin, Z. Evis, S. Şahin, K. Altunbaş, A. Tezcaner. "Structural and biological assessment of boron doped bioactive glass nanoparticles for dental tissue applications." *Ceramics International* (Accepted).

## CONFERENCE PAPERS

1. **R. Moonesi Rad**, D. Keskin, Z. Evis, S. E. Erdoğan, Şahin, A. Tezcaner. “Preparation of a nanobiocomposite scaffold containing boron modified bioactive glass nanoparticles and biopolymers of cellulose acetate/pullulan/gelatin and evaluation of its application in dentin tissue engineering”. International Conference on Polymer Science and Engineering. New Orleans, LA, USA (August 22-24 2016).
2. **R. Moonesi Rad**, A. Z. Alshemary, D. Keskin, Z. Evis, S. Şahin, A. Tezcaner. “Macroporous boron modified bioactive glass scaffolds for hard tissue engineering”. 8th National Biomechanics Congress with International Participation, Ankara, Turkey (October 19-23 2016).
3. **R. Moonesi Rad**, D. Atila, D. Keskin, Z. Evis, A. Tezcaner. “Asymmetric bi-layer composite membrane containing Boron-modified nano bioactive glass for guided bone regeneration” 4th International Conference and Exhibition on Materials Science and Engineering. Orlando, FL, USA (September 14-16, 2015), p.5.
4. **R. Moonesi Rad**, M. Güldiken, D. Keskin, Z. Evis, S. Şahin, A. Tezcaner. “Boron modified nano bioactive glass incorporated polymeric microspheres for hard tissue engineering”. 21st Biomaterials Science and Technology Symposium. Antalya, Turkey (October 22-24 2015), p.173.
5. Sh. Mounesi Rad, **R. Moonesi Rad**, “PLLA/CNT nanocomposite scaffolds for application in nerve tissue engineering: Fabrication and evaluation of their physical and mechanical properties”. 8th National Biomechanics Congress with International Participation, Ankara, Turkey (October 19-23 2016), p.5.
6. **R. Moonesi Rad**, A. Z. Alshemary, D. Keskin, Z. Evis, S. Şahin, A. Tezcaner. “Evaluation of cytotoxicity effect of boron modified bioactive glass nanoparticles on human dental pulp stem cells”. 22<sup>nd</sup> Biomedical Science and Technology Symposium. Ankara, Turkey (May 12-14 2017), p.105.

## HOBBIES

Mountain climbing, Swimming, Visiting natural and historical attractions